



Development of Enzymatic Fuel Cells with Pyranose-2-Oxidase

A Thesis submitted by

Samet Şahin

For the Degree of Doctor of Philosophy

School of Chemical Engineering and Advanced Materials

Newcastle University

February 2017

Abstract

Power harvesting from biological sources has been very popular recently because of the advancements in implantable medical devices. Among all different biofuel cells, utilising enzymes for glucose oxidation plays essential role in developing micro-power sources due to their high bio-catalytic activity.

The aim of this study is to develop enzyme electrodes using pyranose-2-oxidase (P2O, wild type and mutants) and investigate the potential use in enzymatic biofuel cell applications as alternative to commercially available glucose oxidase (GOx) for glucose oxidation. Additional work was also carried out with bilirubin oxidase (BOD) for oxygen reduction. The effect of oxygen on enzyme performance, immobilization of the enzymes on carbon surface and biofuel cell performance were mainly investigated. The electrochemical techniques employed in this study were cyclic voltammetry, linear sweep voltammetry and chronoamperometry. Fuel cell test were carried out in glass cells and custom-made stack cells by recording cell potential on different resistances. Polarization curves were obtained by plotting voltage, current and power values.

P2O and GOx were first tested in solution in the presence of electron mediator ferrocene carboxylic acid (FcCOOH) to investigate the effect of oxygen on enzyme performances. P2O and its mutants showed similar electrochemical behaviour compared to commercial GOx where P2O-T169G mutant showed better performance, especially when oxygen is saturated in the solution. The immobilization of the mutant P2O-T169G and GOx were then achieved using crosslinking on pyrenyl carbon structures, where either FcCOOH was used in solution or ferrocene (Fc) immobilised with nafion® polymer and carbon nanotubes on electrode surface. BOD was also immobilised on electrode using same method without mediator. Results indicate that enhanced current values was achieved compared to solution studies with good affinity towards glucose for both of the enzymes.

Proof of concept biofuel cells were set up using P2O-T169G/GOx and BOD as anodes and cathode, respectively. Initial tests showed that P2O-T169G based enzymatic fuel cell can reach up to a power density of $9.56 \mu\text{W cm}^{-2}$ which is $\sim 25\%$ more power output than it was obtained for GOx in aerobic conditions. Finally, a biofuel cell anode using P2O-T169G was combined with air breathing BOD cathode in a stack design enzymatic biofuel cell with an open circuit potential of 0.558 V and maximum power density of $29.8 \pm 6.1 \mu\text{W cm}^{-2}$ at 0.318 V.

To My Family,

The reason for who I am today.

Thank you for your great support and continuous care.

I couldn't have done it without you.

To Prof. Abdurrahman Tanyolaç,

My greatest inspiration and mentor for life with his exceptional personality.

I will never forget the things you have taught me

and how they have changed my life.

Acknowledgements

First of all, I would like to thank Allah (cc), for blessing me with this achievement and I am eternally grateful for what I have in this life,

I would like to thank my supervisors, Dr. Eileen Yu, for her guidance throughout my studies whom I am so grateful to work with and my second supervisor, Professor Jarka Glassey, for being there whenever I needed,

I would like to thank my research group (based in Merz Court, C318 and Bedson, G10), especially Dr. Henriette Christensen for her kind support,

I would like to thank all CEAM family; technicians, administrative staff and academic staff especially those who had to deal with me. Also, all the student reps, fellow demonstrators and module leaders I worked with in CEAM and SAgE faculty. It was a great pleasure working with you, one which I will never forget.

I would like to thank Prof. Pimchai Chaiyen and her research group, for kindly providing P2O enzyme samples for my studies and their endless support. I would also like to thank Dr. Kamila Zelechowska and her research group, especially Miss. Izabela Kondratowicz, for kindly testing my samples for SEM analysis and the collaboration for the graphene studies.

I would like to thank Republic of Turkey, Ministry of National Education, for sponsoring my PhD and making it all possible.

I am eternally grateful to my family, for being there, cheering me up and taking great care of me. None of my achievements would have been possible without your love and support.

Finally, I would like to thank everyone who has inspired me to do a PhD abroad. These were the best days of my life (so far).

Table of Contents

Abstract.....	i
Acknowledgements	iii
List of Figures.....	ix
List of Tables	xxiii
Nomenclature.....	xxv
Abbreviations	xxvii
Chapter 1. Introduction and Literature Review	1
1.1. Introduction.....	1
1.1.1. Overview of Enzymatic Biofuel Cells.....	1
1.1.2. Aims and Objectives.....	3
1.2. Literature Review	4
1.2.1. Enzymes Used in Enzymatic Biofuel Cells.....	6
1.2.2. Enzymatic Electrode Assemblies for Biofuel Cells	13
1.2.3. Enzymatic Biofuel Cell Configurations and Performance	32
1.3. Review of Methods for Electrochemical Analysis	40
1.3.1. The Cell Set-up.....	41
1.3.2. Electrochemical Characterization.....	41
1.3.3. Fuel Cell Polarization	44
Chapter 2. Electrochemical Glucose Oxidation by Pyranose-2-Oxidase Mutants for Enzymatic Biofuel Cell Applications	47
2.1. Introduction.....	47
2.2. Experimental	49
2.2.1. Materials	49
2.2.2. Electrochemical Measurements.....	50
2.3. Results and Discussion	50

2.3.1. Electrochemical characterization of Pyranose-2-oxidase and its mutants in solution	50
2.3.2. Electrochemical characterization of Glucose Oxidase in solution and comparison with P2O enzymes	64
2.4. Conclusions	70
Chapter 3. Immobilization of Mutant P2O and GOx on Pyrenyl Carbon Structures for Glucose Oxidation	73
3.1. Introduction	73
3.2. Experimental	77
3.2.1. Materials	77
3.2.2. Preparation of Ferrocene-Nafion Redox Polymer with Multi-Walled Carbon Nanotubes (Fc-Nafion-MWCNTs)	78
3.2.3. Fabrication of Enzyme Electrodes	78
3.3. Electrochemical Measurements	80
3.4. Results and Discussion	81
3.4.1. Enzyme electrodes in solution with FcCOOH	81
3.4.2. Enzyme electrodes modified with ferrocene-nafion-multi-walled carbon nanotubes (Fc-Nafion-MWCNTs)	89
3.5. Conclusions	103
Chapter 4. A Glucose-Air Enzymatic Biofuel Cell with Pyranose-2-Oxidase	105
4.1. Introduction	105
4.2. Experimental	107
4.2.1. Materials	107
4.2.2. Preparation of Enzymatic Biofuel Cell Anode	107
4.2.3. Preparation of Enzymatic Biofuel Cell Cathode	107
4.2.4. Electrochemical and Fuel Cell Measurements	108
4.3. Results and Discussion	109
4.3.1. Performance of EBFCs with P2O-T169G, GOx and BOD	109

4.3.2. Stability of EBFC with P2O-T169G and Air-breathing Cathode	121
4.4. Conclusions.....	124
Chapter 5. Conclusion and Recommendations for Future Work	127
5.1. Conclusion	127
5.2. Recommendations for Future Work	128
5.2.1. Optimization of Enzyme Electrodes and EBFC	128
5.2.2. Enzymes	128
5.2.3. Materials for Electrode Fabrication.....	129
5.2.4. Biofuel Cell Design	131
Appendix	133
Appendix A	133
Appendix B.....	141
Appendix C.....	146
Appendix D	148
References	149

List of Figures

Figure 1. 1. Schematic diagram of a membrane-less glucose/oxygen enzymatic biofuel cell. . 1	1
Figure 1. 2. Illustrating the scale of credibility gap for biofuel cells and biosensors in terms of approximate power output ranges (Bullen <i>et al.</i> , 2006).3	3
Figure 1. 3. EBFC publications between 2010 and 2012 (Source: Web of Knowledge). 5	5
Figure 1. 4. The reaction catalyzed by GOx.6	6
Figure 1. 5. Structure of the GOx enzyme and FAD units (Goodsell, 2006).7	7
Figure 1. 6. Structure of the P2O subunit from <i>Trametes multicolor</i> (Martin Hallberg <i>et al.</i> , 2004). 8	8
Figure 1. 7. Cross-section view two subunits (marked as A and C) showing the active site and the channels providing water-accessible structure (Martin Hallberg <i>et al.</i> , 2004). 9	9
Figure 1. 8. A representation of the X-ray-determined crystal structure of (A) laccase III from <i>trametes versicolor</i> (Piontek <i>et al.</i> , 2002) and (B) BOD from <i>myrothecium verrucaria</i> (Cracknell <i>et al.</i> , 2011) (TNC refers to trinuclear cluster (T2 and T3) of the enzyme). 11	11
Figure 1. 9. Mechanisms of DET from electrodes to BOD connected (A) <i>via</i> the T1 site and (B) <i>via</i> the T2/T3 cluster (Ramírez <i>et al.</i> , 2008). 12	12
Figure 1. 10. Schematics of (A) direct and (B) mediated electron transfer-based enzyme electrodes (Alkire <i>et al.</i> , 2013). 14	14
Figure 1. 11. The different locations of enzyme active centres, (A) Enzyme active centre is NAD(H) or NADP(H), (B) the active centre is diffusive and (C) the active centre is located deep buried inside the enzyme (Bullen <i>et al.</i> , 2006). 15	15
Figure 1. 12. Immobilization technology in biofuel cells (Yang <i>et al.</i> , 2012). 17	17
Figure 1. 13. Schematic diagram of LBL fabrication of an enzyme electrode for electrochemical detection of fatty acids (ACOD: Acyl-CoA Oxidase, ACS: Acyl-CoA Synthetase, C SPE: Carbon screen printed electrode, MWCNT: Multi-walled carbon nanotubes) (Kang <i>et al.</i> , 2014). 18	18

Figure 1. 14. Schematic of immobilised enzyme using nanostructured silica sol-gel entrapment method (Lim <i>et al.</i> , 2007).	18
Figure 1. 15. Covalent enzyme immobilization with (A) epoxy-modified silica (B) aminopropyl-modified silica (Jung <i>et al.</i> , 2010).....	19
Figure 1. 16. EDC-NHS crosslinking reaction scheme (Scientific, 2016).....	20
Figure 1. 17. Schematic for crosslinking enzymes on pyrene activated carbon nanotubes using EDC-NHS couple (Krishnan and Armstrong, 2012).	20
Figure 1. 18. (A) The structure of anodic Os polymer with a 13-atom flexible spacer between the polymer backbone and the Os complex (B) Schematics of electron conduction in Os redox hydrogels (Mano <i>et al.</i> , 2002b; Heller, 2006).....	23
Figure 1. 19. Structure of (A) Ferrocene and (B) FcCOOH.	24
Figure 1. 20. Schematic of enzymatic anode based on SWCNTs incorporated with Fc redox polymer (Tran <i>et al.</i> , 2011).	26
Figure 1. 21. Structure of nafion [®]	27
Figure 1. 22. Structure of (A) 1-pyrenebutric acid and (B) 1-pyrenebutanoic acid succinimidyl ester.	29
Figure 1. 23. Schematic of PQQ-GHD and Lc immobilised on pyrenyl carbon nanostructures (Szczupak <i>et al.</i> , 2012).....	30
Figure 1. 24. Enzymatic biofuel cells demonstrated in non-mamal living animals: (A) snail, (B) lobster and (C) clam (Halámková <i>et al.</i> , 2012; Szczupak <i>et al.</i> , 2012; MacVittie <i>et al.</i> , 2013).	33
Figure 1. 25. Enzymatic biofuel cells implanted in (A) rabbit ear and (B) rat (Miyake <i>et al.</i> , 2011; Zebda <i>et al.</i> , 2013).	37
Figure 1. 26. Schematic presentation of (A) microfluidic fuel cell (B) concentric fuel cell (C) fuel cell with air breathing cathode (D) stack design fuel cell (Fischback <i>et al.</i> , 2006; Lim and Palmore, 2007; Habrioux <i>et al.</i> , 2008; Svoboda <i>et al.</i> , 2008).....	39

Figure 1. 27. Simple presentation of an experimental set-up for three-electrode electrochemical cell.	41
Figure 1. 28. (A) CV waveform and (B) typical CV (Princeton).....	42
Figure 1. 29. Plot of peak height for cadmium reduction at various scan rates (Princeton, 2016).	43
Figure 1. 30. (A) Polarization curve and the losses (Gold, 2012) (B) power curve with polarization curve for an EBFC (González-Guerrero <i>et al.</i> , 2013).	44
Figure 2. 1. (A) CV (scan rate: 10 mV s ⁻¹) and (B) LSV (scan rate: 1 mV s ⁻¹) scans of nitrogen saturated solutions with 0 mM and 2 mM concentrations of glucose added to the solution containing 0.5 mM FcCOOH and 1 mg mL ⁻¹ P2O-WT in PBS at pH 7. (GCE surface area: 0.071 cm ²).....	52
Figure 2. 2. LSV (scan rate: 1 mV s ⁻¹) scans of nitrogen saturated solutions with different concentrations of glucose added to the solution containing 0.5 mM FcCOOH and 1 mg mL ⁻¹ P2O-WT in PBS at pH 7. (GCE surface area: 0.071 cm ²).	53
Figure 2. 3. Plot of peak heights at various scan rates for 0 mM and 2 mM concentrations of glucose added to the solution containing 0.5 mM FcCOOH and 1 mg mL ⁻¹ P2O-WT in PBS, at pH 7. Data obtained from Figure A.1 and Figure A.2 in Appendix A.....	54
Figure 2. 4. (A) CV (scan rate: 10 mV s ⁻¹) and (B) LSV (scan rate: 1 mV s ⁻¹) scans of nitrogen saturated solutions with 0 mM (black) and 2 mM (red) concentrations of glucose added to the solution containing 0.5 mM FcCOOH and 1 mg mL ⁻¹ P2O-T169S in PBS, at pH 7. (GCE, surface area: 0.071 cm ²).	55
Figure 2. 5. LSV (scan rate: 1 mV s ⁻¹) scans of nitrogen saturated solutions with different concentrations of glucose added to the solution containing 0.5 mM FcCOOH and 1 mg mL ⁻¹ P2O-T169S in PBS, at pH 7. (GCE, surface area: 0.071 cm ²).....	56
Figure 2. 6. Plot of peak heights at various scan rates for 0 mM and 2 mM concentrations of glucose added to the solution containing 0.5 mM FcCOOH and 1 mg mL ⁻¹ P2O-T169S in PBS, at pH 7. Data obtained from Figure A.3 and Figure A.4 in Appendix A	57

Figure 2. 7. The relationship between peak catalytic current and glucose concentration for P2O-T169S. Inset: Lineweaver-Burk plot.....	58
Figure 2. 8. (A) CV (scan rate: 10 mV s ⁻¹) and (B) LSV (scan rate: 1 mV s ⁻¹) scans of nitrogen saturated solutions with 0 mM (black) and 2 mM (red) concentrations of glucose added to the solution containing 0.5 mM FcCOOH and 1 mg mL ⁻¹ P2O-T169G in PBS at pH 7. (GCE surface area: 0.071 cm ²).....	59
Figure 2. 9. LSV (scan rate: 1 mV s ⁻¹) scans of nitrogen saturated solutions with different concentrations of glucose added to the solution containing 0.5 mM FcCOOH and 1 mg mL ⁻¹ P2O-T169G in PBS at pH 7. (GCE surface area: 0.071 cm ²).....	60
Figure 2. 10. Plot of peak heights at various scan rates for 0 mM and 2 mM concentrations of glucose added to the solution containing 0.5 mM FcCOOH and 1 mg mL ⁻¹ P2O-T169G in PBS, at pH 7. (GCE, surface area: 0.071 cm ²). Data obtained from Figure A.5 and Figure A.6 in Appendix A.....	60
Figure 2. 11. The relationship between peak catalytic current and glucose concentration for P2O-T169G. Inset: Lineweaver-Burk plot.....	61
Figure 2. 12. LSV (scan rate: 1 mV s ⁻¹) scans of nitrogen saturated solutions with 2 mM concentrations of glucose added to the solution containing 0.5 mM FcCOOH and 1 mg mL ⁻¹ concentrations of P2O-WT, P2O-T169S and P2O-T169G at pH 7. (GCE surface area: 0.071 cm ² and 0 mM concentration data is subtracted from 2 mM concentration data).	62
Figure 2. 13. LSV (scan rate: 1 mV s ⁻¹) scans of (A) P2O-T169S and (B) P2O-T169G (both concentrations are 1 mg mL ⁻¹ in PBS) in nitrogen and air saturated solutions with 2 mM concentrations of glucose added to the solution containing 0.5 mM FcCOOH in PBS at pH 7. (GCE surface area: 0.071 cm ²).	63
Figure 2. 14. (A) CV (scan rate: 10 mV s ⁻¹) and (B) LSV (scan rate: 1 mV s ⁻¹) scans of nitrogen saturated solutions with 0 mM (black) and 2 mM (red) concentrations of glucose added to the solution containing 0.5 mM FcCOOH and 1 mg mL ⁻¹ GOx in PBS at pH 7. (GCE surface area: 0.071 cm ²).....	65
Figure 2. 15. Plot of peak heights at various scan rates for 0 mM and 2 mM concentrations of glucose added to the solution containing 0.5 mM FcCOOH and 1 mg mL ⁻¹ GOx in PBS at pH	

7. (GCE surface area: 0.071 cm ²). Data obtained from Figure A.10 and Figure A.11 in Appendix A.	66
Figure 2. 16. The relationship between peak catalytic current and glucose concentration for GOx. Inset: Lineweaver-Burk plot.	67
Figure 2. 17. CAs (1 h length) of air saturated solutions for GOx and P2O-T169G (both 1 mg mL ⁻¹) at 0.350 V for 0 mM and 4 mM concentrations of glucose added to the solution containing 0.5 mM FcCOOH, at pH 7. (GCE, surface area: 0.071 cm ²).	68
Figure 2. 18. CAs (3 h length) of air saturated solutions for GOx and P2O-T169G (both 1 mg mL ⁻¹) at 0.350 V for 4 mM concentration of glucose added to the solution containing 0.5 mM FcCOOH, at pH 7. (GCE, surface area: 0.071 cm ²).	69
Figure 3. 1. Carbon screen printed electrodes (SPEs) used for the electrochemical experiments; DRP-C110 (left) and DRP-C1110 (right) (DropSens, 2016)	77
Figure 3. 2. Schematic representation of crosslinking of enzymes on bare carbon electrode (A) and on Fc-Nafion-MWCNTs (B)	79
Figure 3. 3. Experimental set-up for electrochemical experiments.	80
Figure 3. 4. CV (scan rate: 5 mV s ⁻¹) scans of (A) P2O-T169G and (B) GOx immobilised on carbon SPE. Tested in nitrogen saturated solutions with 0 mM and 4 mM concentrations of glucose added to the solution containing 0.5 mM FcCOOH in 0.1 M PBS at pH 7. Ag is the silver/silver ion reference electrode used on the SPE (SPE surface area: 0.126 cm ²).	82
Figure 3. 5. (A) CA experiment at 0.2 V (<i>vs</i> Ag) of various glucose concentrations for P2O-T169G enzyme immobilised on carbon SPE, (B) Current values for various glucose concentrations derived from (A) and (C) the calibration curve for the linear region. Tested in saturated solutions of 0.5 mM FcCOOH in PBS at pH 7. Ag is the silver/silver ion reference electrode used on the SPE (SPE surface area: 0.126 cm ²). Error bars are sample standard deviations of measurements on n = 2 samples.	84
Figure 3. 6. (A) CA experiment at 0.2 V (<i>vs</i> Ag) of various glucose concentrations for GOx enzyme immobilised on carbon SPE, (B) Current values for various glucose concentrations	

derived from (A) and (C) the calibration curve for the linear region. Tested in saturated solutions of 0.5 mM FcCOOH in PBS at pH 7. Ag is the silver/silver ion reference electrode used on the SPE (SPE surface area: 0.126 cm²). Error bars are sample standard deviations of measurements on n = 2 samples..... 85

Figure 3. 7. CA experiments at 0.2 V (vs Ag) of various glucose concentrations for P2O-T169G and GOx enzymes immobilised on carbon SPE. Tested in air saturated solutions of 0.5 mM FcCOOH in PBS at pH 7. Ag is the silver/silver ion reference electrode used on the SPE (SPE surface area: 0.126 cm²)...... 86

Figure 3. 8. Lineweaver-Burk plot of P2O-T169G and GOx enzymes immobilised on carbon SPE. Tested in air saturated solutions of 0.5 mM FcCOOH in 0.1 M PBS at pH 7. Ag is the silver/silver ion reference electrode used on the SPE (SPE surface area: 0.126 cm²)...... 87

Figure 3. 9. CV (scan rate: 50 mV s⁻¹) scans for the pre-conditioning of the carbon SPEs modified with Fc-Nafion. Tested in 0.1 M PBS at pH 7. Fc-Nafion loading is 0.06 mg cm⁻². Ag is the silver/silver ion reference electrode used on the SPE (SPE surface area: 0.126 cm²). (All 20 scans are shown in Figure B.9) 89

Figure 3. 10. Comparison between Fc-Nafion and Fc-Nafion-MWCNTs coated electrodes after pre-conditioning step. CVs performed at a scan rate of 10 mV s⁻¹, tested in 0.1 M PBS at pH 7. Fc-Nafion and Fc-Nafion-MWCNTs loadings are 0.06 mg cm⁻². Ag is the silver/silver ion reference electrode used on the SPE (SPE surface area: 0.126 cm²)...... 90

Figure 3. 11. (A) CVs (scan rate: 10 mV s⁻¹) showing the effect of the different amounts of Fc-Nafion-MWCNTs coated on SPEs after pre-conditioning step and (B) anodic peak current values of the different electrodes prepared. Tested in 0.1 M PBS at pH 7. Ag is the silver/silver ion reference electrode used on the SPE (SPE surface area: 0.126 cm²). Error bars are sample standard deviations of measurements on n = 3 samples. 91

Figure 3. 12. SEM images of the (A) bare electrode, Fc-Nafion (B) before and (C) after pre-conditioning step and Fc-Nafion-MWCNTs (D) before and (E) after pre-conditioning step . 92

Figure 3. 13. SEM images of (A) unconditioned, (B) pre-conditioned Fc-Nafion-MWCNTs coated electrodes, (C) only MWCNTs and (D) pre-conditioned Fc-Nafion-MWCNTs with higher magnification. 94

Figure 3. 14. CV (scan rate: 5 mV s^{-1}) scans of (A) P2O-T169G and (B) GOx immobilised on Fc-Nafion-MWCNTs pre-conditioned carbon SPE. Tested in nitrogen saturated solution for various glucose concentrations containing 0.5 mM FcCOOH in PBS at pH 7. Ag is the silver/silver ion reference electrode used on the SPE (SPE surface area: 0.126 cm^2). 95

Figure 3. 15. (A) CA experiment at 0.15 V (vs Ag) of various glucose concentrations for P2O-T169G enzyme immobilised on Fc-Nafion-MWCNTs pre-conditioned carbon SPE, (B) Current values for various glucose concentrations derived from (A), (C) CA experiment at 0.15 V (vs Ag) of various glucose concentrations for GOx enzyme immobilised on carbon SPE and (D) Current values for various glucose concentrations derived from (C). Tested in 0.1 M PBS at pH 7. Ag is the silver/silver ion reference electrode used on the SPE (SPE surface area: 0.059 cm^2). Error bars are sample standard deviations of measurements on $n = 2$ samples. 96

Figure 3. 16. (A) CA experiment at 0.15 V (vs Ag) of various glucose concentrations for P2O-T169G enzyme immobilised on Fc-Nafion-MWCNTs pre-conditioned carbon SPE with a surface area of 0.126 cm^2 , (B) Current density values for various glucose concentrations derived from (A) with the data presented in Figure 3.15 (B). Tested in nitrogen saturated 0.1 M PBS at pH 7. Ag is the silver/silver ion reference electrode used on the SPE. Error bars are sample standard deviations of measurements on $n = 2$ samples. 97

Figure 3. 17. Comparison of current densities of P2O-T169G with GOx, both immobilised on Fc-Nafion-MWCNTs pre-conditioned carbon SPE (surface area: 0.126 cm^2). Data obtained from CA experiments at 0.15 V (vs Ag) of various glucose concentrations. Tested in air saturated 0.1 M PBS at pH 7. Ag is the silver/silver ion reference electrode used on the SPE. Error bars are sample standard deviations of measurements on $n = 2$ samples. (Raw data: Figure 3.15 (C) and Figure 3.16 (A) for GOx and P2O-T169G respectively). 98

Figure 3. 18. Calibration curve for P2O-T169G and GOx enzymes immobilised on Fc-Nafion-MWCNTs pre-conditioned carbon SPE. Tested in air saturated 0.1 M PBS at pH 7. Data extracted from Fig 3.17. (SPE surface area: 0.126 cm^2) 99

Figure 3. 19. Lineweaver-Burk plot for P2O-T169G and GOx immobilised on Fc-Nafion-MWCNTs pre-conditioned carbon SPE. Tested in air saturated 0.1 M PBS at pH 7. Data extracted from Fig 3.15 (B) and (D). (SPE surface area: 0.059 cm^2) 100

Figure 3. 20. CA experiments at 0.15 V (<i>vs</i> Ag) of various glucose concentrations for P2O-T169G and GOx enzymes immobilised on Fc-Nafion-MWCNTs pre-conditioned carbon SPE. Tested in air saturated 0.1 M PBS at pH 7. Ag is the silver/silver ion reference electrode used on the SPE (SPE surface area: 0.126 cm ²).....	100
Figure 3. 21. CA experiments at 0.15 V (<i>vs</i> Ag) for (A) P2O-T169G and (B) GOx. Tested in nitrogen and air saturated solutions of PBS at pH 7 containing 4 mM glucose for 12h. Ag is the silver/silver ion reference electrode used on the SPE (SPE surface area: 0.126 cm ²).....	101
Figure 3. 22. CA experiments at 0.15 V (<i>vs</i> Ag) for P2O-T169G and GOx. Tested in air saturated solutions of PBS at pH 7 containing 4 mM glucose for 12 h. Ag is the silver/silver ion reference electrode used on the SPE (SPE surface area: 0.126 cm ²).....	102
Figure 4. 1. Experimental set-up for cells. (A) Fuel cell set-up with a glass cell beaker (B) Fuel cell set-up with stack cell design with air breathing cathode (C) Overall view of the test equipment while operating in batch mode with a glass cell beaker.....	108
Figure 4. 2. CV (scan rate: 5 mV s ⁻¹) scans of a BOD cathode immobilised on MWCNTs coated SPE (MWCNTs loading of 0.08 mg cm ⁻¹) tested in nitrogen and air saturated solution of 0.1 M PBS at pH 7 containing 5.5 mM glucose. Ag is the silver/silver ion reference electrode used on the SPE (SPE surface area: 0.126 cm ²).....	109
Figure 4. 3. (A) Cell voltage-current and (B) fuel cell polarization curves operating in non-aerated and aerated glucose concentrations. All enzymes used to construct EBFCs were at 4 mg mL ⁻¹ concentration and were immobilised on SPE (surface area: 0.126 cm ²). EBFCs were tested at batch mode using a glass cell in non-aerated and aerated glucose concentrations of 5.5 mM in 0.1 M PBS at pH 7.	111
Figure 4. 4. Non-aerated and aerated anode (left) and cathode (right) potentials <i>versus</i> current curves obtained from EBFC tests. All enzymes used to construct EBFCs were at 4 mg mL ⁻¹ concentration and were immobilised on SPE (surface area: 0.126 cm ²). EBFCs were tested at batch mode using a glass cell in non-aerated and aerated solutions of 0.1 M PBS at pH 7 containing 5.5 mM glucose.....	113

Figure 4. 5. (A) Cell voltage-current and (B) fuel cell polarization curves for P2O-T169G and GOx as EBFC anodes combined with BOD cathode. All enzymes used to construct EBFCs were at 4 mg mL⁻¹ concentration and were immobilised on SPE (surface area: 0.126 cm²). EBFCs were tested at batch mode using a glass cell in aerated solutions of 0.1 M PBS at pH 7 containing 5.5 mM glucose. Error bars are sample standard deviations of measurements on n = 2 samples of each EBFC..... 116

Figure 4. 6. Voltage-current curves of anode (dashed line)-cathode (straight line) potentials for P2O-T169G and GOx as EBFC anodes combined with BOD cathode. All enzymes used to construct EBFC were at 4 mg mL⁻¹ concentration and were immobilised on SPE (surface area: 0.126 cm²). EBFCs were tested at batch mode using a glass cell in aerated solutions of 0.1 M PBS at pH 7 containing 5.5 mM glucose. Error bars are sample standard deviations of measurements on n = 2 samples of each EBFC. 117

Figure 4. 7. Cell voltage-current and fuel cell polarization curves showing the performance of P2O-T169G anode and BOD cathode. Enzymes concentrations of 10 mg mL⁻¹ and 4 mg mL⁻¹ were used for anode and cathode respectively and were both immobilised on carbon paper electrodes (surface area: 1.77 cm²). EBFCs were tested at batch mode using stack cell design in aerated solutions of 0.1 M PBS at pH 7 containing 5.5 mM glucose. Error bars are sample standard deviations of measurements on n = 2 samples of each EBFC. 119

Figure 4. 8. Voltage-current curves of anode and cathode potentials for P2O-T169G and BOD respectively. Enzymes concentrations of 10 mg mL⁻¹ and 4 mg mL⁻¹ were used for anode and cathode respectively and were both immobilised on carbon paper electrodes (surface area: 1.77 cm²). EBFCs were tested at batch mode using stack cell design in aerated solutions of 0.1 M PBS at pH 7 containing 5.5 mM glucose. Error bars are sample standard deviations of measurements on n = 2 samples of each EBFC. 120

Figure 4. 9. Fuel cell performance parameters at different times of polarisation for air-breathing EBFCs using P2O-T169G and BOD at the anode and cathode respectively. (A) Voltage-Current (B) Power curve (C) OCP-Max. Power *versus* time. Enzymes concentrations of 10 mg mL⁻¹ and 4 mg mL⁻¹ were used for anode and cathode respectively and were both immobilised on carbon paper electrodes (surface area: 1.77 cm²). EBFCs were tested at batch mode using stack cell design in aerated solutions of 0.1 M PBS at pH 7 containing 5.5 mM glucose. The maximum power values were obtained at 4 kΩ. 122

Figure 4. 10. (A) Cell voltage, anode and cathode potentials and (B) Percentage power density change of the EBFC over time during continuous operation of 18 days. P2O-T169G (10 mg mL⁻¹) and BOD (4 mg mL⁻¹) were used at the anode and cathode respectively and were both immobilised on carbon paper electrodes (surface area: 1.77 cm²). EBFCs were tested at continuous mode using stack cell design with a flow rate of 0.3 mL min⁻¹ in aerated solutions of 0.1 M PBS at pH 7 containing 5.5 mM glucose. 123

Figure 5. 1. Structure of PDH from *Agaricus meleagris* (Tan *et al.*, 2013) 129

Figure 5. 2. Schematic for oxygen reduction by laccase using graphene-multi-walled carbon nanotubes assembly (Lalaoui *et al.*, 2015)..... 130

Figure 5. 3. CVs of BOD immobilised on (A) rGO (inset: SEM image, 4 µm magnification) and (B) rGO+MWCNTs (inset: SEM image, 4 µm magnification) modified electrodes, tested in air and/or nitrogen saturated PBS at pH 7, 5 mV s⁻¹ scan rate..... 131

Figure 5. 4. (A) Scheme of Y-shaped glucose/O₂ microfluidic biofuel cell (B) PDMS-glass device. 132

Figure A. 1. CV (scan rate: 10 mV s⁻¹) scans of nitrogen saturated solution experiments with P2O-WT. Tests were performed at various scan rates of 0.5 V s⁻¹ (outer scan), 0.4 V s⁻¹, 0.3 V s⁻¹, 0.2 V s⁻¹, 0.1 V V s⁻¹, 0.05 V s⁻¹ and 0.01 V s⁻¹ (inner scan) with 0 mM glucose concentration of 0.5 mM FcCOOH in PBS at pH 7. (GCE surface area: 0.071 cm²). 133

Figure A. 2. CV (scan rate: 10 mV s⁻¹) scans of nitrogen saturated solution experiments with P2O-WT. Tests were performed at various scan rates of 0.5 V s⁻¹ (outer scan), 0.4 V s⁻¹, 0.3 V s⁻¹, 0.2 V s⁻¹, 0.1 V V s⁻¹, 0.05 V s⁻¹ and 0.01 V s⁻¹ (inner scan) with 2 mM glucose concentration of 0.5 mM FcCOOH in PBS at pH 7. (GCE surface area: 0.071 cm²). 133

Figure A. 3. CV (scan rate: 10 mV s⁻¹) scans of nitrogen saturated solution experiments with P2O-T169S. Tests were performed at various scan rates of 0.5 V s⁻¹ (outer scan), 0.4 V s⁻¹, 0.3 V s⁻¹, 0.2 V s⁻¹, 0.1 V V s⁻¹, 0.05 V s⁻¹ and 0.01 V s⁻¹ (inner scan) with 0 mM glucose concentration of 0.5 mM FcCOOH in PBS at pH 7. (GCE surface area: 0.071 cm²). 134

Figure A. 4. CV (scan rate: 10 mV s⁻¹) scans of nitrogen saturated solution experiments with P2O-T169S. Tests were performed at various scan rates of 0.5 V s⁻¹ (outer scan), 0.4 V s⁻¹, 0.3 V s⁻¹, 0.2 V s⁻¹, 0.1 V V s⁻¹, 0.05 V s⁻¹ and 0.01 V s⁻¹ (inner scan) with 2 mM glucose concentration of 0.5 mM FcCOOH in PBS at pH 7. (GCE surface area: 0.071 cm²)..... 134

Figure A. 5. CV (scan rate: 10 mV s⁻¹) scans of nitrogen saturated solution experiments with P2O-T169G. Tests were performed at various scan rates of 0.5 V s⁻¹ (outer scan), 0.4 V s⁻¹, 0.3 V s⁻¹, 0.2 V s⁻¹, 0.1 V V s⁻¹, 0.05 V s⁻¹ and 0.01 V s⁻¹ (inner scan) with 0 mM glucose concentration of 0.5 mM FcCOOH in PBS at pH 7. (GCE surface area: 0.071 cm²)..... 135

Figure A. 6. CV (scan rate: 10 mV s⁻¹) scans of nitrogen saturated solution experiments with P2O-T169G. Tests were performed at various scan rates of 0.5 V s⁻¹ (outer scan), 0.4 V s⁻¹, 0.3 V s⁻¹, 0.2 V s⁻¹, 0.1 V V s⁻¹, 0.05 V s⁻¹ and 0.01 V s⁻¹ (inner scan) with 2 mM glucose concentration of 0.5 mM FcCOOH in PBS at pH 7. (GCE surface area: 0.071 cm²)..... 135

Figure A. 7. Raw data for the LSV (scan rate: 1 mV s⁻¹) scans of nitrogen saturated solutions with 2 mM concentrations of glucose added to the solution containing 0.5 mM FcCOOH and 1 mg mL⁻¹ concentrations of P2O-WT, P2O-T169S and P2O-T169G at pH 7. (GCE surface area: 0.071 cm²)..... 136

Figure A. 8. LSV (scan rate: 1 mV s⁻¹) scans of P2O-WT (1 mg mL⁻¹ in PBS) in nitrogen and air saturated solutions with 1 mM concentrations of glucose added to the solution containing 0.5 mM FcCOOH in PBS at pH 7. (GCE surface area: 0.071 cm²)..... 136

Figure A. 9. LSV (scan rate: 1 mV s⁻¹) scans of nitrogen saturated solutions with various glucose concentrations added to the solution containing 0.5 mM FcCOOH and 1 mg mL⁻¹ GOx in PBS at pH 7. (GCE surface area: 0.071 cm²)..... 137

Figure A. 10. CV (scan rate: 10 mV s⁻¹) scans of nitrogen saturated solution experiments with GOx. Tests were performed at various scan rates of 0.5 V s⁻¹ (outer scan), 0.4 V s⁻¹, 0.3 V s⁻¹, 0.2 V s⁻¹, 0.1 V V s⁻¹, 0.05 V s⁻¹ and 0.01 V s⁻¹ (inner scan) with 0 mM glucose concentration of 0.5 mM FcCOOH in PBS at pH 7. (GCE surface area: 0.071 cm²)..... 137

Figure A. 11. CV (scan rate: 10 mV s⁻¹) scans of nitrogen saturated solution experiments with GOx. Tests were performed at various scan rates of 0.5 V s⁻¹ (outer scan), 0.4 V s⁻¹, 0.3 V s⁻¹,

0.2 V s⁻¹, 0.1 V V s⁻¹, 0.05 V s⁻¹ and 0.01 V s⁻¹ (inner scan) with 2 mM glucose concentration of 0.5 mM FcCOOH in PBS at pH 7. (GCE surface area: 0.071 cm²). 138

Figure A. 12. CAs (1 h length) of air saturated solutions for P2O-T169G (1 mg mL⁻¹) at 0.350 V for 0 mM and 4 mM concentrations of glucose added to the solution containing 0.5 mM FcCOOH, at pH 7. (GCE, surface area: 0.071 cm²). 138

Figure A. 13. CAs (1 h length) of air saturated solutions for GOx (1 mg mL⁻¹) at 0.350 V for 0 mM and 4 mM concentrations of glucose added to the solution containing 0.5 mM FcCOOH, at pH 7. (GCE, surface area: 0.071 cm²)..... 139

Figure A. 14. CAs (3 h length) of air saturated solutions for P2O-T169G (1 mg mL⁻¹) at 0.350 V for 4 mM concentration of glucose added to the solution containing 0.5 mM FcCOOH, at pH 7. (GCE, surface area: 0.071 cm²). 139

Figure A. 15. CAs (3 h length) of air saturated solutions for GOx (1 mg mL⁻¹) at 0.350 V for 4 mM concentration of glucose added to the solution containing 0.5 mM FcCOOH, at pH 7. (GCE, surface area: 0.071 cm²). 140

Figure B. 1. CV (scan rate: 5 mV s⁻¹) scans of carbon SPE to show reproducibility of the electrode. Tested in 0.1 M PBS at pH 7. Ag is the silver/silver ion reference electrode used on the SPE (SPE surface area: 0.126 cm²). Error bars are sample standard deviations of measurements on n = 4 samples..... 141

Figure B. 2. CV (scan rate: 5 mV s⁻¹) scans of carbon SPEs to show its activity towards glucose. Tested in 0.1 M PBS at pH 7 containing 0 mM and 5.5 mM glucose. Ag is the silver/silver ion reference electrode used on the SPE (SPE surface area: 0.126 cm²). Graphs shown are mean values based on n = 2 samples. 141

Figure B. 3. CV (scan rate: 5 mV s⁻¹) scans of carbon SPEs modified with Fc-Nafion-MWCNTs and then treated with PBSE to show its activity towards glucose. Tested in 0.1 M PBS at pH 7 containing 0 mM and 5.5 mM glucose. Ag is the silver/silver ion reference electrode used on the SPE (SPE surface area: 0.126 cm²). Graphs shown are mean values based on n = 2 samples. 142

Figure B. 4. CV (scan rate: 5 mV s ⁻¹) scans of GOx adsorbed on carbon SPEs to show its activity towards glucose. Tested in 0.1 M PBS at pH 7 containing 0 mM and 2 mM glucose. Ag is the silver/silver ion reference electrode used on the SPE (SPE surface area: 0.126 cm ²).	142
Figure B. 5. LSV (scan rate: 1 mV s ⁻¹) scans of P2O-T169G immobilised on carbon SPE. Tested in nitrogen saturated solutions with various glucose concentrations added to the solution containing 0.5 mM FcCOOH in 0.1 M PBS at pH 7. Ag is the silver/silver ion reference electrode used on the SPE (SPE surface area: 0.126 cm ²).	143
Figure B. 6. CV (scan rate: 5 mV s ⁻¹) scans of GOx immobilised on carbon SPE. Tested in nitrogen saturated solutions with various glucose concentrations added to the solution containing 0.5 mM FcCOOH in 0.1 M PBS at pH 7. Ag is the silver/silver ion reference electrode used on the SPE (SPE surface area: 0.126 cm ²).	143
Figure B. 7. LSV (scan rate: 1 mV s ⁻¹) scans of GOx immobilised on carbon SPE. Tested in nitrogen saturated solutions with various glucose concentrations added to the solution containing 0.5 mM FcCOOH in 0.1 M PBS at pH 7. Ag is the silver/silver ion reference electrode used on the SPE (SPE surface area: 0.126 cm ²).	144
Figure B. 8. CV (scan rate: 5 mV s ⁻¹) scans of P2O-T169G immobilised on carbon SPE. Tested in nitrogen saturated solutions with various glucose concentrations added to the solution containing 0.5 mM FcCOOH in 0.1 M PBS at pH 7. Ag is the silver/silver ion reference electrode used on the SPE (SPE surface area: 0.126 cm ²).	144
Figure B. 9. CV (scan rate: 50 mV s ⁻¹) scans for the pre-conditioning of the carbon SPEs modified with Fc-Nafion. Tested in 0.1 M PBS at pH 7. Fc-Nafion loading is 0.06 mg cm ⁻² . Ag is the silver/silver ion reference electrode used on the SPE (SPE surface area: 0.126 cm ²).	145
Figure C. 1. CV (scan rate: 5 mV s ⁻¹) scans of MWCNTs modified carbon SPE (MWCNTs loading of 0.08 mg cm ⁻¹) to show its inactivity towards oxygen present. Tested in nitrogen and air saturated solutions containing 0.1 M PBS at pH 7. Ag is the silver/silver ion reference electrode used on the SPE (SPE surface area: 0.126 cm ²).	146

Figure C. 2. Log-log plot of non-aerated and aerated anode-cathode potentials *versus* current curves obtained from enzymatic biofuel cell tests 146

Figure C. 3. Stability of the air-breathing biofuel cell under batch operation 147

List of Tables

Table 1. 1. Enzymes used in EBFCs using glucose as fuel (Half-Cell Reaction: glucose \rightarrow glucono-1,5-lactone + 2H ⁺ + 2e ⁻).....	10
Table 1. 2. Typical mediators used in enzymatic glucose oxidation. (V vs Ag/AgCl = V vs SHE – 0.197; V vs SCE = V vs. SHE – 0.24.) *methylene green exhibits two redox pairs, ** poly-L-lysine, *** polyallylamine.....	22
Table 1. 3. Examples of glucose/air (or O ₂) fuel cells based on mediators and GOx.....	34
Table 2. 1. The properties of the pyronase-2-oxidase enzymes used in solution experiments (Wongnate <i>et al.</i> , 2011))(Kujawa <i>et al.</i> , 2006; Pitsawong <i>et al.</i> , 2010).....	51
Table 2. 2. The electrochemical behaviour of the P2O enzymes used in solution CV experiments. Tested in nitrogen saturated solutions containing 0.5 mM FcCOOH and 1 mg mL ⁻¹ concentrations of P2O-WT, P2O-T169S and P2O-T169G at pH 7. (GCE surface area: 0.071 cm ² , E _{pa} : anodic peak potential, E _{pc} : cathodic peak potential).	63
Table 2. 3. Calculated diffusion coefficients for P2O enzymes using Randles-Sevcik equation at different glucose concentrations.	64
Table 2. 4. Summary of K _m values for the enzymes used	67
Table 3. 1. Summary of the electrochemical characteristics of P2O-T169G and GOx enzymes immobilised on carbon SPE. Tested in nitrogen saturated solutions with 0 mM and 4 mM concentrations of glucose added to the solution containing 0.5 mM FcCOOH in 0.1 M PBS at pH 7. (SPE surface area: 0.126 cm ²).	83
Table 3. 2. The saturation currents and glucose concentrations of P2O-T169G and GOx immobilised on carbon SPE from CA experiments at 0.2 V (vs Ag). All means and sample standard deviations from replicate measurements on n = 2 samples (SPE surface area: 0.126 cm ²).	86

Table 4. 1. Summary of the EBFC performance parameters obtained from non-aerated and aerated glucose concentrations. All enzymes used to construct EBFCs were at 4 mg mL⁻¹ concentration and were immobilised on SPE (surface area: 0.126 cm²). Anode and cathode potentials were also recorded as 0.050 and 0.544 V for non-aerated, 0.082 and 0.541 V for aerated solutions respectively at OCP. The maximum power values were obtained at different external loads of 150 kΩ (giving a cell potential of 0.361 V) and 100 kΩ (giving a cell potential of 0.347 V) representing the values for non-aerated and aerated solutions, respectively..... 110

Table 4. 2. Summary of the enzymatic biofuel cell performance results comparing P2O-T169G and GOx obtained from aerated system test. All enzymes used to construct EBFCs were at 4 mg mL⁻¹ concentration and were immobilised on SPE (surface area: 0.126 cm²). Anode and cathode potentials were 0.093±0.015 and 0.534±0.031 V for P2O-T169G (BOD at the cathode) and 0.072±0.015 and 0.517±0.004 V for GOx (BOD at the cathode) at OCP respectively. The maximum power values were obtained at 100 kΩ for P2O-T169G and 125 kΩ for GOx. All means and sample standard deviations from replicate measurements on n = 2 samples of each EBFC..... 115

Table 4. 3. Summary of the enzymatic biofuel cell performance results obtained from P2O-T169G anode and air breathing BOD cathode. Anode and cathode potentials were -0.019±0.035 and 0.524±0.014 V for P2O-T169G and BOD at OCP. The maximum power values were obtained at 2.5 kΩ. All means and sample standard deviations from replicate measurements on n = 2 samples of each EBFC..... 118

Nomenclature

A	Area
Ag	Silver
AgCl	Silver chloride
C	Concentration
D	Diffusion coefficient
E	Potential
F	Faraday constant
H ₂ O ₂	Hydrogen peroxide
i	Current
j	Current density
K _m	Michaelis-Menten constant
n	Number of electrons
Os	Osmium
O ₂	Oxygen
R	Ideal gas constant
SO ₃	Sulfonate
T	Temperature

Abbreviations

ABTS	2, 2'-azino-bis (3-ethylbenzthiazoline-6-sulfonic acid)
ACOD	Acyl-CoA oxidase
ACS	Acyl-CoA synthetase
ADH	Alcohol dehydrogenase
BOD	Bilirubin oxidase
CA	Chronoamperometry
CE	Counter electrode
CV	Cyclic voltammetry
CDH	Cellobiose dehydrogenase
CNT	Carbon nanotube
COx	Cytochrome oxidase
DET	Direct electron transfer
EBFC	Enzymatic biofuel cell
EDC	1-ethyl-3-(3-dimethylaminopropyl) carbodiimide hydrochloride
FAD	Flavin adenine dinucleotide
Fc	Ferrocene
FcCOOH	Ferrocene carboxylic acid
GDH	Glucose dehydrogenase
GOx	Glucose oxidase
HQS	8-hydroxyquinoline-5-sulfonic acid
HRP	Horseradish peroxidase
LBL	Layer by layer
Lc	Laccase

LSV	Linear sweep voltammetry
MET	Mediated electron transfer
MFC	Microbial biofuel cell
MP-11	Microperoxidase-11
MWCNT	Multi-walled carbon nanotube
NAD	Nicotinamide adenine dinucleotide
NHS	N-hydroxysulfosuccinimide
OCP	Open circuit potential
PBS	Potassium phosphate buffer
PBSE	1-pyrenebutanoic acid succinimidyl ester
PEGDGE	Poly(ethylene glycol) diglycidyl ether
PDH	Pyranose dehydrogenase
PTFE	Polytetrafluoroethylene
PQQ	Pyrrroloquinoline quinone
P2O	Pyranose-2-oxidase
RE	Reference electrode
rGO	Reduced graphene oxide
SEM	Scanning electron spectroscopy
SHE	Standard hydrogen electrode
SPE	Screen-printed electrode
SWCNT	Single-walled carbon nanotube
WE	Working electrode

Chapter 1. Introduction and Literature Review

1.1. Introduction

1.1.1. Overview of Enzymatic Biofuel Cells

The relationship between electricity and biology was first discovered by Galvani in 1780 (Galvani, 1791). It was reported that the muscles of dead frogs' legs twitched when struck by an electrical spark (Galvani, 1791). This can be considered one of the first studies in the field of bioelectricity. The chemical fuel cell concept, on the other hand, has been known for almost two centuries since Grove first used hydrogen fuel cells in series to produce water and electrical current by reversing the action of the electrolysis (Grove, 1839). However, the connection between biology and electricity was not demonstrated in a fuel cell until the early 20th century and later expanded with the development of the microbial fuel cells (MFCs) (Cohen, 1931) and enzymatic biofuel cells (EBFCs) (Davis and Yarbrough, 1962) (Yahiro *et al.*, 1964).

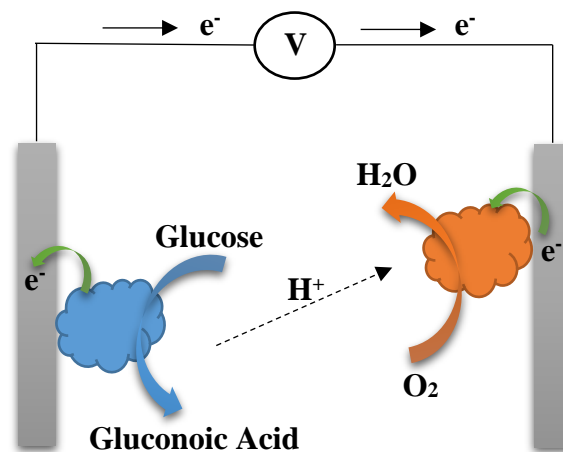


Figure 1. 1. Schematic diagram of a membrane-less glucose/oxygen enzymatic biofuel cell.

Enzymes are utilised instead of traditional metal catalysts or living microorganisms (Calabrese Barton *et al.*, 2004) in EBFCs. A typical EBFC consists of two electrodes; anode and cathode in which each enzyme has unique reactions due to its substrate selectivity (Calabrese Barton *et al.*, 2004). This eliminates the need for other elements, such as a membrane, required by traditional fuel cells (Heller, 2004). Figure 1.1 shows a schematic diagram of a membrane-less EBFC utilising immobilised enzymes on anode and cathode and using glucose and oxygen as fuel and oxidant respectively. The fuel is oxidized at the anode and the electrons are driven through an external circuit to the cathode, where they combine with an oxidant which is usually

oxygen (Ivanov *et al.*, 2010). The chosen electrode material should be conductive and inert within the potential range of the cell, the most commonly used ones being carbon and its allotropes or gold (Zhang *et al.*, 2004b; Wang *et al.*, 2009a).

EBFCs can be classified into two types based on their functions (Hao Yu and Scott, 2010). If the enzyme takes part in the production of the fuel substrate for the fuel cell *via* bio-reaction process, it is called product type (Hao Yu and Scott, 2010). Hydrogen production from glucose for traditional hydrogen-oxygen fuel cell can be an example of this type of EBFCs (Woodward *et al.*, 1996; Mertens and Liese, 2004). If the enzyme takes part directly in the bio-reaction for energy production, it is called direct type (Hao Yu and Scott, 2010). These types of EBFCs are the most popular fuel cells in recent research studies in which the performance of the fuel cell mainly depends on the enzyme (Hao Yu and Scott, 2010).

Enzymes are known as excellent catalysts and highly efficient electro-catalysts for biological reactions (Hao Yu and Scott, 2010). The properties of enzymes such as activity under physiological temperature and pH, high turnover numbers and utilisation of more complex fuels can be considered as unique when compared to the conventional low temperature oxidation-reduction catalysts (Calabrese Barton *et al.*, 2004; Ivanov *et al.*, 2010). EBFCs are not also dependent on any nutrient or biomass acclimation and can be controlled more easily (Calabrese Barton *et al.*, 2004). These properties allow this technology to find applications in the area of implanted devices as a source of electricity e.g. in human or animal tissues or larger cells implanted in blood vessels (Calabrese Barton *et al.*, 2004). The highly selective nature of the enzymes is perhaps their most significant attribute since it allows the development of membrane-less enzymatic biofuel cells (Calabrese Barton *et al.*, 2004). This simplifies the design and allows for miniaturization of implanted devices (Calabrese Barton *et al.*, 2004).

Enzymes, as catalysts in fuel cells, can perform better than conventional catalysts in many aspects such as reaction rates, specificity, miniaturization and low over-potentials (Leech *et al.*, 2012). However, there are still important problems that need to be solved such as: long term stability of the enzyme electrodes, efficient electron transfer between enzyme and electrode surfaces and improved enzyme bio-catalytic activity with enhanced power output (Hao Yu and Scott, 2010).

Figure 1.2 demonstrates the potential of the biofuel cells to reach required power output ranges. The credibility gap needs to be overcome for EBFCs to become commercially viable (Bullen *et al.*, 2006). Some major advancements have been achieved during the last three decades in the field focusing on the potential problems and their solutions (Bullen *et al.*, 2006).

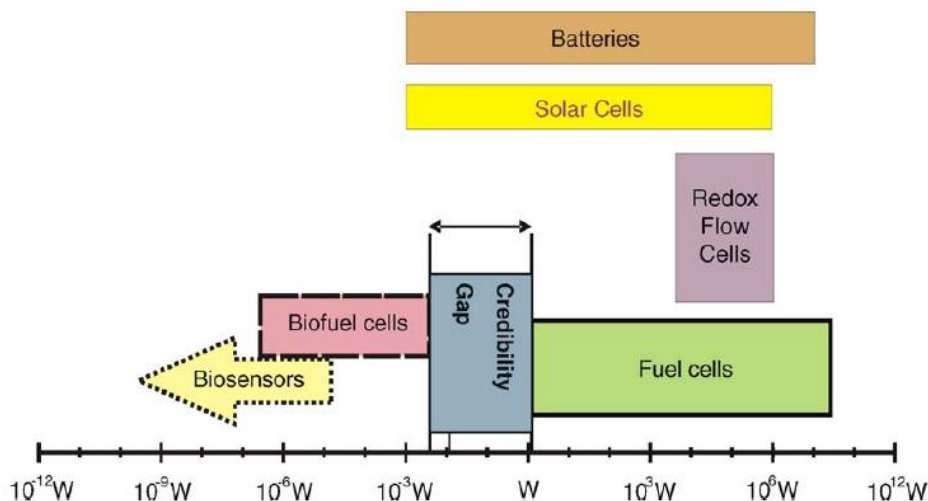


Figure 1. 2. Illustrating the scale of credibility gap for biofuel cells and biosensors in terms of approximate power output ranges (Bullen *et al.*, 2006).

These advancements can be listed as increased open circuit potential (OCP) from 0.175 V to almost 1 V and current densities from the nA scale to mA cm^{-2} (Rasmussen *et al.*, 2016). However, further improvements are necessary especially in fuel cell performance and stability for implantation of micro electronic systems to be viable.

1.1.2. Aims and Objectives

Aim

The aim of this project is to develop an enzymatic biofuel cell that can produce power from glucose using the pyronase-2-oxidase enzyme (P2O). The investigation will focus on the electrochemical behaviour of P2O in solution and immobilization on to the electrode as well as comparison with commercially available glucose oxidase (GOx).

Objectives

It can be possible to fabricate an enzymatic anode and cathode using promising enzymes such as P2O and bilirubin oxidase (BOD) for biofuel cell applications. An enzymatic biofuel cell

operating under human physiological conditions can be developed with high power output and good stability. Such a biological fuel cell could be used as an implantable power device or to power micro electronic devices. The investigation of these promising enzymes in terms of oxygen utilisation, performance and stability, the immobilization technique used and choice of materials for electrode fabrication will be given attention to construct a successful enzymatic biofuel cell.

In this scope, the following objectives should be achieved in this study:

- a) To characterize P2O and its oxygen resistant mutants in solution using electrochemical techniques in terms of catalytic activity, glucose affinity, effect of oxygen on enzyme performance and stability as well as comparison with the performance of GOx.
- b) To develop an immobilization technique achieving successful electron transfer from the biological species to the electrode for glucose oxidation.
- c) To test the enzyme immobilised electrodes developed at step (b) using the same approach from step (a)
- d) To construct an enzymatic biofuel cell producing a stable output using glucose and oxygen.

The solution experiments with P2O and its mutants is discussed in Chapter 2, followed by the work on enzyme immobilization for developing enzymatic biofuel cell anodes in Chapter 3. Chapter 3 also shows the electron transfer behaviour of the mediator, ferrocene (Fc), first in solution and then immobilised on electrode surface with the enzyme, in the presence of carbon nanotubes (CNTs) and nafion[®] polymer. Chapter 4 covers the performance analysis of the enzymatic biofuel cells constructed as well as comparisons between enzymes. The overall conclusions and recommendations of future work are given in Chapter 5. The appendix contains the supplementary information that supports the work in the body of the thesis that is referred to whenever necessary.

1.2.Literature Review

Biofuel cell research has been very popular in the literature for decades. Several established groups often have frequently reviewed the field, some of the most important include Minteer and co-workers (Cooney *et al.*, 2008), focusing on three-dimensional (3-D) structures and characterization techniques, Kannan *et al.* (Kannan *et al.*, 2009) and Armstrong (Cracknell *et al.*, 2008) focusing on enzymes and their properties, Heller (Heller, 2004) and Willner (Willner

et al., 2009), focusing on their novel studies in the enzymatic biofuel cell (EBFC) field as well as some wide reviews by Barton *et al.* (Calabrese Barton *et al.*, 2004) and Bullen *et al.* (Bullen *et al.*, 2006).

There have been an increasing number of papers published per year on EBFCs over the past 6 years obtained from the search results using web of knowledge database with the keyword “enzymatic biofuel cell”.

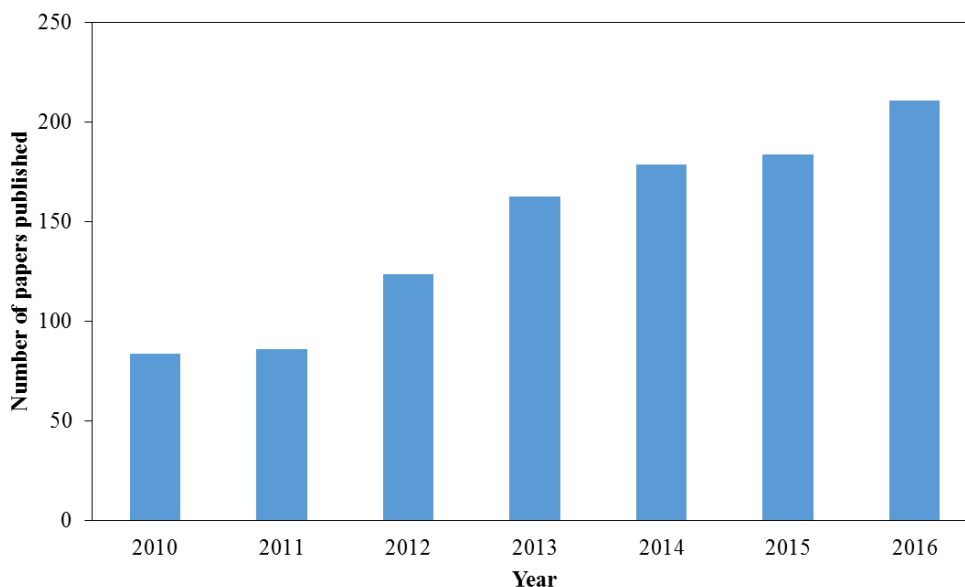


Figure 1. 3. EBFC publications between 2010 and 2012 (Source: Web of Knowledge).

Figure 1.3 shows this trend where an increasing interest in the field of EBFC research over the past 6 years until 2015 where it plateaued and then started to increase in 2016. 1186 papers were found with 146 of them marked as review papers, 991 of them were articles and rest of them were other documents types such as meetings, abstracts *etc*. It is important to note that approximately 50 % of the papers were published during last three years. On the other hand, when refined with the key word, “Glucose Oxidase” there are 330 papers out of 1186 (28 %) and only 11 papers (0.9 %) when refined with the key word “Pyranose Oxidase”. There are 134 (11 %) and 204 (17 %) papers for the key word “Bilirubin Oxidase” and “Laccase” respectively. Only 58 out of 1186 papers (5 %) could be found by refining “implantable” key word. These analysis show that a fuel cell design utilising pyranose oxidase with bilirubin oxidase was used only 3 times during the last 6 years none of which utilised both of them in one fuel configuration but just in related studies (such as using pyranose dehydrogenase).

In this chapter of the thesis, the following aspects were reviewed in the context of this study: Enzymes used in enzymatic biofuel cells, enzymatic electrode assemblies for biofuel cells, enzymatic biofuel cell configurations and performance and finally the electrochemical techniques for the investigation of the enzyme electrodes.

1.2.1. Enzymes Used in Enzymatic Biofuel Cells

Enzymes for Anodic Reaction

Among all the enzymes used in enzymatic biofuel cells, GOx (EC 1.1.3.4) is the most widely used enzyme for glucose oxidation (Ivanov *et al.*, 2010). GOx is a dimeric flavoprotein catalysing the oxidation of β -d-glucose by oxygen (O_2) to d-gluconolactone which is further oxidized to gluconic acid and hydrogen peroxide (H_2O_2) (Figure 1.4) (Hecht *et al.*, 1993a).

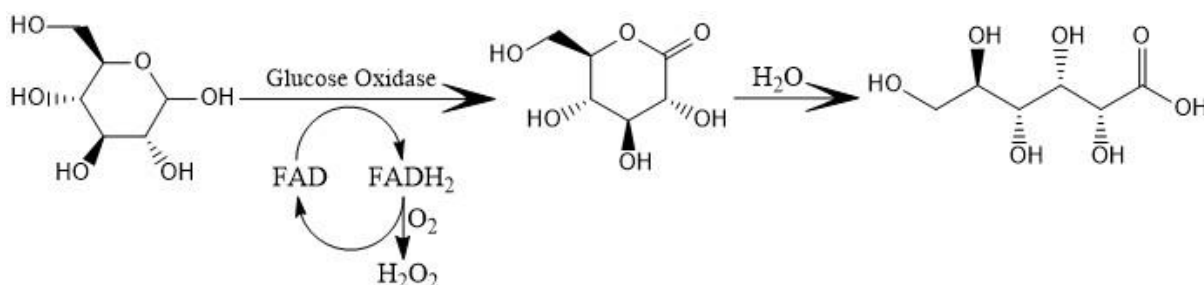


Figure 1. 4. The reaction catalyzed by GOx.

GOx has two identical subunits with a mean total molecular mass of 150 - 180 kDa, an average diameter of 8 nm and isoelectric point of about 4.2 (Wilson and Turner, 1992). Figure 1.5 shows the structure of the GOx enzyme indicating two flavin adenine dinucleotide (FAD) units as cofactors located in each apoenzyme (Yahiro *et al.*, 1964). This co-factor, FAD, is responsible for the catalytic function of GOx, in the glucose oxidation reaction (Ivanov *et al.*, 2010) where it is reduced to FADH₂ at -0.05 V vs standard hydrogen electrode (SHE) (\sim -0.25 V vs silver/silver chloride (Ag/AgCl)) (Degani and Heller, 1988).

GOx has a rigid structure and the FAD centres are located deeper than 8 Å from the surface of the molecule that makes the direct electron transfer to the electrode difficult. (Hecht *et al.*, 1993b). Thus, mediators are necessary to shuttle the electrons between the enzyme and the electrodes. The natural electron acceptor for GOx is O_2 where H_2O_2 is produced as a result of the reaction (Ivanov *et al.*, 2010). This, however, is one of the most important drawbacks of

using GOx in enzymatic biofuel cells as the generation of the H₂O₂ should be avoided due to its highly oxidative nature.

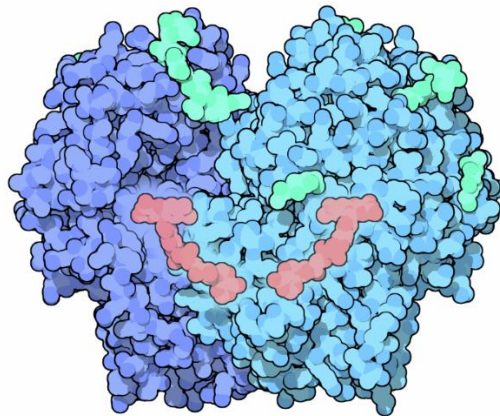


Figure 1. 5. Structure of the GOx enzyme and FAD units (Goodsell, 2006).

In systems where an electron transfer mediator is needed, the natural electron acceptor O₂ would compete with the mediator resulting decreased anodic current density (Ivanov *et al.*, 2010). The optimum pH of GOx for glucose oxidation reaction is 5.5 when O₂ is utilised as electron acceptor. Below pH 2 and above pH 8, the catalytic activity of the enzyme is rapidly lost (Wilson and Turner, 1992).

GOx is a very popular choice of enzyme in the field of glucose biosensors and enzymatic biofuel cells due to its inexpensive, stable and practical use. However, many other enzymes have been recently utilised in biofuel cell applications. For example, glucose dehydrogenase (EC 1.1.1.47, GDH), has a big advantage since its natural electron acceptor is not oxygen; however it needs a soluble co-factor called nicotinamide adenine dinucleotide (NAD) (Ivanov *et al.*, 2010).

Glucose dehydrogenase (Pyrroloquinoline quinone (PQQ)-dependent) GDH (EC 1.1.5.2) (Tsujimura *et al.*, 2002; Wu *et al.*, 2009; Güven *et al.*, 2016) is also another enzyme from dehydrogenase family that has been used in enzymatic biofuel cells for glucose oxidation. Cellobiose dehydrogenase (EC 1.1.99.18, CDH), is another promising enzyme whose natural substrate is cellobiose but it can also oxidize different monosaccharides including glucose (Tasca *et al.*, 2008).

In the recent years, there has been some interest in using P2O enzyme (pyranose:oxygen 2-oxidoreduc-tase, EC 1.1.3.10) instead of GOx especially in the field of biosensors and there are only few studies in the field of enzymatic biofuel cells (mostly preliminary). P2O is a wood

degrading enzyme which can oxidase glucose as well as variety of other sugar substrates by utilising alternative electron acceptors (Leitner *et al.*, 2001). It can oxidize sugars such as 2-deoxy-D-glucose, 2-keto-D-glucose and methyl β -D-glucosides using the Ping Pong Bi Bi mechanism similarly to other oxidoreductases at position C-2 and also at position C-3, (Martin Hallberg *et al.*, 2004; Wongnate *et al.*, 2011). Figure 1.6 shows the structure of one subunit of the P2O enzyme.

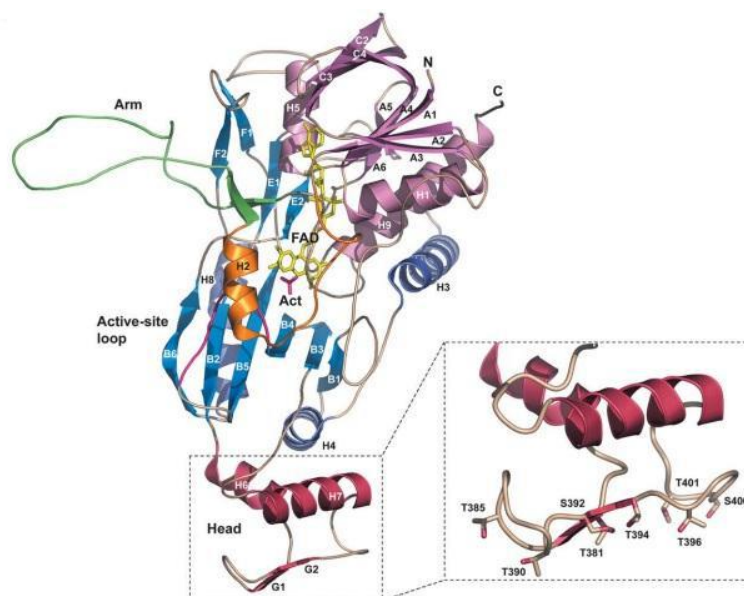


Figure 1. 6. Structure of the P2O subunit from *Trametes multicolor* (Martin Hallberg *et al.*, 2004).

P2O catalyses the same reaction as GOx using the FAD units however with a wider range of substrate selectivity and ability to be used without showing any anomeric selectivity (Spadiut *et al.*, 2010). Although GOx has been very popular in the field of enzymatic biofuel cells, one of its important drawbacks is having a restricted turnover rate for glucose. In aqueous solutions, only 64% of the glucose is present as the β -form and GOx oxidizes glucose only at the C-1 position which is a limiting factor as it is only one anomeric form of the substrate (Zafar *et al.*, 2010).

P2O has a homotetrameric structure with a molecular mass of 270 kDa (overall surface area of $81,616 \text{ \AA}^2$) and an isoelectric point in the range 4.4–4.8 (Kujawa *et al.*, 2006). Each of the four subunits carries one FAD molecule covalently bound to a histadine group, (Kujawa *et al.*, 2006) and one active site (Martin Hallberg *et al.*, 2004). The approximate dimensions of each subunit

molecule are 50 Å x 55 Å x 90 Å which is a peanut shape body consisting of arm and head sections.

The homotetrameric assembly dimensions are approximately 80 Å x 90 Å x 90 Å. The cross-section of the two subunits is shown in Figure 1.7. The active site of the P2O enzyme is located approximately 11 Å to 14 Å below the protein surface (which is slightly more buried than GOx). To be able to access to any of the four active sites, substrate must enter a void (roughly 15,000 Å³ in volume) through the channels and then diffuse to the active site from the void.

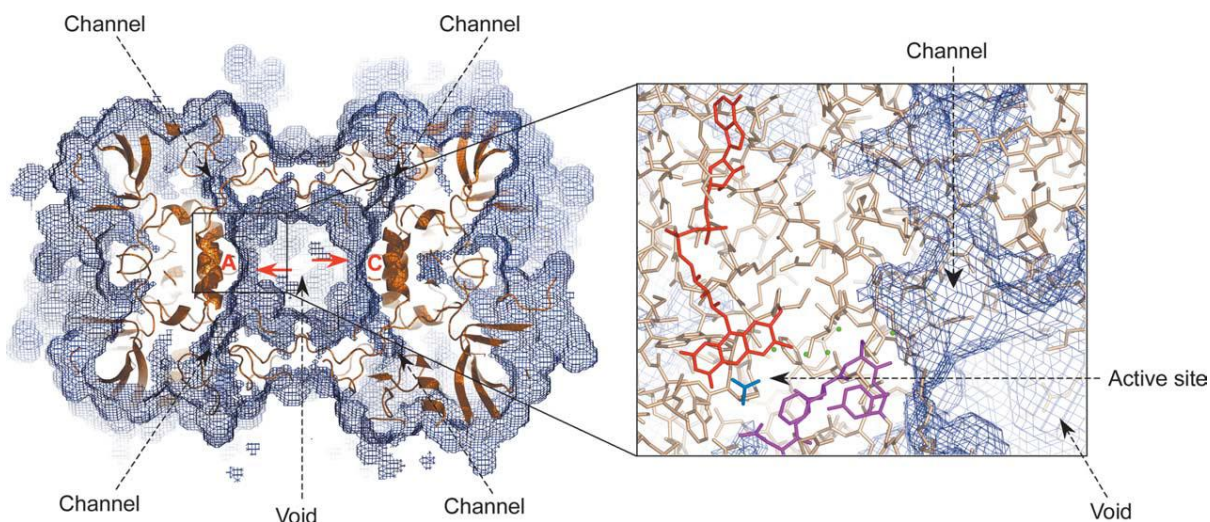


Figure 1. 7. Cross-section view two subunits (marked as A and C) showing the active site and the channels providing water-accessible structure (Martin Hallberg *et al.*, 2004).

The enzymes used in glucose oxidation for biofuel cell applications are summarized alongside their co-factors, half-reactions and natural electron acceptors in Table 1.1. The presented enzymes are the most commonly reported anodic enzymes for enzymatic biofuel cells with the addition of the promising enzyme P2O.

Each of the anodic enzymes has their own specific limitations regarding their structure, ability to oxidize sugars in different positions, ability to perform in different conditions such as pH or in the presence of an electron acceptor. Selecting an enzyme for an enzymatic biofuel cell is still an important challenge since their initial designs, improvements in technology and nanotechnology, have led to the development of a variety of mutant enzymes with enhanced properties which could provide commercially viable alternatives to those currently on the market.

Fuel (Substrate)	Enzyme	Co-Factor	Natural Electron Acceptor
Glucose	Glucose Oxidase (EC 1.1.3.4, GOx)	FAD	O ₂
	Glucose Dehydrogenase (EC 1.1.1.47, GDH)	NAD	NAD
	PQQ-dependent GDH (EC 1.1.5.2)	PQQ	quinone
	Cellobiose Dehydrogenase (EC 1.1.99.18, CDH),	FAD, heme	Not known (Baminger <i>et al.</i> , 2001)
	Pyranose-2-Oxidase (EC 1.1.3.10, P2O)	FAD	O ₂

Table 1. 1. Enzymes used in EBFCs using glucose as fuel (Half-Cell Reaction: glucose → glucono-1,5-lactone + 2H⁺ + 2e⁻).

Enzymes for Cathodic Reaction

Two of the most widely used enzymes for oxygen reduction in the field of EBFCs are laccase (EC 1.10.3.2, Lc) and BOD (EC 1.3.3.5) both of which are multi-copper oxidases. These enzymes can oxidize a range of substrates and retain four metal ion sites classified as types T1, T2 and T3 (Ivanov *et al.*, 2010). Each site has a different functionality where T1 binds the organic substrate and T2/T3 cluster catalyses the four electron reduction of oxygen to water (Shleev *et al.*, 2005; Ramírez *et al.*, 2008). Figure 1.8 shows the structure of Lc (Figure 1.8-A) and BOD (Figure 1.8-B) from *Trametes versicolor* and *Myrothecium verrucaria*, respectively.

Lc shows better activity in acidic conditions typically at pH 5, whereas BOD is better in more neutral to alkaline pH (Ivanov *et al.*, 2010). It was also stated that one of the Lc centres (T2) is inactive at neutral pH and is inhibited by Cl⁻ ions unlike BOD (Mano *et al.*, 2002b). Depending on the fuel cell configuration in which they are to be utilised, the choice of the enzyme could change, however, for implantable devices, BOD is considered to be more appropriate because of its superior qualities such activity in physiological conditions

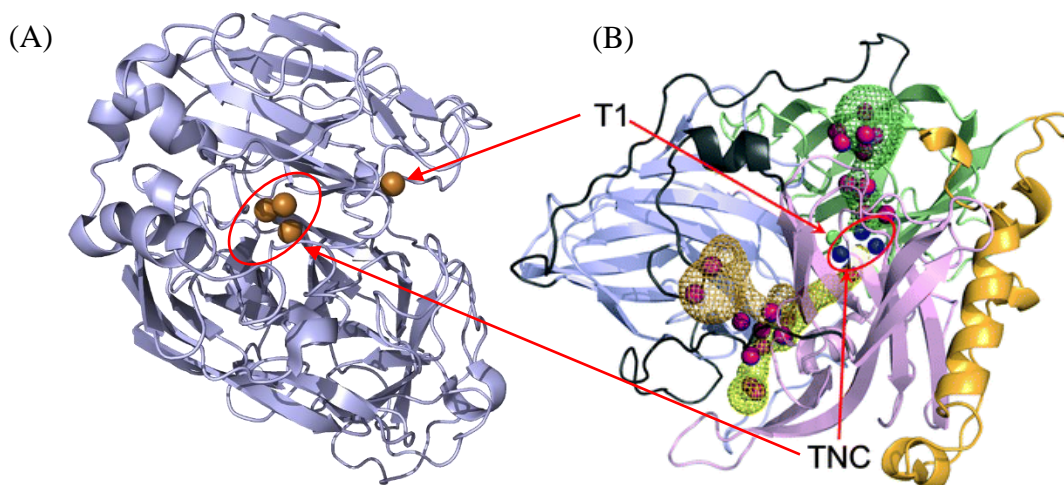


Figure 1. 8. A representation of the X-ray-determined crystal structure of (A) laccase III from *trametes versicolor* (Piontek *et al.*, 2002) and (B) BOD from *myrothecium verrucaria* (Cracknell *et al.*, 2011) (TNC refers to trinuclear cluster (T2 and T3) of the enzyme).

BOD is a monomeric enzyme which has a molar mass around 52 kDa (from *myrothecium verrucaria*) (Mano *et al.*, 2002a). Figure 1.9 shows the proposed DET mechanism *via* different sites of BOD due to its orientation when used with graphite and gold electrodes. The distance between the enzyme surface and T1 site is less than 10 Å at its closest approach (Ramírez *et al.*, 2008). This is short enough for electrons to be transferred from the electrode to the T1 site but enzymes should be oriented accordingly (Ramírez *et al.*, 2008). BOD has several advantages over Lc apart from the pH, such as, being less sensitive to high concentrations of bromide deactivating Lc (Calabrese Barton *et al.*, 2004). This could be an important parameter where blood is used in the EBFC (Kim *et al.*, 2009).

BOD can also retain a high activity in the presence of high concentration of molecular oxygen and it is relatively well stable (Weigel *et al.*, 2007). Importantly for EBFC designs, BOD was reported to have redox potentials between 0.47-0.67 V (*vs* Ag/AgCl) (Kim *et al.*, 2003; Christenson *et al.*, 2006) which would be positive enough to generate sufficient cell voltage when used with anodic enzymes such as P2O or GOx. Lc also shows similar redox potentials around 0.550 - 0.585 V (*vs* Ag/AgCl) (Barrière *et al.*, 2006; Güven *et al.*, 2016).

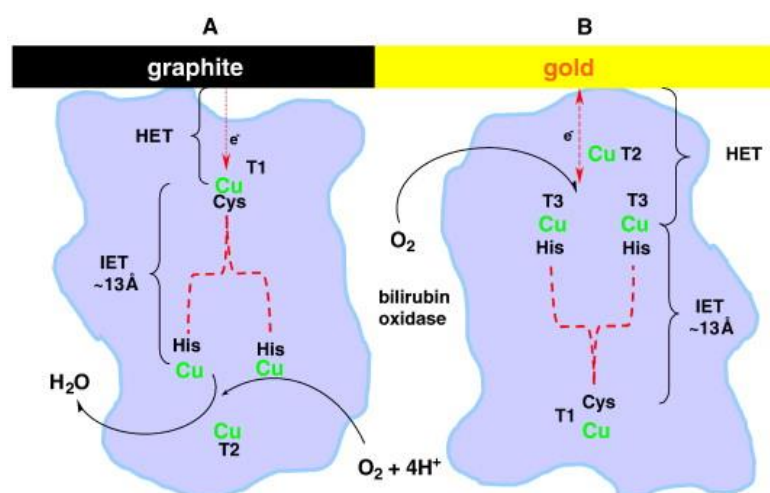


Figure 1. 9. Mechanisms of DET from electrodes to BOD connected (A) *via* the T1 site and (B) *via* the T2/T3 cluster (Ramírez *et al.*, 2008).

There are on the other hand different enzymes that can be used for the oxygen reduction reactions such as cytochrome oxidase (EC 1.9.3.1, COx) (Katz *et al.*, 1999b), and cytochrome c both of which have heme as a catalytic centre. When H_2O_2 is utilised at the cathode, microperoxidase-11 (MP-11) (Willner *et al.*, 1998b) and horseradish peroxidase (EC 1.11.1.7, HRP) (Pizzariello *et al.*, 2002) can also be used.

Outlook on Enzyme Choice for Biofuel Cells

Enzyme selection for both anodic and cathodic reactions is a real challenge to improve EBFCs. The improvement of the biocatalyst is equally as important as choosing one. GOx, despite being very advantageous in theory, has many drawbacks in practice especially in limiting the performance of the fuel cell long term with its natural electron acceptor O_2 as well as substrate selectivity.

Therefore, there has always a search for alternative enzymes or modified forms of GOx to enhance its properties using methods like purification (Gao *et al.*, 2009) or deglycosylation (Courjean *et al.*, 2009). Engineering the enzyme, on the other hand, is another recent approach which can theoretically be fine-tuned for targeted applications. Rational design (Willner *et al.*, 1998b) and directed evolution (Zhu *et al.*, 2006) are the two main approaches used in protein engineering to serve this purpose. GOx was previously used in protein engineering studies (Zhu *et al.*, 2006).

Recently, however, different mutants of P2O enzyme have been developed using semi-rational protein design (Pitsawong *et al.*, 2010). These mutants are reported not to utilise as much oxygen as their wild type form (Pitsawong *et al.*, 2010), but still retain the advantages of the wild type enzyme. This makes these mutant enzymes a promising candidate for glucose oxidation in enzymatic fuel cells especially for long term applications.

The four-electron electrochemical reduction of O₂ at pH 7 has been the basis of the enzymatic biofuel cells. The blue copper oxidases with copper centres are closer to the surface of the enzymes such as BOD, can provide direct electron transfer (DET) from the electrode, and are very promising for their use in enzymatic fuel cell applications. Utilising a stable glucose oxidizing enzyme that does not require oxygen as an electron acceptor (no electron competition with cathode) and has a wide sugar substrate selectivity, combined with a suitable cathodic enzyme (for oxygen reduction) presents a good design for future EBFCs. As a result, a P2O and BOD combination in a membrane-less EBFC (as anodic and cathodic enzymes respectively) might perform well under human physiological conditions.

1.2.2. Enzymatic Electrode Assemblies for Biofuel Cells

Electron Transfer

Enzymes catalysing oxidation-reduction reactions (redox reactions) are often called redox enzymes. These enzymes consist of two components: apoenzyme (the protein component) and cofactor(s) (nonproteinaceous) (Leech *et al.*, 2012). The cofactor is responsible for the electron transfer between the enzyme and its substrate (Leech *et al.*, 2012). Electron transfer in the enzymatic biofuel cells can take place in two different directions. Firstly, the transfer of the generated electrons from the enzymes (oxidative reactions) to the electrodes (at the anode) and secondly the electrons transferred from the electrodes to the enzyme (reductive reaction). These electrons can be transferred *via* different mechanisms which either includes a mediator or direct enzyme-electrode communication (Bullen *et al.*, 2006).

One of the most important issues in the development of enzymatic electrodes for biofuel cell applications is the successful and efficient electron transfer between the enzyme and electrode. This type of electron transfer can occur either directly between enzyme and electrode (one way or another), and is called DET, or in the presence of a mediator shuttling the electrons between enzyme and electrode, which is called mediated electron transfer (MET) (Bullen *et al.*, 2006; Cooney *et al.*, 2008; Ivanov *et al.*, 2010).

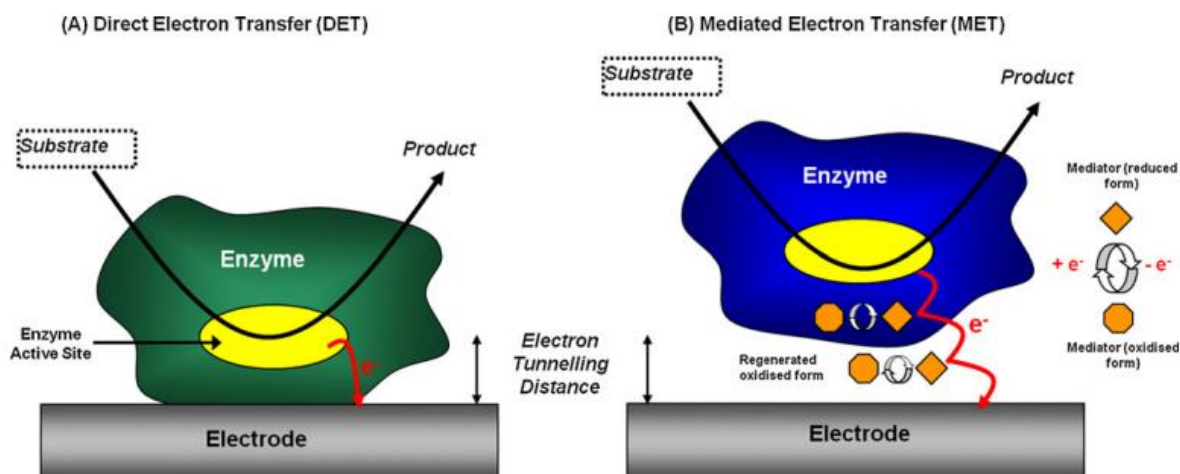


Figure 1. 10. Schematics of (A) direct and (B) mediated electron transfer-based enzyme electrodes (Alkire *et al.*, 2013).

Figure 1.10 shows the schematic of a DET and MET based enzyme electrodes. The common structure of the enzymes which can exhibit DET is that their active centres are closer to the protein surface, whereas the enzymes that have deep buried active centres in the protein structure need a redox mediator. However, only less than 100 out of 1000 redox enzymes in the literature are known to achieve DET (Ramanavicius and Ramanaviciene, 2009).

Although DET is considered to be very convenient for the simplicity of the fabrication of the enzyme electrodes, there are still several challenges that need to be overcome to achieve significant rates of DET with high current densities. For instance, it was reported that for distances beyond 2 nm between electron donor and acceptor, the rate of electron transfer could be negligible (Alkire *et al.*, 2013).

Redox enzymes can be classified as three types based on the electron transfer mechanism (can also be defined as the location of enzyme active centres) (Bullen *et al.*, 2006; Hao Yu and Scott, 2010) as shown in Figure 1.11. In the first group, enzymes have diffusive active centres (Figure 1.11. (A)). These enzymes often have weakly bounded active centres such as (NADH/NAD⁺) or nicotinamide adenine dinucleotide phosphate (NADPH/NADP⁺) (Bullen *et al.*, 2006; Hao Yu and Scott, 2010). The weakly binding redox centres act as an electron transfer mediator by diffusing away from the enzyme (Bullen *et al.*, 2006). For example, GDH and alcohol dehydrogenase (ADH) can be classified within this group.

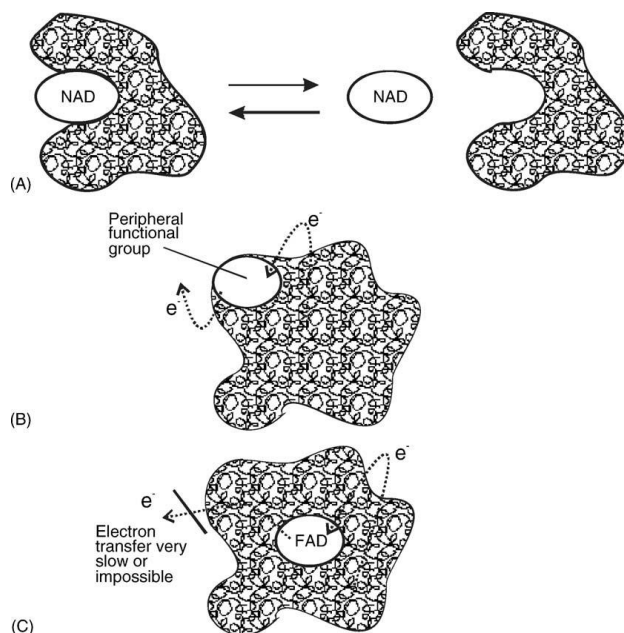


Figure 1. 11. The different locations of enzyme active centres, (A) Enzyme active centre is NAD(H) or NADP(H), (B) the active centre is diffusive and (C) the active centre is located deep buried inside the enzyme (Bullen *et al.*, 2006).

The second group are the enzymes that have active centres at or close to the protein surface (Figure 1.11. (B)). Many of the multi copper enzymes such as Lc and BOD as well as peroxidases such as HPR and cytochrome c belong in this group. The first two groups are able to maintain DET between the enzyme active centres and the electrode surface. Among the most widely used enzymes, it is still a matter of debate on which mechanism GOx can maintain for glucose oxidation. There are several reports presenting DET for GOx (Liu and Dong, 2007a; Wang *et al.*, 2009a; Zhao *et al.*, 2009) while others claim due to its structure only MET is possible (Mano *et al.*, 2003b). For the studies claiming to achieve DET with GOx, carbon nanomaterials are generally incorporated in the immobilization methods as they are reported to communicate with the enzyme active site (Liu and Dong, 2007a; Wang *et al.*, 2009a; Zhao *et al.*, 2009).

The evidence of the DET is generally proved by the appearance of an FAD/FADH₂ redox peak, however, most of the studies failed to show the oxidation currents in the presence of glucose (Kim *et al.*, 2009; du Toit *et al.*, 2016). There also could be possible protein denaturation induced by CNTs according to reported reviews showing that the presence of free or exposed FAD close to the electrode surface should be considered (Kannan *et al.*, 2009).

The orientation of the enzymes is very important to achieve DET (Hao Yu and Scott, 2010), it should be noted that both the orientation and the diffusional access for the substrate should be considered when fabricating this type of enzyme electrodes. Finally, even in cases where the electrode can approach close enough to the enzyme active site to achieve DET, this still might not be guaranteed that the bio-electro-catalytic current will be generated as the electrode can block the access to the active site of the enzyme (Leech *et al.*, 2012).

The last group is the enzymes which has an active centre buried deep in the protein structure (Figure 1.11. (C)). In this case, the electrochemical connection between enzyme and electrode can only be established in the presence of an electron-transfer mediator (aka redox mediator). Glucose oxidase by far the most studied enzyme, is the best example for this group with a deep buried FAD group. However as mentioned above, it should be noted that there are studies showing DET can be possible with GOx.

Enzyme Immobilization Technology

Biological species are very sensitive to restrictive environmental conditions and their fluctuations because of their nature (Yang *et al.*, 2012). In practice, the lifetime of an isolated biological species such as enzymes is limited. However, immobilization of enzymes supplies an efficient and sustainable solution to overcome this problem offering high stability and extended lifetime and activity (Yang *et al.*, 2012).

Such immobilization matrixes can offer a biological environment which can preserve the enzymes from harmful environmental conditions such as shear forces, pH, temperature fluctuations, organic solvents and toxins (Shuler *et al.*, 1986; Yang *et al.*, 2012). Other benefits such as increased cell-line stability and easy regulation of culture environment are very important aspects for the design of enzymatic biofuel cells (Dörnenburg and Knorr, 1995).

Figure 1.12 summarises the immobilization technology, classified by three categories: the immobilization methods (*i.e.* adsorption, covalent binding and entrapment *etc.*), the immobilization structure (*i.e.* zero/one/two/three dimensional nanostructures *etc.*) and the immobilization material (*i.e.* carbon, sol-gel *etc.*).

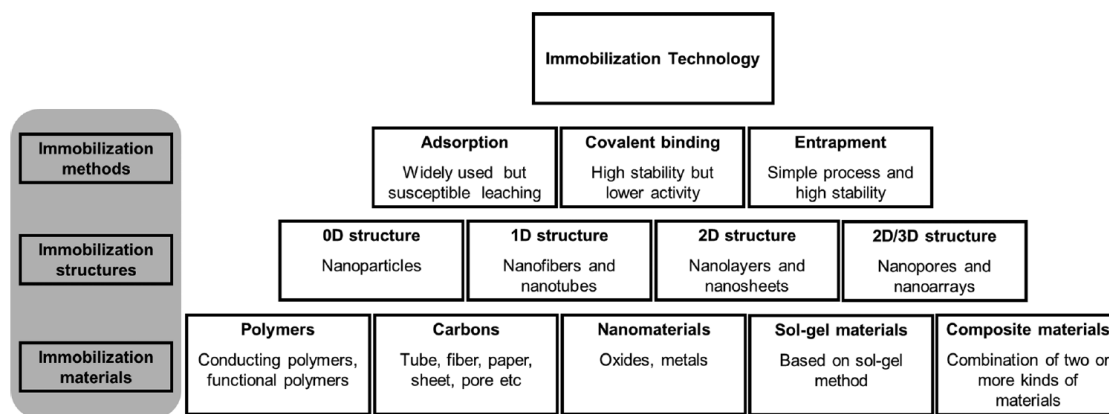


Figure 1. 12. Immobilization technology in biofuel cells (Yang *et al.*, 2012).

Immobilization Methods

Several different immobilization methods have been studied over the years which can achieve high enzyme densities on electrode surfaces providing enhanced performance and improved electron transfer kinetics (Shuler *et al.*, 1986; Cosnier, 2000; Nguyen *et al.*, 2004; Cooney *et al.*, 2008; Costa *et al.*, 2011). The most widely used methods can be summarized as adsorption, entrapment and covalent binding.

Adsorption - The most straight forward and easy immobilization method is the adsorption of the enzymes on electrode surface. As well as being simple, it is a mild and reversible process, which can be applied to different structures such as sponges (Ahmadi *et al.*, 2006), fibres (Facchini and DiCosmo, 1990), sheets (Danilov and Ekelund, 2001) and foams (Yin *et al.*, 2006). The efficiency of adoption depends on the physicochemical condition such as pH or ionic strength as well as the pore size or structure of the support (Yang *et al.*, 2012). However, the leaching of the adsorbed enzymes to the solution is the main challenge for this type of immobilization. Recently layer-by-layer (LBL) assemblies based on electrostatic interaction are a point of interest especially in the area of constructing enzyme electrodes.

Strong polycations such as poly(dimethyldiallylammonium chloride) (PDDA) were shown to be well adsorbed on carbon or gold electrodes (Alexeyeva and Tammeveski, 2008; Zhang *et al.*, 2008). Figure 1.13 shows a schematic diagram of LBL fabrication of an enzyme electrode for electrochemical detection of fatty acids.

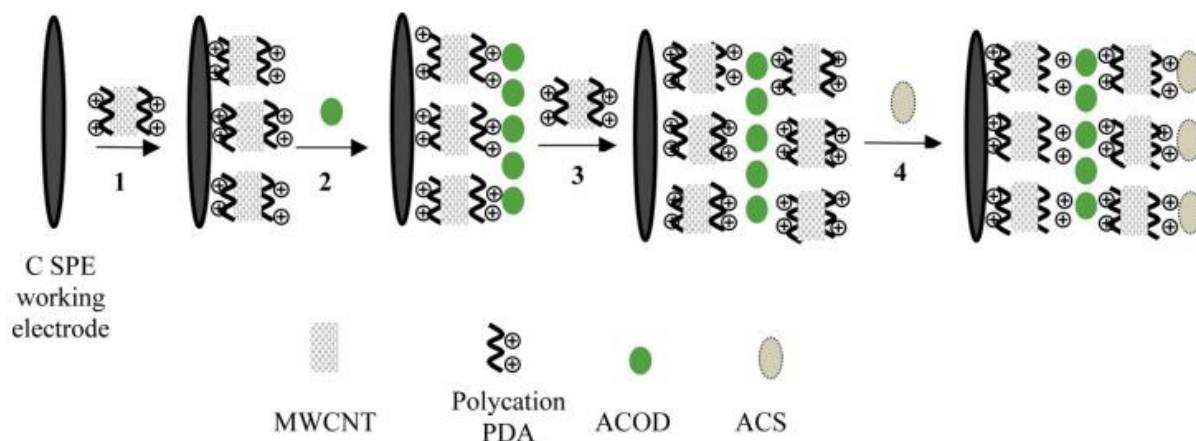


Figure 1. 13. Schematic diagram of LBL fabrication of an enzyme electrode for electrochemical detection of fatty acids (ACOD: Acyl-CoA Oxidase, ACS: Acyl-CoA Synthetase, C SPE: Carbon screen printed electrode, MWCNT: Multi-walled carbon nanotubes) (Kang *et al.*, 2014).

Entrapment - Entrapment of enzymes is often used in the field of enzymatic electrode design especially using polymeric materials, as it is an easy process with good mechanical strength and stability (Yang *et al.*, 2012). It was reported that such systems can solve the leaching problem up to a point but cannot eliminate it for good (Cooney *et al.*, 2008).

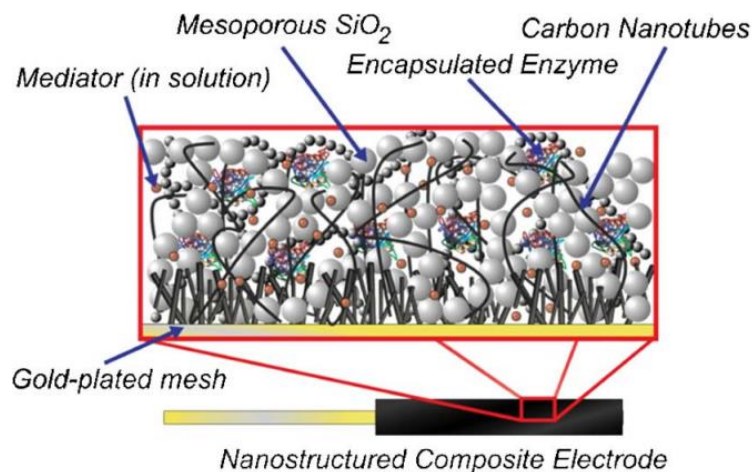


Figure 1. 14. Schematic of immobilised enzyme using nanostructured silica sol-gel entrapment method (Lim *et al.*, 2007).

One example of this type of immobilization method is shown in Figure 1.14 where the enzyme was encapsulated in sol-gel silica matrices and carbon nanotubes were incorporated within the

matrix to provide enhanced electronic conduction (Lim *et al.*, 2007). It was reported that uniform carbon nanotube inside sol-gel film was achieved using polyethylene glycol and the enzyme maintained its activity on the developed enzymatic electrode.

Covalent Binding - Covalent binding is similar to adsorption as a way of forming monolayer coverage of enzyme on the electrode surface, through chemical bonds are formed between the enzyme and the electrode (Cooney *et al.*, 2008). In this approach, stability and leaching of the enzymes can be improved, yet enzymes show lower activity than the native form due to the chemical bonds formed (Cooney *et al.*, 2008; Yang *et al.*, 2012).

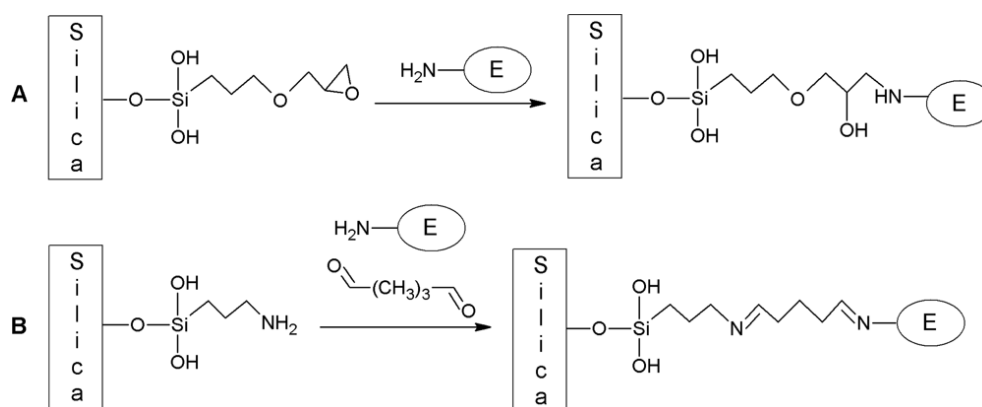


Figure 1. 15. Covalent enzyme immobilization with (A) epoxy-modified silica (B) aminopropyl-modified silica (Jung *et al.*, 2010).

The functional groups involved in covalent binding are amino, carboxyl, alcohol, thiol, and phenolic functions (Iqbal *et al.*, 2013). These groups can be involved in different reactions include diazotization followed by coupling, amide bond formation, and Schiff's base formation (Girelli and Mattei, 2005). An example of covalent enzyme immobilization using epoxy-modified silica or aminopropyl-modified silica resulting different reactions with enzyme is shown in Figure 1.15 (Jung *et al.*, 2010).

Cross-linking, often classified in covalent binding method, can achieve successful immobilization of enzymes on electrode surfaces. This can be achieved using either covalent bonding or ionic bonding. The most widely used cross-linking agents include carboxyl-reactive chemical groups that used for crosslinking carboxylic acids to primary amines. 1-ethyl-3-(3-dimethylaminopropyl) carbodiimide hydrochloride (EDC) is an example for this type crosslinker where it often used with N-hydroxysulfosuccinimide (NHS) to improve efficiency or create dry-stable (amine-reactive) intermediates.

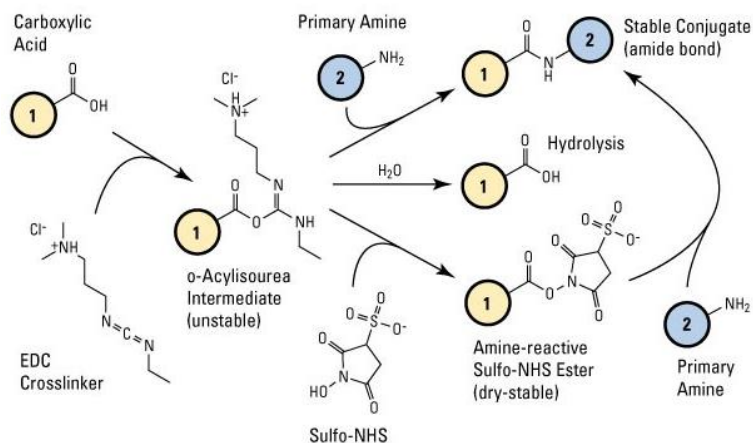


Figure 1. 16. EDC-NHS crosslinking reaction scheme (Scientific, 2016).

Figure 1.16 shows the reaction scheme for the EDC-NSH crosslinking reaction with amine. NHS is important to use in this type of crosslinking reaction as it forms NHS ester (dry stable) which is more stable than o-acylisourea formed by EDC, therefore more efficient conjugation can be achieved. There are several studies using EDC-NHS crosslinking methodology especially incorporating carbon nanotubes with pyrenyl activated sites as it provides carboxylic acid groups for enzyme linkage (Krishnan and Armstrong, 2012). Figure 1.17 is example of EDC-NHS crosslinking or an anodic and cathodic enzyme on Pyrolytic graphite ‘edge’ electrodes.

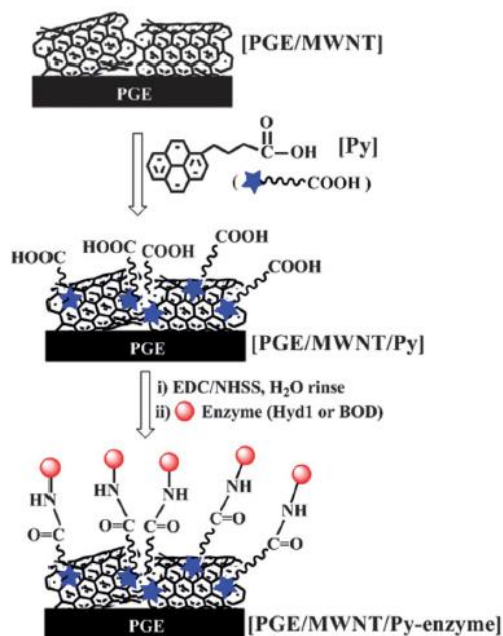


Figure 1. 17. Schematic for crosslinking enzymes on pyrene activated carbon nanotubes using EDC-NHS couple (Krishnan and Armstrong, 2012).

Enzyme Electrodes Based on Diffusional and Immobilised Mediator

Mediator based electrodes have been widely studied in literature due to the low number of enzymes which can achieve DET and their limitations (Ivanov *et al.*, 2010). The mediator used for electron transfer in the field of EBFCs can be divided into two categories: free diffusive and immobilised mediators (Ivanov *et al.*, 2010).

Table 1.2 presents a list of mediators for commonly used enzymes for glucose oxidation and their redox potentials. Mediators are mostly specific to the enzyme and their redox potentials depend on conditions such as pH or whether they are soluble or immobilised. EBFCs using diffusional mediators are limited in use because of their impracticality for most of the foreseen applications such as implantable healthcare devices.

Although some of the mediators have been reported as non-toxic to humans such as Ferrocene (Fc) (Stepnicka, 2008), there are also few others which are toxic such as osmium (Os) (Hao Yu and Scott, 2010). Therefore, diffusional mediators, such as ferrocene mono carboxylic acid (FcCOOH) are generally employed alongside novel immobilization methods in the literature. For example, CNTs-Chitosan (Liu *et al.*, 2005) or ionic liquids (IL) (Liu and Dong, 2007b) suspension systems were used with FcCOOH as mediator with GOx entrapped in the polymer matrix. FcCOOH was also used in different studies such as CNTs mixtures of GOx using different immobilization techniques (Yan *et al.*, 2007a; Tan *et al.*, 2009).

Different mediators such as benzoquinone and N,N,N',N'-tetramethyl-p-phenylenediamine (TMPD) have been used in similar approaches with GOx covalently attached to the electrode using different coupling techniques (Zhang *et al.*, 2006; Kuwahara *et al.*, 2007). Diffusional mediators were also used in microfluidic designs as both enzyme and mediator solution mixtures can be used as a separate phase without mixing into other phases due to very slow flow rates (Bedekar *et al.*, 2007).

Several reports have been published for different methods of immobilizing enzymes with mediators in literature (Gao *et al.*, 2007; Togo *et al.*, 2007; Deng *et al.*, 2008; Nazaruk *et al.*, 2008; Zhou *et al.*, 2009). Most of the research focused on using 3-D matrices like polymers, lipids and CNTs or combination of these to incorporate mediator and enzyme in a practical way such as entrapment (Ivanov *et al.*, 2010).

Mediator		Redox Potential / V (vs Ag/AgCl)	pH	Reference
Ferrocene carboxylic acid		~-0.34	7	(Yan <i>et al.</i> , 2007a)
p-benzoquinone		~-0.06	7	(Kuwahara <i>et al.</i> , 2007)
Phenazine methosufate		~-0.12	6	(Bedekar <i>et al.</i> , 2007)
Pyrroloquinoline quinone		~ (-0.09)	7	(Willner <i>et al.</i> , 1998b)
8-hydroxyquinoline-5-sulfonic acid		~-0.11	5	(Brunel <i>et al.</i> , 2007)
Tetrathiafulvalene		~-0.22	7	(Nazaruk <i>et al.</i> , 2008)
Poly(methylene blue)		-0.10	6	(Yan <i>et al.</i> , 2006)
Poly(brilliant cresyl blue)		-0.11	7	(Gao <i>et al.</i> , 2007)
Methylene green*		-0.20/-0.05	6	(Li <i>et al.</i> , 2008)
Meldola blue		-	-	(Zhou <i>et al.</i> , 2009)
Nile blue		-0.35	7	(Yan <i>et al.</i> , 2007b)
Thionine		-	-	(Deng <i>et al.</i> , 2008)
Os polymer		-0.19	5	(Mano <i>et al.</i> , 2003b)
		-0.19	7	(Mano <i>et al.</i> , 2002b)
		0.095	5	(Chen <i>et al.</i> , 2001b)
		-0.16	7	(Kim <i>et al.</i> , 2003)
		-0.11	5	(Barrière <i>et al.</i> , 2006)
poly(vinylferrocene)		0.30	7	(Tamaki and Yamaguchi, 2006)
2-methyl-1,4-napthoquinone (vitamin K3)	on PLL**	-0.27	7	(Togo <i>et al.</i> , 2007)
	on PAAm***	-0.25	7	(Sato <i>et al.</i> , 2005)

Table 1. 2. Typical mediators used in enzymatic glucose oxidation. (V vs Ag/AgCl = V vs SHE - 0.197; V vs SCE = V vs. SHE - 0.24.) *methylene green exhibits two redox pairs, ** poly-L-lysine, *** polyallylamine.

Polypyrrole electropolymerization for enzyme entrapment for both anodic and cathodic enzyme electrodes, as well as using poly(ethylene glycol) diglycidyl ether (PEGDGE) for subsequent cross-linking of the proteins, has been used to immobilize different mediators such as 8-hydroxyquinoline-5-sulfonic acid (HQS) and 2, 2'-azino-bis (3-ethylbenzthiazoline-6-sulfonic acid) (ABTS) (Brunel *et al.*, 2007; Merle *et al.*, 2009). However, in many cases the electrode stability has been a real concern due to mediator leaching in this type of entrapment approach.

One of the most widely studied immobilised mediator has been Os polymer based redox hydrogels to overcome this problem. Figure 1.18 shows the structure of the Os polymer and the electron conduction takes places in the redox hydrogel. The main advantage of using Os polymers is the wide redox potential ranges for different redox reactions, fast electron transfer rate and good chemical stability (Hao Yu and Scott, 2010). Since one of the first reports of an Os polymer system by the Heller group in 1991 (Gregg and Heller, 1991) based on electrostatic interactions (hydrogel being polycationic and enzymes being polyanionic), various polymer backbones have been developed and used in the field of biosensors and biofuel cells (Barton *et al.*, 2001; Kang *et al.*, 2006).

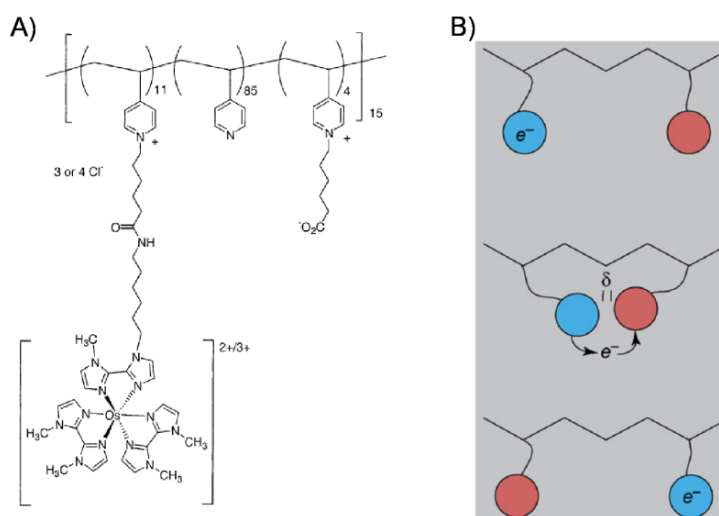


Figure 1. 18. (A) The structure of anodic Os polymer with a 13-atom flexible spacer between the polymer backbone and the Os complex (B) Schematics of electron conduction in Os redox hydrogels (Mano *et al.*, 2002b; Heller, 2006).

However, biocompatibility is the main problem for long term applications where Os polymer is used. Since Os compounds are toxic, possible leaching problems raise much concern in using this redox hydrogels especially in implantable systems (Hao Yu and Scott, 2010). In addition

to Os polymers, which can be used for both anode and cathode enzymatic electrode preparation there have been specific mediators reported for oxygen reduction systems. The most notable example of this mediator type is ABTS that was utilised for both Lc (Palmore and Kim, 1999) and BOD (Habrioux *et al.*, 2009). The redox potentials reported for ABTS is around 0.49 V *versus* Ag/AgCl (0.69 V *vs* SHE) at pH 7 which is closer to the redox potentials of multi copper oxidases (Nazaruk *et al.*, 2008). However, as multi copper oxidases can exhibit DET efficiently, recent research focuses on using these enzymes without any mediator.

Enzyme Electrodes with Ferrocene Polymer Systems

Fc and its derivatives have been widely used as mediators for enzymatic bio-anode fabrication for decades (Li *et al.*, 1997; Miao *et al.*, 2001; Razumien *et al.*, 2003; Kase and Muguruma, 2004). In one of the earliest reports by Cass, they demonstrated that the Fc and its derivatives are able to accept electrons from GOx enzyme and shuttle the electrons to the electrode as confirmed by voltammograms (Cass *et al.*, 1984). The structure of Fc and its widely used derivative Ferrocene carboxylic acid (FcCOOH) are shown in Figure 1.19.

Fc is known to be insoluble in water, on the other hand, its most widely used derivative FcCOOH is soluble due to its $-\text{COOH}$ group attached to the Fc molecule (O'Gorman, 1998). This is an important aspect when the mediator is required in aqueous media, however recent EBFC designs require immobilised systems predominantly due to their suitability in implant applications.

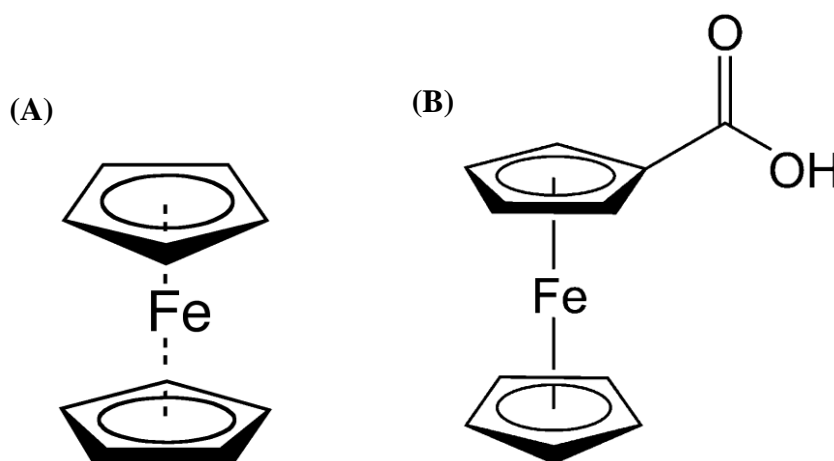


Figure 1. 19. Structure of (A) Ferrocene and (B) FcCOOH.

Fc based mediators are rapid oxidants (Cass *et al.*, 1984), stable in oxidized or reduced forms (Harper and Anderson, 2010), easy to derivatize (Harper and Anderson, 2010), even reported as harmless for human body up to certain levels (Stepnicka, 2008) and its redox potential is independent of pH (Katz *et al.*, 1999a). However, the rate of the reaction between GOx and Fc is lower than the reaction between GOx and O₂. The presence of O₂ would result in decreased catalytic current as it will accept the electrons faster than Fc to form H₂O₂ excessively, therefore it either would decrease the catalytic current related to the reaction with Fc or the system will be affected by the oxidative nature of H₂O₂ (Cass *et al.*, 1984).

Different methods have been applied to immobilize the Fc and/or its derivatives to obtain a stable fast electron transfer enzymatic electrodes. Early methods generally include the entrapment of Fc into polymer such as polyacrylamide gels (Lange and Chambers, 1985) or ferrocene/siloxane polymer (Gorton *et al.*, 1990). Entrapment within the polymer aimed at preventing the enzyme and mediator diffusing away from the electrode resulting in stable electrodes. Although these methods appear to work successfully, the long term leaching of both enzyme and mediator is inevitable (Brooks *et al.*, 1988).

The encapsulating method has been used many times using conducting polymers such as polypyrrole (Fiorito and Torresi, 2001; Vidal *et al.*, 2002), polyphenols (Nakabayashi *et al.*, 1998), cellulose acetate membranes (Tkáč *et al.*, 2002). Although promising results have been obtained the fabricated electrodes suffer from several problems such as low conductivity of the films formed and some interferences due to electro polymerization processes.

Cross-linking of glutaraldehyde on top of a sandwich conformation involving chitosan, Fc and GOx has been developed and it was stated that the bio electrode maintained 65% of its activity after 30 days of storage in buffer solution (Miao *et al.*, 2001). However, glutaraldehyde is known as a strong sterilant, toxin and strong irritant which makes its use suspicious in enzymatic electrodes especially in terms of biocompatibility.

Sol-gel materials (Yang *et al.*, 2003) and hydrogels (Bu *et al.*, 1998) were also other materials studied to utilise Fc and its derivatives. Physical entrapment of sol-gel materials with the enzyme and Fc has issues with leaching of materials used in electrode fabrication. On the other hand even when covalently bonded, the chemical binding of enzyme to electrode tend to decrease enzyme stability due to affecting its 3-D structure or limiting the ability of the internal movements of the enzyme to catalyze the reactions (Cooney *et al.*, 2008). Poly(ethylenimine)

(PEI), is one of the most promising polymer material used in conjunction with carbon nanomaterials cross-linked to Fc for enzymatic bioanode fabrication. Several number of good quality reports have been published incorporating PEI with single-walled CNTs (SWCNTs) (Tran *et al.*, 2011) or multi-walled CNTs (MWCNTs) (Arribas *et al.*, 2007; Rubianes and Rivas, 2007; Laschi *et al.*, 2008; Yan *et al.*, 2008). Figure 1.20 shows the incorporation of SWCNTs with PEI polymer to construct enzymatic electrodes by immobilizing GOx with Fc used as mediator.

However most of these reports relate to the design an amperometric glucose detection. On the other hand, in the field of enzymatic biofuel cells, PEI was also used by incorporating SWNTs with redox polymer–enzyme hydrogels in which Fc was attached to linear poly(ethylenimine) (Meredith *et al.*, 2011). Although many different approaches have been investigated to utilise Fc with different anodic enzymes in fabricating enzyme electrodes for biofuel cell anodes, enzyme leaching from the polymer films still is a concern especially in continuous monitoring systems or biofuel cells requiring long term operation.

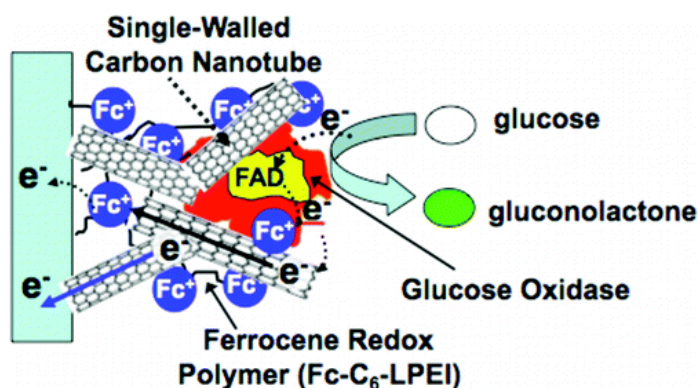


Figure 1. 20. Schematic of enzymatic anode based on SWCNTs incorporated with Fc redox polymer (Tran *et al.*, 2011).

Nafion[®], a perfluorosulfonic acid cation-exchange polymer, on the other hand, could be a possible solution to this problem if used as a protective and encapsulating material in the fabrication of enzyme electrodes (Harkness *et al.*, 1993). Nafion[®] consists of hydrophobic perfluorocarbon backbone with side chains terminated by the hydrophilic sulfonate (SO_3^-) groups with counter ions (Vishnyakov and Neimark, 2001). Figure 1.21 shows the structure of nafion[®] where in a typical membrane x varies between 5 and 14, y varies between 200 and 1000 and $z = 1$. The hydrated nafion[®] membrane can hold between 1 and 30 water molecules per SO_3^- group (Blake *et al.*, 2005).

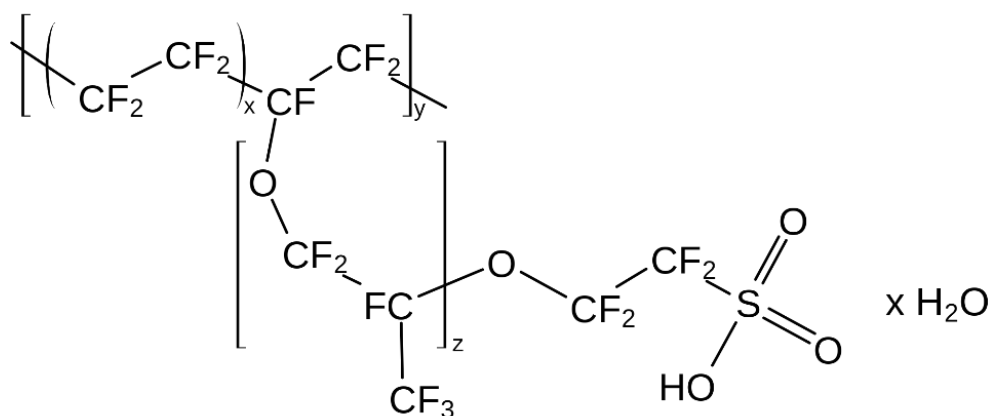


Figure 1. 21. Structure of nafion®.

Ion conductivity takes place in the hydrophilic domain of the nafion® where water can be adsorbed into both hydrophobic and hydrophilic domains (Blake *et al.*, 2005). Nafion® has excellent ion conduction properties (Moore *et al.*, 2004), biocompatible interface & compatibility with mammalian tissue (which are essential for implantable medical applications) (Turner *et al.*, 1990), hydrophilic and hydrophobic properties, as well as being chemically inert with a long-term chemical stability due to its polytetrafluoroethylene (PTFE) backbone (Blake *et al.*, 2005).

Positively charged redox-active species have been previously entrapped into nafion® membranes showed promising results (Rubinstein and Bard, 1980) and used for different purposes such as reference electrodes (Rubinstein, 1984). In another example, N-methylphenazonium (NMP) was adsorbed onto the nafion® layer for glucose bio sensing applications containing GDH enzyme where successful electron transfer through NMP was achieved (Malinauskas *et al.*, 2004).

Mediators can be reduced and oxidized to shuttle the electrons between the enzyme active sites and the electrode. During this operation the mediator can be re-oxidized at the electrode (to its cationic form). If this process were occurring inside the nafion® film, the mediator would be ion-exchanged out of the film. However, since nafion® has a high selectivity coefficient for cations with a hydrophobic character, this can provide a potential solution to the problem of mediator leaching (Martin and Freiser, 1981).

Nafion® contains large segments of hydrophobic uncharged chain material in the polymer which has strong interactions with hydrophobic ions resulting in strong retention of hydrophobic cations by nafion® (Espenscheid *et al.*, 1986). This can provide a strong base for

stable mediator incorporation into nafion[®] films and can be achieved with Fc (Espenscheid *et al.*, 1986). Nafion[®] coating was also reported to protect electrode surface (Robertson and Yeager, 1996). Although having difficulties in respect to controlling film thickness and uniformity between different electrodes, the protective function of nafion[®] was shown to be reproducible (Harrison *et al.*, 1988).

Incorporating Fc with nafion[®] as polymeric films has been reported as a straightforward method for amperometric glucose detection (White *et al.*, 1982; Chen *et al.*, 1992; Dong *et al.*, 1992; Harkness *et al.*, 1993; Brown and Luong, 1995; Vaillancourt *et al.*, 1999). Fc containing nafion[®] polymer films can be applied to enzymatic electrode fabrication in many ways which can be summarized into 3 simple types:

- Drop casting of enzymes after coating the electrodes with Fc-Nafion film (Dong *et al.*, 1992)
- Drop casting of enzymes before coating the electrodes with Fc-Nafion films to trap the enzyme (Ghica and Brett, 2005; Mani *et al.*, 2013)
- Physical entrapment of enzyme inside the Fc-Nafion polymer films (Harkness *et al.*, 1993; Vaillancourt *et al.*, 1999) or electro-polymerizing a conducting polymer/Fc derivative on nafion[®]-enzyme electrode (Brown and Luong, 1995)

Nafion[®] tends to deactivate enzymes with increasing pH and diluting nafion[®] suspensions to solve this problem was reported to form unstable and non-uniform films (Moore *et al.*, 2004). Therefore, dilutions must be achieved without compromising the film quality on the electrode surface. High ethanol content (90%) nafion[®] suspensions were reported to maintain stable membranes on electrode surfaces (Karyakin *et al.*, 1996). Using the high ethanol content in suspensions showed better performance in terms of stability compared to excessive water diluted nafion[®] suspensions (Harkness *et al.*, 1993; Karyakin *et al.*, 1996).

Nafion[®] incorporated with Fc might be a solution for fabricating long term stable and electrochemically active enzyme electrodes for glucose oxidation in enzymatic biofuel cells as nafion[®] is also readily permeable to glucose (Harkness *et al.*, 1993). However, there is still room for improvement as these films can be enhanced using better materials and methods.

Enzyme Electrodes Based on Carbon Nanotube Deposits

There has been great interest in using CNTs especially during the last two decades because of their unique properties of biocompatibility and excellent conductivity. CNTs are divided into two main groups according to their layered structures which are SWCNTs (consists of one layer, straw like structure) and MWCNTs (group of nested tubes, up to 100 tubes surrounded each other) (Babadi *et al.*, 2016).

One of the most important advantages of utilising CNTs in the area of enzymatic electrode fabrication for enzymatic biofuel cells is their highly specific 3-D structured surface area of more than $1000 \text{ m}^2 \text{ g}^{-1}$ (Peigney *et al.*, 2001). Different modifications can be applied to the CNTs by attaching specific sites to immobilize enzymes or mediators which makes this nanostructures very suitable for biofuel cell electrode design (Cosnier *et al.*, 2014). CNTs can either maintain electrical communication between the enzymes and the electrodes directly (such as with BOD as a cathodic enzyme) and/or can enhance indirect electrical communication (such as enzyme mediator CNTs composites) (Cosnier *et al.*, 2014). Functionalized CNTs show excellent properties including, film forming ability, good adhesion, high mechanical strength and amenable to chemical modifications (e.g. hydroxyl or amino groups) which makes them very attractive for enzyme immobilization (Zhang *et al.*, 2004a; Luo *et al.*, 2005; Zhou *et al.*, 2007). Such immobilization methods might include cross-linking (Zhang *et al.*, 2004a) (Wei *et al.*, 2002), dip coating and covalent bonding.

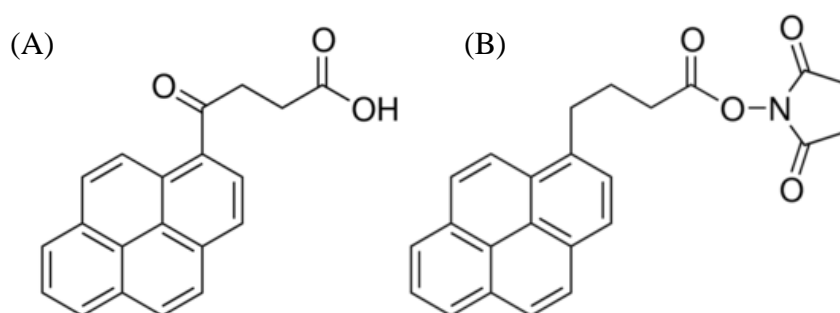


Figure 1. 22. Structure of (A) 1-pyrenebutric acid and (B) 1-pyrenebutanoic acid succinimidyl ester.

Non-covalent functionalization of CNTs using with pyrene derivatives and enabling π - π stacking interactions with CNT wall was reported several years ago and attracted many researchers (Chen *et al.*, 2001a; Krishnan and Armstrong, 2012; Bourourou *et al.*, 2013). Figure

1.22 illustrates the structure of two different pyrenyl compounds: (A) 1-pyrenebutric acid and (B) 1-pyrenebutanoic acid succinimidyl ester.

Although earlier reports used 1-pyrenebutric acid for the crosslinking of enzymes using the EDC-NHS couple (Krishnan and Armstrong, 2012), recently another pyrenyl compound, 1-pyrenebutanoic acid succinimidyl ester (PBSE) has become popular in the field of constructing electrodes (Halámková *et al.*, 2012; Szczupak *et al.*, 2012; MacVittie *et al.*, 2013; Güven *et al.*, 2016). Having the ester group (as in PBSE) attached to the pyrene structure makes this compound attractive as it involves less complicated modification of the electrodes. When functionalized with PBSE, CTNs side-walls form π - π stacking of the polyaromatic pyrenyl moiety. This structure provides covalent binding with amino groups of the enzymes. Figure 1.23 shows a simple representation of the process where PQQ-GDH and Lc enzymes are both immobilised on CNT buckypaper electrode (Szczupak *et al.*, 2012).

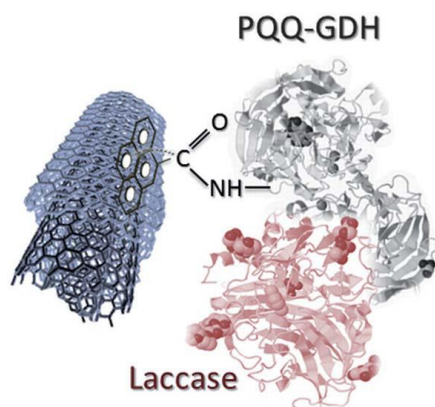


Figure 1. 23. Schematic of PQQ-GHD and Lc immobilised on pyrenyl carbon nanostructures (Szczupak *et al.*, 2012).

PBSE results in a random orientation of the enzyme molecules relative to the electrode surface because of the large number of amino acid groups randomly positioned in the protein structure (Katz, 1994). However incorporation of the CNTs might be a problem especially in the case of cathodic enzyme electrodes where DET is depending on the orientation of the enzyme.

Graphene, is a 2-D nanomaterial of carbon, with very high surface areas of $2630 \text{ m}^2 \text{ g}^{-1}$ and shows promising properties such as high mechanical conductivity and easy of functionalization for the field of enzymatic biofuel cell electrode fabrication (Babadi *et al.*, 2016). It was introduced as a favourable alternative electrode material in different applications to enhance the properties of the electrode.

More recently, mixtures of graphene with CNTs have been studied to combine the excellent properties of both materials for enzymatic bio-cathode design (Lalaoui *et al.*, 2015). More studies incorporating graphene with CNTs were reported to be on the increase due to promising preliminary results.

Outlook on Enzyme Electrode Assemblies

One of the most important aspects for designing enzymatic biofuel cell anodes and cathodes is selecting the most suitable assembly to immobilize enzymes onto electrode surface. Over decades, there have been many studies to achieve highly stable, biocompatible and high current density electrode configurations.

Electrode transfer is the first step to develop the right approach for the chosen enzyme. Hence, the biochemistry of the enzymatic electrode transfer should be understood well. In theory, DET presents an easy and efficient choice, however the downside of such electrical communication should be considered. As explained in section 1.2.2 about only limited numbers of enzymes can achieve DET and even within this small proportion there are concerns and even debatable results regarding the enzyme orientation and ability to transfer electrons.

The widely used and promising enzymes such as GOx and P2O on the anodic side and BOD on the cathode side can be employed in the presence or absence of mediators. Although there are no reports claiming DET for P2O enzymes, there are a remarkable number of studies claiming DET for GOx. Most of these incorporate CNTs as they claim that this nano-scale material can reach the active site of the enzyme to maintain communication between the enzyme and the electrode. Nonetheless, there is no clear information whether such systems harm the enzymatic structure especially in the long term. It is, on the other hand, well-established for that BOD like other multi copper oxidases, can facilitate the transport of electrons from electrode itself because of the fact that its active site is very close to the protein surface.

In contrast, the structure of the GOx shows that the active site of the enzyme is deep buried under the protein shell and in fact even if it was possible to wire nanomaterials inside the enzyme, this might not actually work at the desired performance or stability. Due to the possible damage that might be caused during the wiring processes such modifications should be considered when designing enzyme electrodes as was previously reported (Kannan *et al.*, 2009).

On the other hand, some mediators such as Fc have been widely studied in the literature showing successful mediation of the electrons for enzymatic glucose oxidation. In particular, incorporating Fc with biocompatible and stable polymers such as nafion[®] could be a good approach for fabricating enzymatic electrodes. CNTs could also be added to form a composite which might provide better electrical conductivity. In conclusion, an easy step modification process combined with biocompatible and long term stable design is extremely desired for fabrication of enzymatic electrodes for enzymatic biofuel cells.

1.2.3. Enzymatic Biofuel Cell Configurations and Performance

One of the earliest reports on enzymatic biofuel cells was by Willner and Katz based on NADH and H₂O₂ for anode and cathode reactions respectively (Willner *et al.*, 1998a). This type of fuel cell had an OCP of 0.32 V with a maximum power of 8 μ W using an external load of 3 k Ω (Willner *et al.*, 1998a). Then, a glucose/O₂ EBFC was reported by the same group leading the way to the improvements with these types of EBFCs for many applications to power microelectronics in implantable micro devices. The maximum power was 4 μ W at an external load of 0.9 k Ω with 1 mM glucose concentration (Katz *et al.*, 1999b).

Enzymatic Biofuel Cells Based on Glucose and Air/O₂

Many different configurations have been published based on different enzymes for anodic and cathodic reactions where glucose and oxygen are utilised at the anode and cathode respectively. Most of these studies focused on developing fuel cells for implantation under physiological conditions to use the glucose present naturally in human blood. As discussed in Section 1.2.1, GOx is the most widely utilised enzyme for enzymatic biofuel cell anodes.

EBFCs based on GOx and Os derivatized polymer mediators have been very popular and attracted many researchers since the first biofuel cell design for glucose oxidation. One of the examples for this type of enzymatic biofuel cells is presented by Soukharev *et al.* wiring both GOx and Lc enzymes for anode and cathode respectively using Os-based redox polymers (Soukharev *et al.*, 2004). This configuration provided power outputs of 350 μ W cm⁻² in 15 mM glucose containing citrate buffer (pH 5) at 37.5 °C. In another study, researchers developed a GOx-BOD based glucose/O₂ EBFC with a power output of 244 μ W cm⁻² in 15 mM glucose containing 0.15 M chloride at (pH 7.4) at ~37 °C (Mano and Heller, 2003). Both of these studies do not present any stability information which is a concern when using these Os-based

polymers. For implantable medical devices, nontoxic mediators, unlike Os, are essential (Hao Yu and Scott, 2010).

Other mediators such as tetrathiafulvalene (TTF) (Komaba *et al.*, 2008; Nazaruk *et al.*, 2008) and HQS (Habrioux *et al.*, 2008) have been used for enzymatic biofuel cell anodes with GOx, and ABTS is commonly used (Liu and Dong, 2007b; Habrioux *et al.*, 2008; Komaba *et al.*, 2008) for Lc and BOD containing cathodes. However, mediators like Fc and its derivatives have attracted more researchers due to their promising properties (Liu and Dong, 2007b) (Lim *et al.*, 2007; Liu and Dong, 2007b). Most of the recent studies report using the DET properties of Lc and BOD enzymes in combination with CNTs or gold nano particles (Krishnan and Armstrong, 2012; du Toit *et al.*, 2016). Table 1.3 shows examples of fuel cells that all use a mediator based on GOx anodes and redox mediators and cathodes with Lc and BOD.

Recently there has been growing interest in implantable fuel cells. In this context, researchers demonstrated power production from the hemolymph of snails (Halámková *et al.*, 2012), “cyborg” lobsters (MacVittie *et al.*, 2013), and serially connected clams (Szczupak *et al.*, 2012). A biofuel cell was even inserted in an insect (Rasmussen *et al.*, 2012). Figure 1.24 shows examples of these demonstrations.

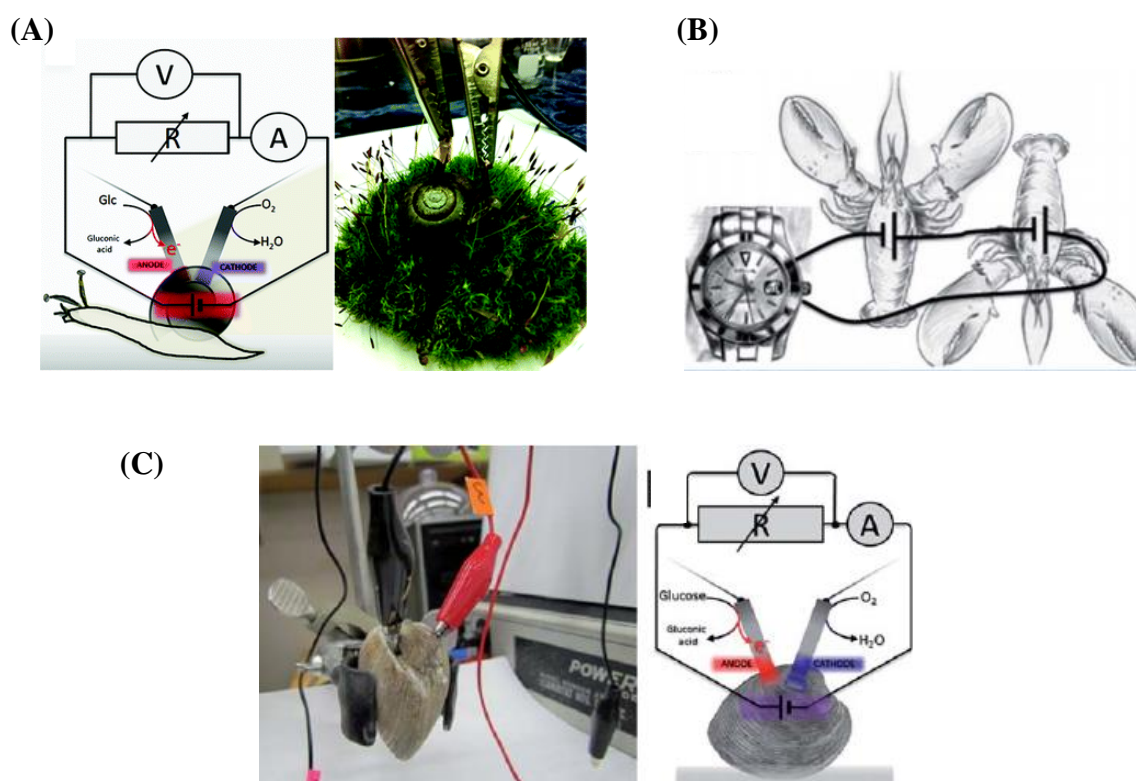


Figure 1. 24. Enzymatic biofuel cells demonstrated in non-mammalian living animals: (A) snail, (B) lobster and (C) clam (Halámková *et al.*, 2012; Szczupak *et al.*, 2012; MacVittie *et al.*, 2013).

Enzymes Anode / Cathode	Mediators Anode/Cathode	Fuel Concentration / mM	Power Density / ($\mu\text{W cm}^{-2}$)	Comments	Ref
GOx/Lc	TTF/ABTS	15	7	Two glassy carbon electrodes (GCE) modified with enzymes embedded in lyotropic liquid-crystalline cubic phase were used for the biofuel cell construction. McIlvaine buffer, pH 7 solution. No stability information.	(Nazaruk <i>et al.</i> , 2008)
GOx/Lc	Os polymer/ Os polymer	15	137	Carbon fiber electrodes (7 μm diameter, 2 cm long) were used. At 23 $^{\circ}\text{C}$, pH 5.0 citrate buffer (0.2 M). The cell operated for 24 h with <10% loss; after 72 h of continuous operation the power output dropped by ~25%. The external load in the test was 1 M Ω .	(Chen <i>et al.</i> , 2001b)
GOx/Lc	Os polymer/ Os polymer	15	350	2 cm long carbon fiber anode coated with “wired” glucose oxidase and with a 7 μm diameter, 2 cm long carbon fiber cathode coated with the PVI-Os-tpy “wired” laccase and with the novel polymer I “wired” laccase cathode, pH 5 citrate buffer at 37.5 $^{\circ}\text{C}$. No stability information.	(Soukharev <i>et al.</i> , 2004)
GOx/Lc	The ferrocene carboxylic acid or ferrocene dicarboxylic acid/ABTS	15	10	Enzyme entrapment in multi-walled carbon nanotubes-ionic liquid gel. Air-saturated acetate acid buffer solution containing saturated FcCOOH solution (pH 5.86). Stability at OCP (0.33V) is 72 h. Stability under 40 k Ω was dramatically bad.	(Liu and Dong, 2007b)

Table 1. 3. Examples of glucose/air (or O₂) fuel cells based on mediators and GOx.

Enzymes Anode / Cathode	Mediators Anode/Cathode	Fuel Concentration / mM	Power Density / ($\mu\text{W cm}^{-2}$)	Comments	Ref
GOx/Lc	Fc/DET	10	15.8	Carbon nanotubes-hydroxyapatite nano composite-based anode and cathode. 0.10 M pH 6.0 phosphate buffer, temperature 20 ± 2 °C was used. No stability information.	(Zhao <i>et al.</i> , 2009)
GOx/Lc	Fc/DET	10	29.4	Lc immobilised <i>via</i> polymerization of dopamine with CNTs. GOx with Nafion-Fc-MWCNTs on glassy carbon. Operating in Britton–Robinson buffer solution (pH 5.0). After 5 h operation at 20k Ω , performance decreased to 94 % of initial value. No info for long term stability.	(Tan <i>et al.</i> , 2010)
GOx/BOD	Os polymer/ Os polymer	15	50	A biofuel cell under physiological conditions air saturated, pH 7.4, 0.14 M NaCl, 37.5 °C. No stability information.	(Kim <i>et al.</i> , 2003)
GOx/BOD	Os polymer/ Os polymer	20	244	A miniature biofuel cell operating under physiological conditions phosphate buffer, pH 7.4, 0.15 M chloride at ~ 37 °C. No stability information.	(Mano and Heller, 2003)
GOx/BOD	TTF/ABTS	100	150	Enzymes and mediators were entrapped in polyion complex matrix on CNTs modified glassy carbon electrode. Tested in O ₂ saturated 40 mM PBS buffer at 37 °C.	(Komaba <i>et al.</i> , 2008)

Table 1.3 continued.

Enzymes Anode / Cathode	Mediators Anode/Cathode	Fuel Concentration / mM	Power Density / (μW cm^{-2})	Comments	Ref
GOx/BOD	Ferrocenemethanol /ABTS	100	120	Sol-gel-CNTs enzyme composite electrodes, air saturated solution, operated at room temperature. No stability information.	(Lim <i>et al.</i> , 2007)
GOx/BOD	Ferrocenemethanol /ABTS	100	24.3	The anode of the biofuel cell consists of a gold electrode with co-immobilised graphene – glucose oxidase using silica sol–gel matrix. Air saturated glucose solution in PBS. The system was stored in pH 7.4 PBS solution at 4 °C and tested every day with a 15 k Ω external load. After the first 24 h, it had lost 6.2% of its original power output. Power output become 50% of its original power output after 7 days	(Liu <i>et al.</i> , 2010)
GOx/BOD	HQS/ABTS	10	42	Concentric BFC based on carbon tubular electrodes set up. The enzymes and the mediators were entrapped at the electrode surfaces by a film of polypyrrole film followed by a glutaraldehyde treatment. Phosphate buffered solution (pH 7.4) at 37 °C. No stability information.	(Habrioux <i>et al.</i> , 2008)
GOx/BOD	Fc/ABTS	5	26	Fc containing redox polymer. Tested O ₂ sat PBS at 37 °C. No stability information	(Bunte <i>et al.</i> , 2014)
GOx/BOD	Fc/DET	10	13	The MWCNT, Fc, enzymes and chitosan were sequentially coated on a glassy carbon electrode. No stability information.	(Park <i>et al.</i> , 2011)

Table 1.3 continued.

In terms of the implantable applications in mammals, the first demonstration of an implanted biofuel cell (fully biological) for generating electricity was in a rat (Cinquin *et al.*, 2010). The fuel cell was able to generate electrical power using the glucose in the rat with an OCP value of 0.275 V and maximum power output of 6.5 μW (Cinquin *et al.*, 2010). Similar to this study, rabbit ear (partially implanted, anode compartment only) (Miyake *et al.*, 2011) and brain of a living rat (Andoralov *et al.*, 2013) were used to power up an enzymatic biofuel cells resulting 0.42 μW and 2 $\mu\text{W cm}^{-2}$ power and power density values respectively.

Incorporating CNTs technology and DET properties, researchers managed to raise the power to 38.7 μW by implanting an enzymatic biofuel cell in a rat and lit up an LED or a digital thermometer using special circuits with capacitors (Zebda *et al.*, 2013). Examples illustrating mammalian implanted fuel cells are shown in Figure 1.25. A glucose/oxygen biofuel cell using FAD-dependent glucose dehydrogenase enzyme at the anode side operating in human serum was also reported and produced maximum power densities of 39.5 ± 1.3 and $57.5 \pm 5.4 \mu\text{W cm}^{-2}$ for EBFCs at 21 °C and 37 °C, respectively (Milton *et al.*, 2015).

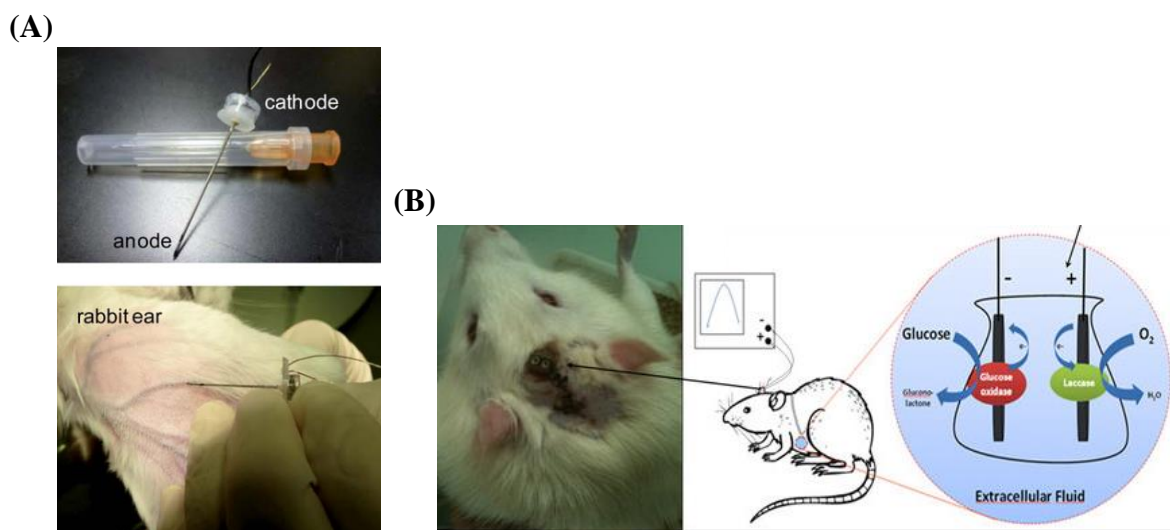


Figure 1. 25. Enzymatic biofuel cells implanted in (A) rabbit ear and (B) rat (Miyake *et al.*, 2011; Zebda *et al.*, 2013).

More recently, a model study using human serum has been reported where anodic and cathodic electrodes were made of carbon nanotube-buckypaper modified with PQQ-dependent glucose dehydrogenase and laccase, respectively. Power densities of 16.12 $\mu\text{W cm}^{-2}$ were achieved in human serum for lower than physiological glucose concentrations (Güven *et al.*, 2016).

Increasing the glucose concentration to 24.89 mM and biofuel cell temperature to 37 °C caused an increase in power output leading up to 49.16 $\mu\text{W cm}^{-2}$ (Güven *et al.*, 2016).

The progress in the area of enzymatic biofuel cells is slower than previous years because of operational limitations especially for human implants such as pacemakers. Although there are preliminary reports concerning powering up pacemakers (MacVittie *et al.*, 2013) using enzymatic biofuel cells, it is still not stable enough for the long-term applications. However, in the short term, there are other potential applications might be important, for example, in plants. In this content, there are reports demonstrating enzymatic biofuel cells extracting power from glucose or fructose in plants such as from grape (Mano *et al.*, 2003a), fruit juice (Liu and Dong, 2007a) or more recently an orange (MacVittie *et al.*, 2015).

EBFC Designs

Most of the present EBFC designs are at the level of proof-of-concept and generally designed for immersing the electrodes in related fuel stock solution (Ivanov *et al.*, 2010). In the case of implantable designs, it is still at the stage of utilising electrodes inside the plant, non-mammals or mammals using appropriate electrode design such as wires or small surfaces (Miyake *et al.*, 2011; Halámková *et al.*, 2012).

There are, on the other hand, several reports demonstrating different possible designs for enzymatic biofuel cells including microfluidic cells (Bedekar *et al.*, 2007; Togo *et al.*, 2007), concentric cells (Habrioux *et al.*, 2008), fuel cells with air breathing cathodes (Sakai *et al.*, 2009) and modular stack cells (Kamitaka *et al.*, 2007). Figure 1.26 shows examples of different fuel cell designs reported previously.

The design of the enzymatic biofuel cells is an important issue as miniaturization is a very important aspect especially for implantable power devices (Ivanov *et al.*, 2010). Each design addresses particular problems and offers a solution, however, there are no absolute solutions covering all of the problems of limited power output and low long term stability simultaneously. Microfluidic biofuel cell design appears to be a solution for the miniaturization problem, however most of the presented reports based on the diffusional enzyme and mediator demonstrated that they dissolved in the electrolyte solution flowing through a microchannel (Zebda *et al.*, 2009; González-Guerrero *et al.*, 2013).

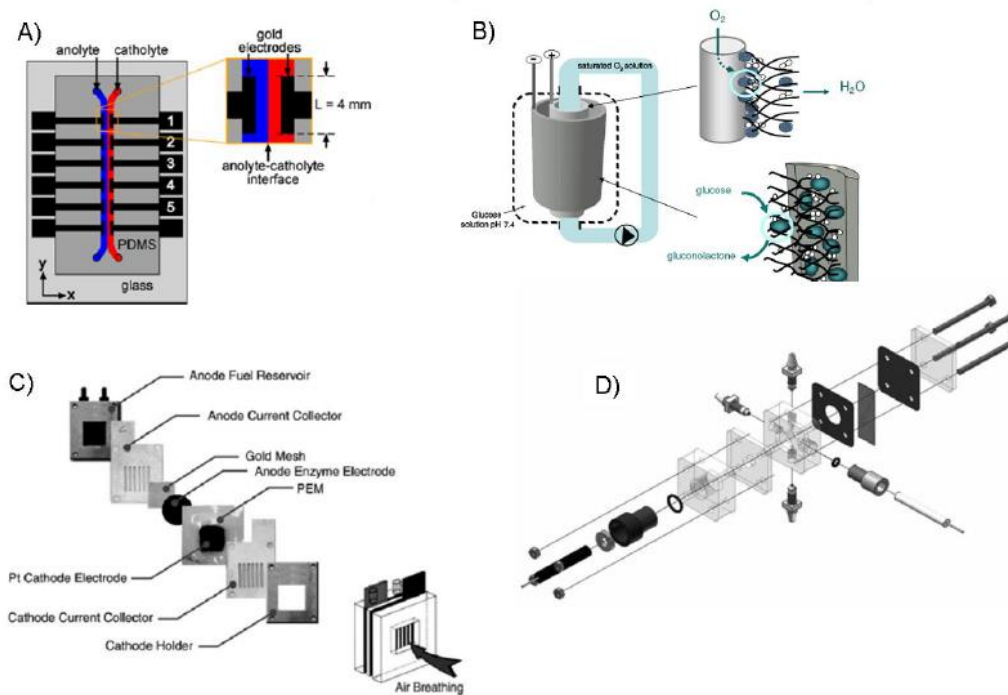


Figure 1. 26. Schematic presentation of (A) microfluidic fuel cell (B) concentric fuel cell (C) fuel cell with air breathing cathode (D) stack design fuel cell (Fischback *et al.*, 2006; Lim and Palmore, 2007; Habrioux *et al.*, 2008; Svoboda *et al.*, 2008).

Air-breathing cathodes also addresses the problem about the low O₂ solubility in aqueous solutions which could be a potential solution for cathode limiting enzymatic biofuel cells by utilising the gas phase O₂ (Smolander *et al.*, 2008). A concentric biofuel cell design similar to air-breathing cathodes could be used to utilise gas phase O₂, however its functionality especially for implantable applications could be a problem (Habrioux *et al.*, 2008). Stack cells on the other hand are very suitable for lab scale experiments with their flexible design allowing electrochemical characterization as well as fuel cell performance measurements (Svoboda *et al.*, 2008).

Conclusions and Future Outlook on EBFCs

The typical fuel used in current development of the enzymatic biofuel cells is glucose and the typical oxidant is O₂ with GOx being the most widely utilised enzyme for glucose oxidation. However, other promising enzymes such as P2O could be an alternative with its wide range of sugar selectivity and structural properties (such as having 4-FAD groups). Fc and its derivatives are also the most promising mediators when used with an appropriate immobilization strategy. Depending on the conditions used, Lc or BOD could be utilised for the oxygen reduction

reaction. BOD has the advantage as it can be used under physiological conditions such as neutral pH and its DET properties have been extensively reported.

The essential problem for future enzymatic biofuel cells is long-term stability. Unfortunately, studies addressing this issue in the literature are in the minority. Flow systems using microfluidic cells could be used to solve this problem as batch designs will not achieve the desired stability values. Genetically modified enzymes could be another solution to improve the enzyme stability especially in aerobic conditions. Incorporation of membranes such Nafion[®] could also help to improve the stability of the enzymatic electrodes in the biofuel cell. In the case of implantable devices, long term stable fuel cells are required to compete with the current technology. Conventional batteries for pacemakers can work up to 10 years where the best examples of the EBFCs can only go up to months (MacVittie *et al.*, 2015).

There are also thermodynamic limitations such as the potential difference between the anode and cathode which is dependent on the redox potentials of the enzymes used. This limitation is followed by kinetic, ohmic and mass transport limitations when extracting power from the biofuel cell. Therefore, to maintain the voltages required by even the smallest electrical device, devices such as charge pumps and capacitors could be used. These systems provide sufficient temporary current without changing the design or construction of the biofuel cell. In this way, the voltage requirements would be met (Hanashi *et al.*, 2011).

There are different problems and possible solutions for future EBFC designs. However, these solutions require a multi-disciplinary approach including protein engineering to improve the properties of biocatalysts, new and better immobilization strategies for more stable electrodes, incorporation of nanotechnology such as carbon nanomaterials and novel designs such as microfluidics combined with air breathing designs. Only then, the energy production from enzymes can make a real impact and benefit medical science and healthcare management.

1.3.Review of Methods for Electrochemical Analysis

Electrochemistry can be defined as the field in which the chemical response of systems to electrical stimulations is associated with charge separation (Bard *et al.*, 1980; Brett *et al.*, 1993). There is a huge array of different phenomena covered by the field of electrochemistry involving electroanalytical sensors and fuel cells (Bard *et al.*, 1980).

There are different purposes that electrochemistry can be employed which might involve investigations of the electrochemical properties of developed power sources such as fuel cells. Such investigations can be made by employing electrochemical methods (Bard *et al.*, 1980). Oxidation/reduction (redox) reactions are often used to provide information about the concentration, kinetics, reaction mechanism, chemical status and behaviour of a species in solution.

1.3.1. The Cell Set-up

Most of electrochemical techniques requires three electrodes; the working electrode (WE, e.g. carbon, graphite, gold *etc.*), the reference electrode (RE, e.g. SHE, Ag/AgCl, *etc.*) and the counter (or auxiliary) electrode (CE, e.g. carbon, platinum, *etc.*) (Brett *et al.*, 1993). These three electrodes are placed in a cell connected to a potentiostat (an instrument that controls the potential of the WE and measures the corresponding current) shown in Figure 1.27. The potentiostat can control the potential difference and measure the current flow between electrodes. The RE is essential to control the effects from the electrolyte and CE-electrolyte interface (Larminie *et al.*, 2003). The current flow takes places between CE and WE whilst the potential difference is measured between RE and WE.

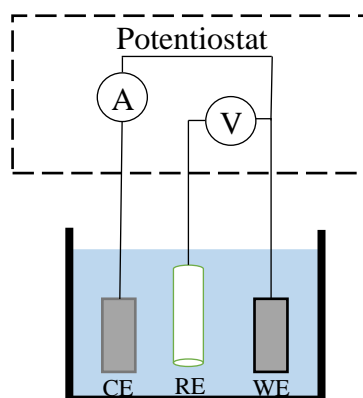


Figure 1. 27. Simple presentation of an experimental set-up for three-electrode electrochemical cell.

1.3.2. Electrochemical Characterization

Various parameters can be altered when applying different methods for the investigation of the electrochemical systems. Such methods involve voltammetry (cyclic voltammetry and linear sweep voltammetry) and amperometry (chronoamperometry) as well others (such as pulsed techniques or polarography) (O'Gorman, 1998).

Voltammetry

Cyclic voltammetry (CV) and Linear Sweep Voltammetry (LSV) are two of the most commonly used electroanalytical techniques in electrochemical systems (Brett *et al.*, 1993). There are many applications where CV and LSV can be used to gather information about the reversible/irreversible behavior of redox couples as well as reaction mechanism and diffusion coefficients (Bard *et al.*, 1980).

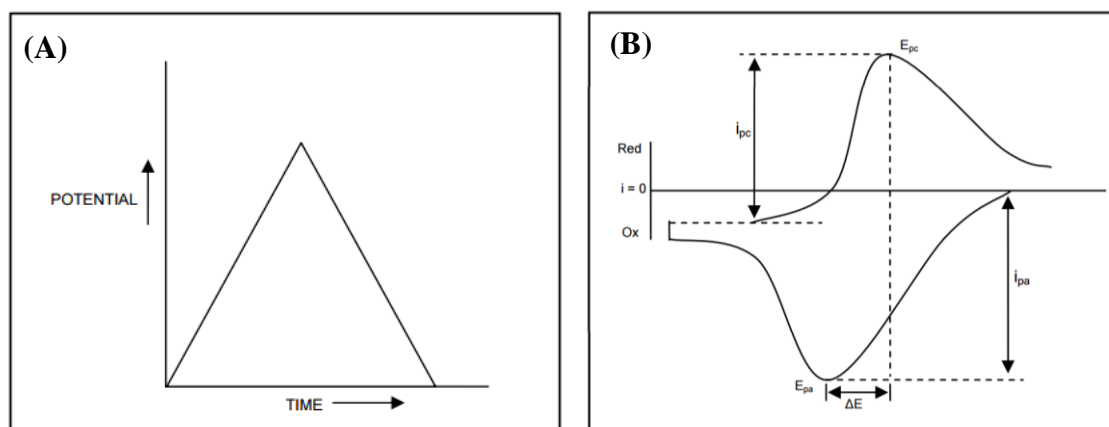


Figure 1.28. (A) CV waveform and (B) typical CV (Princeton)

The CV experiment can be performed using a potentiostat which can apply a potential ramp between two chosen potentials and reverse it back to the initial potential. The current is measured during this potential sweep and then can be plotted *versus* applied potential. In LSV, on the other hand, the potential is swept in one direction only, rather than cycling it back. Both can be run as single or multi cycles, however most of the time multi scans are used to allow the system to reach steady state. A CV waveform and the typical CV voltammogram are shown in Figure 1.28.

Data Interpretation

There are quite a few parameters that can be extracted from a single CV scan. These include the cathodic peak height (I_{pc}), the anodic peak height (I_{pa}), the cathodic peak potential (E_{pc}) and the anodic peak potential (E_{pa}). These parameters can provide information about the nature of the redox reaction takes place (Nicholson, 1965; Brett *et al.*, 1993).

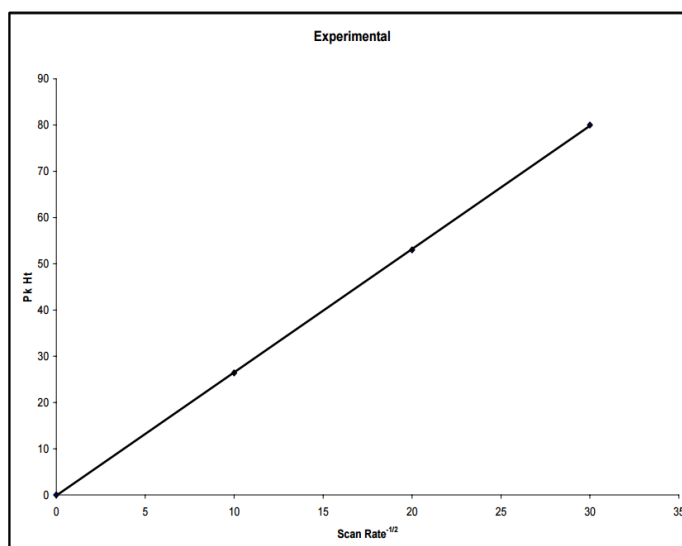


Figure 1. 29. Plot of peak height for cadmium reduction at various scan rates (Princeton, 2016).

In general the peak separation is expressed by the equation: where; n is the number of electrons transferred (Nicholson, 1965). The optimum potential difference between E_{pa} and E_{pc} for one electron transfer was reported to be 57 mV (Nicholson, 1965).

$$\Delta E_p = E_{pa} - E_{pc} = \frac{57 \text{ mV}}{n} \quad (\text{Eq. 1. 1})$$

The scan rate of the CV can be varied to determine the diffusion coefficient of the redox species. For a reversible system the peak height will increase linearly with the square root of scan rate. The slope of the resulting line will be proportional to the diffusion coefficient as seen in Figure 1.29.

This relationship is explained by the Randles-Sevcik equation (Brett *et al.*, 1993):

$$i_p = 0.4463nG = FAC \left(\frac{nFvD}{RT} \right)^{\frac{1}{2}} \quad (\text{Eq. 1. 2})$$

where i_p is the peak current height (A), n is the number of electrons transferred, F is the Faraday constant ($C \text{ mol}^{-1}$), A is the electrode area (cm^2), C is the concentration of the electron transferring species (mol cm^{-3}), v is the scan rate ($V \text{ s}^{-1}$), D is the diffusion coefficient of the electron transferring species ($\text{cm}^2 \text{ s}^{-1}$), R is the gas constant ($VC \text{ K}^{-1} \text{ mol}^{-1}$) and T is temperature (K).

Chronoamperometry

Chronoamperometry (CA) is another commonly used electroanalytical technique especially used in biosensor and biofuel cell studies to obtain calibration curves and stability studies. In a typical CA experiment the current response at a certain potential is recorded and can be plotted as a function of time.

CA experiments can be used to obtain calibration curves by adding the sensing substrate into the solution and recording the steady state current response over time. For example, in the case of developing a glucose sensor using glucose based EBFC, the glucose *versus* steady state graphs can be obtained. Such graphs then can be used to extract more information such as the sensitivity, glucose affinity *etc.*

1.3.3. Fuel Cell Polarization

A polarization curve can be defined as the plot of current (or current density) *versus* cell potential (E) as shown in Figure 1.30.

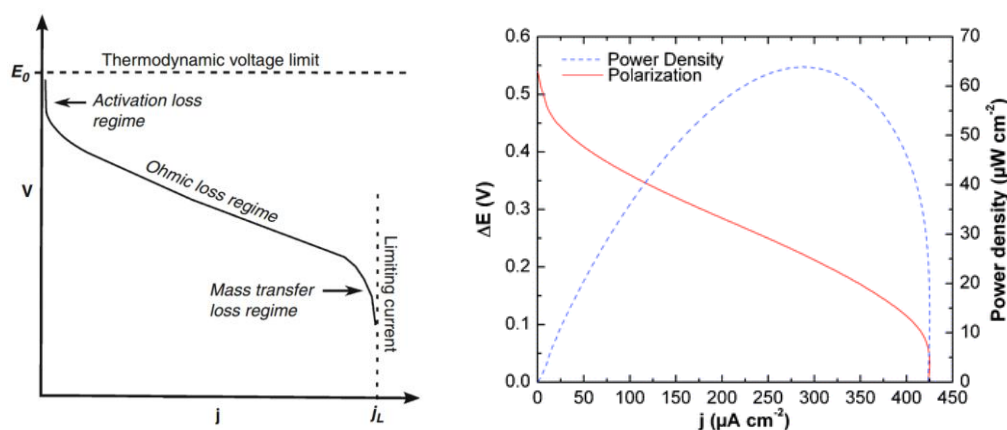


Figure 1. 30. (A) Polarization curve and the losses (Gold, 2012) (B) power curve with polarization curve for an EBFC (González-Guerrero *et al.*, 2013).

This type of curves can be obtained by applying various resistances to the fuel cell and recording the voltage-current values generated by the cell (Güven *et al.*, 2016). Figure 1.30 also indicates that the fuel cell voltage achieved is lower than the theoretical thermodynamic values and the voltage decreases when the current going through the cell is increased. Polarization curves (with power curves) can provide very useful information in order to understand and improve the fuel cell performance such as power and current densities as well as some limitations regarding to

the system. These limitations are defined as activation-related losses, Ohmic losses and mass transport related losses (Rayment and Sherwin, 2003; Stolten, 2010)

Briefly the reasons for the losses in different regions can be summarized as follows (Rayment and Sherwin, 2003; Stolten, 2010):

- Activation-related losses: Because of the activation energy of the electrochemical reaction at the electrodes.
- Ohmic losses: Could be caused by many reasons including the ionic resistance in the electrolyte, electronic resistance in the electrodes or connectors and components *etc.*
- Mass-transfer related losses: Because of the mass transport of the reactant and product on the electrode.

All of these factors should be taken into account while designing a fuel cell especially complicated system such as EBFCs because of the involvement of bio-electro-active species.

Chapter 2. Electrochemical Glucose Oxidation by Pyranose-2-Oxidase Mutants for Enzymatic Biofuel Cell Applications

In this chapter, the performance of the pyranose-2-oxidase (P2O) enzyme and its mutants were electrochemically tested for glucose oxidation and the results were compared with the more widely used enzyme glucose oxidase (GOx). Electrochemical characterization of the enzymes was performed in solution with the diffusive mediator ferrocene carboxylic acid (FcCOOH) using cyclic voltammetry (CV), linear sweep voltammetry (LSV) and chronoamperometry (CA). Electrochemical tests showed the activity of P2O enzymes for glucose oxidation and successful electron transfer from enzymes to the electrode *via* electron transfer mediator. P2O and its mutants showed similar electrochemical behaviour compared to commercial GOx where P2O-T169G mutant demonstrated better performance especially when oxygen is saturated in the solution. Stability studies also showed that P2O-T169G mutant was not significantly affected by the presence of oxygen, whereas GOx was seriously affected. Results indicate that P2O-T169G is a promising enzyme with good stability and can be used in enzymatic biofuel cell (EBFC) applications as an alternative to GOx.

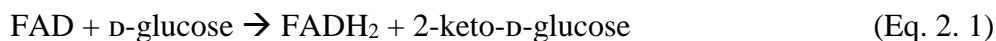
2.1. Introduction

P2O (pyranose:oxygen 2-oxidoreductase, EC 1.1.3.10) is a wood degrading enzyme that has excellent reactivity with alternative electron acceptors for a range of sugar substrates. It was purified and characterized from several different fungal sources, with *trametes multicolor* being the best studied (Leitner *et al.*, 2001; Martin Hallberg *et al.*, 2004).

The first crystal structure of P2O from *Trametes multicolor* was reported by Hallberg *et al.* (2004) using single anomalous dispersion. P2O can oxidase sugars at position C-2 by the *Ping Pong Bi Bi* mechanism similar to other oxidoreductases (Wongnate *et al.* (2011)), as well as other substrates at position C-3, such as 2-deoxy-D-glucose, 2-keto-D-glucose and methyl β -D-glucosides (Martin Hallberg *et al.*, 2004; Wongnate *et al.*, 2011). This enzyme, therefore, has recently become very popular in the field of enzymatic sensors and biofuel cells because of its wide range of substrate selectivity and lack of any anomeric selectivity (Spadiut *et al.*, 2010).

The reaction mechanism of P2O consists of oxidative and reductive half reactions. During the reductive half reaction, the sugar is oxidized to the corresponding sugar derivative and the flavin adenine dinucleotide (FAD) is reduced to FADH₂ shown in (Eq. 2.1). The oxidative half

reaction consists of the reduction of oxygen (O₂) to hydrogen peroxide (H₂O₂) and the re-oxidation of FADH₂ to FAD shown in (Eq. 2.2) (Kujawa *et al.*, 2006).



GOx, on the other hand, is the most widely used for glucose oxidation in biofuel cells because of its well-known structure and good selectivity for glucose (Wilson and Turner, 1992). GOx catalyses the oxidation of D-glucose into D-glucono-1, 5-lactone which then hydrolyses to gluconic acid. GOx uses FAD as the co-factor responsible for the catalytic reaction (Ivanov *et al.*, 2010). However, it has significant drawbacks include GOx having restricted turnover rate for glucose. GOx oxidizes glucose only at the C-1 position, which is a limiting factor in terms of coulombic efficiency (Zafar *et al.*, 2010). It also has a high turnover rate for O₂, that risks excessive H₂O₂ production (Zafar *et al.*, 2010). Enzyme turnover rate for O₂ becomes essential in EBFC applications where fuel and oxidant are in the same solution.

The use of P2O in the development of biosensors has been reported in literature, wherein the co-immobilization of P2O with peroxidase on a carbon paste electrode was one of the earliest reports (Lidén *et al.*, 1998). A few studies have been reported recently using P2O in biosensor applications such as wiring different flexible osmium functionalized polymers with P2O on graphite electrodes (Timur *et al.*, 2006) (Tasca *et al.*, 2007; Zafar *et al.*, 2010). This approach was reported to provide more efficient electron transfer from the reduced reaction centres of the enzyme (Timur *et al.*, 2006). A similar strategy was also used in another study supporting the idea of enhanced electron transfer rate of P2O when wired with osmium polymers (Tasca *et al.*, 2007).

Although these reports show promising results with osmium polymers, there is a concern about their use as implantable devices. Osmium compounds are toxic and not biocompatible, therefore leaching is a serious concern posing a high risk for long term applications (Hao Yu and Scott, 2010). Another study demonstrates the use of carbon nanotubes (CNTs) with carbon paste electrodes to fabricate P2O based biosensors (Odaci *et al.*, 2008). Determination of the glucose levels in wine samples were shown to be consistent with the standard methods (Odaci *et al.*, 2008). Gold nanoparticles (AuNPs) - polyaniline(PANI)/AgCl/gelatin nanocomposite on glassy carbon electrode (GCE) was another immobilization method used for P2O where the enzyme was shown to maintain its bioactivity and stability for glucose sensing applications

(Ozdemir *et al.*, 2010). Although all the previous reports showed promising results, the wide sugar selectivity of P2O is reported to have significant disadvantage on its use in biosensor applications. However, this could be an advantage if it is used in biofuel cells which have not yet been fully investigated.

One of the biggest challenges for EBFCs is to fabricate long-term stable enzymatic electrodes for implantable devices or other micro-electronic applications (Calabrese Barton *et al.*, 2004). Since O₂ plays a key role in the enzymatic glucose oxidation reaction as an electron acceptor, using an enzyme that does not utilise oxygen is a big advantage (Ivanov *et al.*, 2010) because the enzyme will not have to compete with the electron transfer mediator (if used) to accept electrons and also the production of H₂O₂ will be minimized (Ivanov *et al.*, 2010). P2O, in wild type form, also utilises O₂ as an electron acceptor, therefore, H₂O₂ production during the oxidation of glucose is a concern.

In this chapter, the use of different mutant P2O enzymes, which have lower turnover rates for O₂, have been investigated in bio-electrochemical systems. The redox behaviour of P2O enzymes and GOx were characterised using cyclic voltammetry, linear sweep voltammetry and chronoamperometry with FcCOOH used as an electron mediator. Finally, the results were compared with commercially available GOx to determine possible applications of P2O in electrochemical systems.

2.2. Experimental

2.2.1. Materials

FcCOOH, D-(+)-Glucose and GOx (from *Aspergillus niger* lyophilized, powder, ~200 U mg⁻¹) were purchased from Sigma-Aldrich (Dorset, UK). P2O-WT (22 U mg⁻¹) and its mutants were kindly donated by Prof Chaiyen's research group in Faculty of Science, Mahidol University, Thailand. Mutants P2O-T169S (0.6 U mg⁻¹) and P2O-T169G (0.2 U mg⁻¹) were prepared as described previously using Site-directed mutagenesis at the conserved residue threonine position (Thr¹⁶⁹) of P2O (Pitsawong *et al.*, 2010; Wongnate *et al.*, 2011). The GCE was purchased from IJ Cambria Scientific Ltd. (Llanelli UK). Stock solutions of glucose were allowed to mutarotate for minimum 24 h before use and were subsequently kept refrigerated at 4 °C. Stock solution of 1 mM FcCOOH were prepared by dissolving FcCOOH in 100 mM phosphate buffer solution (PBS) at pH 7 and were subsequently kept refrigerated at 4 °C. All

the enzyme solutions were made by dissolving and/or diluting the enzyme stock solutions with 100 mM PBS at pH 7 and were subsequently kept at -70 °C.

2.2.2. Electrochemical Measurements

The solutions for the electrochemical tests were prepared by mixing enzyme solutions with FcCOOH to give a final concentration of 1 mg mL⁻¹ enzyme and 0.5 mM FcCOOH concentration in a total volume of 2 mL. The electrochemical tests were performed in a three-electrode electrochemical cell system, in which the working electrode (WE) was GC, a platinum coil was used as the counter electrode (CE) and the reference electrode (RE) was Ag/AgCl (~4M saturated KCl gel filled). The GC WE had a diameter of 3 mm and a surface area of 0.071 cm².

GCE was polished before each experiment with 1 µm diamond and 0.05 µm alumina powder, rinsed thoroughly with de-ionized (DI) water between each polishing step, sonicated no more than 3 min in DI water and dried under nitrogen. Prior to the electrochemical tests, the solutions were saturated with either air or nitrogen between each consecutive glucose additions under constant stirring.

The potentials described are all *versus* Ag/AgCl reference electrode unless otherwise specified. CV, LSV and CA were used to characterize the electrochemical experiments. CV experiments were performed at different scan rates from 500 mV s⁻¹ to 10 mV s⁻¹, LSV experiments were performed at 1 mV s⁻¹ and CA experiments carried out applying a constant voltage of 0.35 V for 1 h and 3 h. All the electrochemical measurements were carried out by an Autolab potentiostat-galvanostat (PGSTAT101) purchased from Methrom Autolab (Utrecht, Netherlands).

2.3. Results and Discussion

2.3.1. Electrochemical characterization of Pyranose-2-oxidase and its mutants in solution

The properties of the different P2O enzymes used in this chapter are listed in Table 2.1. It has been reported previously that the conserved residue Thr¹⁶⁹ is situated strategically in the P2O active site, positioned immediately above the flavin (Martin Hallberg *et al.*, 2004). Therefore, the mutants prepared by changing the position of Thr¹⁶⁹ show different behaviour to the wild type form regarding glucose oxidation and oxygen affinity (Pitsawong *et al.*, 2010).

The rate constant (k_{cat}) of P2O-T169S was reported to be higher than P2O-WT and P2O-T169G for the enzymatic oxidation of glucose. A two-step glucose oxidation mechanism was previously proposed for P2O-WT, including the flavin reduction and C4a-hydroperoxyflavin decay in contrast the mutants' reaction mechanism was proposed to be limited only by the flavin reduction (Pitsawong *et al.*, 2010). As a result, the k_{cat} of P2O-T169S demonstrated higher values than it was for P2O-WT. However, the reductive catalytic efficiency ($k_{cat}/(K_m\text{-Glucose})$) for P2O-T169S was similar to that of P2O-WT but very low for P2O-T169G (11 fold lower value) showing that the reductive half reaction is less affected in P2O-T169S compared to T169G. When the oxidative catalytic efficiency ($k_{cat}/(K_m\text{-O}_2)$) values are compared, P2O-T169S and P2O-T169G have 8 and 549 fold lower values respectively than P2O-WT. This indicates that the modification at the Thr¹⁶⁹ position highly affects the oxidative half reaction of the enzymes.

Parameters	Enzymes		
	P2O-WT	P2O-T169S	P2O-T169G
Rate constants for glucose oxidation - k_{cat} / s^{-1}	9.7 ± 0.15	13.7 ± 0.2	0.7 ± 0.01
Catalytic efficiency for glucose oxidation - $k_{cat}/(K_m\text{-Glucose}) / (mM^{-1} s^{-1})$	8.6	8.1	0.8
Catalytic efficiency for oxygen reduction - $k_{cat}/(K_m\text{-O}_2) / (mM^{-1} s^{-1})$	110.0	13.8	0.2
Reduction Potential / mV	-105	-106	-1

Table 2. 1. The properties of the pyronase-2-oxidase enzymes used in solution experiments (Wongnate *et al.*, 2011)(Kujawa *et al.*, 2006; Pitsawong *et al.*, 2010).

The reduction potentials of P2O-WT and P2O-T169S are in the same range indicating that the oxidative power of the mutant P2O-T169S is preserved. For T169G, on the other hand, the reduction potential is significantly higher than the other enzymes (-1 mV *versus* -105 mV or lower) showing an inverse effect for reduction rate constants (more than 10 fold decrease in reduction rate constant). This suggests that the binding mode of D-Glucose in P2O-T169G is

different from what in P2O-WT and P2O-196S, thus resulting in lower efficiency of the hydride transfer from sugar to flavin (Pitsawong *et al.*, 2010). However, P2O-T169G stands out because of its very low $k_{cat}/(K_m-O_2)$ values imply poor oxygen affinity which is desirable for EBFCs.

Electrochemical characterization of P2O-WT

Figure 2.1 shows the electrochemical response of P2O-WT (1 mg mL^{-1}) enzyme in solution with 0.5 mM FcCOOH as an electron mediator in PBS, pH 7. The oxidation and reduction peaks were observed at 0.370 V and 0.273 V respectively vs Ag/AgCl at 10 mV s^{-1} scan rate.

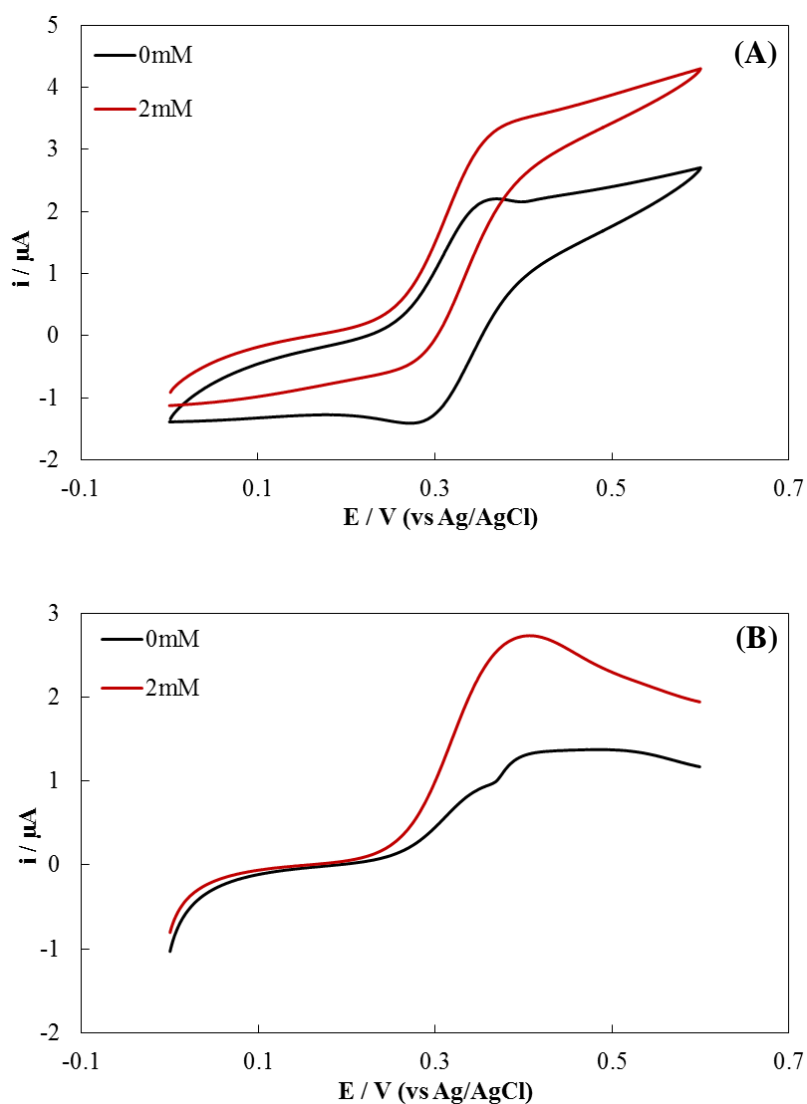


Figure 2. 1. (A) CV (scan rate: 10 mV s^{-1}) and (B) LSV (scan rate: 1 mV s^{-1}) scans of nitrogen saturated solutions with 0 mM and 2 mM concentrations of glucose added to the solution containing 0.5 mM FcCOOH and 1 mg mL^{-1} P2O-WT in PBS at pH 7. (GCE surface area: 0.071 cm^2).

The peak potentials for both oxidation and reduction processes show a typical FcCOOH electrochemical response as reported before (Fernández and Carrero, 2005). The difference in potential between the oxidation (E_{pa}) and reduction (E_{pc}) (peak separation) is 0.097 V and the peak current ratio (i_{pa}/i_{pc}) is equal to ~ 1.6 when there is no glucose is present in the solution.

The peak separation for a reversible process is given by the equation explained in Chapter 1 Section 1.3.2. In most cases when ΔE is greater than $(0.057/n)$ the process is called “quasi-reversible” and it is called “irreversible” when only a single peak is observed for one of the potential scans (Allen and Larry, 2001). However, in some processes showing slow electron processes, the peaks can be reduced in size and slightly separated (Ndlovu *et al.*, 2012).

When 2 mM glucose was added to the solution, the oxidation peak was increased and the reduction peak disappeared. The reason for this disappearance can be explained in terms of fast kinetics of the oxidative reaction when glucose is present, resulting in the ferrocene (Fc) not having sufficient time to be reduced on the electrode surface at the given scan rate. This behaviour suggests the enzyme is active for catalysing glucose oxidation and successful electron transfer from enzyme to the electrode *via* the electron transfer mediator.

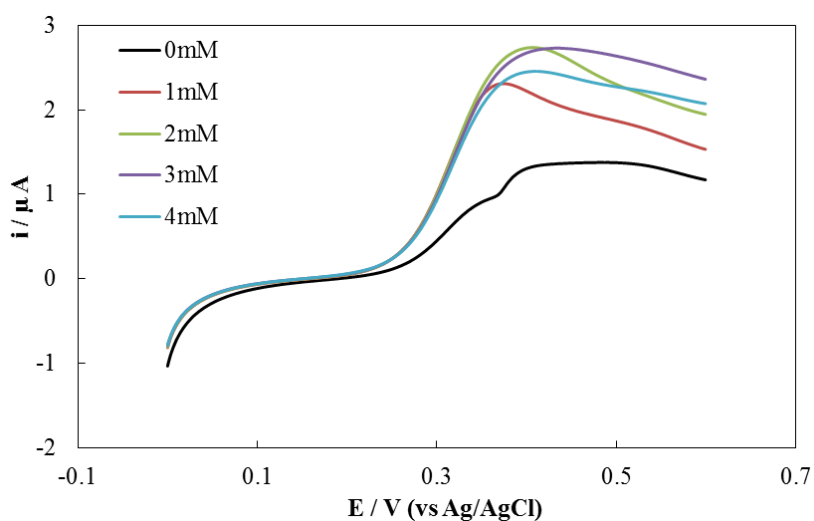


Figure 2. 2. LSV (scan rate: 1 mV s^{-1}) scans of nitrogen saturated solutions with different concentrations of glucose added to the solution containing 0.5 mM FcCOOH and 1 mg mL^{-1} P2O-WT in PBS at pH 7. (GCE surface area: 0.071 cm^2).

In the LSV results, the anodic peak was increased by 2 fold upon addition of 2 mM glucose, on the other hand it did not change much at higher concentrations than this as shown in Figure 2.2. This type of response indicates the saturation of the catalytic current response due to glucose

oxidation at the concentration of 2 mM. This saturation current might depend on the enzyme concentration as well as the glucose oxidation mechanism.

CV scans of the solution experiments with P2O-WT were performed at various scan rates from 0.5 V s^{-1} to 0.01 V s^{-1} (original data from Figure A.1 and Figure A.2 in Appendix A). Figure 2.3 shows the peak height (I_{pc}) is linearly proportional to the square root of scan rate for both 0 mM and 2 mM glucose concentrations. For a reversible diffusive system, the peak height should increase linearly with the square root of scan rate. Although the peak separation and peak current ratio data from the CV do not suggest a perfect reversible system, all the scan rates demonstrate a good degree of linearity. The effect of the glucose can be observed better at slower scan rates suggesting a slow reaction rate for the system.

It can be seen from Figure 2.3 that the slope of the resulting forward scan is proportional to the diffusion coefficient by the Randles-Sevcik equation (E.q 1.2 in Chapter 1 Section 1.3.2. Diffusion coefficient for FcCOOH was calculated as 1.78 and $0.85 \times 10^{-6} \text{ cm}^2 \text{ s}^{-1}$ for 0 mM and 2 mM glucose concentrations respectively (presented in Table 2.2). This decrease might indicate slower diffusion for FcCOOH when glucose is present in the solution because increased concentration of the total species in the solution can be affecting the diffusion of FcCOOH. As the current is increased due to the oxidation of glucose especially at lower scan rates, more FcCOOH will be diffusing to electrode at given scan rate and the diffusion of the species will be adversely affected.

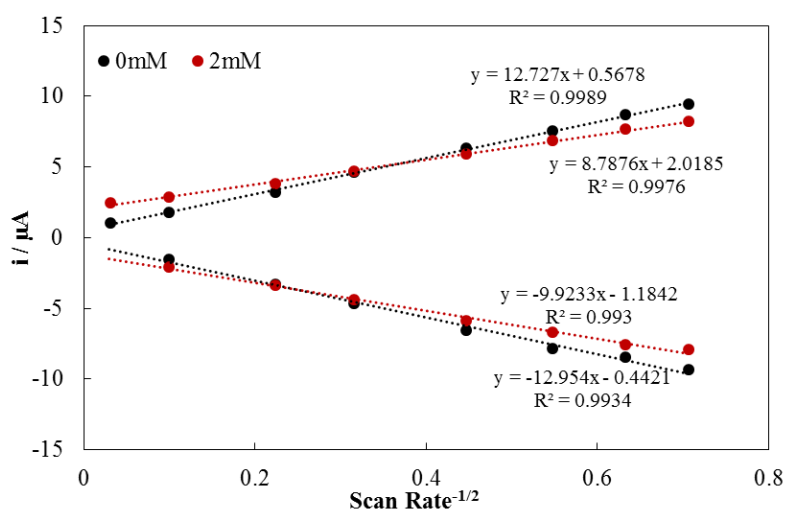


Figure 2. 3. Plot of peak heights at various scan rates for 0 mM and 2 mM concentrations of glucose added to the solution containing 0.5 mM FcCOOH and 1 mg mL^{-1} P2O-WT in PBS, at pH 7. Data obtained from Figure A.1 and Figure A.2 in Appendix A.

Electrochemical characterization of P2O-T169S

Figure 2.4 shows the electrochemical response of P2O-T169S (1 mg mL^{-1}) enzyme in solution with 0.5 mM FcCOOH as an electron mediator in PBS, pH 7.

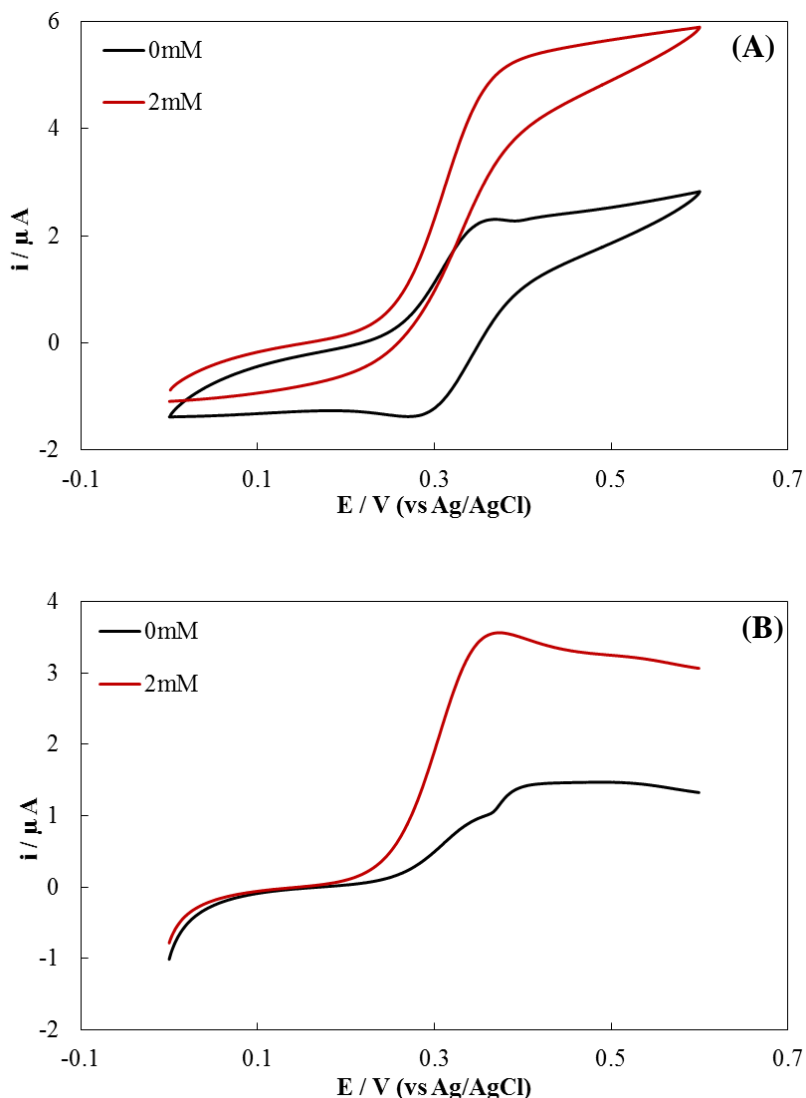


Figure 2. 4. (A) CV (scan rate: 10 mV s^{-1}) and (B) LSV (scan rate: 1 mV s^{-1}) scans of nitrogen saturated solutions with 0 mM (black) and 2 mM (red) concentrations of glucose added to the solution containing 0.5 mM FcCOOH and 1 mg mL^{-1} P2O-T169S in PBS, at pH 7. (GCE, surface area: 0.071 cm^2).

The oxidation and reduction peaks were observed at 0.366 V and 0.273 V respectively vs Ag/AgCl at 10 mV s^{-1} scan rate, the peak separation was 0.093 V and the peak current ratio (i_{pa}/i_{pc}) was equal to ~ 1.7 when there was no glucose is present in the solution. This was very similar to the results obtained from P2O-WT suggesting similar electron transfer processes.

The reduction peak disappeared upon addition of 2 mM glucose and the oxidation peak was increased. LSV scan showed that the anodic peak was increased by almost 3 fold after 2 mM glucose addition. It can be concluded for the P2O-T169S enzyme that the activity for catalysing glucose oxidation and successful electron transfer from enzyme to the electrode *via* electron transfer mediator was achieved.

The P2O-T169S enzyme also showed increased activity up to 6 mM glucose concentrations as displayed in Figure 2.5. This value is higher than that observed for P2O-WT. As it was explained before based on the values presented in Table 1.1, this kind of behaviour between these two enzymes was expected as P2O-T169S has higher rate constants for the glucose oxidation reaction.

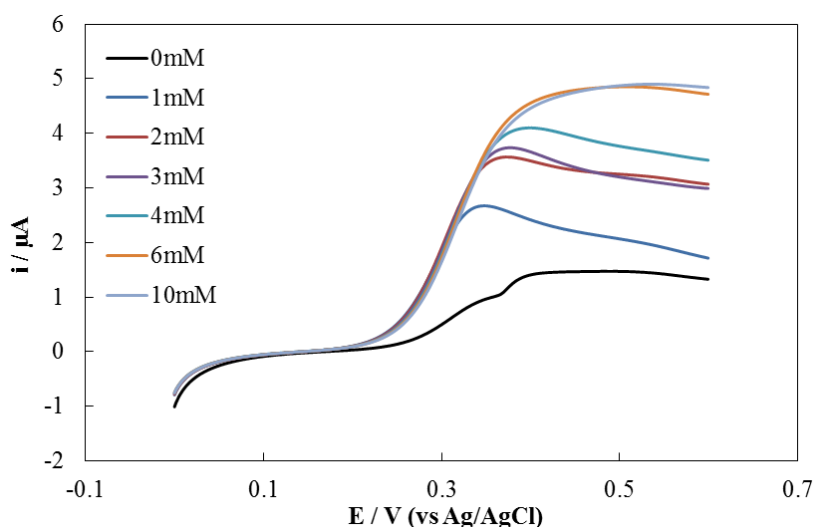


Figure 2. 5. LSV (scan rate: 1 mV s^{-1}) scans of nitrogen saturated solutions with different concentrations of glucose added to the solution containing 0.5 mM FcCOOH and 1 mg mL^{-1} P2O-T169S in PBS, at pH 7. (GCE, surface area: 0.071 cm^2).

CV scans of the solution experiments with P2O-T169S were performed at various scan rates from 0.5 V s^{-1} to 0.01 V s^{-1} (Figure A.3 and Figure A.4 in Appendix A). Figure 2.6 shows the relationship between the peak height (I_{pc}) and the square root of scan rate for 0 mM and 2 mM glucose concentrations which is similar to that of the P2O-WT enzyme.

All the scan rates demonstrate a good degree of linearity for both anodic and cathodic current peak heights. This result supports the voltammograms discussed previously. Diffusion coefficients for FcCOOH were calculated as 2.28 and $1.00 \times 10^{-6} \text{ cm}^2\text{s}^{-1}$ for 0 mM and 2 mM glucose concentrations respectively.

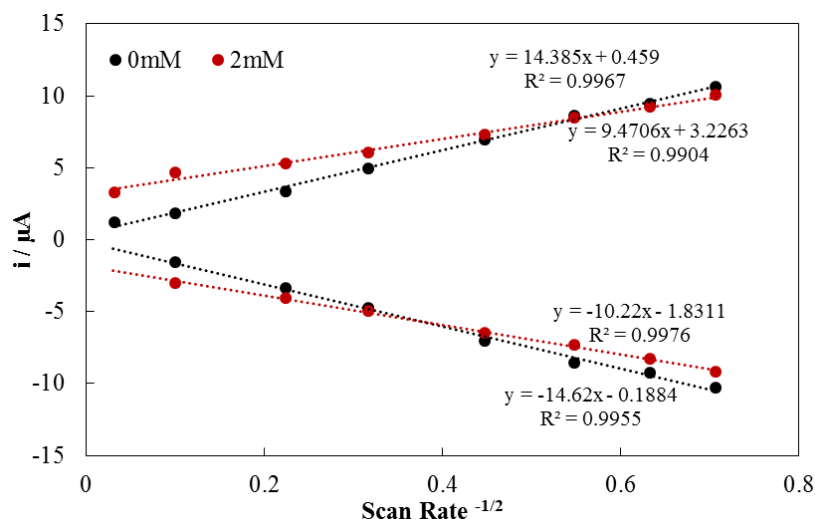


Figure 2. 6. Plot of peak heights at various scan rates for 0 mM and 2 mM concentrations of glucose added to the solution containing 0.5 mM FcCOOH and 1 mg mL⁻¹ P2O-T169S in PBS, at pH 7. Data obtained from Figure A.3 and Figure A.4 in Appendix A

The relationship between the catalytic current and the concentration of glucose can yield information about the enzyme substrate kinetics especially when the enzyme is responsive to increasing additions of glucose. (Thevenot *et al.*, 1999). The apparent Michaelis-Menten constant K_m represents the analyte concentration yielding a response equal to half of its maximum value for infinite substrate concentration (Thevenot *et al.*, 1999). The K_m value can be calculated using Lineweaver-Burk equation:

$$\left(\frac{1}{i}\right) = \left(\frac{K_m}{i_{max}}\right)\left(\frac{1}{C}\right) + \left(\frac{1}{i_{max}}\right) \quad (\text{Eq. 2. 3})$$

where; i and i_{max} and C represent the steady state current, maximum current and glucose concentration, respectively. Figure 2.7 shows the plot of $1/i$ versus $1/C$ that gives a straight line with a slope equal to K_m/i_{max} and intercept to $1/i_{max}$.

Substituting values for intercept and slope in the equation gave the value of 0.91 mM for K_m . This value is close to the value of 1.7 mM presented before calculated using steady state kinetic assays (Pitsawong *et al.*, 2010). The reason of the shift from the linearity of the Lineweaver-Burk plots could also be due to mass transport or kinetic limitations caused by the electron

transfer mechanism between the enzyme/mediator and mediator/electron systems (Uang and Chou, 2003).

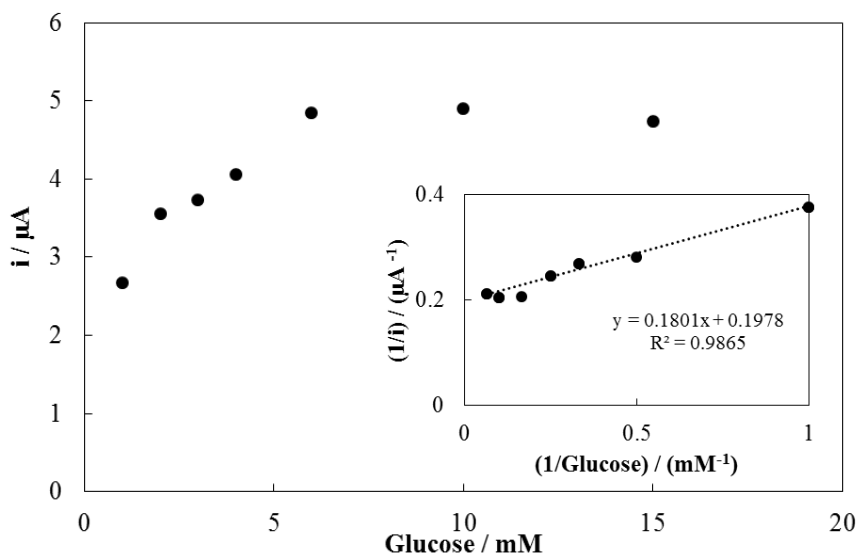


Figure 2.7. The relationship between peak catalytic current and glucose concentration for P2O-T169S. Inset: Lineweaver-Burk plot.

Electrochemical characterization of P2O-T169G

Figure 2.8 shows the electrochemical response of the P2O-T169G (1 mg mL^{-1}) enzyme in solution with 0.5 mM FcCOOH as an electron mediator in PBS, pH7. The oxidation and reduction peaks were observed at 0.374V and 0.277V vs Ag/AgCl at 10 mV s^{-1} scan rate respectively, the peak separation is 0.097 V and the peak current ratio (i_{pa}/i_{pc}) is equal to ~ 1.7 when there is no glucose is present in the solution. This is also very similar to the results obtained from P2O-WT and P2O-T169S.

P2O-T169G also demonstrated a very similar catalytic current response after 2 mM glucose addition. LSV scans also showed that the anodic peak was increased 1.63 fold after 2 mM glucose addition which as anticipated was smaller than both P2O-WT and P2O-T169S. However, P2O-T169G demonstrated activity for catalysing glucose oxidation and successful electron transfer from enzyme to the electrode *via* electron transfer mediator.

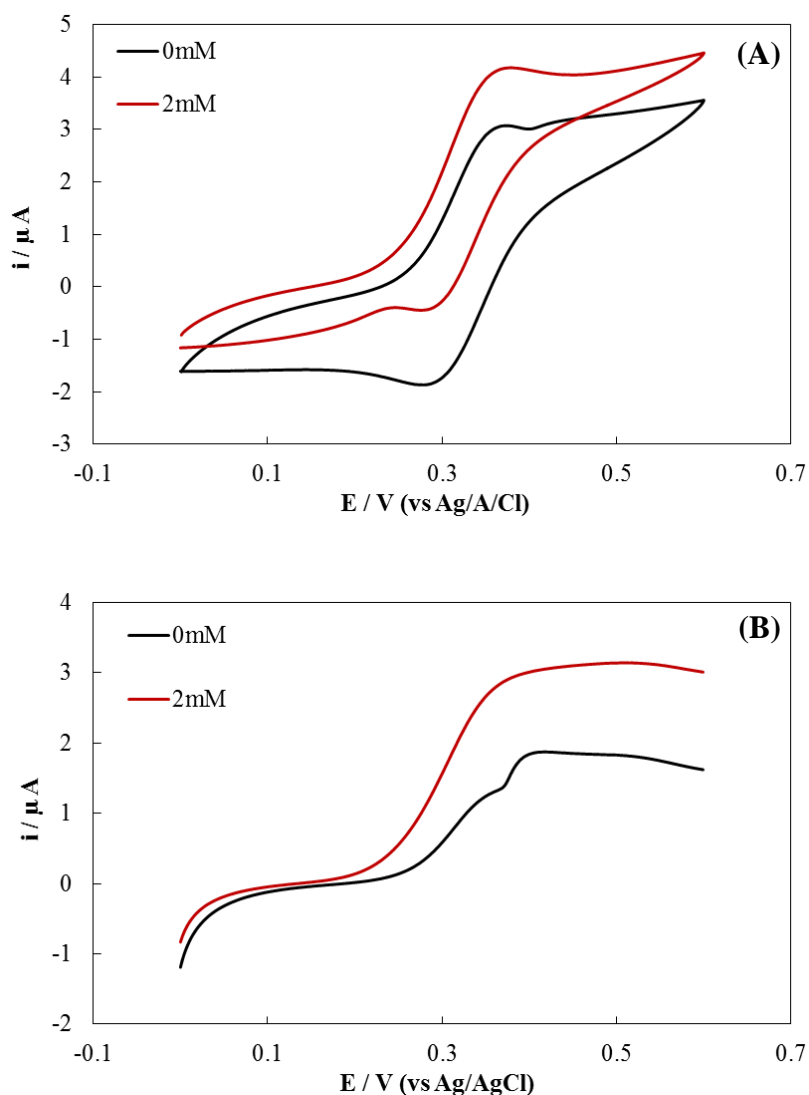


Figure 2. 8. (A) CV (scan rate: 10 mV s^{-1}) and (B) LSV (scan rate: 1 mV s^{-1}) scans of nitrogen saturated solutions with 0 mM (black) and 2 mM (red) concentrations of glucose added to the solution containing 0.5 mM FcCOOH and 1 mg mL^{-1} P2O-T169G in PBS at pH 7. (GCE surface area: 0.071 cm^2).

Figure 2.9 shows that the P2O-T169G enzyme also showed increasing activity for up to 6 mM glucose concentrations. It is interesting to note that the catalytic current response of P2O-T169G is very similar to P2O-T169S although it has lower reaction rate constant. However, as discussed before, the glucose binding mechanism of P2O-T169G was reported to be different than that for the wild type and P2O-T169S. It should also be noted that, although the saturation concentrations are similar, the catalytic current response did not reach the same high values as P2O-T169S.

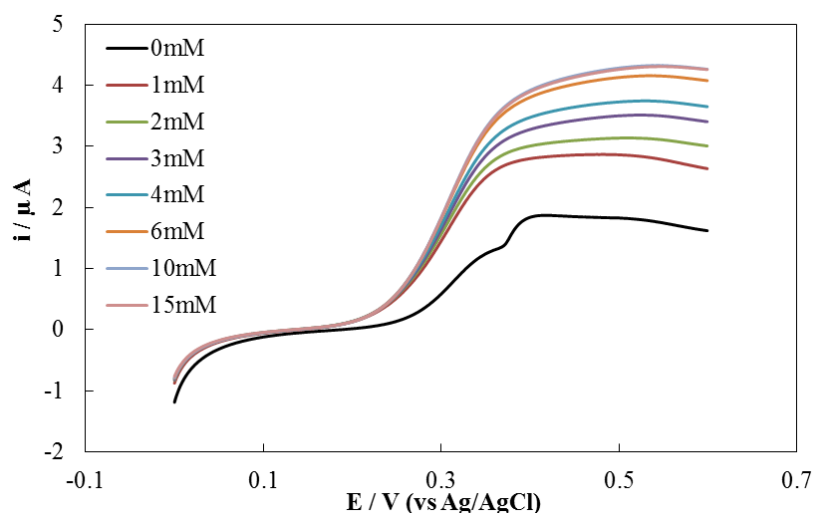


Figure 2. 9. LSV (scan rate: 1 mV s^{-1}) scans of nitrogen saturated solutions with different concentrations of glucose added to the solution containing 0.5 mM FcCOOH and 1 mg mL^{-1} P2O-T169G in PBS at pH 7. (GCE surface area: 0.071 cm^2).

CV scans of the solution experiments with P2O-T169G were performed at various scan rates from 0.5 V s^{-1} to 0.01 V s^{-1} (Figure A.5 and Figure A.6 in Appendix A). The relationship between the peak height (I_{pc}) and the square root of scan rate for 0 mM and 2 mM glucose concentrations can be seen in Figure 2.10.

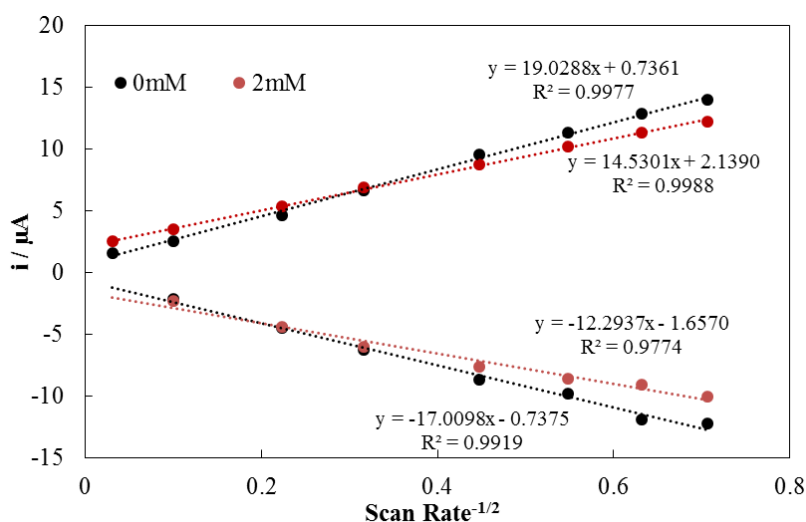


Figure 2. 10. Plot of peak heights at various scan rates for 0 mM and 2 mM concentrations of glucose added to the solution containing 0.5 mM FcCOOH and 1 mg mL^{-1} P2O-T169G in PBS, at pH 7. (GCE, surface area: 0.071 cm^2). Data obtained from Figure A.5 and Figure A.6 in Appendix A

The behaviour observed for P2O-T169G was similar to that observed for P2O-WT and P2O-T169S. Experimental data indicates a good degree of linearity with oxidation and reduction current peak heights. The diffusion coefficients for FcCOOH calculated using (Eq. 1.2) were 3.98 and $2.32 \times 10^{-6} \text{ cm}^2 \text{ s}^{-1}$ respectively for 0 mM and 2 mM glucose concentrations.

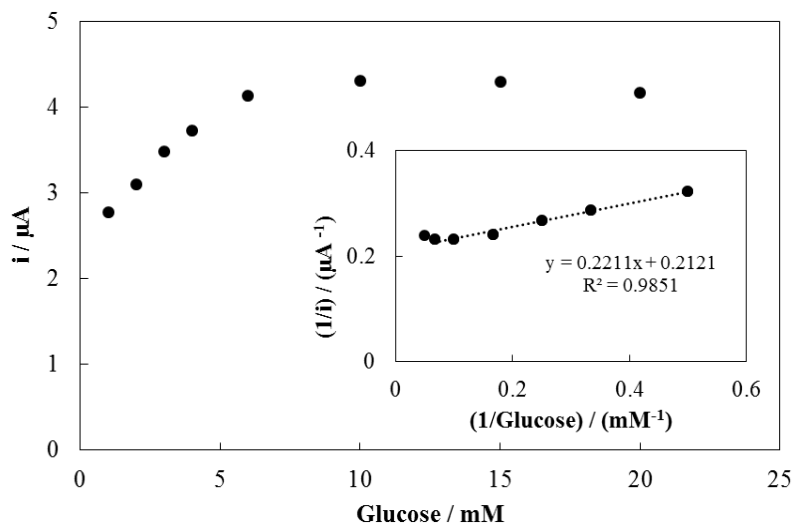


Figure 2. 11. The relationship between peak catalytic current and glucose concentration for P2O-T169G. Inset: Lineweaver-Burk plot.

Figure 2.11 shows the plot of $1/i$ versus $1/C$ that gives a straight line with a slope equal to K_m/i_{\max} and intercept to $1/i_{\max}$. According to the intercept and the slope of the equation, K_m was estimated to be 1.04 mM . It is very similar to the previously reported value of 0.9 mM was calculated using steady state kinetic assays although the electrochemical method has a R^2 value of 0.98506 (Pitsawong *et al.*, 2010).

Comparison between P2O enzymes

Figure 2.12 shows the electrochemical response of the P2O-WT, P2O-T169S and P2O-T169G enzymes each in solutions of 0.5 mM FcCOOH as an electron mediator in PBS at pH 7 in the presence of 2 mM glucose concentration. The data is presented in terms of relative increase from 0 mM glucose concentration to demonstrate the increase from background current (Raw data is presented in Figure A.7 in Appendix A). The data shows that P2O-T169S has the highest relative difference response towards glucose.

Both mutants P2O-T169G and P2O-T169S demonstrated a similar response in terms of where the catalytic current responses start around 0.2 V ; the start potential (of oxidation) was slightly

higher for the P2O-WT at 0.25 V. This could be due to role of Thr¹⁶⁹ position and its effect in the binding mechanism for the glucose oxidation by P2O (Pitsawong *et al.*, 2010). The P2O-WT showed the same peak current with P2O-T169G, but it also showed a decreased current in the mass transport region. On the other hand, P2O-T169G was not as affected as by mass transport as P2O-WT or P2O-T169S. This kind of behaviour could be related to the hemo-tetrameric structure of the enzyme.

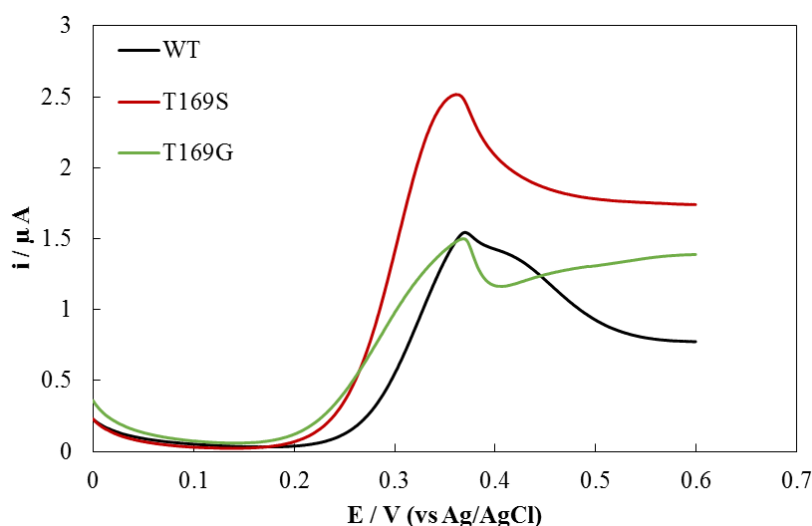


Figure 2. 12. LSV (scan rate: 1 mV s^{-1}) scans of nitrogen saturated solutions with 2 mM concentrations of glucose added to the solution containing 0.5 mM FcCOOH and 1 mg mL^{-1} concentrations of P2O-WT, P2O-T169S and P2O-T169G at pH 7. (GCE surface area: 0.071 cm^2 and 0 mM concentration data is subtracted from 2 mM concentration data).

The electrochemical behaviour during CV experiments of the three different P2O enzymes have been summarised in Table 2.2. The enzymes showed similar E_{pa} and E_{pc} values. The peak current ratios were ca 1.7 for all enzymes. However, the values are all higher than the theoretical value of 0.059 V, this may be an indication of the quasi-reversible process.

LSV results showed that the increase of catalytic current, upon addition of glucose, from 0 mM to 2 mM was different for each enzyme. With P2O-T169S showing the highest increase (3 fold) from 0 mM glucose concentration to 2 mM followed by P2O-WT (2 fold) and P2O-T169G (1.6 fold). These results quasi match the results presented in Figure 2.12.

Enzyme	E_{pa} / V	E_{pc} / V	$\Delta E / V$	I_{pa}/I_{pc}
P2O – WT	0.370	0.273	0.097	1.6
P2O – T169S	0.366	0.273	0.093	1.7
P2O – T169G	0.374	0.273	0.097	1.7

Table 2. 2. The electrochemical behaviour of the P2O enzymes used in solution CV experiments. Tested in nitrogen saturated solutions containing 0.5 mM FcCOOH and 1 mg mL⁻¹ concentrations of P2O-WT, P2O-T169S and P2O-T169G at pH 7. (GCE surface area: 0.071 cm², E_{pa} : anodic peak potential, E_{pc} : cathodic peak potential).

Figure 2.13 shows the effect of oxygen on the performance of the P2O mutants in solution. It can be seen that when oxygen is present in the solution it affects the P2O-T169S enzyme remarkably (~34 % decrease in the current), but not so much for the P2O-T169G (~10%). This matches the $k_{cat}/(K_m-O_2)$ values presented in Table 2.1 (8.1 and 0.8 mM⁻¹ s⁻¹ for P2O-T169S and P2O-T169G respectively). After reaching the peak potential the current did not decrease for P2O-T169G, however, it changed by 15-20 % for P2O-T169S in both nitrogen and air saturated conditions. This is an important outcome regarding the enzyme behaviour in the mass-transport region.

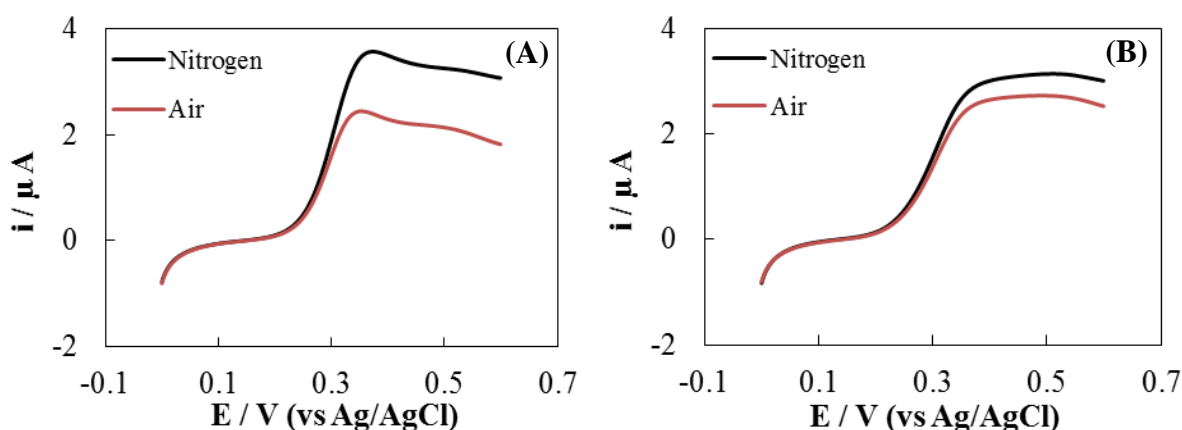


Figure 2. 13. LSV (scan rate: 1 mV s⁻¹) scans of (A) P2O-T169S and (B) P2O-T169G (both concentrations are 1 mg mL⁻¹ in PBS) in nitrogen and air saturated solutions with 2 mM concentrations of glucose added to the solution containing 0.5 mM FcCOOH in PBS at pH 7. (GCE surface area: 0.071 cm²).

This behaviour of P2O-T169G might not be as affected by mass transport limitations as T169S. This could be an important attribute for P2O-T169G in biofuel cell applications as an alternative enzyme (P2O-WT shows no difference at 2 mM glucose probably because it is the saturation glucose concentration). However, the 1 mM glucose result shows remarkable difference when air is applied as displayed in Figure A.8 in Appendix A).

Enzyme	Diffusion coefficient of FcCOOH / $\text{cm}^2 \text{s}^{-1} \times 10^{-6}$	
	0 mM	2 mM
P2O – WT	1.78	0.85
P2O –T169S	2.28	1.00
P2O – T169G	3.98	2.32

Table 2. 3. Calculated diffusion coefficients for P2O enzymes using Randles-Sevcik equation at different glucose concentrations.

Table 2.3 presents diffusion coefficients calculated using Randles-Sevcik equation for FcCOOH when used with P2O enzymes at different glucose concentrations. These values are within the range of previously reported values of $5.73 \times 10^{-6} \text{ cm}^2 \text{ s}^{-1}$ for FcCOOH when used with GOx; a widely employed enzyme in EBFCs from CV experiments (Bartlett and Pratt, 1995).

The diffusion coefficients of the enzymes were decreased upon addition of glucose in all cases following the trend of P2O-WT < P2O-T169S < P2O-T169G. The diffusion coefficient was expected to be lower in the presence of glucose as more species in the solution would affect the FcCOOH being a diffusive mediator. P2O-T169G has the highest value implying better diffusivity, adds weight to results showing it to be least affected enzyme in the mass transport limited region of operation.

2.3.2. Electrochemical characterization of Glucose Oxidase in solution and comparison with P2O enzymes

Figure 2.14 shows the electrochemical response of the GOx enzyme in solution with 0.5 mM FcCOOH as an electron mediator in PBS, pH 7. The anodic and cathodic peaks were observed at 0.366 V and 0.270 V respectively vs Ag/AgCl at 10 mV s^{-1} scan rate, the peak separation

was 0.096 V and the current peak ratio (i_{pa}/i_{pc}) was ~ 1.6 when no glucose was present in the solution.

This is very similar to results obtained with the P2O enzymes indicating P2O enzymes show similar behaviour in electrochemical systems to GOx. The response of GOx upon addition of 2 mM glucose was also similar to P2O enzymes with the reduction peak disappearing and the oxidation peak was increasing. Also, LSV scans showed that the oxidation peak was increased 3.3 fold after 2 mM glucose addition which is around the value obtained for P2O-T169S.

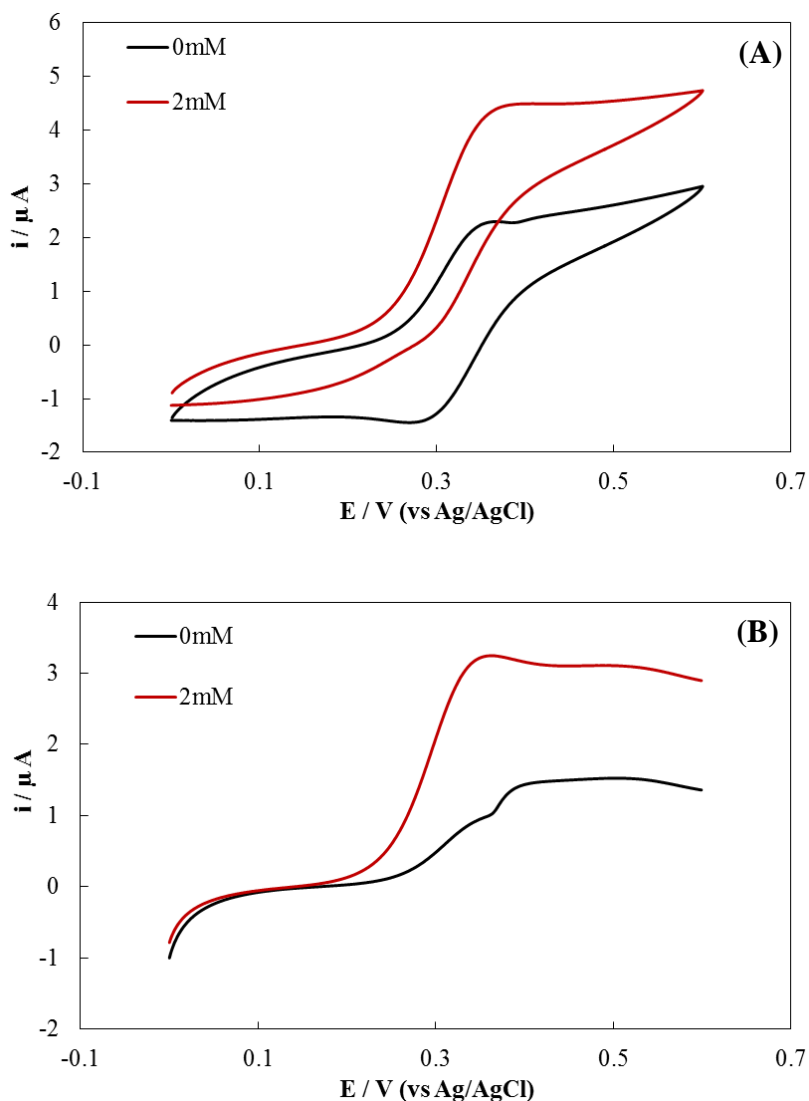


Figure 2. 14. (A) CV (scan rate: 10 mV s^{-1}) and (B) LSV (scan rate: 1 mV s^{-1}) scans of nitrogen saturated solutions with 0 mM (black) and 2 mM (red) concentrations of glucose added to the solution containing 0.5 mM FcCOOH and 1 mg mL^{-1} GOx in PBS at pH 7. (GCE surface area: 0.071 cm^2).

GOx also showed increasing activity for up to 15 mM glucose concentrations (Figure A.9 in Appendix A) which is higher than any of the P2O enzymes. This can be explained by differences in enzyme activities for every mg of enzyme in solution. Although the enzyme concentrations were same (1 mg mL^{-1}), GOx has higher activity for every mg of enzyme. The catalytic current response toward glucose starts around 0.2 V which is similar to P2O-T169S and P2O-T169G whereas the GOx oxidation peak current reached $3.2 \mu\text{A}$ in LSV at 2 mM glucose. This is ~ 1.2 fold higher than P2O-T169S in LSV at 2 mM glucose.

CV scans of the solution experiments with GOx were carried out at various scan rates from 0.5 V s^{-1} to 0.01 V s^{-1} (Figure A.10 and Figure A.11 in Appendix A). Figure 2.15 indicates the relationship between the peak height (I_{pc}) and the square root of scan rate for 0 mM and 2 mM glucose concentrations. Similarly, results show a good degree of linearity for P2O enzymes against oxidation and reduction current peak heights.

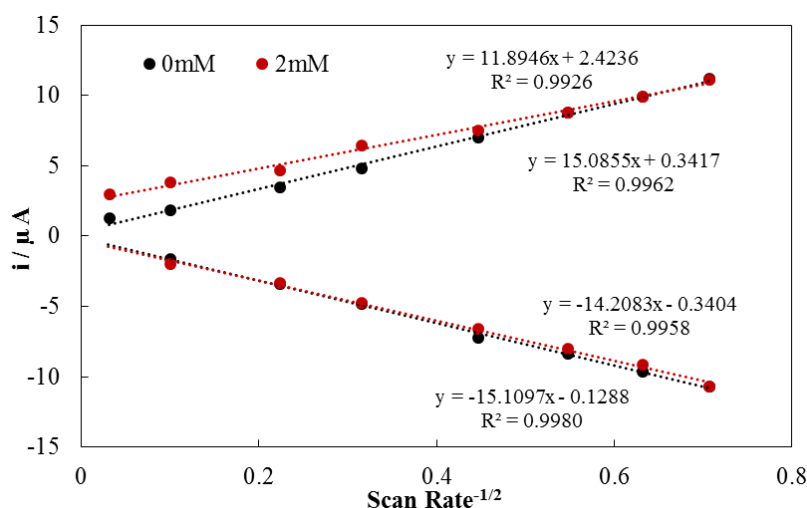


Figure 2. 15. Plot of peak heights at various scan rates for 0 mM and 2 mM concentrations of glucose added to the solution containing 0.5 mM FcCOOH and 1 mg mL^{-1} GOx in PBS at pH 7. (GCE surface area: 0.071 cm^2). Data obtained from Figure A.10 and Figure A.11 in Appendix A.

Diffusion coefficients for FcCOOH with GOx were calculated to be 2.5 and $1.6 \times 10^{-6} \text{ cm}^2 \text{ s}^{-1}$ for 0 mM and 2 mM glucose concentrations respectively. As previously mentioned these are also in the same region as previously published values for FcCOOH when used with GOx ($5.73 \times 10^{-6} \text{ cm}^2 \text{ s}^{-1}$) (Bartlett and Pratt, 1995).

Figure 2.16 shows the plot of $1/i_{ss}$ versus $1/C$ that gives a straight line with a slope equal to K_m/i_{max} and intercept to $1/i_{max}$. From the intercept and slope of the graph, K_m was estimated to be 2.95 mM. The K_m value of GOx has been published in literature through data mainly acquired using immobilised electrodes and therefore hard to compare with solution experiments.

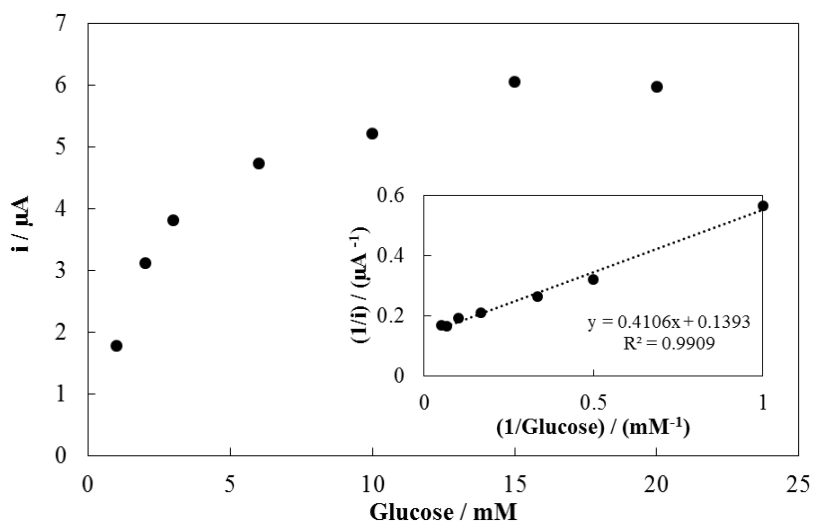


Figure 2. 16. The relationship between peak catalytic current and glucose concentration for GOx. Inset: Lineweaver-Burk plot.

Enzyme	K_m from this study / mM	K_m reported in literature / mM
P2O –T169S	0.91	1.7 (Pitsawong <i>et al.</i> , 2010)
P2O – T169G	1.04	0.9 (Pitsawong <i>et al.</i> , 2010)
GOx	2.95	1.5 -27 (Rogers and Brandt, 1971; Qiu <i>et al.</i> , 2009; Fatoni <i>et al.</i> , 2013; Du Toit and Di Lorenzo, 2014)

Table 2. 4. Summary of K_m values for the enzymes used

K_m values for P2O-T169S and P2O-T169G can be used to measure the affinity between the enzymes and glucose where high K_m values are indicative of weak affinity (Sekretaryova, 2014). For the solution experiments comparing the K_m values can help us to understand the affinities of the enzymes used towards glucose. Table 2.4 summarises the K_m values calculated

in this study and reported in literature for P2O mutant enzymes and GOx. The K_m value for P2O-T169S was similar to that of P2O-T169G (0.91 mM *versus* 1.04 mM). The K_m values of 1.7 mM and 0.9 mM reported previously from steady-state kinetic experiments (Pitsawong *et al.*, 2010) for the P2O-T169S and P2O-T169G, are similar to those obtained electrochemically, but with P2O-T169S showing slightly better affinity in the electrochemical system.

The reported values of K_m for GOx show wide range of values from 1.5 mM to 27 mM (Rogers and Brandt, 1971; Qiu *et al.*, 2009; Fatoni *et al.*, 2013; Du Toit and Di Lorenzo, 2014). The value of 2.95 mM for GOx is ~ 3 fold higher than the values calculated for P2O-T169S and P2O-T169G in this study showing P2O mutants have greater affinity towards glucose when compared to GOx which is an essential discovery when considering the use of P2O enzymes for biofuel cell applications.

Effect of oxygen for glucose oxidation with P2O-T169G

To compare the effect of oxygen, chronoamperometry was carried out between the widely used enzyme GOx and the oxygen resistant mutant P2O-T169G. Experimental conditions were the same as for the voltammogram experiments and the duration of the experiments were 1 h (Figure 2.17) and 3 h long (Figure 2.18).

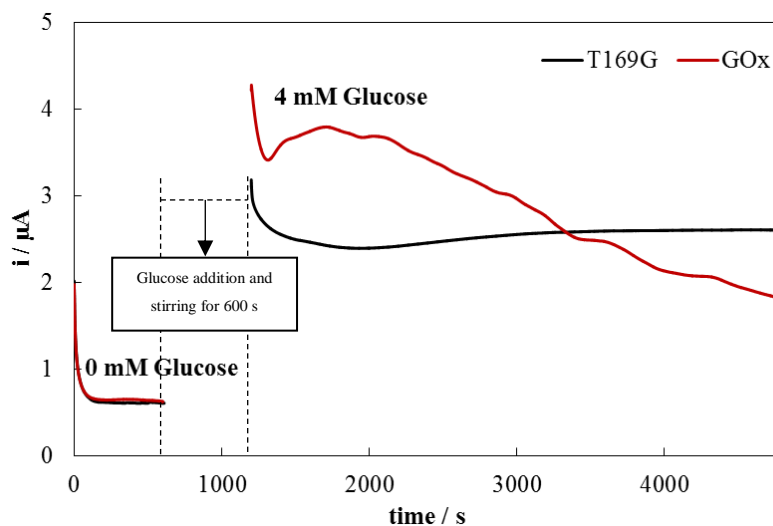


Figure 2. 17. CAs (1 h length) of air saturated solutions for GOx and P2O-T169G (both 1 mg mL⁻¹) at 0.350 V for 0 mM and 4 mM concentrations of glucose added to the solution containing 0.5 mM FcCOOH, at pH 7. (GCE, surface area: 0.071 cm²).

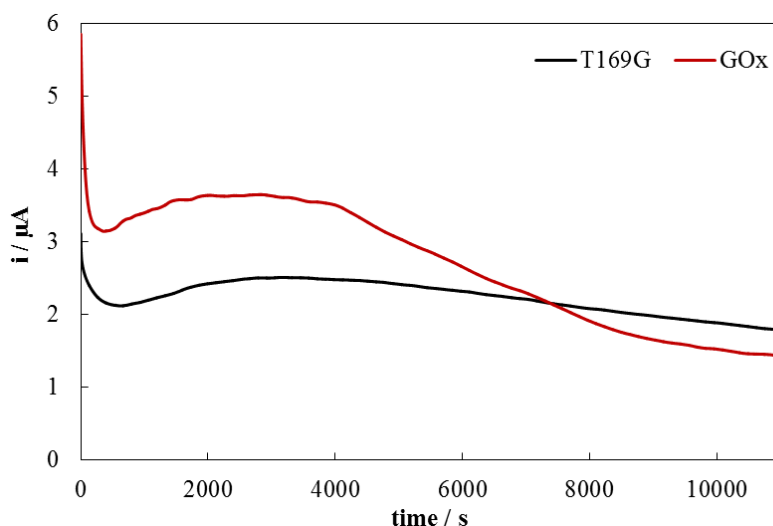


Figure 2. 18. CAs (3 h length) of air saturated solutions for GOx and P2O-T169G (both 1 mg mL⁻¹) at 0.350 V for 4 mM concentration of glucose added to the solution containing 0.5 mM FcCOOH, at pH 7. (GCE, surface area: 0.071 cm²).

In the short (1 h) CA experiments, where no glucose is present in solution, the current lost ~67 % and ~70 % of its initial value and stabilised within few min for GOx and P2O-T169G respectively while the presence of oxygen did not significantly alter the current. After the addition of 4 mM glucose, the current showed a sharp drop from its initial value and then reached a plateau. By looking at the difference in current density between the plateau region and at the end of 1 hr, GOx shows a ~53 % drop under air-saturated conditions while there is no remarkable change for P2O-T169G.

Although the current value for P2O-T169G was initially lower than that for GOx in line with voltammogram experiments, the current value for P2O-T169G remained higher than GOx after 1 h. It was deduced that the net current difference at the end of 1 hr between GOx and P2O-T169G was 0.8 μA with P2O-T169G having 1.45 fold higher current. This demonstrates that the effect of oxygen on the performance of P2O-T169G is low, whereas it causes a significant performance loss for GOx. (The raw data for both enzymes were presented in Figure A.12 and Figure A.13 in Appendix A). Figure 2.18 shows the behavior of enzymes with 4 mM glucose concentration over 3 h. As with the 1 h CA experiments, the differences in current values were calculated from the plateau to the end of the 3 h. The change in current density under air saturated conditions for GOx was ~61%, whereas it was ~28 % for P2O-T169G. Also, the net current difference at the end of 3 hrs between GOx and P2O-T169G was ~21 %.

P2O-T169G was not affected from the presence of oxygen as much as GOx as confirmed by 1 h and 3 h stability experiments. Although ~28 % of its initial current density was lost during the 3-hrs, this loss was observed both in air and nitrogen saturated conditions suggesting that oxygen is not the reason for the decreased current (Figure A.14 in Appendix A). This could be because a consequence of it being in solution as it is known that enzymes are very instable when used in solution (Wu *et al.*, 2015). In contrast, it was observed that GOx lost more of its current under air saturated conditions (Figure A.15 in Appendix A). The results from 1-hr and 3-hrs experiments show that P2O-T169G could be a good alternative to GOx because of its good stability and oxygen resistance.

2.4. Conclusions

In this chapter, the performance and the feasibility of P2O enzymes have been investigated for EBFCs using solution experiments (enzyme free in solution and not immobilised on electrode). The electrochemical tests showed P2O activity for catalysing glucose oxidation and successful electron transfer from enzyme to the electrode *via* an electron transfer mediator FcCOOH.

P2O enzymes showed similar electrochemical behaviour between each other and commercial GOx with P2O-T169S exhibiting the highest catalytic current response. P2O-T169S and P2O-T169G also had higher glucose saturation concentrations than the wild type enzyme. Also the affinities of P2O-T169S and P2O-T169G towards glucose was found to be better than GOx which is an important consideration for EBFCs. Voltammograms showed that the current response of P2O-T169G in the region of mass transport limitations was better than other enzymes.

The oxygen resistance and its effect on stability of the enzymes has been tested with P2O-T169G showing a very good resistance against oxygen. The decrease in current for P2O-T169G was found to be only ~10% whereas it was ~34% for P2O-T169S when oxygen was present in the solution (shown from LSV data). Further stability experiments have been carried out to compare the promising performance of P2O-T169G with GOx. The results showed that oxygen had negligible effect on P2O-T169G activity with oxygen (10%), whereas GOx lost ~53% and ~61% of its current in short and long stability experiments respectively. This is very important finding for P2O-169G which recommends this enzyme as an alternative for GOx.

These results are similar to the results reported based on steady-state kinetic experiments, therefore electrochemical validation of the values in literature was achieved. In conclusion, this

study suggests that P2O-T169G could be an alternative to GOx by virtue of its good oxygen resistance and stability in EBFC applications. Using enzymes in solution, however, is not practical. If used in immobilised systems, performance and long-term stability of EBFCs could be even greater enhanced. Further studies on enzyme electrode with immobilised enzymes for glucose oxidation and EBFCs are discussed in Chapter 3 and Chapter 4.

Chapter 3. Immobilization of Mutant P2O and GOx on Pyrenyl Carbon Structures for Glucose Oxidation

In this chapter, immobilization onto an electrode of the oxygen resistant mutant P2O-T169G was carried out and compared with glucose oxidase (GOx) using electrochemical characterization techniques. In the first part, enzymes were immobilised on carbon surface by crosslinking on pyrenyl carbon structures and ferrocene carboxylic acid (FcCOOH) was used as an electron mediator in solution. This was followed by immobilization of both enzyme and mediator using a novel immobilization technique, in which, a mixture of ferrocene (Fc), nafion[®] and multi-walled carbon nanotube (MWCNT) was coated on electrode surface, followed by an electrochemical treatment where enzymes were crosslinked on pyrenyl carbon nanostructures. The Fc-Nafion-MWCNTs electrode was optimized using voltammetry and the morphology of the electrode was investigated by scanning electron spectroscopy (SEM). The performance of the oxygen resistant P2O-T169G was compared with GOx in terms of electrochemical activity, glucose affinity and effect of oxygen on enzyme performance and stability. Enzymatic electrodes demonstrated enhanced current values compared to solution studies when immobilised on electrode surface. The Michaelis-Menten constant, K_m values of 0.68 mM and 0.17 mM for P2O-T169G and GOx, respectively, suggest good affinity towards glucose for both of the enzymes. Finally, P2O-T169G showed promising performance especially in terms of stability.

3.1. Introduction

One of the most important aspects for enzymatic electrode fabrications is stability because enzymes are very sensitive to environmental conditions because of their intrinsic nature (Yang *et al.*, 2012). Immobilization matrixes might solve this problem by protecting the biological species from environmental effects and result in more efficient and stable performance (Yang *et al.*, 2012). Immobilization can also achieve high density of enzymes on electrode surfaces providing enhancement in performance and improved electron transfer kinetics (Shuler *et al.*, 1986; Cooney *et al.*, 2008).

There are different ways of constructing enzyme electrodes for enzymes and mediators including physical and chemical methods in which the electrode material is a crucial aspect. Some of the most widely used processes are basic physical adsorption, covalent attachment, crosslinking, wiring and entrapments in polymeric gels (Cooney *et al.*, 2008; Hao Yu and Scott,

2010; Ivanov *et al.*, 2010). All techniques have their specific advantages and disadvantages based on the applications employed.

The use of Fc and its derivatives as redox mediators between enzymes and electrodes have been very popular (Li *et al.*, 1997; Miao *et al.*, 2001; Razumien *et al.*, 2003; Kase and Muguruma, 2004). This is because ferrocene/ferrocinium (Fc/Fc⁺) can replace O₂ in the reaction as explained in Chapter 2.1, eq. 2.2. because it's a good electron acceptor (Cass *et al.*, 1984; Ghica and Brett, 2005). The diffusive feature of Fc makes it very attractive as a mediator because it can shorten the electron transfer distance (Bartlett and Pratt, 1995). One of the first reports about electron transfer based on mediators demonstrated that Fc and its different derivatives are efficient electron acceptors for enzymes such as glucose oxidase (Cass *et al.*, 1984).

Some of the most important properties of Fc and its derivatives can be summarized as easy derivatization, fast electron transfer kinetics and stable structure either in oxidized or reduced state (Harper and Anderson, 2010). Fc was also suggested as a possible dietary iron supplement ('haematinic') at appropriate doses in humans (Stepnicka, 2008) which is important as biomedical applications requires biocompatibility. Fc molecule is known to be insoluble in water, however, some of its derivatives such as FcCOOH are water soluble due to having the carboxylic acid group (O'Gorman, 1998). FcCOOH could be a good alternative to Fc in the applications of redox reactions in aqueous media. There is, however, a need for immobilizing Fc onto electrodes for enzyme-mediator immobilised systems in biomedical applications.

Polymeric materials are widely used in fabricating enzyme electrodes for biosensor and biofuel cell applications (Sarma *et al.*, 2009; Wang *et al.*, 2009b). It is possible to use different polymeric materials for many different purposes such as mediation of electrons, ion-selective membranes or in the form of polymer matrixes for entrapment of proteins (Yang *et al.*, 2012). The most widely used polymers can be listed as nafion[®], chitosan, poly-pyrrole polyaniline, polyphenol, poly-thiophene, poly-1,3-phenylenediamine, polyvinyl pyridine, polyvinyl alcohol, polycarbonate, and nylon (Haccoun *et al.*, 2006; Linford and Schlindwein, 2006; Zheng *et al.*, 2006). Early studies about Fc mediated enzyme electrodes had low stability as they were suffering from enzyme leaching or denaturation (Brooks *et al.*, 1988).

Different configurations utilising Fc with polymeric materials have been studied to overcome the problems of Fc mediated enzyme electrodes. The encapsulating method uses conducting polymers such as polypyrrole (Fiorito and Torresi, 2001; Vidal *et al.*, 2002), polyphenols

(Nakabayashi *et al.*, 1998) or cellulose acetate membranes (Tkáč *et al.*, 2002). Chitosan, for instance, was used with Fc in a “sandwich” configuration followed by the immobilization of GOx using glutaraldehyde (Miao *et al.*, 2001). Fc was also entrapped in polyacrylamide-based redox hydrogels (Bu *et al.*, 1998) or in sol-gel materials (Li *et al.*, 1997; Bu *et al.*, 1998; Yang *et al.*, 2003) to obtain efficient enzymatic electrodes. Among all different methods, crosslinking of Fc to polymers such poly-ethylenimine (PEI) (Merchant *et al.*, 2007), utilising single-walled (Nazaruk *et al.*, 2010) or multi-walled carbon nanotubes (Qiu *et al.*, 2009) and also mixture of PEI with MWCNTs (Arribas *et al.*, 2007; Rubianes and Rivas, 2007; Laschi *et al.*, 2008; Yan *et al.*, 2008) and SWCNTs (Tran *et al.*, 2011) have also been reported for amperometric glucose detection. Enzyme leaching from the polymer films, on the other hand, still is a concern especially for continuous monitoring systems or biofuel cells requiring long operational times.

Among all other polymers used in the field, nafion[®], a perfluorosulfonic acid cation-exchange polymer, can be used as a protective and encapsulating material in the fabrication of enzyme electrodes (Harkness *et al.*, 1993). Nafion[®] consists of a hydrophilic and hydrophobic phase (Vishnyakov and Neimark, 2001). Water can be adsorbed into these two domains with ion conductivity taking place in the hydrophilic phase (Blake *et al.*, 2005). Nafion[®] has many advantages for its use in enzymatic electrode fabrication summarised as: excellent ion conduction properties (Moore *et al.*, 2004), biocompatible interface and compatibility with mammalian tissue (essential for implantable medical applications) (Turner *et al.*, 1990), hydrophilic and hydrophobic properties, being chemically inert, and exhibiting long-term chemical stability due to its polytetrafluoroethylene (PTFE) backbone (Blake *et al.*, 2005).

Incorporating Fc with nafion[®] in polymeric films is a straightforward method for amperometric glucose detection (Chen *et al.*, 1992; Dong *et al.*, 1992; Harkness *et al.*, 1993; Brown and Luong, 1995; Vaillancourt *et al.*, 1999). Fc containing nafion[®] polymer films can be applied to enzymatic electrode fabrication in many ways. The attachment of the enzymes to the surface of a nafion[®] modified electrode (Dong *et al.*, 1992), electro-polymerizing a conducting polymer or Fc derivative on nafion[®]-enzyme electrode (Brown and Luong, 1995) or casting enzyme solution before the nafion[®] layer to trap the enzyme (Ghica and Brett, 2005; Mani *et al.*, 2013) and entrapping the enzyme within the nafion[®] polymer (Harkness *et al.*, 1993; Vaillancourt *et al.*, 1999) have been previously reported to utilise Fc and nafion[®] with enzymes for fabrication of enzyme electrodes. When used in enzymatic systems nafion[®] content plays essential role in deactivation of the enzymes because of its acidic nature (Karyakin *et al.*, 1996; Moore *et al.*,

2004). Solutions of nafion[®] with high ethanol content was reported to have well dissolved nafion[®] and more stable films were observed compared to conventional methods including excessive dilution of nafion[®] (Merotra, 2013). However, more stable films can be obtained by incorporating enhanced materials such as carbon nanotubes (CNTs).

Nanomaterials have been very popular for electrode modification processes over a decade. One of the most commonly used nanomaterial in enzymatic electrodes are CNTs mainly because of their enhanced mechanical and electrical properties (Britto *et al.*, 1999; Baughman *et al.*, 2002). In particular, non-covalent binding of molecules to the CNTs sidewalls has become very popular recently. Obtaining strong π - π interactions using pyrene and its derivatives provides wide range of possibilities for enzyme immobilization (Jönsson-Niedziolka *et al.*, 2010). This approach has been widely used in the field of enzymatic biofuel cell electrodes (Halámková *et al.*, 2012; Szczupak *et al.*, 2012; MacVittie *et al.*, 2013; Güven *et al.*, 2016).

Incorporating MWCNTs into Fc-Nafion solutions might increase the electrical and mechanical properties of coated films. High surface area carbon material on the electrode surface can provide successful crosslinking of enzymes using pyrene and/or its derivatives. It has been reported that dispersions prepared using MWCNTs and Nafion[®] showed promising results for CNTs based biosensors such as for bilirubin determination (Filik *et al.*, 2015), electrochemically reduced graphene oxide (rGO) / MWCNTs glucose biosensors (Mani *et al.*, 2013) and graphene/gold/Nafion bio-composite materials (Zhou *et al.*, 2010).

The use of P2O in the literature was summarised in Chapter 1, Section 1.2.1 and Chapter 2, Section 2.21. The immobilization of P2O was recently achieved by direct adsorption of the enzyme on meso-porous carbon and dried electrodes were coated with nafion[®] solution which was then tested as biosensor and biofuel cell (Kwon *et al.*, 2014). Although the biosensor and biofuel cell tests showed promising results, there was no information in the preliminary study about the leaching of adsorbed enzyme species into solution or the stability of the system.

MWCNT dispersions of Fc-Nafion mixture in high ethanol content can be used as electrically conductive, stable and biocompatible electrode coating. Functionalizing the sidewalls of coated MWCNTs with pyrene and/or its derivatives can provide simple and effective way of immobilizing enzymes for biofuel cell applications. P2O-T169G demonstrated promising results due to its low turnover rates and good stability in the presence of oxygen (Chapter 2,

Section 2.3.1). Immobilizing oxygen resistant P2O-T169G enzyme to construct enzymatic electrodes can represent a new approach in the literature for biofuel cell applications.

3.2. Experimental

3.2.1. Materials

Fc, 1-pyrenebutyric acid (pyrene), 1-pyrenebutyric acid N-hydroxysuccinimide ester (PBSE), 1-ethyl-3-(3-dimethylaminopropyl) carbodiimide (EDC), N-Hydroxysuccinimide (NHS), nafion[®] (perfluorinated resin solution, 5 wt. % in mixture of lower aliphatic alcohols and water contains 45% water), dimethylformamide (DMF), ethanol (EtOH) and sodium hydroxide (NaOH) were purchased from Sigma-Aldrich (Dorset, UK). Universal indicator paper was purchased from VWR International LTD (Leicestershire, UK). Multi-walled carbon nanotubes (MWCNTs) (inner diameters of 20-50 nm and outer diameters of 70-200 nm) were obtained from Applied Sciences Inc. (Ohio, USA).

Stock solutions of 0.01 M pyrene and PBSE were prepared by dissolving pyrene and PBSE in DMF and kept refrigerated in a dark bottle at 4 °C. A fresh mixture of EDC and NHS was dissolved in deionized water (~18 MΩ-cm) before each experiment to give final concentrations of 0.1 M and 0.4 M respectively. All the enzyme solutions were made by dissolving and/or diluting the enzyme stock solutions with 0.1 M PBS at pH 7 and were subsequently kept at -70 °C.

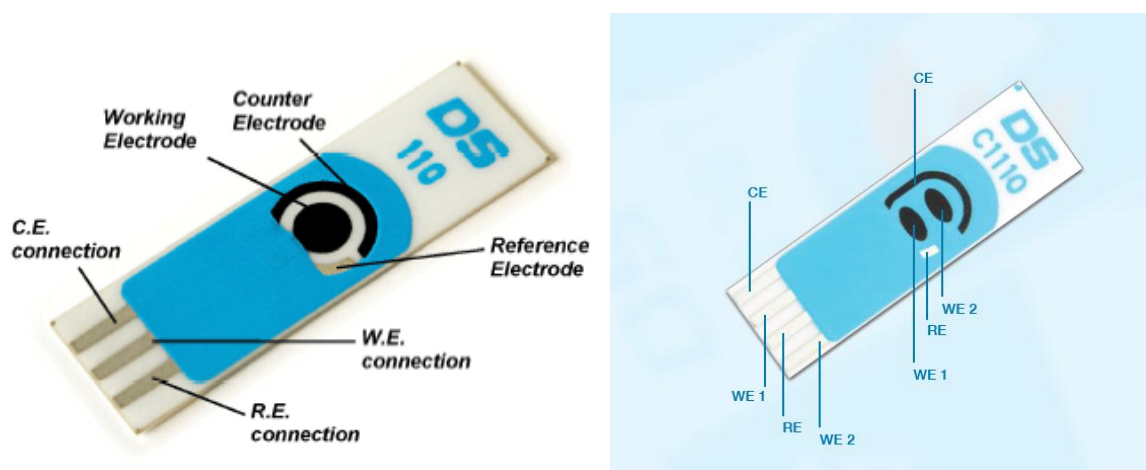


Figure 3. 1. Carbon screen printed electrodes (SPEs) used for the electrochemical experiments; DRP-C110 (left) and DRP-C110 (right) (DropSens, 2016)

Carbon screen-printed electrodes (Carbon SPE, model DRP-C110 and model DRP-C1110) were purchased from DropSens (Oviedo, Spain). Figure 3.1 shows the carbon SPEs where, the DRP-C110 model has a WE diameter of 0.40 cm and a surface area of 0.126 cm² and the DRP-C1110 model has two elliptic working electrodes with a surface area of 0.059 cm². Before used, the reproducibility of the SPEs were investigated to ensure the electrodes are stable throughout the study (Figure B.1 in Appendix B). The reference electrodes were silver/silver ion (Ag/Ag⁺) (~ -0.15 V vs Ag/AgCl) and the counter electrodes were carbon. The dimensions of the electrodes are 33 x 10 x 0.5 mm (Length x Width x Height) respectively. The electrodes were stored at room temperature in a dry place and no pre-treatment was required. All other materials were purchased as described in Section 2.2.1.

3.2.2. Preparation of Ferrocene-Nafion Redox Polymer with Multi-Walled Carbon Nanotubes (Fc-Nafion-MWCNTs)

The preparation of Fc-Nafion redox polymer was reported previously in the literature (Merotra, 2013). In order to increase the electrical conductivity of the redox polymer and incorporation of a high surface area carbon support for enzyme immobilization, a new modified procedure was carried out. Briefly, nafion[®] (5 wt. %) was diluted to 1 wt. % in solution with 90 % EtOH. Then, this solution was neutralized to pH 7 with dropwise addition of concentrated NaOH. The pH of the solution was checked with pH indicator paper between each step until desired pH was achieved. Fc was then dissolved in the neutralized solution to give 0.025 M of Fc-Nafion solution. The final form of the solution was achieved by mixing 1 mg of MWCNTs with the solution and sonicating for 3 h.

3.2.3. Fabrication of Enzyme Electrodes

Fabrication of crosslinked enzyme electrodes on unmodified carbon SPE

Enzyme immobilization based on chemical crosslinking of the enzymes on pyrenyl carbon nanostructures has been reported in the literature (Krishnan and Armstrong, 2012). In this study, immobilization of the enzymes on carbon surface of the carbon SPE was carried out using similar procedure, as follows; 20 µL of pyrene solution (10 mM in DMF) was absorbed on carbon SPE in the dark for 40 min to obtain strong π - π stacked structures between carbon and pyrene. Then, the electrode was rinsed with de-ionized water consecutively. The free carboxylic groups of pyrene were treated for 20 min using freshly prepared 20 µL of 0.4 M EDC and 0.1 M NHS mixture. The electrode was then again rinsed with de-ionized water. Finally, the

enzyme electrode was rinsed with PBS at pH 7 before it was electrochemically tested. This process is outlined in Fig 3.2 (A)

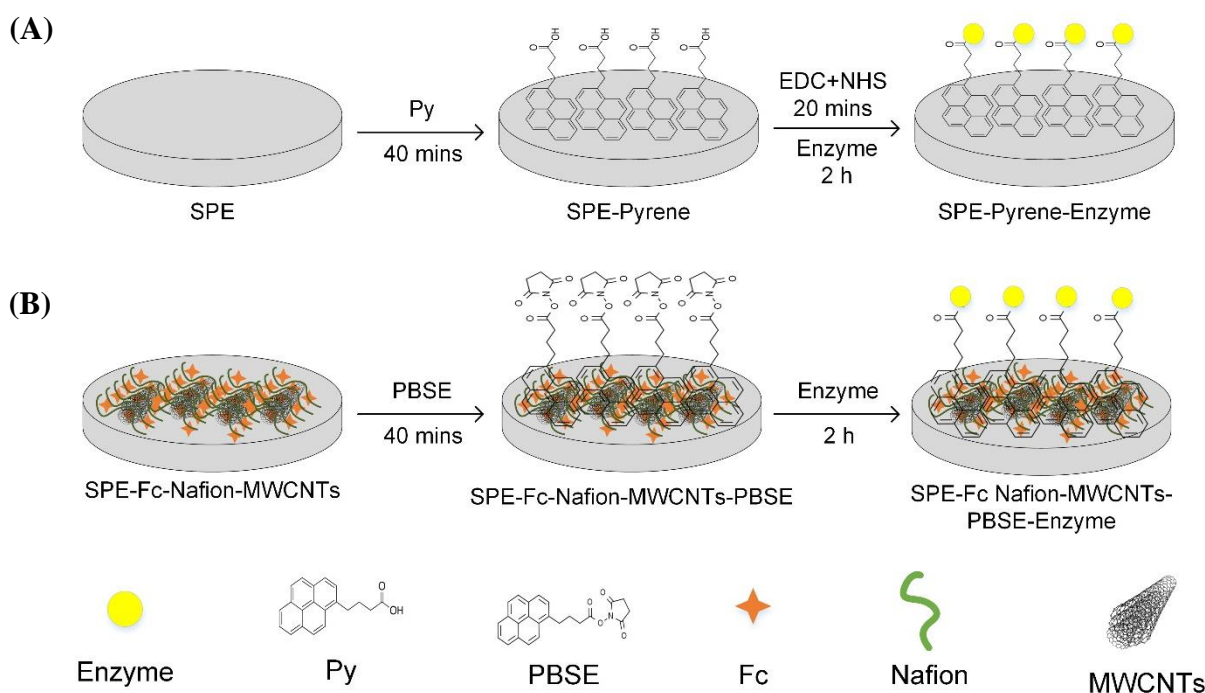


Figure 3. 2. Schematic representation of crosslinking of enzymes on bare carbon electrode (A) and on Fc-Nafion-MWCNTs (B)

Fabrication of Fc-Nafion-MWCNTs modified enzyme electrodes

A solution of Fc-Nafion-MWCNTs (preparation described in Section 3.2.2) was drop coated onto carbon SPE in small additions with drying time allowed between each step. Then, the dried electrode was placed in a cell and a preconditioning step of 20 cyclic voltammetry (CV) scans at 50 mV s^{-1} between -0.4 V and 0.4 V (*vs* Ag) was applied, similar to the reports elsewhere (Dong *et al.*, 1992). It was reported that the preconditioning step accumulates Fc^+ inside the ionic structure of Nafion[®] decreases the hydrophobicity of the Nafion[®] layer resulting in better enzyme immobilization (Merotra, 2013). After the preconditioning step, the electrode was washed with de-ionized water, dried in an oven at $35 \text{ }^\circ\text{C}$ for 10 mins and stored at room temperature ready for enzyme immobilization. Immobilization of the enzymes was performed as shown Figure 3.2 (A). A different pyrenyl compound, PBSE (10 mM in DMF) was used to activate Fc-Nafion-MWCNTs electrode for 1h. Since it has an N-hydroxysuccinimide group attached to the acid, it eliminates the extra EDC+NSH step hence resulting in easier fabrication of enzyme electrodes. The fabrication of crosslinked enzyme electrodes is shown in Figure 3.2

(B). SPEs, Fc-Nafion-MWCNTs modified SPEs, PBSE activated Fc-Nafion-MWCNTs modified SPEs and enzyme adsorbed Fc-Nafion SPEs were tested to ensure this method provides successful crosslinking of the enzymes and successful electron transfer between the enzyme and electrode. These results were shown in Figure B.2, B. 3 and B. 4 in Appendix B)

3.3. Electrochemical Measurements

All the electrochemical measurements were carried out by an Autolab potentiostat-galvanostat (PGSTAT101) in an electrochemical cell (shown in Figure 3.3) containing 500 μ L of electrolyte solution (either 0.5 mM FcCOOH in PBS or PBS only, both at pH 7).

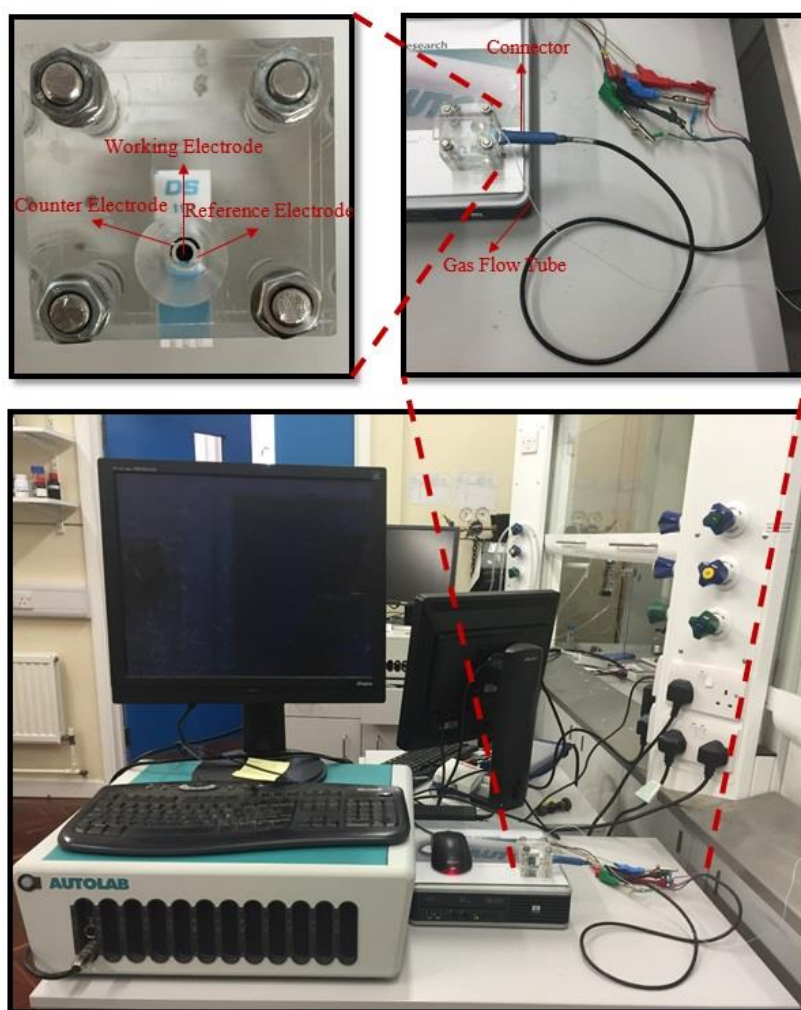


Figure 3. 3. Experimental set-up for electrochemical experiments.

Prior to the electrochemical tests the solutions were saturated with either air or nitrogen before and between each consecutive glucose additions. Cyclic voltammetry (CV), linear sweep voltammetry (LSV) and chronoamperometry (CA) were used to characterize the enzyme

electrodes. CV experiments were performed at different scan rates from 500 mV s^{-1} to 5 mV s^{-1} , LSV experiments were performed at 1 mV s^{-1} and CA experiments were carried out by applying constant voltage over time and recording the steady state current after consecutive glucose additions in every 10 min. Also, CA for longer hours under constant nitrogen or air sparging was carried out for stability analysis.

3.4. Results and Discussion

3.4.1. Enzyme electrodes in solution with FcCOOH

P2O-T169G and GOx enzymes were immobilised on pyrene activated carbon surface by cross-linking and electrochemically tested using cyclic and linear sweep voltammetry techniques in solutions of 0.5 mM FcCOOH (as an electron mediator) in PBS at pH 7. Figure 3.4 shows the electrochemical response of P2O-T169G and GOx to 0 mM and 4 mM glucose in solution with 0.5 mM FcCOOH.

Redox potentials obtained from Fc and its derivatives used in glucose oxidation were reported in literature in the range of 0.25 and 0.6 V vs Ag/AgCl (Nakabayashi *et al.*, 1998; Koide and Yokoyama, 1999; Fiorito and Torresi, 2001; Miao *et al.*, 2001; Tkáč *et al.*, 2002; Kase and Muguruma, 2004) for different solvents. The results showed the activity of FcCOOH when there is no glucose present in the solution (Figure 3.4 black line). The electrochemical response of the enzymes was observed upon glucose addition into the solution at around the same redox potentials of FcCOOH suggesting successful mediation of the electrons from enzyme to electrode had been achieved.

Although both enzymes showed similar onset potentials of around -0.1 V when glucose was added, the peak potential of P2O-T169G shifted negatively by about 0.07 V . This could be related to the experimental conditions of the CV as this difference was not observed for LSV at 1 mV s^{-1} (5 fold slower than CV, Figure B5 in Appendix B). The negative potential shifts of the oxidation current peaks were reported previously when Fc is used in solution with enzymes (Stepnicka, 2008).

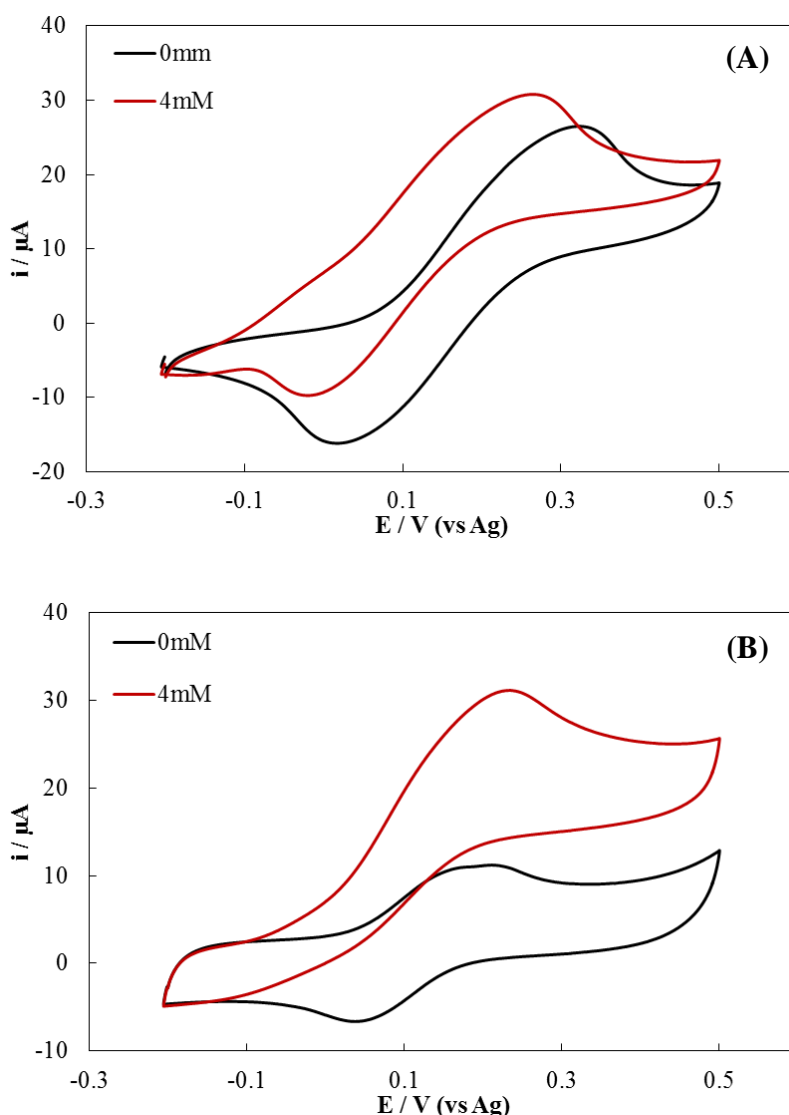


Figure 3. 4. CV (scan rate: 5 mV s^{-1}) scans of (A) P2O-T169G and (B) GOx immobilised on carbon SPE. Tested in nitrogen saturated solutions with 0 mM and 4 mM concentrations of glucose added to the solution containing 0.5 mM FcCOOH in 0.1 M PBS at pH 7. Ag is the silver/silver ion reference electrode used on the SPE (SPE surface area: 0.126 cm^2).

GOx showed a similar response with the solution experiments discussed in Chapter 2, where the reduction peak for the reaction between the enzymes and the mediator disappeared due to the fast kinetics of the oxidative reaction. The enzymatic electrode showed increasing activity up to 10 mM glucose concentration (Figure B.6 and Figure B.7 in Appendix B). On the other hand, when P2O-T169G was used, the electrode showed increasing activity only up to 6 mM glucose concentration (Figure B. 8, also LSV results: Figure B.5 in Appendix B). This is similar to the results where both enzymes and the mediator were in the same solution discussed in Chapter 2.

Although the same concentrations of the both enzymes were used in the cross-linking reaction (1 mg mL^{-1}) there could be different enzyme loadings on the carbon surface. As previously discussed in Chapter 1, Section 1.2.1, P2O enzyme has a different structure than GOx and this could be affecting the cross-linking reaction. It should also be noted that the activity of the mutant enzyme P2O-T160G is lower than the commercial GOx. The electrochemical responses of both enzymes were similar to each other, however, P2O-T169G showed higher background current than GOx when there was no glucose present. This could be related to the intramolecular electrostatic interactions between the enzymes and FcCOOH mediator (Stepnicka, 2008).

Enzyme		E_{pa} / V	E_{pc} / V	$\Delta E / \text{V}$	I_{pa}/I_{pc}
P2T169G	0 mM	0.320	0.020	0.300	1.64
	4 mM	0.270	-0.020	0.290	3.17
GOx	0 mM	0.210	0.040	0.170	1.69
	4 mM	0.230	-	-	-

Table 3. 1. Summary of the electrochemical characteristics of P2O-T169G and GOx enzymes immobilised on carbon SPE. Tested in nitrogen saturated solutions with 0 mM and 4 mM concentrations of glucose added to the solution containing 0.5 mM FcCOOH in 0.1 M PBS at pH 7. (SPE surface area: 0.126 cm^2).

The summary of the electrochemical data derived from the CV results is presented in Table 3.1. It was noted that the anodic potential for P2O-T169G was more positive than the GOx when there is no glucose present, however, the results grew closer upon addition of glucose. This might be related to the electrostatic interaction between the enzymes and Fc. P2O is a bigger molecule with 4 times more FAD centres as explained before (Chapter 1, Section 1.2.1) so it might cause different interactions with Fc. The differences in potential between anodic and cathodic peaks were higher than the theoretical value of a reversible reaction (Scholz, 2010). The reason for this could be the crosslinked enzyme on the electrode surface affecting the redox reaction. The high peak current ratios also suggest that the anodic reaction was faster than the cathodic reaction and increased further when more glucose was added showing fast reaction and mediation by FcCOOH at given scan rate.

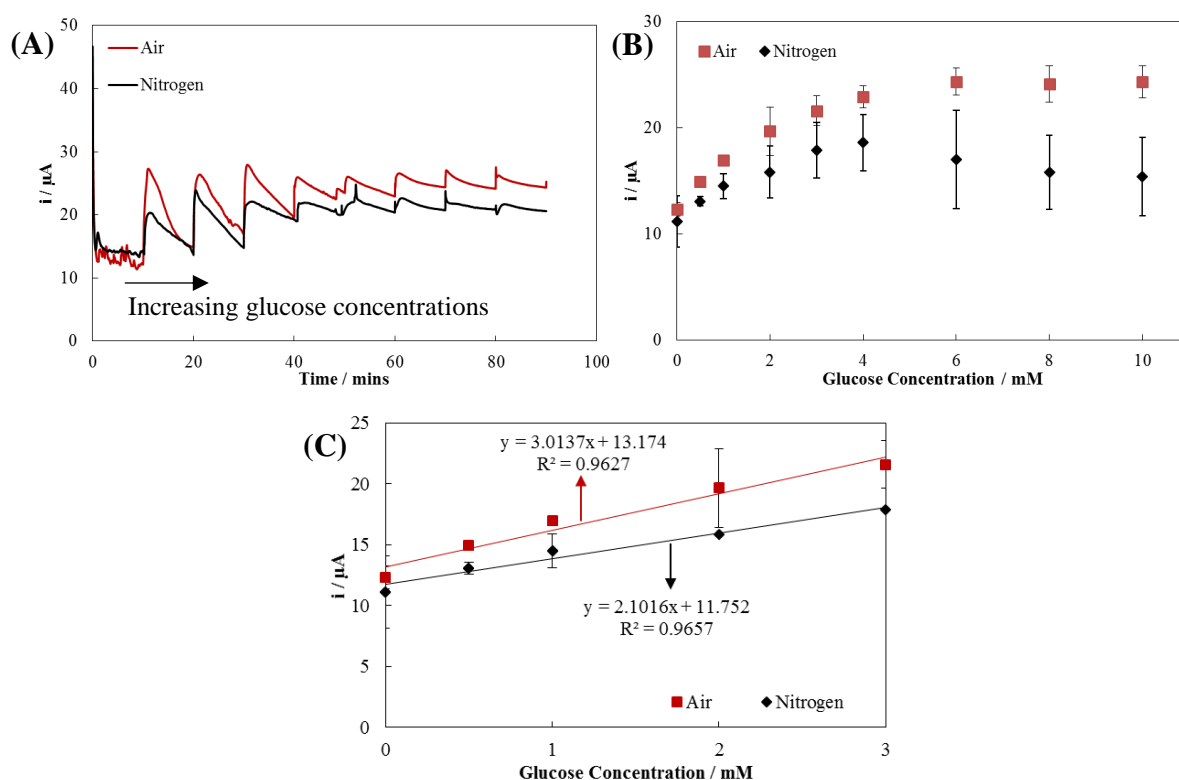


Figure 3. 5. (A) CA experiment at 0.2 V (vs Ag) of various glucose concentrations for P2O-T169G enzyme immobilised on carbon SPE, (B) Current values for various glucose concentrations derived from (A) and (C) the calibration curve for the linear region. Tested in saturated solutions of 0.5 mM FcCOOH in PBS at pH 7. Ag is the silver/silver ion reference electrode used on the SPE (SPE surface area: 0.126 cm²). Error bars are sample standard deviations of measurements on n = 2 samples.

Figure 3.5 shows the results derived from CA experiments performed at 0.2 V by recording the steady state current after consecutive glucose additions every 10 min under air and nitrogen saturated solution conditions. P2O-T169G showed increasing current after every glucose addition up around 4 mM glucose concentration and linearity up to 3 mM glucose concentration ($R^2=0.97$ and $R^2=0.96$ for nitrogen and air respectively). The performance of the enzyme did not decrease in the presence of oxygen, the current was also slightly higher which could be because of the oxidative nature of the oxygen.

The CA results of GOx showed similarities to P2O-T169G with the current increasing after each glucose addition up to around 8 mM glucose concentration and linearity up to 6 mM glucose concentration ($R^2=0.98$ and $R^2=0.97$ for nitrogen and air respectively). Figure 3.6 shows the results derived from CA experiments for GOx performed at 0.2 V by recording the

steady state current after consecutive glucose additions every 10 min under air and nitrogen saturated solution conditions. GOx showed higher current values and slightly better linearity compared to P2O-T16G which was expected due to the higher activity of GOx.

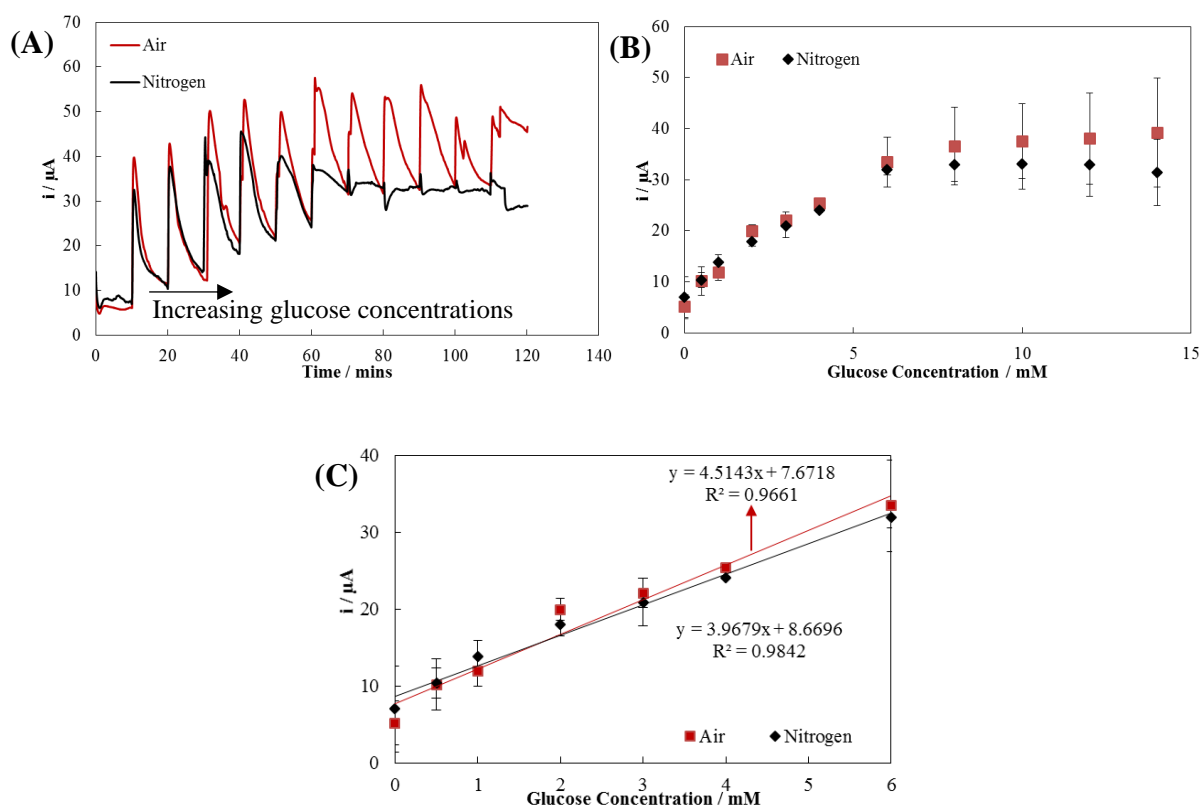


Figure 3. 6. (A) CA experiment at 0.2 V (*vs* Ag) of various glucose concentrations for GOx enzyme immobilised on carbon SPE, (B) Current values for various glucose concentrations derived from (A) and (C) the calibration curve for the linear region. Tested in saturated solutions of 0.5 mM FcCOOH in PBS at pH 7. Ag is the silver/silver ion reference electrode used on the SPE (SPE surface area: 0.126 cm²). Error bars are sample standard deviations of measurements on $n = 2$ samples.

The saturation currents and saturation concentrations for glucose have been summarized in Table 3.2 for GOx and P2O-T169G. Both enzymes demonstrated similar behaviour in the mass transport limited region where GOx showed bigger deviation in the presence of air. This could be due to the effect of oxygen in the solution competing with the mediator as an electron acceptor for GOx. GOx, also have ~ 2 times higher saturation concentration than P2O-T169G for glucose. This shows this enzyme have better selectivity for glucose sensing. However this could also be related to the activities of both enzymes where GOx is higher for the same enzyme concentrations.

Enzyme	Saturation Current / μA		Saturation Concentrations for Glucose / mM	
	Nitrogen	Air	Nitrogen	Air
P2O-T169G	16.5 ± 4.2	24.3 ± 2.2	4	4
GOx	32 ± 7.1	38 ± 9.3	8	8

Table 3. 2. The saturation currents and glucose concentrations of P2O-T169G and GOx immobilised on carbon SPE from CA experiments at 0.2 V (*vs* Ag). All means and sample standard deviations from replicate measurements on $n = 2$ samples (SPE surface area: 0.126 cm^2).

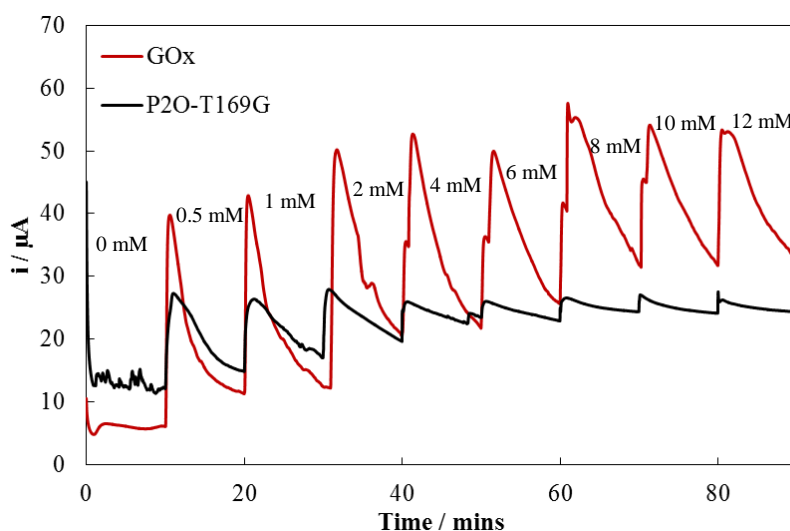


Figure 3. 7. CA experiments at 0.2 V (*vs* Ag) of various glucose concentrations for P2O-T169G and GOx enzymes immobilised on carbon SPE. Tested in air saturated solutions of 0.5 mM FcCOOH in PBS at pH 7. Ag is the silver/silver ion reference electrode used on the SPE (SPE surface area: 0.126 cm^2).

Figure 3.7 shows the comparison between P2O-T169G and GOx with air at a constant voltage of 0.2 V with consecutive glucose additions every 10 mins. The background current for P2O-T169G was higher than GOx similar to the results obtain the CV experiments. GOx showed an instant jump in current upon addition of glucose with each step following by a sharp decrease. At lower glucose levels (where the linearity is), the drop in current between each glucose concentrations for GOx was much higher than for P2O-T169G and the current after 10 min is

also lower. GOx loses its initial current response faster than P2O-T169G during first 10 min indicating relatively poor performance of GOx compared to P2O-T169G.

A similar response was observed for GOx in the nitrogen saturated CA experiments at lower glucose concentrations (Figure 3.6 (A)), hence it might be due to instability or poor performance of the immobilised enzyme and not necessarily because of the oxygen present. At higher glucose concentrations, on the other hand, the current does not show as sharp decreases as in nitrogen saturated solution. The effect of oxygen might be more pronounced around the saturation region where glucose oxidation is at its maximum and hence more electrons for oxygen to compete with Fc.

P2O-T169G showed more stable current responses with consecutive glucose additions. Most importantly it showed almost no significant current spikes on glucose addition in the saturation region which might indicate that it could be beneficial for the stability of the systems where P2O-T169G might be used. This kind of response could be because of its low affinity towards oxygen and also the channelled structure of the enzyme would be controlling the mass transport of the substrate and the products (Martin Hallberg *et al.*, 2004). Similar results were obtained from CA experiments for P2O-T169G under nitrogen saturation concentrations where there is a slight decrease in current spikes on addition of glucose at lower glucose concentrations and almost no decrease under high glucose concentrations (Figure 3.5 (A)).

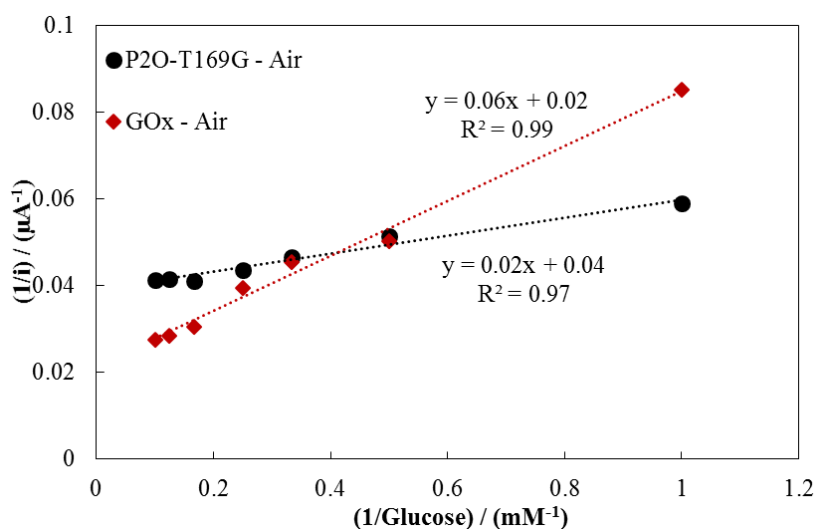


Figure 3. 8. Lineweaver-Burk plot of P2O-T169G and GOx enzymes immobilised on carbon SPE. Tested in air saturated solutions of 0.5 mM FcCOOH in 0.1 M PBS at pH 7. Ag is the silver/silver ion reference electrode used on the SPE (SPE surface area: 0.126 cm²).

Figure 3.8 shows the Lineweaver-Burk plot for P2O-169G and GOx tested in air saturated solution derived from CA experiment data. As explained before in Chapter 2.3.1, the Lineweaver-Burk equation (Eq 2.5) can be used to get information about enzyme kinetics in systems when enzyme is responsive to increasing glucose concentrations.

Each enzyme might have different affinities (tendency to bind their substrate, usually shown as K_m) defined as the substrate concentration at which half of the enzyme's active sites form complexes with the substrate. In this case the enzymes will have different affinities towards glucose. Where an enzyme is reported to have a high K_m value for glucose oxidation, it means that excessive amount of glucose must be present to saturate the enzyme that can be also expressed as the enzyme having a low affinity for glucose. Therefore, low K_m values are important to show the affinity of the enzyme towards glucose as it will only need a small amount of glucose to saturate the enzyme (Berg *et al.*, 2002).

The K_m values for P2O-T169G and GOx in air saturated solutions were calculated as 0.53 mM and 2.97 mM respectively between 1 and 10 mM glucose concentration range ($R^2=0.97$ and $R^2=0.99$ for P2O-T169G and GOx respectively). The lower K_m value for P2O-T169G suggests higher affinity toward glucose than GOx. Since increasing the glucose concentration would not always increase the rate of glucose oxidation by the enzyme, saturation will be reached when there is enough glucose to fill the enzymes' active sites and where the maximum possible electrochemical current i_{max} will be reached (Berg *et al.*, 2002). The i_{max} values for P2O-T169G and GOx were calculated as 25.64 μA and 46.73 μA , respectively. These calculated results based on the Lineweaver-Burk plot are suggesting higher currents for GOx due to its activity similar to experimental data presented and discussed in Table 3.2 within the given standard deviation range.

The effectiveness, stability and turnover of the enzyme towards its substrate is highly dependent on the immobilization of the enzyme on the electrode surface (Sarma *et al.*, 2009). Results from the immobilization of the enzymes showed higher current, higher glucose concentration and better affinities towards glucose compared to the results where enzyme and mediator are in solution. As a result, enhanced electron transfer and stability can be achieved by immobilizing Fc on electrode surface.

3.4.2. Enzyme electrodes modified with ferrocene-nafion-multi-walled carbon nanotubes (Fc-Nafion-MWCNTs)

Figure 3.9 shows the CVs for the pre-conditioning step of Fc-Nafion modified carbon SPE performed at 50 mV s^{-1} scan rate in PBS at pH 7. The current increased with increasing scan number and become saturated around the 20th cycle. The anodic peak of the first cycle behaved different than the rest of the scans as the species might be moving into different domains of the nafion® layer in the first cycle. This is similar to studies reported in literature (Dong *et al.*, 1992; Merotra, 2013).

The incorporation of a cationic redox couple into an anionic perfluorsulfonated polymer such as nafion® has been reported previously (Vaillancourt *et al.*, 1999). As more scans were applied, the positively charged Fc^+ accumulated inside the anionic sulphonate group of nafion® resulting in increasing anodic and cathodic peaks until a constant redox couple of Fc formed. It was suggested before that this processes increased the conductivity and stability of the coated film (Dong *et al.*, 1992).

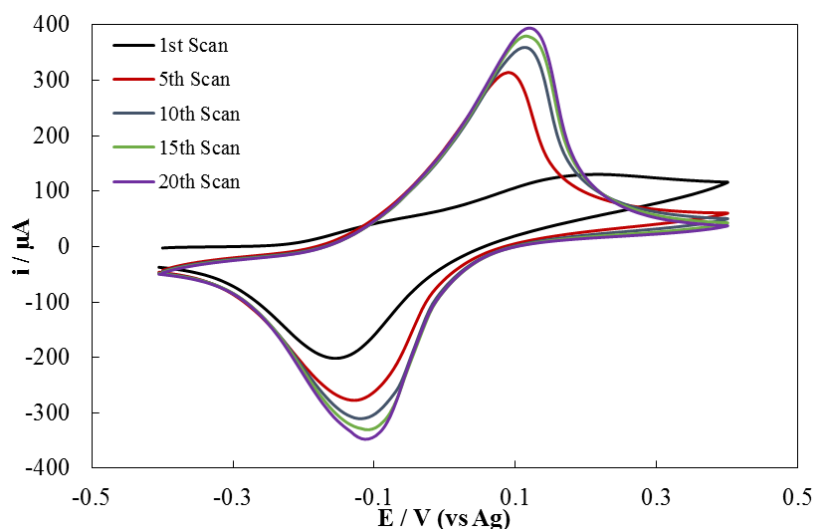


Figure 3. 9. CV (scan rate: 50 mV s^{-1}) scans for the pre-conditioning of the carbon SPEs modified with Fc-Nafion. Tested in 0.1 M PBS at pH 7. Fc-Nafion loading is 0.06 mg cm^{-2} . Ag is the silver/silver ion reference electrode used on the SPE (SPE surface area: 0.126 cm^2). (All 20 scans are shown in Figure B.9)

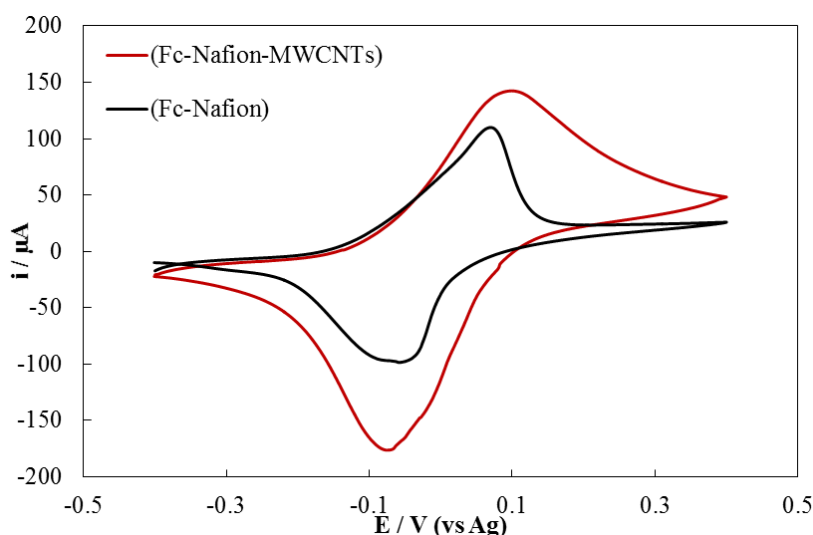


Figure 3. 10. Comparison between Fc-Nafion and Fc-Nafion-MWCNTs coated electrodes after pre-conditioning step. CVs performed at a scan rate of 10 mV s^{-1} , tested in 0.1 M PBS at $\text{pH } 7$. Fc-Nafion and Fc-Nafion-MWCNTs loadings are 0.06 mg cm^{-2} . Ag is the silver/silver ion reference electrode used on the SPE (SPE surface area: 0.126 cm^2).

In this section, a new approach for fabricating Fc-Nafion films on carbon electrodes was investigated. MWCNT dispersions (1 mg mL^{-1}) of Fc-Nafion mixture in high ethanol content were prepared to achieve stable, biocompatible and electrically conductive Fc-Nafion films. Figure 3.10 shows the difference between two preconditioned carbon SPEs with Fc-Nafion and Fc-Nafion-MWCNTs films tested in PBS at $\text{pH } 7$. The MWCNTs modified new film showed larger current in both anodic and cathodic processes suggesting more efficient electron transfer from Fc to the electrode due to high electrical conductive nature of the nanomaterial.

Different film loadings were applied on carbon SPEs and CVs was performed to test the performance of the electrodes. The main purpose of this experiment was to find the minimum film loading on the electrode with maximum concentration of Fc possible. In doing so, the thickness of the nafion[®] layer can be minimised and the number of the mediator molecules can be maximized on the electrode for more efficient electron transfer between enzyme and the mediator.

Figure 3.11 shows the effect of different Fc-Nafion-MWCNTs coating amounts on the current response of the electrodes. CVs were performed observing the anodic and cathodic processes as more of the film was loaded onto the electrodes (Figure 3.11 (a)). Then, the peak currents were presented as a function of film loading (Figure 3.11 (b)). The current response showed

increasing current values until 0.06 mg cm^{-2} loading. It was observed that the error margin was getting larger as the film loading was increased. This could be due to excessive loading of the material hence resulting in leaching or instability of the film. The optimum film loading was selected as 0.06 mg cm^{-2} and used as the electrode configuration for enzyme immobilization procedures.

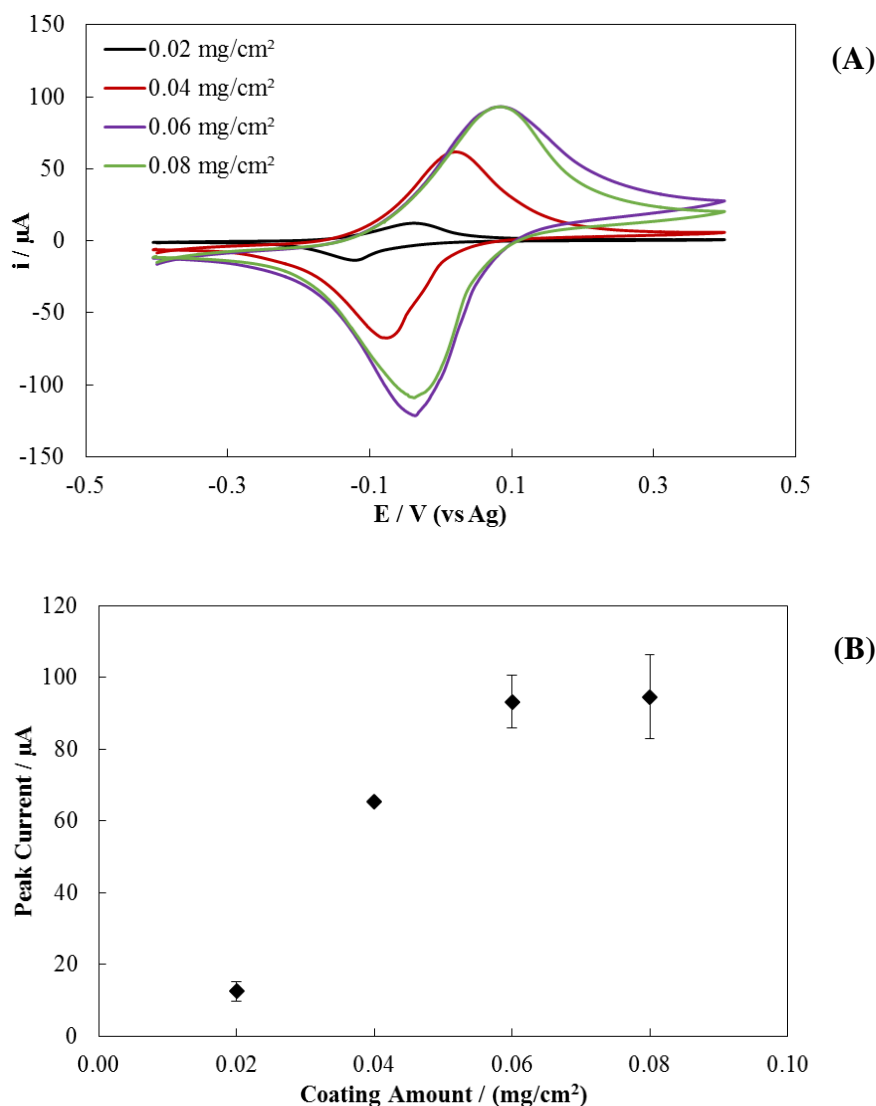


Figure 3. 11. (A) CVs (scan rate: 10 mV s^{-1}) showing the effect of the different amounts of Fc-Nafion-MWCNTs coated on SPEs after pre-conditioning step and (B) anodic peak current values of the different electrodes prepared. Tested in 0.1 M PBS at pH 7. Ag is the silver/silver ion reference electrode used on the SPE (SPE surface area: 0.126 cm^2). Error bars are sample standard deviations of measurements on $n = 3$ samples.

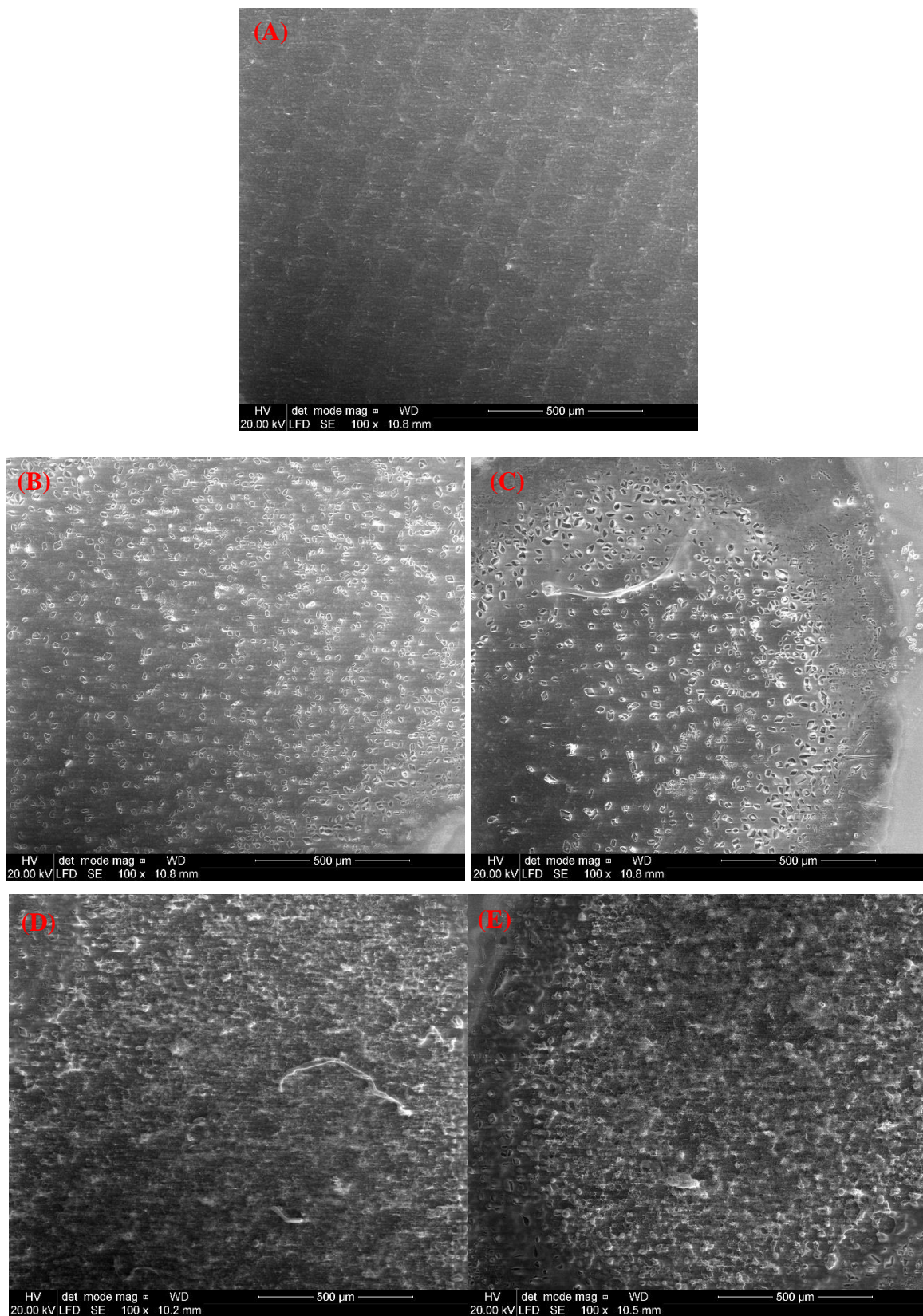


Figure 3. 12. SEM images of the (A) bare electrode, Fc-Nafion (B) before and (C) after pre-conditioning step and Fc-Nafion-MWCNTs (D) before and (E) after pre-conditioning step

The morphology of the Fc-Nafion-MWCNTs film coated electrodes at different stages of the electrode modification process were investigated using SEM. Figure 3.12 shows the images of all the steps applied during the preparation of the electrodes.

Fc can be seen in the form of micrometric crystals in the SEM images, for both Fc-Nafion (Fig 3.12 (B)) and Fc-Nafion-MWCNTs (Fig 3.12 (D)) electrode samples. By looking at the distribution of the crystals in these samples, it can be concluded that they are distributed fairly even. The SEM of the Fc-Nafion-MWCNTs samples show that Fc is surrounded by MWCNTs structure which is good considering the immobilization of the enzymes will take place on the carbon surface therefore successful electron transfer can be achieved.

The conformation of the coating might be changing after the pre-conditioning steps as the Fc crystals are observed to be accumulating to the sides of the electrode for both samples as seen from the Fig. 3.12 (C). This could be due to the accumulation of the Fc⁺ ions in the negatively charged sulphonate clusters of nafion[®] film as explained before.

Figure 3.13 shows unconditioned and pre-conditioned Fc-Nafion-MWCTNs (A) and (B) respectively, also the MWCNTs (C) and conditioned Fc-Nafion-MWCNTs with higher magnifications for comparison. The pre-conditioned electrode gave clearer images when higher magnification were used. This could suggest that the nafion[®] film structure may be changing during the pre-conditioning step by accumulation of Fc.

The effect on the nafion[®] when mixed with MWCNTs is clarified if Figure 3.13 (c) and (d) are compared. MWCNTs are observed to be integrated inside the nafion[®] and this could increase the electron conductive properties of the film. This approach provides two main advantages to conventional Fc-Nafion films:

- i.** Electrically conductive structure
- ii.** High surface area carbon support for protein immobilization

These two major improvements can be used to fabricate enzyme electrodes for enzymatic biofuel cells. The pre-conditioning step might provide more stable electrodes due to the advantages of the electrochemical treatment especially can prevent Fc leaching which may be very important for implantable systems.

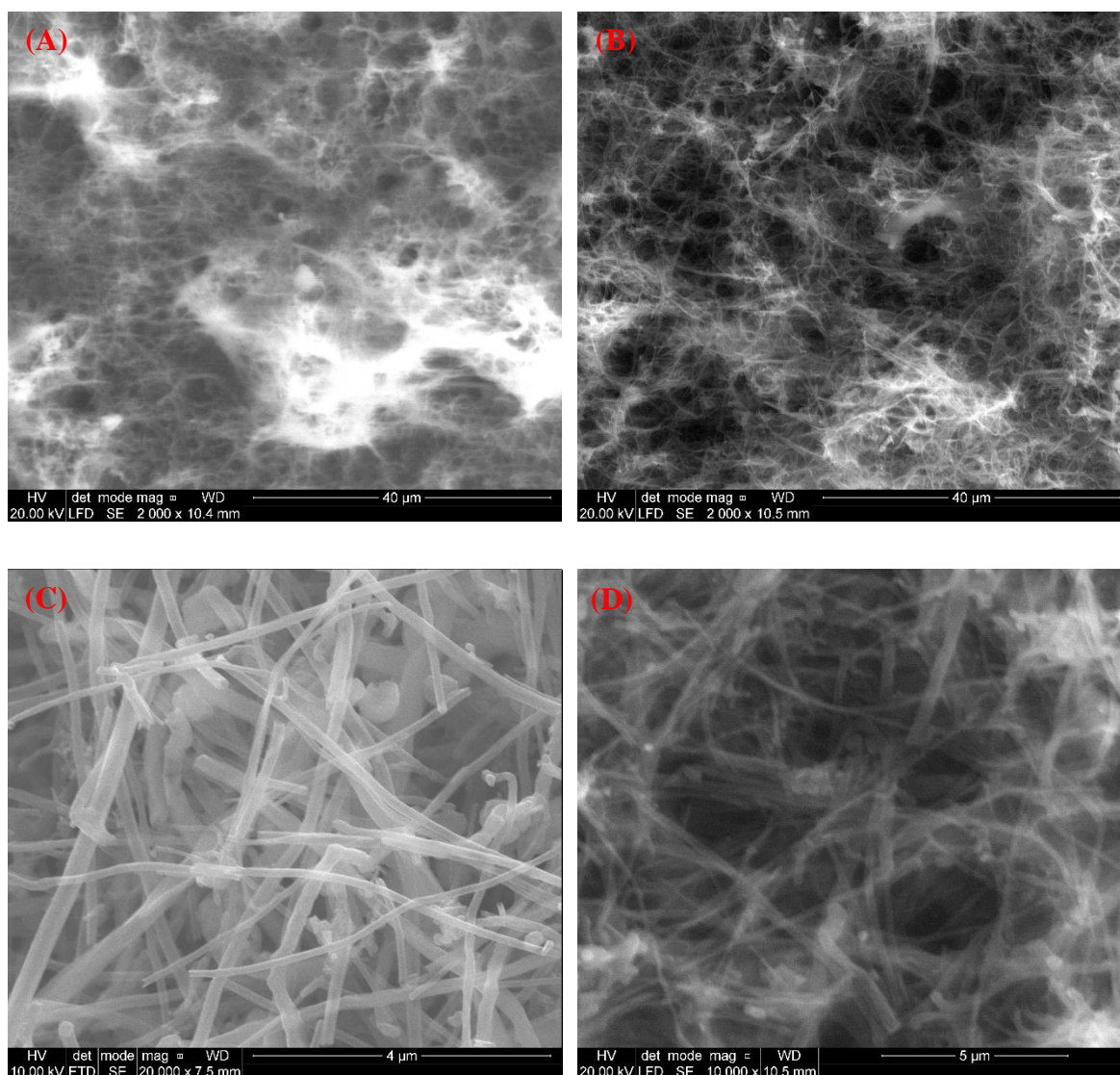


Figure 3. 13. SEM images of (A) unconditioned, (B) pre-conditioned Fc-Nafion-MWCNTs coated electrodes, (C) only MWCNTs and (D) pre-conditioned Fc-Nafion-MWCNTs with higher magnification.

Figure 3.14 shows the electrochemical response of the P2O-T169G (a) and GOx (b) immobilised on Fc-Nafion-MWCNTs pre-conditioned electrode (coating amount: 0.06 mg cm^{-2}) by crosslinking the enzymes on pyrene activated carbon nanostructures as explained in Figure 3.2 (B). The electrodes were placed in a pyrex cell (shown in Figure 3.3) and tested in nitrogen saturated PBS at pH 7.

The catalytic current response of the electrodes without any glucose present in the solution was similar either showing very low activity (P2O-T169G) or no activity (GOx). Both enzymes

demonstrated an increased catalytic current response up to 4 mM glucose concentrations similar to the results with FcCOOH in solution.

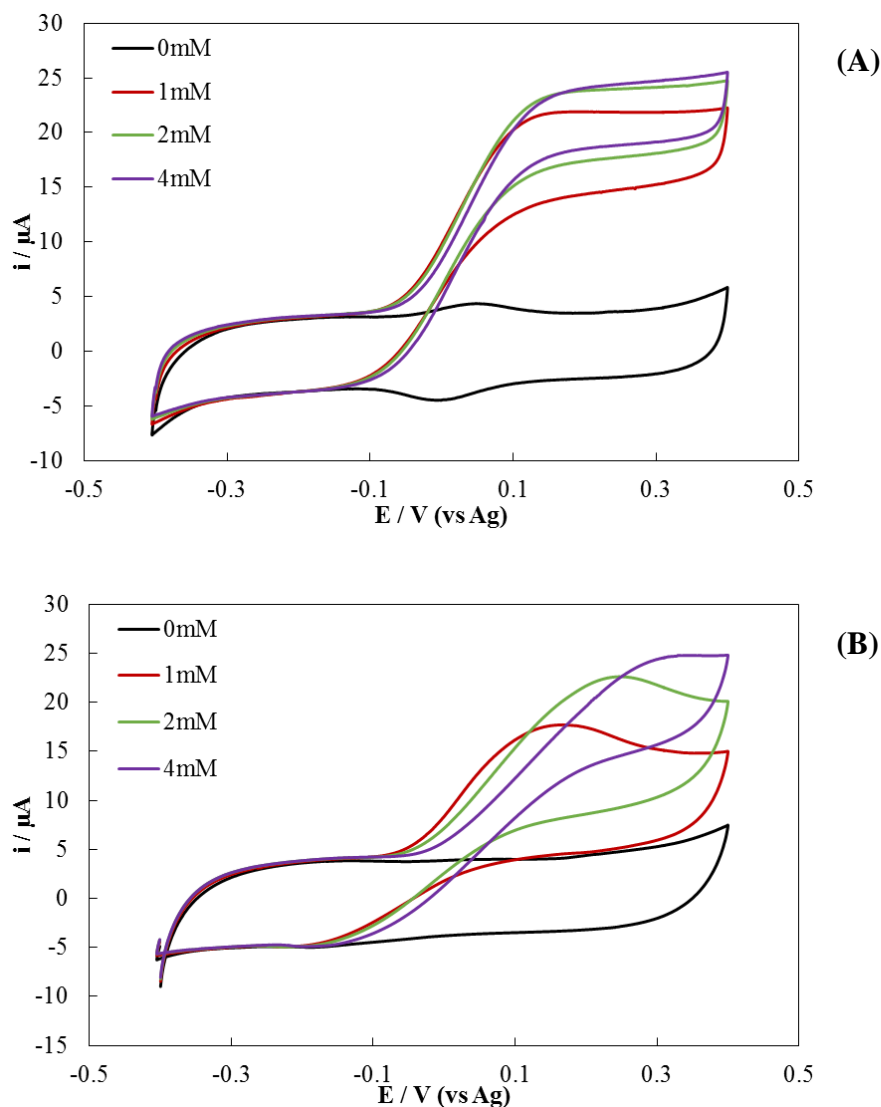


Figure 3. 14. CV (scan rate: 5 mV s^{-1}) scans of (A) P2O-T169G and (B) GOx immobilised on Fc-Nafion-MWCNTs pre-conditioned carbon SPE. Tested in nitrogen saturated solution for various glucose concentrations containing 0.5 mM FcCOOH in PBS at pH 7. Ag is the silver/silver ion reference electrode used on the SPE (SPE surface area: 0.126 cm^2).

P2O-T169G showed a sharp increase in the presence of glucose whereas GOx showed similar behaviour only in low glucose concentrations. They both displayed the same onset potential (around -0.1 V vs Ag) dependant on the activation of the glucose oxidation reaction for different glucose concentrations which is also similar as when FcCOOH was in solution. This suggests

the successful immobilization of the enzymes on the electrode surface and successful electron transfer between the enzyme and electrode *via* Fc mediator.

The different shapes obtained from CVs are also similar to the experiments discussed in Section 3.4.1, however P2O-T169G did not show significant shift in peak potentials with a 5 mV s^{-1} scan rate. On the other hand, the peak potentials for GOx were positively shifted as the glucose amount is increased in solution. This could be due the saturation glucose concentrations that affects the behaviour of the enzyme at peak potentials as it might change the reaction rate of the glucose oxidation. The shape of the voltammograms for P2O-T169G and GOx was also different. This could be because of the structural differences between two enzymes and different sugar binding mechanism of P2O-T169G enzyme than GOx.

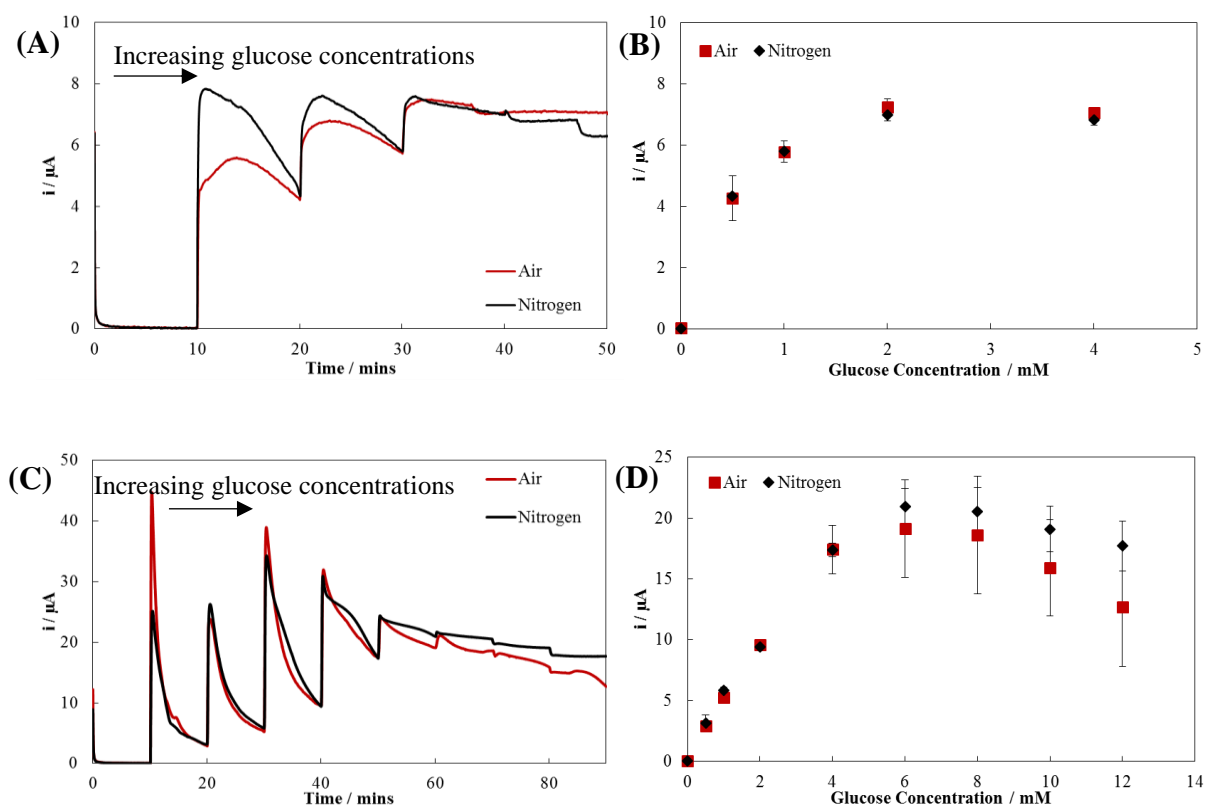


Figure 3. 15. (A) CA experiment at 0.15 V (*vs* Ag) of various glucose concentrations for P2O-T169G enzyme immobilised on Fc-Nafion-MWCNTs pre-conditioned carbon SPE, (B) Current values for various glucose concentrations derived from (A), (C) CA experiment at 0.15 V (*vs* Ag) of various glucose concentrations for GOx enzyme immobilised on carbon SPE and (D) Current values for various glucose concentrations derived from (C). Tested in 0.1 M PBS at pH 7. Ag is the silver/silver ion reference electrode used on the SPE (SPE surface area: 0.059 cm^2). Error bars are sample standard deviations of measurements on $n = 2$ samples.

Figure 3.15 shows the results derived from CA experiments performed at 0.15 V by recording the steady state current after consecutive glucose additions every 10 min under air and nitrogen saturated solution conditions. P2O-T169G demonstrated increasing current after each glucose addition up to around 2 mM glucose concentration where GOx showed increasing current up to 6 mM. The performance of the enzymes was lower than where the FcCOOH was used in the solution (Figures 3.5 and 3.6). This sort of behaviour was expected due to the entrapped Fc inside nafion[®] clusters since it is a diffusive mediator. Voltammetry experiments showed the background current for the system was approximately 6 and 3 fold lower than where FcCOOH was in the solution for P2O-T169G and GOx respectively. It could be the fact that less amount of Fc trapped inside the nafion[®] layer than where it was free moving in the solution. The amount of Fc interacting with the electrode surface was calculated to be approximately 2.7 fold less than where it was used in the solution experiments.

Another set of experiments were carried out to test bigger surface area electrode and the catalytic responses were compared with GOx. Figure 3.16 shows the behaviour of P2O-T169G immobilised on different surface area electrodes (0.059 cm² and 0.126 cm²).

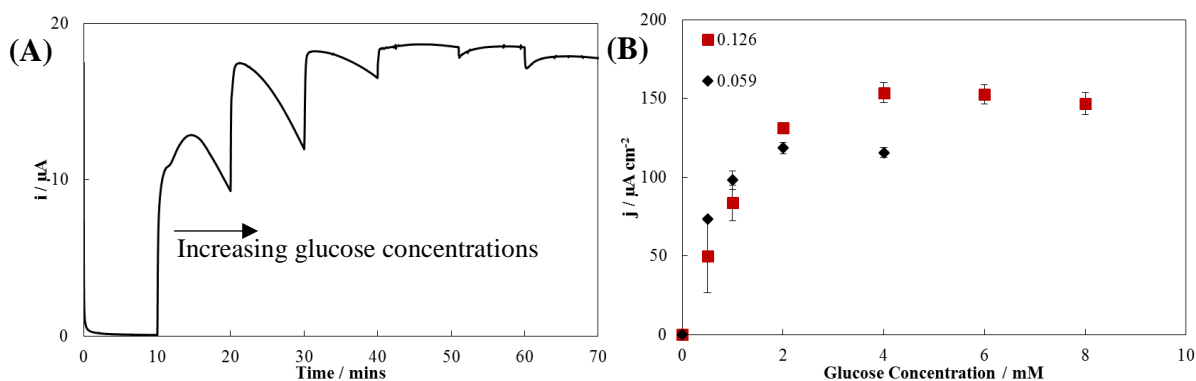


Figure 3. 16. (A) CA experiment at 0.15 V (*vs* Ag) of various glucose concentrations for P2O-T169G enzyme immobilised on Fc-Nafion-MWCNTs pre-conditioned carbon SPE with a surface area of 0.126 cm², (B) Current density values for various glucose concentrations derived from (A) with the data presented in Figure 3.15 (B). Tested in nitrogen saturated 0.1 M PBS at pH 7. Ag is the silver/silver ion reference electrode used on the SPE. Error bars are sample standard deviations of measurements on n = 2 samples.

The catalytic current response of P2O-T169G increased when bigger surface electrode was used, however, the glucose concentration region where the catalytic current is linear did not change significantly (between 0 to 2 mM). Better immobilization of the enzyme on a bigger

surface area might have caused higher current values, yet showed similar saturation behaviour. This could be related to the immobilization efficiency of the enzyme. P2O-T169G is relatively bigger molecule compared to GOx, therefore, the orientation of the enzyme molecules on small area electrode could be different than GOx.

The performance of the P2O-T169G was similar at low glucose concentrations, and showed similar linearity in parallel to previous tests, when compared to GOx. Figure 3.17 shows the difference on performance between P2O-T169G and GOx enzymes under air saturated solutions. Similar to previous results, GOx performs a lot less in terms of catalytic current at high glucose concentrations (mass transport limited region) whereas P2O-T169G showed more consistent response yet with lower current values.

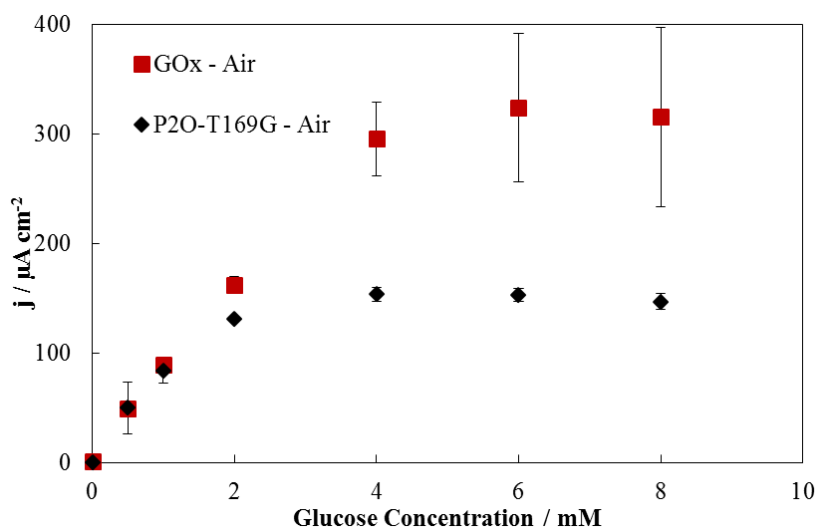


Figure 3. 17. Comparison of current densities of P2O-T169G with GOx, both immobilised on Fc-Nafion-MWCNTs pre-conditioned carbon SPE (surface area: 0.126 cm^2). Data obtained from CA experiments at 0.15 V (vs Ag) of various glucose concentrations. Tested in air saturated 0.1 M PBS at pH 7. Ag is the silver/silver ion reference electrode used on the SPE. Error bars are sample standard deviations of measurements on $n = 2$ samples. (Raw data: Figure 3.15 (C) and Figure 3.16 (A) for GOx and P2O-T169G respectively).

The linearity of the both systems are shown in Figure 3.18 where the GOx showed linear response up to 4 mM glucose concentration ($R^2=0.99$) and P2O-169G was 2 mM ($R^2= 0.97$). It was noted that whether Fc was used in the solution or immobilised, P2O-T169G enzyme showed lower current values and not as good linearity as GOx. The main reason for this kind of behaviour might be the lower activity of the mutant in comparison to commercial GOx

enzyme. P2O-T169G has a different structure than GOx as described previously (Chapter 1, Section 1.2.1) which might affect the immobilization of the protein and the interactions with the diffusive mediator although they both oxidize glucose by similar reactions.

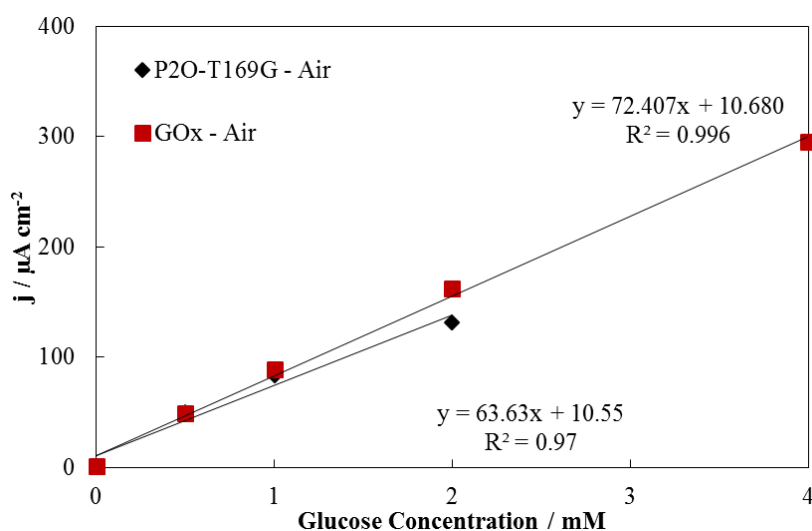


Figure 3. 18. Calibration curve for P2O-T169G and GOx enzymes immobilised on Fc-Nafion-MWCNTs pre-conditioned carbon SPE. Tested in air saturated 0.1 M PBS at pH 7. Data extracted from Fig 3.17. (SPE surface area: 0.126 cm²)

Figure 3.19 shows the Lineweaver-Burk plot for P2O-169G and GOx tested in air saturated solution derived from CA experiment data. The K_m values for P2O-T169G and GOx in air saturated solutions were calculated as 0.68 mM and 0.17 mM respectively for 0.5-10 mM glucose concentration range ($R^2=0.98$ and $R^2=0.99$ for P2O-T169G and GOx respectively). The i_{max} values for P2O-T169G and GOx were calculated as 201 $\mu\text{A cm}^{-2}$ (25.3 μA) and 642 $\mu\text{A cm}^{-2}$ (37.9 μA) respectively.

Compared to the system where Fc was used in the solution, both of the enzymes showed better affinity towards glucose (decreased K_m values), however GOx performs better in this system (in relation to lower K_m). This is also similar to the voltammogram and amperometry experiments where GOx showed better performance and linearity. The saturation current densities calculated using the Lineweaver-Burk equation, was significantly higher than the experimentally measured value for GOx. Considering relatively higher error margins for GOx, this result can be expected. In the case of P2O-T169G the value of the maximum current density was closer to the experimentally measured values.

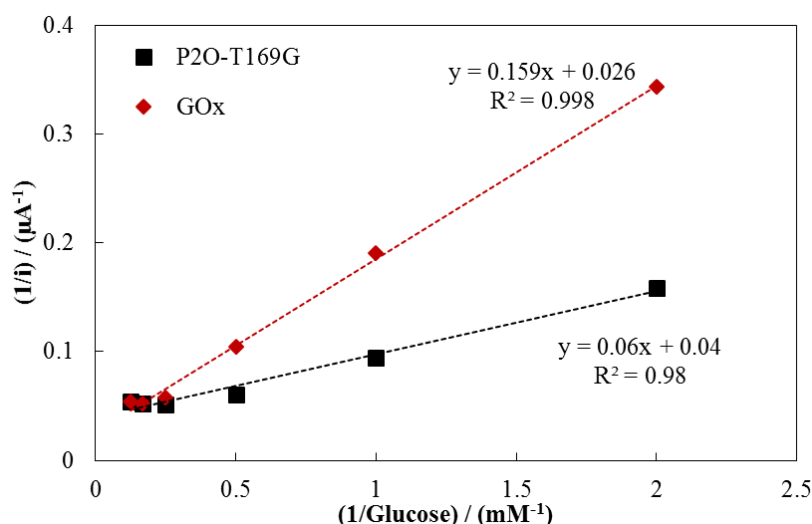


Figure 3. 19. Lineweaver-Burk plot for P2O-T169G and GOx immobilised on Fc-Nafion-MWCNTs pre-conditioned carbon SPE. Tested in air saturated 0.1 M PBS at pH 7. Data extracted from Fig 3.15 (B) and (D). (SPE surface area: 0.059 cm²)

Stability

Stability is a very important parameter especially for continuous systems such as enzymatic biofuel cells. Figure 3.20 shows the difference in current density values for short term stability when solution is saturated with air after different glucose concentrations are added.

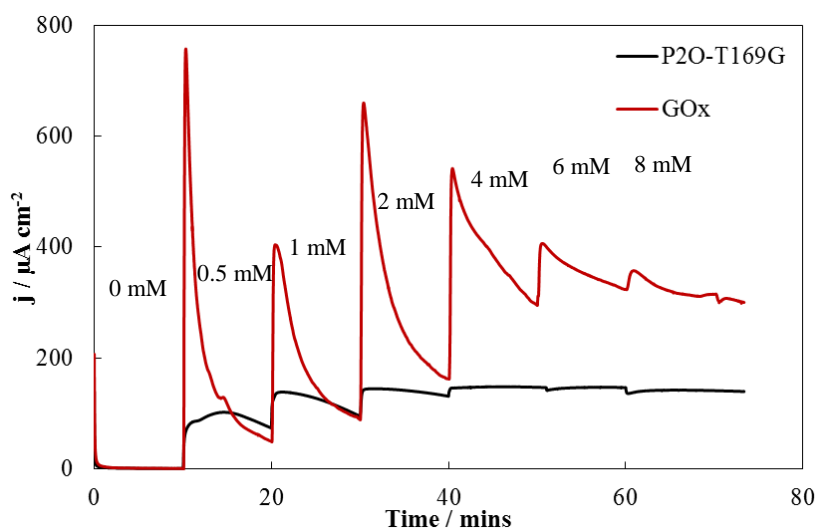


Figure 3. 20. CA experiments at 0.15 V (vs Ag) of various glucose concentrations for P2O-T169G and GOx enzymes immobilised on Fc-Nafion-MWCNTs pre-conditioned carbon SPE. Tested in air saturated 0.1 M PBS at pH 7. Ag is the silver/silver ion reference electrode used on the SPE (SPE surface area: 0.126 cm²).

Upon addition of each glucose concentration, GOx showed higher spikes in current density than P2O-T169G following by a sharp decrease. P2O-T169G, on the other hand, showed consistent and stable current values upon each additional glucose amount. Although this behaviour of GOx provided higher currents, the currents were lower than what it achieved for P2O-T169G at the end of each 10 min period (between glucose additions).

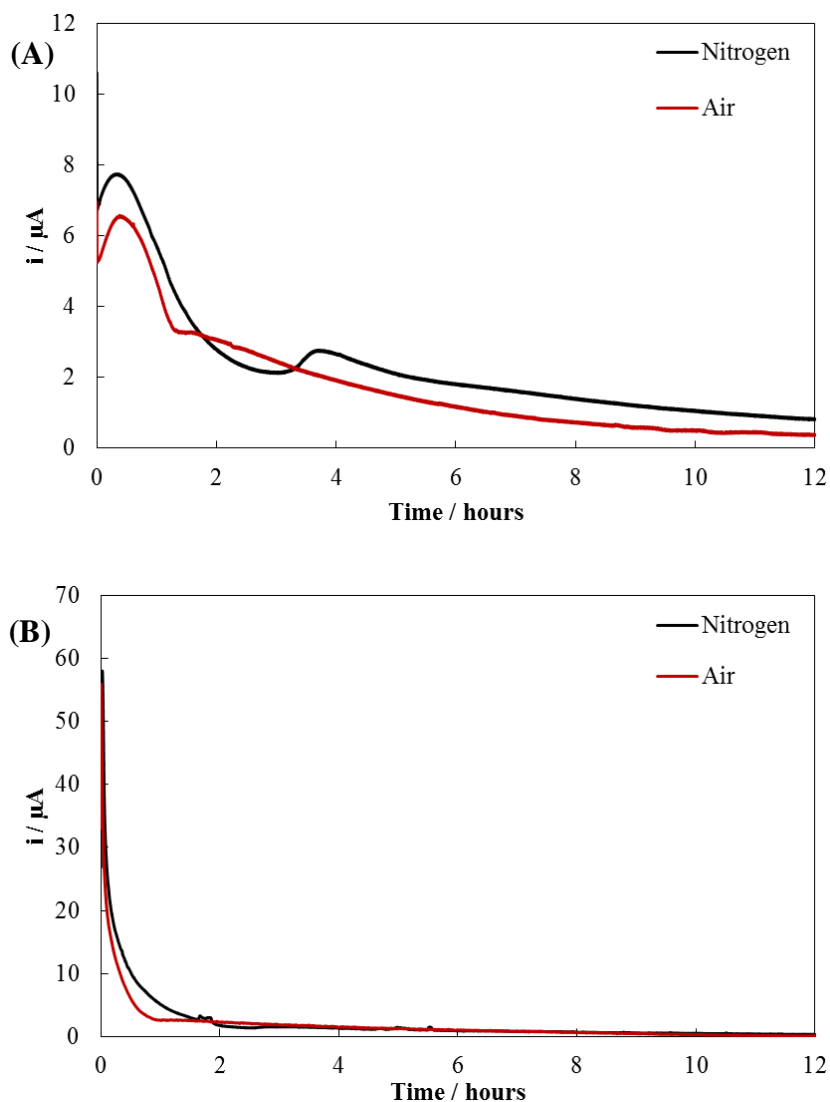


Figure 3. 21. CA experiments at 0.15 V (vs Ag) for (A) P2O-T169G and (B) GOx. Tested in nitrogen and air saturated solutions of PBS at pH 7 containing 4 mM glucose for 12h. Ag is the silver/silver ion reference electrode used on the SPE (SPE surface area: 0.126 cm²).

CA experiments for 12 h were also performed when solution is saturated with air and nitrogen and 4 mM glucose concentration was present to compare the differences of the current

responses for 12 h duration. The duration of 12 h was chosen based on the performance of the enzymes, defined as the time when the current drops more than 50% from their initial readings.

Figure 3.21 shows the stability results for P2O-T169G (Figure 3.21 (A)) and GOx (Figure 3.21 (B)) enzymes when the solutions are saturated with nitrogen and air. In the case of GOx, the current response showed a sharp decrease for both conditions (oxygen present or not) in which it was even sharper when oxygen was present and kept decreasing until almost negligible current values. On the other hand it showed a similar trend for P2O-T169G, keeping the initial catalytic current difference mainly throughout 12 h. Both of the enzymes maintained their trend of decreasing current over a time period of 12 h. This observation could be related to enzyme activity and/or decreasing glucose concentrations or the combination of both. The film stability is also another aspect that might be affecting the general performance of the electrodes.

These results are very similar to the stability experiments conducted where both enzyme and mediator are in the solution in Chapter 2. This suggests that P2O-T169G enzyme might not be utilising oxygen as an electron acceptor and the free oxygen is positively affecting the current response.

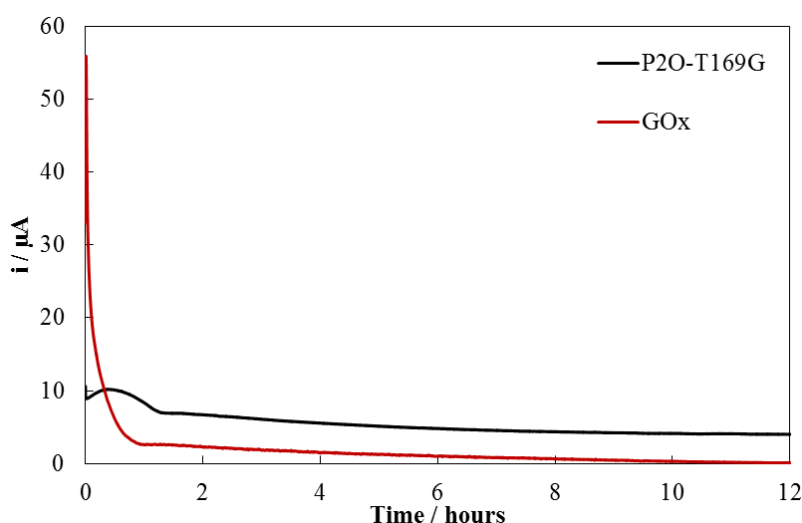


Figure 3. 22. CA experiments at 0.15 V (*vs* Ag) for P2O-T169G and GOx. Tested in air saturated solutions of PBS at pH 7 containing 4 mM glucose for 12 h. Ag is the silver/silver ion reference electrode used on the SPE (SPE surface area: 0.126 cm²).

Figure 3.22 shows the CA experiments for 12 h comparing the performance of the two enzymes. GOx, despite having more than 5 fold higher current response than P2O-T169G (initial current around 55 μA and 10 μA for GOx and P2O-T169G respectively), almost shows no catalytic

activity (around 0.1 μA) after 12 h of operation with 4 mM glucose present, with a sharp decrease of 90% within the first hour of operation. However, P2O-T169G, after losing approximately 30 % of its initial current in the first hour, continues to maintain current with just a further 30% loss over the next 10 h (final current after 12 h is around 4 μA). The initial current loss for both of the enzymes could be related to the activity of the enzyme and the further decrease a combination of glucose consumption and activity. The results obtained from CA experiments for 12 h suggests that P2O-T169G can provide more stable current than GOx under the same conditions. This is an important finding for an enzymatic biofuel cell design requiring stable current flow.

Based on the results obtained from voltammetry and amperometry experiments, GOx showed higher current values, better linearity and even better affinity towards glucose in some cases. However, P2O-T169G showed very promising results, in spite of its lower enzyme activity, by virtue of its stability, glucose affinity and not showing decreasing catalytic current behaviour in the in the mass transport limited region. These results suggests that the use of P2O-T1269G can enhance the performance of the enzymatic fuel cells (EBFCs) especially for long term stable operation.

3.5. Conclusions

In this chapter, the performance of P2O-T169G enzyme was investigated using two different enzyme immobilization approaches where the mediator was either in solution or immobilised on electrode surface. The results were then compared with commercial GOx enzyme to investigate the feasibility of utilising P2O-T169G enzyme for enzymatic biofuel cell applications.

Different immobilization strategies were successfully applied to immobilize the enzymes on the carbon electrode surface. First, enzymes crosslinked onto pyrene activated carbon surface and tested in solution contains the diffusive mediator Fc. In the second part, a novel immobilization approach incorporating MWCNTs within Fc-Nafion film was successfully developed and tested in PBS solution. The morphology of the fabricated Fc-Nafion-MWCNTs electrodes were also characterized by SEM. The electrochemical tests showed successful electron transfer from enzymes to the electrode *via* Fc mediator.

Both enzymes showed enhanced current values when Fc was immobilised on the electrode compared to the results where Fc was in solution. When FcCOOH was used in solution and

enzymes were immobilised, the current density values were 2.8 and 1.9 fold higher than when both enzyme and FcCOOH were in the solution for P2O-T169G and GOx respectively (Chapter 2). Furthermore, co-immobilisation of Fc with the enzymes resulted in 3.3 and 2.3 fold higher current densities for P2O-T169G and GOx respectively compared to when FcCOOH was used in solution. These results show that a significant improvement was provided due to immobilisation of enzymes and the mediator.

GOx, in general, demonstrated higher current values and broader linearity towards glucose due to its high activity. However, P2O-T169G showed promising performance despite its low activity and considering the fact that only 1 mg mL⁻¹ enzyme was utilised for the experiments. In agreement with the results in Chapter 2, P2O-T169G showed very consistent behaviour in the voltammetry experiment where its current response in the region of mass transport limitations was better than GOx.

CA experiments suggest that the stability of P2O-T169G was better than GOx. Although GOx showed higher current values initially, it lost all of its activity over a 12 h period under constant voltage, with a sharp decrease of approximately 90% within the first hour. P2O-T169G, on the other hand, showed better stability with a 60% total current loss with 30% lost within the first hour. It should be noted that the current decrease can be related to enzyme stability as well as glucose consumption amount over time. However, considering both possibilities it can be concluded that P2O-T169G might not be utilising oxygen as an electron acceptor for glucose oxidation and hence was not affected by to the same extent as GOx does.

In conclusion, P2O-T169G has been successfully immobilised on a carbon surface using a novel immobilization method and its performance compared to GOx. Further studies on enzymatic biofuel cell studies are discussed in Chapter 4.

Chapter 4. A Glucose-Air Enzymatic Biofuel Cell with Pyranose-2-Oxidase

In this chapter, different glucose/air enzymatic biofuel cells have been designed and tested using pyranose-2-oxidase-T169G (P2O-T169G) and glucose oxidase (GOx) as anodic enzymes and bilirubin oxidase (BOD) as cathodic enzyme. Enzymatic anodes were prepared by crosslinking enzymes (P2O and GOx) on ferrocene nafion multi-walled carbon nanotubes (Fc-Nafion-MWCNTs) modified electrodes as previously investigated in Chapter 3 and enzymatic cathodes were prepared by crosslinking BOD on MWCNTs modified electrodes.

Initially, a proof of concept enzymatic biofuel cell was designed using P2O-T169G and BOD enzymes for anode and cathode respectively and tested in a simple electrochemical cell with 5.5 mM glucose solution at pH 7. The performance of the enzymatic fuel cell was then compared when GOx was utilised as an anodic enzyme. A biofuel cells were set up using P2O-T169G/GOx and BOD as anodes and cathode, respectively for comparative analysis. Initial tests showed that P2O-T169G based enzymatic fuel cell can reach up to a power density of $9.56 \mu\text{W cm}^{-2}$.

Further tests also showed P2O-T169 based enzymatic biofuel cell can produce ~25 % more power output than GOx when oxygen is present in the solution. Finally, a biofuel cell anode using P2O-T169G was combined with air breathing BOD cathode in a stack design enzymatic biofuel cell (shown in Figure 1.26 (D)). The characteristics of the fuel cell design were investigated in terms of cell voltage, maximum power, power density and stability. An assembly of P2O-T169G – BOD based biofuel cell with an open circuit potential of 0.558 V and maximum power density of $29.8 \pm 6.1 \mu\text{W cm}^{-2}$ at 0.318 V.

4.1. Introduction

Employing enzymes for glucose oxidation and oxygen reduction has attracted many researchers for the last 30 years (Rasmussen *et al.*, 2016). Promising results have been achieved in different applications involving living animals (Schröder, 2012; Falk *et al.*, 2013b) such as insects (Rasmussen *et al.*, 2012), snail and clams (Halámková *et al.*, 2012; Szczupak *et al.*, 2012), lobsters (MacVittie *et al.*, 2013), rats (Cinquin *et al.*, 2010; Andoralov *et al.*, 2013; Castorena-Gonzalez *et al.*, 2013; Cheng *et al.*, 2013; Sales *et al.*, 2013; Zebda *et al.*, 2013) and rabbits (Miyake *et al.*, 2011). Plants (Mano *et al.*, 2003a) and even fruit juice (Liu and Dong, 2007a), were used to power enzymatic biofuel cells for applications such as wireless transmitting

systems (MacVittie *et al.*, 2015) or more recently enzymatic biofuel cells were integrated with contact lenses for glucose sensing (Falk *et al.*, 2013a).

Glucose is one of the most studied fuels for fuel cell applications especially for implantable devices mostly because of its role in human metabolism. Developing efficient and long term stable glucose/O₂ fuel systems is therefore very essential for future applications. Since the first membrane-less glucose enzymatic fuel cell was developed in 1999 (Katz *et al.*, 1999b), different enzymes and approaches have been used to improve the performance and stability of the fuel cells.

According to the best of current knowledge, there is only one study reported utilising P2O in an EBFC (Kwon *et al.*, 2014): researchers employed P2O and GOx in a fuel cell, however, they used air-breathing platinum as cathode so this system was not a fully enzymatic system (only anode is enzymatic). A redox mediator, benzoquinone, was added to the glucose solution of 200 mM used (~35 fold more concentrated glucose than used in this study) and a proton exchange membrane was also added to separate anode and cathode compartments. As a result, a maximum power densities of 11.6 $\mu\text{W cm}^{-2}$ and 40.7 $\mu\text{W cm}^{-2}$ were reported with and without the presence of the mediator, respectively. This values were also higher than it was for GOx tested (8.4 $\mu\text{W cm}^{-2}$ and 31.4 $\mu\text{W cm}^{-2}$ respectively). However, there was no information about the electrochemistry of the proposed direct electron transfer from enzymes and the mediator was used in solution which is not very practical especially for implantable applications. Several other fuel cell designs were also summarised in Chapter 1, Section 1.2.3.

In the scope of this study, the investigation of the P2O enzymes in solution (Chapter 2), different immobilisation strategies to employ P2O for biofuel cell applications (Chapter 3) have been investigated so far and the performance parameters were compared with widely used GOx enzyme. According to the results obtained, it was concluded that P2O is a very promising candidate for biofuel cell applications especially with significant advantages in stability. In this chapter, to best of current knowledge, a membrane-less fully enzymatic biofuel cell based on P2O-T169G – BOD enzymes were studied for the first time. Comparative studies were again conducted using GOx to demonstrate using P2O-T169G in biofuel cell applications.

4.2. Experimental

4.2.1. Materials

Carbon paper with gas diffusion layer was purchased from Freudenberg (Weinheim, Germany). BOD (from *myrothecium verrucaria*, lyophilized powder, 15-65 unit mg^{-1} protein) was purchased from Sigma-Aldrich (Dorset, UK). Watson Marlow 101U/R peristaltic pump was borrowed from School of Chemical Engineering and Advanced Materials (CEAM), Newcastle University BioLab (Newcastle, UK). Resistor box Model RS-500 (range: 1Ω -10 $\text{M}\Omega$) was purchased from Elenco Electronics (Wheeling, US). High resolution data logger ADC-16 was purchased from Pico Technology (Cambridgeshire, UK). The stack cells used in fuel cell experiments were made by the mechanical workshop in CEAM (Newcastle, UK). All the chemicals and other materials were purchased, handled and used as described in Chapter 3.2.1 and 2.2.1.

4.2.2. Preparation of Enzymatic Biofuel Cell Anode

Enzymatic biofuel cell anodes were prepared using the same method described in Chapter 3.2.3. Briefly, a solution of Fc-Nafion-MWCNTs was drop-coated onto carbon SPE (0.126 cm^2) or carbon paper (1.767 cm^2) to give 0.06 mg cm^{-2} loading amount (dried at room temperature). The dried electrode was then pre-conditioned using cyclic voltammetry (CV) for 20 scans at 50 mV s^{-1} between -0.4 V and 0.4 V (*vs* Ag/Ag^+) for SPE and 5 scans between -0.3 and 0.7 V (*vs* Ag/AgCl) for carbon paper electrode. After the pre-conditioning step, the electrodes were washed with de-ionized water and dried in oven at $35 \text{ }^\circ\text{C}$ for 10 min. The electrodes were activated by 1-pyrenebutyric acid N-hydroxysuccinimide ester (PBSE, 10 mM in DMF) for 1 h and rinsed with de-ionized water. Finally, 4 mg mL^{-1} and/or 10 mg mL^{-1} of P2O-T169G and/or GOx were added on freshly activated electrodes at $4 \text{ }^\circ\text{C}$ for 2 h and rinsed with PBS at pH 7 before use.

4.2.3. Preparation of Enzymatic Biofuel Cell Cathode

Enzymatic biofuel cell cathodes were prepared using carbon SPE and carbon paper electrodes used for the anode preparation. A dispersion of MWCTNs (1 mg mL^{-1} in DMF) was drop coated onto the electrodes to give 0.08 mg cm^{-2} nanomaterial loading and dried at room temperature. The electrodes then were activated by 10 mM PBSE in DMF for 1 h and rinsed with de-ionized

water. Finally, 4 mg mL^{-1} of BOD was added on freshly activated carbon SPE and carbon paper electrodes at $4 \text{ }^\circ\text{C}$ for 2 h respectively and rinsed with PBS at pH 7 before use.

4.2.4. Electrochemical and Fuel Cell Measurements

CV were used to characterise BOD in non-aerated and aerated solutions mimicking the same conditions used in the fuel cell measurements. Fuel cell measurements were performed using a resistor box to apply load and the output voltage was recorded by data logger. The anode and cathode potentials were also recorded *versus* Ag/AgCl reference electrode. The current and power were calculated using Ohm's Law ($V = I \times R$ and $P = I \times V$). The glucose concentration used for the fuel cell measurements were 5.5 mM to mimic the glucose in levels human blood. The measurements were carried out at room temperature.

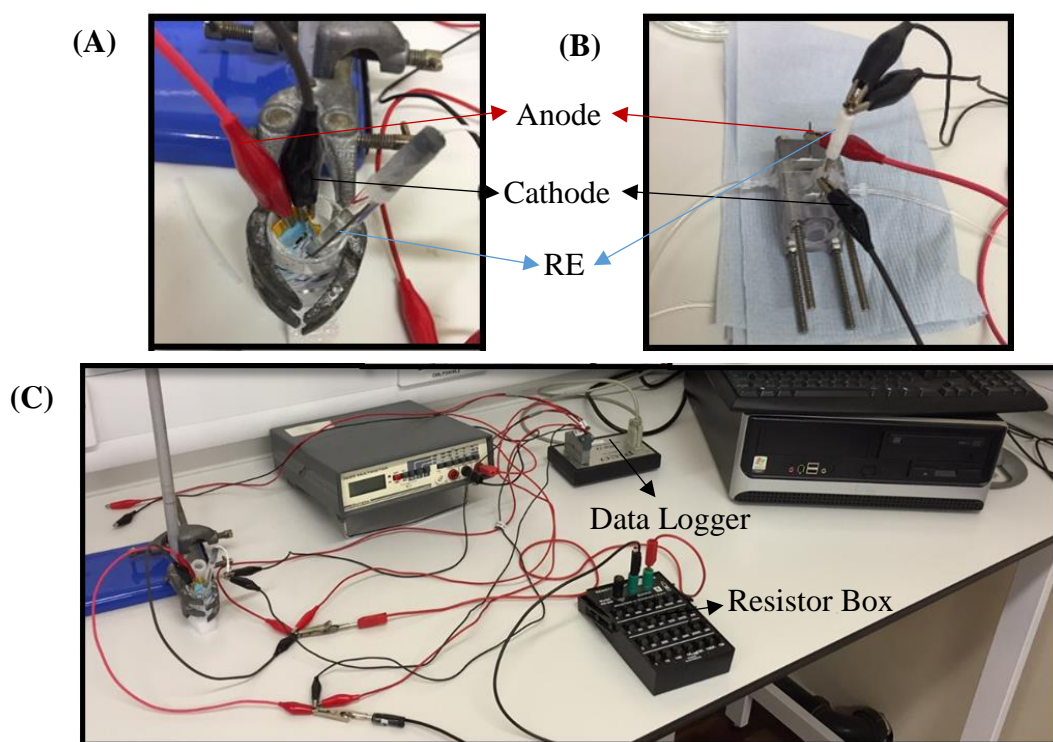


Figure 4. 1. Experimental set-up for cells. (A) Fuel cell set-up with a glass cell beaker (B) Fuel cell set-up with stack cell design with air breathing cathode (C) Overall view of the test equipment while operating in batch mode with a glass cell beaker.

In this study, two different modes were used for fuel cell operation: batch mode and continuous mode. Batch mode was used to obtain performance parameters such as current-voltage and power curves and continuous mode was used to obtain stability information. There were also two different cell designs to make use of different type of electrodes for fuel cell tests. A glass

cell beaker was used to test SPEs and a stack cell design was used to test carbon paper electrodes. The fuel cell set-ups used in this chapter are shown in Figure 4.1.

4.3. Results and Discussion

4.3.1. Performance of EBFCs with P2O-T169G, GOx and BOD

The EBFC anodes used in this chapter was prepared using the immobilization technique developed in Chapter 3, Section 3.4.2. The EBFC cathodes were prepared using a similar approach (explained in section 4.2.3) without using an electron transfer mediator because BOD can exhibit direct electron transfer (DET) between its active site and the electrode (Ramírez *et al.*, 2008). The EBFC cathode was first characterised using CV to validate whether functionalised electrode is capable of electron transfer to the electrode.

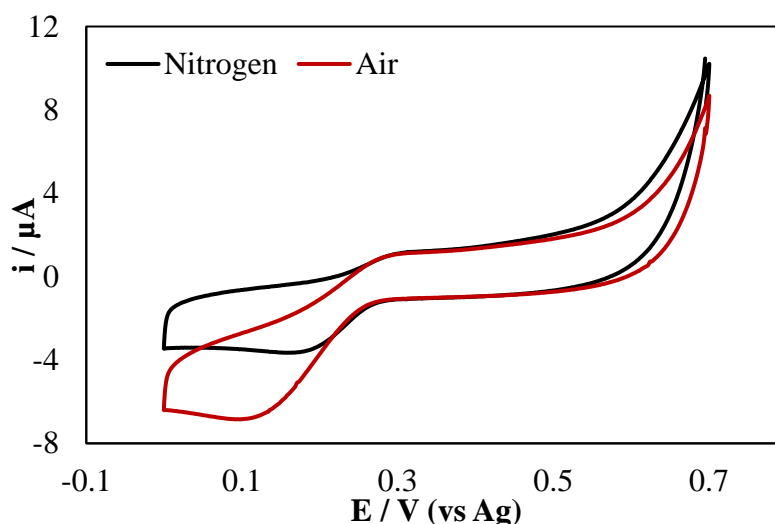


Figure 4. 2. CV (scan rate: 5 mV s^{-1}) scans of a BOD cathode immobilised on MWCNTs coated SPE (MWCNTs loading of 0.08 mg cm^{-1}) tested in nitrogen and air saturated solution of 0.1 M PBS at pH 7 containing 5.5 mM glucose. Ag is the silver/silver ion reference electrode used on the SPE (SPE surface area: 0.126 cm^2).

CVs of a BOD cathode on the SPE were obtained in 5.5 mM glucose solution is shown in Figure 4.2. This solution was chosen to maintain the same conditions used in the EBFC experiments tested in this chapter. The solution was deaerated with N_2 to obtain a baseline and then aerated with air to test the electrochemical activity of BOD. The presence of O_2 in glucose solution clearly resulted in the formation of catalytic currents where the O_2 reduction peak starts at around 0.3 V vs Ag . This appearance of the cathodic current obtained is similar to the previously

reported currents based on immobilization on MWCNTs (Weigel *et al.*, 2007). DET between BOD and electrode was successfully achieved and this electrode configuration was used to prepare the cathodes throughout this chapter. Another set of experiments were also performed to ensure the electron transfer is provided by BOD. In these experiments MWCNTs coated SPEs without BOD were tested and no catalytic current change was observed suggesting no activity when BOD is not present (Figure C.1 in Appendix C).

Effect of Oxygen on the Performance of EBFC

Oxygen is a key parameter for EBFCs as its presence is often not desired at anode but it is essential at cathode. The oxygen-resistant properties and relatively stable performance of P2O-T169G was displayed in Chapter 3 previously, making it attractive for EBFCs. An EBFC was set up using P2O-T169G and BOD as anode and cathode, respectively.

Parameters	EBFCs	
	Non-aerated	Aerated
OCP / V	0.494	0.458
Max Power / μW	0.87	1.20
Max Power Density / ($\mu\text{W cm}^{-2}$)	6.89	9.56
Limiting Current / μA	2.40	3.47
Limiting Current Density / ($\mu\text{A cm}^{-2}$)	19.10	27.54

Table 4. 1. Summary of the EBFC performance parameters obtained from non-aerated and aerated glucose concentrations. All enzymes used to construct EBFCs were at 4 mg mL^{-1} concentration and were immobilised on SPE (surface area: 0.126 cm^2). Anode and cathode potentials were also recorded as 0.050 and 0.544 V for non-aerated, 0.082 and 0.541 V for aerated solutions respectively at OCP. The maximum power values were obtained at different external loads of $150 \text{ k}\Omega$ (giving a cell potential of 0.361 V) and $100 \text{ k}\Omega$ (giving a cell potential of 0.347 V) representing the values for non-aerated and aerated solutions, respectively.

The EBFC cell tests were carried out in 5.5 mM glucose solution at pH 7. This concentration of glucose and pH were chosen to mimic the blood sugar levels in human (Digital, 2016). P2O-

T169G and BOD concentrations used in this part were 4 mg mL^{-1} and the summary of the EBFC performance parameters obtained from non-aerated and aerated glucose solutions are summarised in Table 4.1.

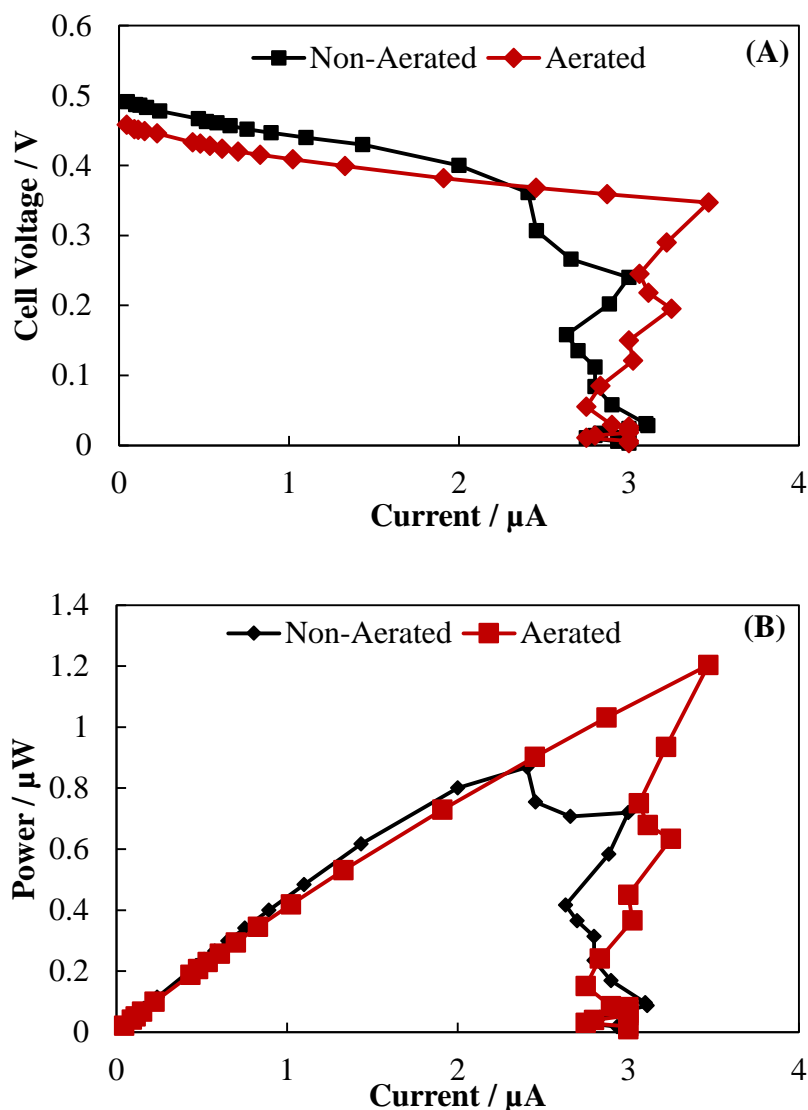


Figure 4. 3. (A) Cell voltage-current and (B) fuel cell polarization curves operating in non-aerated and aerated glucose concentrations. All enzymes used to construct EBFCs were at 4 mg mL^{-1} concentration and were immobilised on SPE (surface area: 0.126 cm^2). EBFCs were tested at batch mode using a glass cell in non-aerated and aerated glucose concentrations of 5.5 mM in 0.1 M PBS at pH 7.

Figure 4.3 shows the cell voltage and power as a function of current, also known as the polarization curve. The EBFCs showed OCP values of 0.494 and 0.458 V for non-aerated and aerated solutions of glucose, respectively. Anode and cathode potentials were also recorded as

0.050 and 0.544 V for non-aerated, 0.082 and 0.541 V for aerated solutions respectively at OCP.

Open circuit potential (OCP) is defined as the potential difference between anode and cathode of a fuel cell (Güven *et al.*, 2016). In practice, OCP is substantially lower than the theoretical value due to various potential losses, particularly activation and kinetic losses (Güven *et al.*, 2016). The anodic potential obtained from the experiments conducted in Chapter 3 (Section 3.4.2) was started around -0.1 V *vs* Ag and the cathodic potential from Figure 4.2 was observed at 0.3 V. Therefore, the OCP of 0.4 V between the reactions at the anode and cathode can theoretically be achieved.

The OCP values for EBFCs were observed higher than the theoretically possible values. This can be explained by analysing anode and cathode potentials recorded during polarization. The anode showed a positive shift of 0.182 V from its theoretical value that was expected as it should not reach or be more negative than its theoretical value. This value, on the other hand, might show closer values to its theoretical value than it was in the polarisation test considering the CV experiment was conducted at 5 mV s⁻¹ scan rate. The cathode also showed a positive shift of ~0.240 V, which was unexpected. Although CV experiment suggests a theoretical redox potential of 0.3 V *vs* Ag, BOD was reported to show electron transfer properties at potentials between 0.32-0.52 V *vs* Ag (Christenson *et al.*, 2006). Therefore, the CV experiments at the given scan rate perhaps does not reflect the real value of the redox potential. If the reported values are taken into consideration, an OCP value of 0.458 V is possible from the designed EBFC in this study.

The power reached up to a maximum value of 0.87 μ W (power density and current density of 6.9 μ W cm⁻² and 19.10 μ A cm⁻² respectively) when the solution is not aerated. Then, increased up to 1.2 μ W (power density and current density of 9.56 μ W cm⁻² and 27.57 μ A cm⁻² respectively) showing ~ 40 % increase in performance when the solution is aerated. After the fuel cell reached its maximum value, which was where the external resistance was equal to its total internal resistance (Menicucci *et al.*, 2006), it started to decay mainly due to mass transport losses. The maximum power values were obtained at different external loads of 150 k Ω (giving a cell potential of 0.361 V) and 100 k Ω (giving a cell potential of 0.347 V) representing the values for non-aerated and aerated solutions, respectively.

At high current density values, polarisation curves show fluctuations and power overshoot (Zhu *et al.*, 2013). This type of behaviour of a biological fuel cell was reported several times in literature (Ieropoulos *et al.*, 2010; Nien *et al.*, 2011; Winfield *et al.*, 2011; Güven *et al.*, 2016). It was observed that the internal resistance of the biofuel cell was also increased when power overshoot occurs (Ieropoulos *et al.*, 2010; Nien *et al.*, 2011; Winfield *et al.*, 2011). However, the reasons of power overshoot are yet not be fully understood (Zhu *et al.*, 2013).

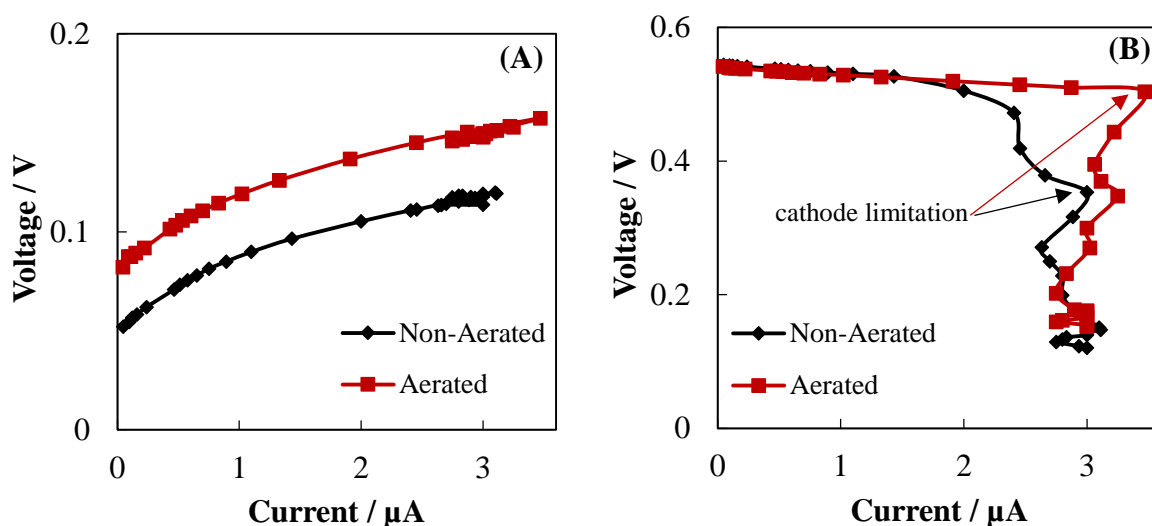


Figure 4. 4. Non-aerated and aerated anode (left) and cathode (right) potentials *versus* current curves obtained from EBFC tests. All enzymes used to construct EBFCs were at 4 mg mL^{-1} concentration and were immobilised on SPE (surface area: 0.126 cm^2). EBFCs were tested at batch mode using a glass cell in non-aerated and aerated solutions of 0.1 M PBS at pH 7 containing 5.5 mM glucose.

Figure 4.4 indicates anode and cathode performance throughout the fuel cell test for non-aerated and aerated solutions. Electron transfer occurs between the anode and cathode, in which the change in energy level can be measured as open circuit potential *versus* Ag/AgCl reference electrode (Jadhav *et al.*, 2014). Therefore, anodic and cathodic potentials were measured during polarization. Anode potentials performed similar for both conditions whereas cathode potential behaviour changed in the presence of oxygen significantly. The results indicate that cathode is a main limiting parameter for the power generation depending on the oxygen levels in the solution.

The fuel cell can produce more power under higher load (also higher internal resistance) than when oxygen is present in the solution. This is a significant discovery as it shows that P2O-

T169G was not affected by the presence of oxygen, on the contrary the performance of the fuel cell was enhanced as possibly in accordance with cathode. In other words, presence of oxygen increased the cathode performance without affecting anode hence the overall EBFC power output was increased.

The anodic potentials between non-aerated and aerated conditions showed a difference of ~ 0.032 V when the cell operates at open circuit and kept this difference during the test without any significant change. The proof of this same trend can be checked by simplifying the Figure 4.4 (A) using log scale giving a slope of 0.02 for both lines (see Figure C.2 in Appendix C). This shows that the anode performance is relatively same but limited to its initial capacity. The cathodic potential, however, showed very similar values at the beginning until the fuel cell was limited. This suggests that difference for OCP values are caused by the initial anode performance. This could be due to the efficiency of the enzyme immobilization as discussed in Chapter 3.

The EBFC was limited by cathode at the current value of $3 \mu\text{A}$ and $3.47 \mu\text{A}$ for non-aerated and aerated solutions, respectively (the points where the cell voltage showed sharp decrease and current values started to read the same value for different cell voltage values, marked on Fig. 4.4) for non-aerated and aerated glucose solutions respectively. This type of outcome was expected when the oxygen in the solution were not sufficient. However, the cathode was still limited although the solution was aerated. This shows that the aeration process was not sufficient enough to maintain the desired current requirements by the electrochemical reaction at the cathode. This is an expected discovery for batch systems where the oxygen depletion is inevitable in particular when continuously consumed by the cathode.

Performance Comparison between P2O-T169G and GOx

After demonstrating P2O-T169G in a biofuel cell, comparative fuel cell tests were carried out using GOx. The performance parameters of P2O-T169G and GOx based EBFCs were summarised in Table 4.2. The same fuel cell design and operating conditions with the oxygen study were also used in this section of the chapter. The EBFCs showed OCP values of 0.442 and 0.444 V for P2O-T169G and GOx, respectively. Anode and cathode potentials were 0.093 ± 0.015 and 0.534 ± 0.031 V for P2O-T169G (BOD at the cathode) and 0.072 ± 0.015 and 0.517 ± 0.004 V for GOx (BOD at the cathode) respectively at OCP. The maximum power values were obtained at $100 \text{ k}\Omega$ and $125 \text{ k}\Omega$ for P2O-T169G and GOx, respectively.

Parameters	EBFC Anode	
	P2O-T169G	GOx
OCP / V	0.442±0.02	0.444±0.02
Max Power / μW	1.06±0.2	0.8±0.1
Max Power Density / ($\mu\text{W cm}^{-2}$)	8.45±1.6	6.34±0.88
Limiting Current / μA	3.26±0.3	2.52±0.18
Limiting Current Density / ($\mu\text{A cm}^{-2}$)	25.83±2.41	20.03±1.4

Table 4. 2. Summary of the enzymatic biofuel cell performance results comparing P2O-T169G and GOx obtained from aerated system test. All enzymes used to construct EBFCs were at 4 mg mL⁻¹ concentration and were immobilised on SPE (surface area: 0.126 cm²). Anode and cathode potentials were 0.093±0.015 and 0.534±0.031 V for P2O-T169G (BOD at the cathode) and 0.072±0.015 and 0.517±0.004 V for GOx (BOD at the cathode) at OCP respectively. The maximum power values were obtained at 100 k Ω for P2O-T169G and 125 k Ω for GOx. All means and sample standard deviations from replicate measurements on n = 2 samples of each EBFC.

The cell voltage-current and power curves are displayed in Figure 4.5. P2O-T169G showed better performance than GOx. P2O-T169G had ~ 25 % more power output with a maximum power density value of 8.45 $\mu\text{W cm}^{-2}$ than GOx when oxygen is present in the glucose solution (max. power of 1.06 and 0.8 μW for P2O-T169G and GOx, respectively). Despite having slightly different anode and cathode potentials, the difference between the OCP values were very close to each other. Another important parameter worth mentioning is the limiting current density, in which, P2O-T169G has a higher value than GOx (3.26 μA versus 2.52 μA). Enhanced short circuit density suggests the contribution of more enzymes into the bio-electrochemical reaction as reported before (Halámková *et al.*, 2012).

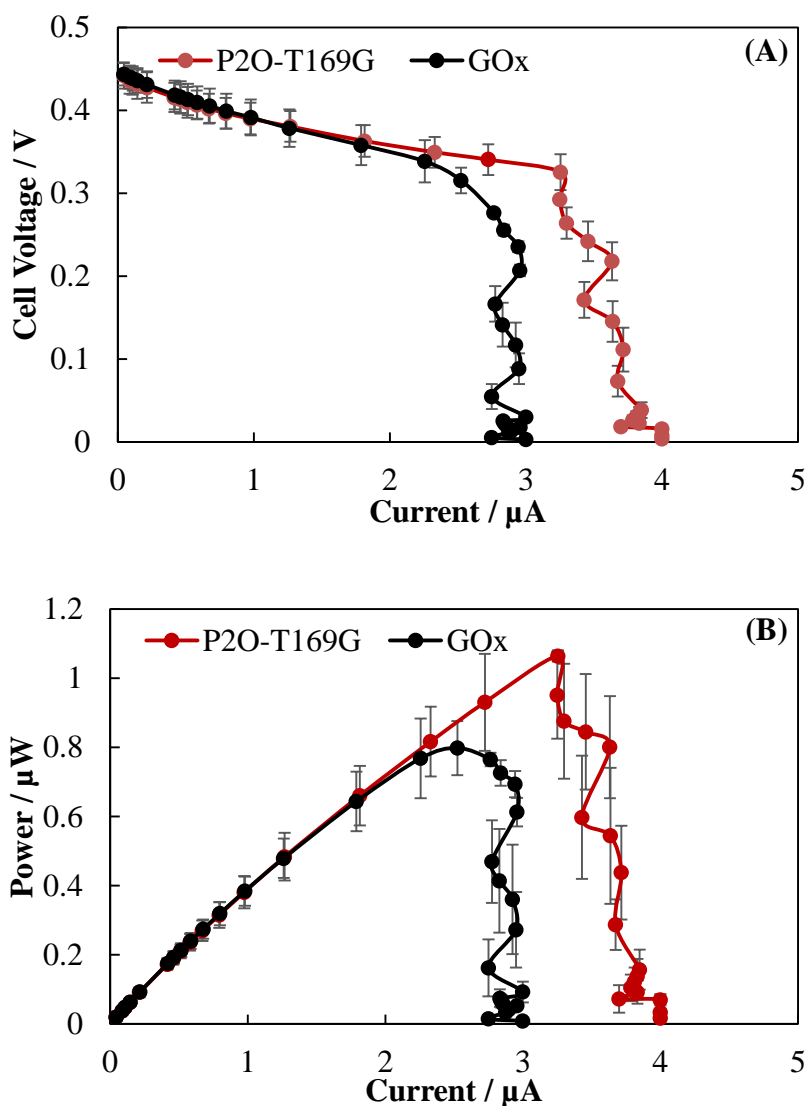


Figure 4. 5. (A) Cell voltage-current and (B) fuel cell polarization curves for P2O-T169G and GOx as EBFC anodes combined with BOD cathode. All enzymes used to construct EBFCs were at 4 mg mL^{-1} concentration and were immobilised on SPE (surface area: 0.126 cm^2). EBFCs were tested at batch mode using a glass cell in aerated solutions of 0.1 M PBS at pH 7 containing 5.5 mM glucose. Error bars are sample standard deviations of measurements on $n = 2$ samples of each EBFC.

Figure 4.6 shows the anode-cathode potentials *versus* current during polarisation test. The GOx based fuel cell was limited by cathode at lower current values than the P2O-T169G based fuel cell. Although both the cathodes were saturated with air prior to tests, P2O-T169G based fuel cell cathode showed better performance which is noteworthy. As discussed in Chapter 1, section 1.2.1, oxygen is the natural electron acceptor of GOx whereas P2O-T169G mutant was genetically modified not to utilise oxygen. Therefore, the enhanced performance of P2O-

T169G might be because it does not utilise oxygen at the anode, hence there is no competition with cathode regarding to oxygen. On the other hand, poor cathodic performance of the GOx based fuel cell, under same aerobic conditions with P2O-T169G, suggests that GOx might be competing with the cathode for oxygen resulting decreased fuel cell performance.

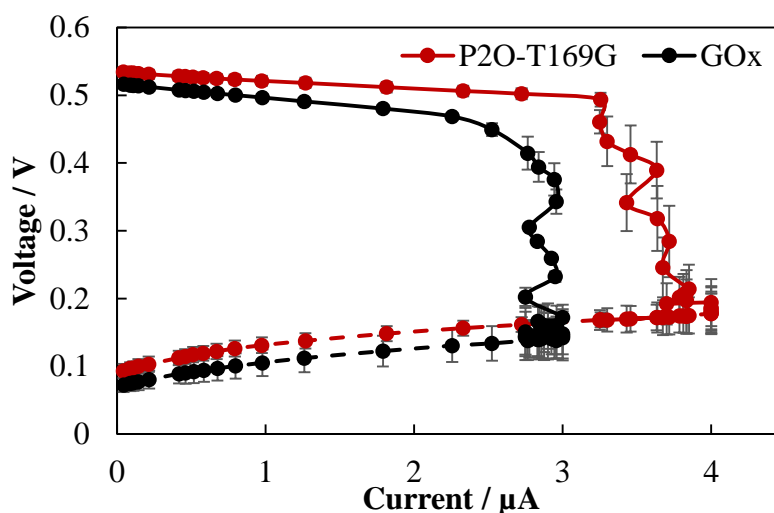


Figure 4. 6. Voltage-current curves of anode (dashed line)-cathode (straight line) potentials for P2O-T169G and GOx as EBFC anodes combined with BOD cathode. All enzymes used to construct EBFC were at 4 mg mL^{-1} concentration and were immobilised on SPE (surface area: 0.126 cm^2). EBFCs were tested at batch mode using a glass cell in aerated solutions of 0.1 M PBS at pH 7 containing 5.5 mM glucose. Error bars are sample standard deviations of measurements on $n = 2$ samples of each EBFC.

Performance of EBFC with P2O-T169G and Air-breathing Cathode

Oxygen resistant properties of the P2O-T169G was shown to have significant advantage over GOx in biofuel cell tests. The cathode limitation, on the other hand, is still a concern for batch type fuel cells where oxygen will decay over time resulting decreased fuel cell performance. A stack cell design with an air breathing carbon paper based cathode compartment was used to improve the cathode performance of the fuel cell. The surface area of the carbon paper electrode used in the stack cell was 1.77 cm^2 , 14 fold larger than it was for previous fuel cell electrodes (SPE) presented in this study. Enzyme concentrations of 10 mg mL^{-1} and 4 mg mL^{-1} were used for P2O-T169G and BOD respectively. The enzyme concentration for the anode was increased to avoid decreased anodic performance in the case of improved cathodic performance would be

achieved. The performance parameters of P2O-T169G –BOD based EBFCs were summarised in Table 4.3.

Parameters	EBFCs
OCP / V	0.558
Max Power / μW	52.3 \pm 10.8
Max Power Density / ($\mu\text{W cm}^{-2}$)	29.8 \pm 6.1
Limiting Current / mA	0.15 \pm 0.02
Limiting Current Density / (mA cm^{-2})	0.08 \pm 0.01

Table 4. 3. Summary of the enzymatic biofuel cell performance results obtained from P2O-T169G anode and air breathing BOD cathode. Anode and cathode potentials were -0.019 ± 0.035 and 0.524 ± 0.014 V for P2O-T169G and BOD at OCP. The maximum power values were obtained at $2.5\text{ k}\Omega$. All means and sample standard deviations from replicate measurements on $n = 2$ samples of each EBFC.

The air-breathing EBFC showed an OCP value of 0.558 V where the anode and cathode potentials were measured -0.019 ± 0.035 and 0.524 ± 0.014 V. This is ~26 % more of that observed when air-breathing cathode was not used. The reason of the enhanced OCP value can be explained by looking at the change in anode and cathode potentials. The anode potential was shifted negatively by 0.091 V and the cathode potential was shifted 0.007 V showing improved values for the electrodes.

Figure 4.7 shows the polarisation curve for air-breathing biofuel cell. The power generation from the biofuel cell reached its maximum value at an external resistance of around $2.5\text{ k}\Omega$ which is 40 times more load applied to the biofuel cell than previous results. This results a maximum power of $52.3\text{ }\mu\text{W}$ ($60.2\text{ }\mu\text{W}$ for the best test) and a power density of $29.8\text{ }\mu\text{W cm}^{-2}$ ($34\text{ }\mu\text{W cm}^{-2}$ for the best test). This is 3.4 times higher than the obtained values of when air-breathing cathode was not used (49 fold increase when power is compared with the EBFC where SPEs were used, from $1.07\text{ }\mu\text{W}$ to $52.57\text{ }\mu\text{W}$). Also, significant improvement was achieved for limiting current giving values of 0.14 mA (increased by 43 fold).

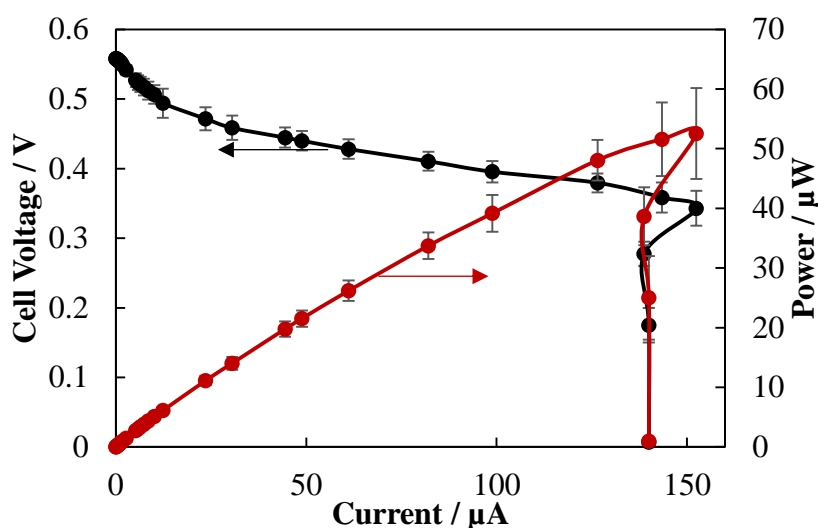


Figure 4. 7. Cell voltage-current and fuel cell polarization curves showing the performance of P2O-T169G anode and BOD cathode. Enzymes concentrations of 10 mg mL^{-1} and 4 mg mL^{-1} were used for anode and cathode respectively and were both immobilised on carbon paper electrodes (surface area: 1.77 cm^2). EBFCs were tested at batch mode using stack cell design in aerated solutions of 0.1 M PBS at pH 7 containing 5.5 mM glucose. Error bars are sample standard deviations of measurements on $n = 2$ samples of each EBFC.

Another important discovery for air-breathing EBFC is shown in Figure 4.8. The limitation of the biofuel cell was switched from cathode to anode suggesting that the air-breathing add-on to the fuel cell design significantly improved the cathode performance. These analyses show that the oxygen concentration is highly important for the fuel cell performance. Oxygen resistant properties of P2O-T169G combined with oxygen rich cathode leading an OCP and power output values in the EBFC.

Kwon *et al.*, 2014 demonstrated for the first time using P2O in an EBFC (Kwon *et al.*, 2014). However, they used air-breathing platinum as cathode not suggesting a fully enzymatic system (only anode is enzymatic) producing maximum power densities of $11.6 \mu\text{W cm}^{-2}$ and $40.7 \mu\text{W cm}^{-2}$ with and without the presence of the mediator, respectively. Although the systems are not fully comparable due to having different designs and enzyme-mediator assemblies, fully enzymatic, air-breathing, membrane-less EBFC developed in this study demonstrated comparable power density values of $29.8 \mu\text{W cm}^{-2}$ ($34 \mu\text{W cm}^{-2}$ for the best test) obtained in 5.5 mM glucose solution in 0.1 M PBS at pH 7 (200 mM used in the study by Kwon *et al.*, 2014)

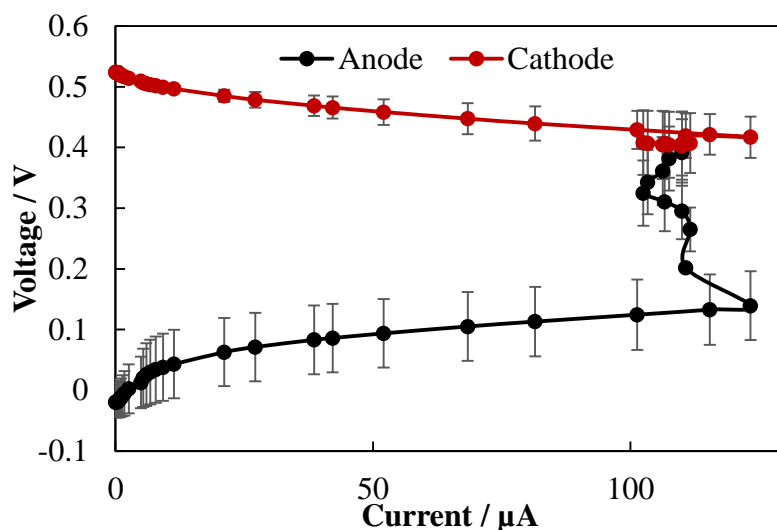


Figure 4. 8. Voltage-current curves of anode and cathode potentials for P2O-T169G and BOD respectively. Enzymes concentrations of 10 mg mL^{-1} and 4 mg mL^{-1} were used for anode and cathode respectively and were both immobilised on carbon paper electrodes (surface area: 1.77 cm^2). EBFCs were tested at batch mode using stack cell design in aerated solutions of 0.1 M PBS at pH 7 containing 5.5 mM glucose. Error bars are sample standard deviations of measurements on $n = 2$ samples of each EBFC.

In the case of co-immobilizing GOx and Fc on the electrodes, the power density of $29.8 \pm 4.31 \text{ } \mu\text{W cm}^{-2}$ at 0.318 V obtained in this study is 3 fold higher than that where FcCOOH was used in solution and GOx entrapped in MWCNT-ionic liquid gel ($10 \text{ } \mu\text{W cm}^{-2}$) and ~ 3 fold higher than that where GOx and Fc were directly crosslinked on the electrode without using nanomaterials ($13 \text{ } \mu\text{W cm}^{-2}$) (Shim *et al.*, 2011) and where Fc, MWCNTs and chitosan were employed on the electrode ($13 \text{ } \mu\text{W cm}^{-2}$) (Park *et al.*, 2011).

Furthermore, it is ~ 2 fold higher than the reported values ($15.8 \text{ } \mu\text{W cm}^{-2}$) where Fc was used with carbon nanocomposite materials (Zhao *et al.*, 2009) and higher performance than that where graphene nano-sheets were used ($24.3 \text{ } \mu\text{W cm}^{-2}$), however the EBFC was tested in the presence of 100 mM glucose solution which 18 fold higher than in this study (5.5 mM) (Liu *et al.*, 2010).

The performance of the biofuel cell in this study was also showed power densities in the same range with that in which Fc is used as a mediator at the anode incorporation with nafion[®] and MWCNTs similar to this study (Tan *et al.*, 2010). However, this fuel cell lost 94 % of its initial performance after 5 h of operation (also operated at pH 5).

4.3.2. Stability of EBFC with P2O-T169G and Air-breathing Cathode

The stability of the air-breathing EBFCs was investigated using two different approaches. In the first approach, the operational stability of the EBFC was tested under constant external load of 4 k Ω after the initial polarization test. Then, the external load was removed after EBFC lost more than 60-70 % of its initial potential and left to rest until it reached steady-state. As the glucose was consumed in the solution, a fresh solution of glucose was prepared and another polarization and stability tests were carried out each time. This process was performed 3-times in total resulting 4 polarization and 3 stability tests. The fuel cell performance parameters of these tests are shown in Figure 4.9. (Raw data for stability: Figure C. 3 in Appendix C).

The maximum power output of the EBFC showed a decreasing trend in every test performed after each stability test. The final value of 26.7 μ W was obtained from the test performed on the 37th hour. This is ~40 % less than its initial value of 45.4 μ W. OCP values of the EBFC before polarization tests showed similar trend with the maximum power output values with a slight drift at the last test (Figure 4.9 (C)). This can also be seen from the voltage-current and power curves (Figure 4.9 (A-B)). OCP of the EBFC was first decreased from 0.558 V to 0.539 V and then increased to 0.547 V. This might be because of the instabilities of the EBFC over time such as; the solution of the EBFC was refreshed before each polarization test, the electrodes were disturbed from their steady-state. Thus, fluctuations from expected trends can be possible.

Although the same glucose concentration was added before each polarization test, a continuous feeding system would be a better solution to test the stability of the EBFC. Another approach to test the stability was taken to have better view of the performance of the EBFC. A constant glucose feeding system was designed using a peristaltic pump operating at a flow rate of 0.3 mL min⁻¹. The flow rate of glucose stock solution was chosen an estimate to be high enough to maintain same glucose concentrations and low enough to prevent leaking due to excessive pressure in the stack cell. However, optimization of the flow rate would be necessary for future studies. Figure 4.11 shows the stability of the air breathing EBFC under 4 k Ω external load. Anode and cathode potentials were recorded individually *versus* Ag/AgCl electrode to have a better view on the performance of the biofuel cell.

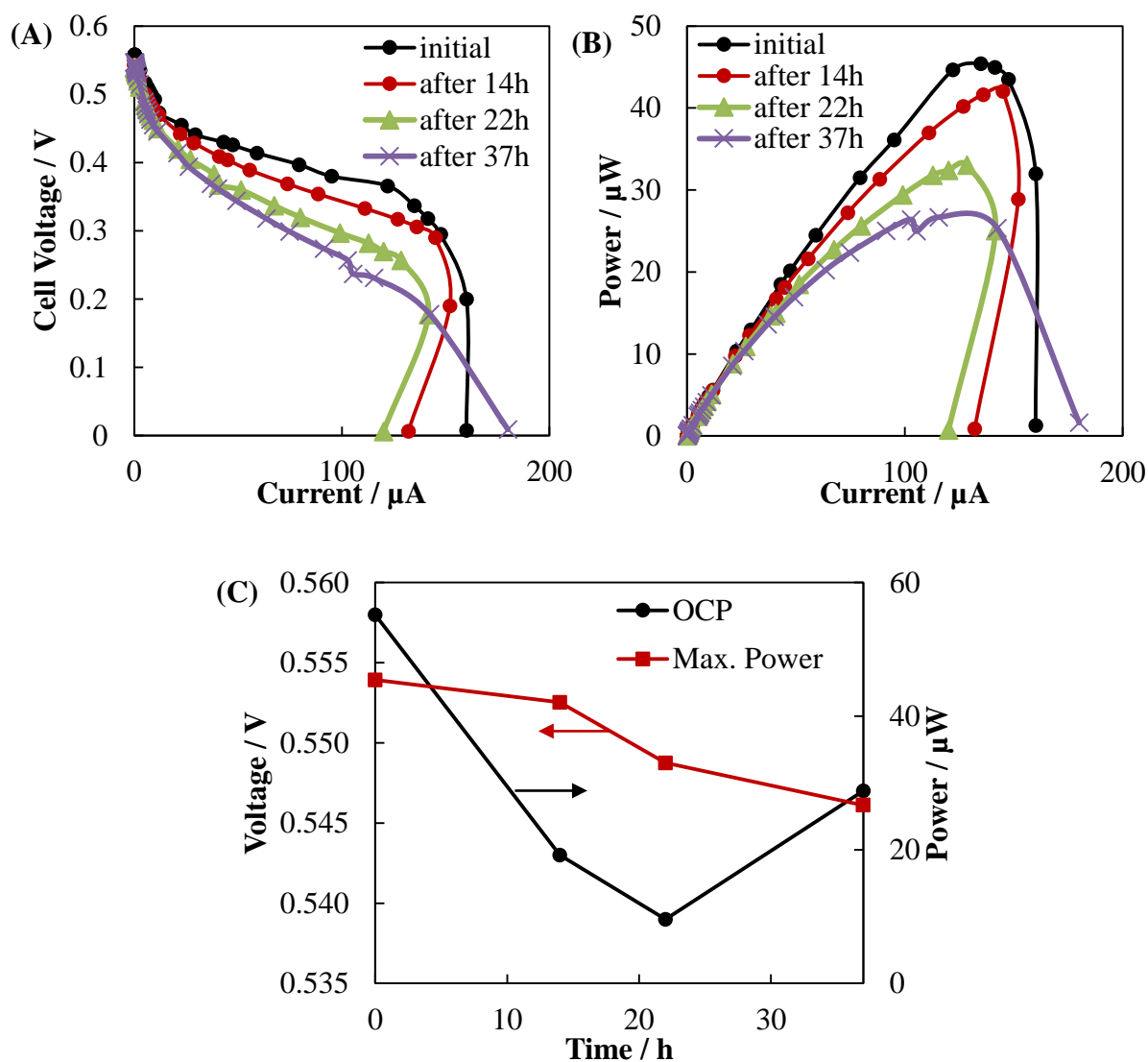


Figure 4.9. Fuel cell performance parameters at different times of polarisation for air-breathing EBFCs using P2O-T169G and BOD at the anode and cathode respectively. (A) Voltage-Current (B) Power curve (C) OCP-Max. Power *versus* time. Enzymes concentrations of 10 mg mL^{-1} and 4 mg mL^{-1} were used for anode and cathode respectively and were both immobilised on carbon paper electrodes (surface area: 1.77 cm^2). EBFCs were tested at batch mode using stack cell design in aerated solutions of 0.1 M PBS at $\text{pH } 7$ containing 5.5 mM glucose. The maximum power values were obtained at $4 \text{ k}\Omega$.

Figure 4.10 shows the continuous potential values of the cell and the power production from the air breathing biofuel cell for 18 days. The cell voltage values showed a consistent decay during the first 24 h (down to $\sim 32\%$ capacity) and stabilized for the following 2 days (~ 23 and $\sim 21\%$ capacity on 2nd and 3rd day respectively) resulting an average power density value of a $5.3 \mu\text{W cm}^{-2}$.

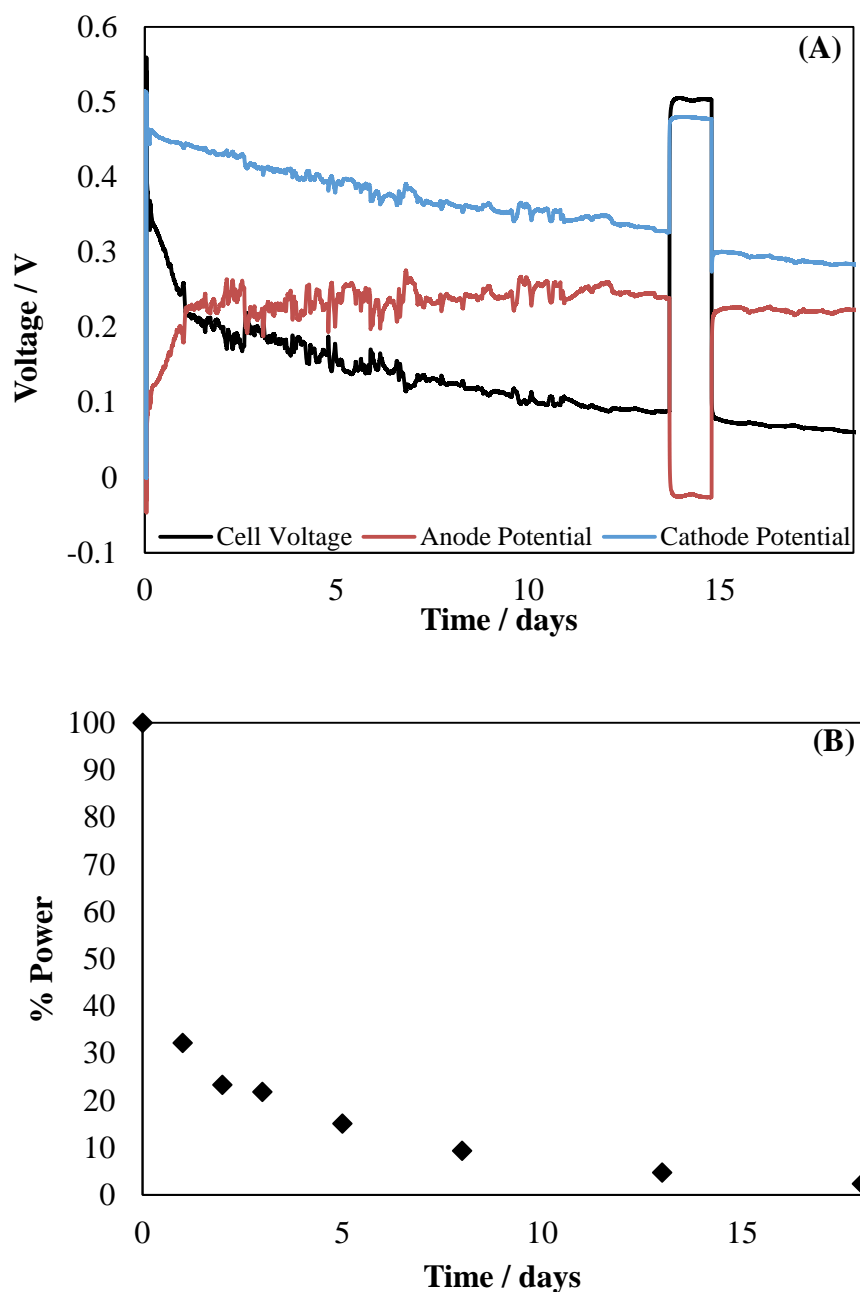


Figure 4. 10. (A) Cell voltage, anode and cathode potentials and (B) Percentage power density change of the EBFC over time during continuous operation of 18 days. P2O-T169G (10 mg mL^{-1}) and BOD (4 mg mL^{-1}) were used at the anode and cathode respectively and were both immobilised on carbon paper electrodes (surface area: 1.77 cm^2). EBFCs were tested at continuous mode using stack cell design with a flow rate of 0.3 mL min^{-1} in aerated solutions of 0.1 M PBS at pH 7 containing 5.5 mM glucose.

The cell voltage then exponentially decayed for the next two weeks of operation reaching a final value of 60 mV with a power density value of a $0.57 \mu\text{W cm}^{-2}$. During the 13th day of the

operation, the load on the cell was removed and left at OCP for 24 h. It was intended to observe the behaviour of the cell during the OCP state and re-applying load. It was found out that after the resting period the cell was maintained the cell voltage from where it was left of. This indicates that the decrease in cell voltage strongly depended of the enzyme activities. The anode and cathode potentials suggest that the overall cell performance was limited by anode especially during the first week of the operation. This is similar with the findings obtained from polarisation experiments. The reason for the initial decay might be due to denaturation and/or inactivation of the enzyme at the anode during a week of operation (Wieckowski, 2009). Later the cathode also showed decreasing voltage characteristics accordingly with anode.

Furthermore, the reason why the sharp decay in the first 24 h following by moderate decrease in the next few days might be also because of the external load chosen as it was rather closer to the maximum current density of the biofuel cell. Selecting the external resistance that is associated with the maximum sustainable power is very difficult as the rate of the charge transfer at the current limiting electrode or the potential across the fuel cell cannot be controlled externally (Menicucci *et al.*, 2006). High instantaneous electric currents might be achieved which results higher than the maximum sustainable rate of charge transfer from the current limiting electrode, in this case, the anode (Menicucci *et al.*, 2006). As a result, more studies should be carried out regarding to determining the optimum external load for sustainable power production. Cathode potential, on the other hand, was only decreased by 10 % during 3 days of operation. This is promising because if the anode is improved, more stable biofuel cells can be obtained.

4.4. Conclusions

In this chapter, the performance and stability of glucose/O₂ fuel cells were investigated using P2O-T169G, GOx at the anode and BOD at the cathode. The EBFC based on P2O-T169G showed an increasing performance by 40 % when oxygen is present in the glucose solution (from 6.89 to 9.56 $\mu\text{W cm}^{-2}$) which suggests that P2O-T169G was not affected from oxygen which is a significant improvement for EBFC anodes. On the other hand, EBFC was limited by cathode due to insufficient oxygen concentration in the solution although it was aerated prior to tests. Oxygen limitation was found to be an important parameter for stable cathode to enhance overall biofuel cell performance As a result, this becomes a design problem as the amount of dissolved oxygen in liquid phase will always be limited to a point.

The performance of P2O-T169G based biofuel cell was also compared with GOx based biofuel cells using aerated glucose solutions. Maximum power density values of 8.45 ± 1.6 and $6.34 \pm 0.88 \mu\text{W cm}^{-2}$ were obtained for P2O-T169G and GOx respectively. P2O-T169G based anode showed ~25 % more current density than GOx. Furthermore, GOx based biofuel cell showed poorer cathodic performance suggesting that GOx might be utilizing oxygen. This is an important discovery towards the use of P2O-T169G as an alternative to GOx in biofuel cell applications. Further investigation of P2O-T169G based anode configuration should also be conducted to improve the anodic performance of the biofuel cell.

Finally, an air breathing bio fuel cell based on P2O-T169G and BOD was successfully achieved resulting an OCP of 0.558 V and the maximum power density of $29.8 \pm 6.1 \mu\text{W cm}^{-2}$ ($34 \mu\text{W cm}^{-2}$ for the best test) at 0.318 V. The stability of fuel cell was observed for a duration of 18 days and the current-limiting electrode was found to be the anode. Power density of $5.3 \mu\text{W cm}^{-2}$ was achieved after the fast decay within the first 24 h and stabilised for 2 days. The cell voltage then exponentially decayed for the next two weeks of operation reaching a final value of 60 mV with a power density value of a $0.57 \mu\text{W cm}^{-2}$. The results were relatively good compared to literature, however, further investigations of fuel cell operation conditions needs to be carried out to optimise the sustainable power output of the biofuel cell.

Chapter 5. Conclusion and Recommendations for Future Work

5.1. Conclusion

The aim of this project was to develop an enzymatic biofuel cell that can produce power from glucose using pyronase-2-oxidase (P2O) enzyme. This study demonstrated the electrochemical behaviour of P2O in solution or immobilised onto electrode surface under human physiological conditions. A membrane-less enzymatic biofuel cell was developed based on P2O with good current density and stability. Comparative analyses were conducted using glucose oxidase (GOx) since it is one of the most employed enzymes in enzymatic electrode fabrication.

P2O and its mutants was first characterised when free in solution with ferrocene carboxylic acid (FcCOOH) mediator using electrochemical techniques in terms of catalytic activity, glucose affinity, oxygen utilisation and stability. P2O-T169G mutant exhibited promising performance with good catalytic activity and stability suggesting significant advantage over GOx in aerobic conditions. Although providing simplicity in design and operation, using enzymes in solution is not practical. It was, however, helpful to understand the electrochemical behaviour of P2O enzymes towards their utilisation for immobilised systems.

The performance of P2O-T169G and GOx were later investigated using different immobilization techniques. A novel immobilisation method incorporating MWCNTs into Fc-Nafion films was developed to achieve successful immobilisation. This is one of the good methods for using Fc mediator in literature, however, it should further be improved and tested in terms of enzyme deactivation or denaturation. P2O-T169G was showed not to utilise oxygen for glucose oxidation where, GOx was significantly affected. This is an important outcome from this study validating the steady-state kinetic experiments reported in literature using electrochemical methods.

Finally, the performance and stability of glucose/O₂ fuel cells were investigated. Fc-Nafion-MWCTNs based anode combined with the promising properties of P2O-T169 showed better performance than widely studied GOx under same circumstances. This is one of the most significant outcomes of this study as it leads the way towards the use of P2O enzyme instead of GOx in biofuel cell applications. Furthermore, a well-stable biocathode based on BOD showed very good performance especially with the air-breathing cathode design. Further investigations could be made to enhance mechanical properties of the enzyme electrode to have

even more stable cathodes using new materials such as graphene. It is expected that developed electrodes will be helpful to take a step forward for the applications of EBFCs and also useful for the development of biosensors.

5.2. Recommendations for Future Work

5.2.1. Optimization of Enzyme Electrodes and EBFC

An enzymatic fuel cell using P2O-T169G and BOD enzymes at the anode and cathode side respectively have been successfully developed in this study. However, further optimization of enzymatic electrodes is needed to get better performance of the enzymatic fuel cell and improve its stability. Therefore, following project objectives are outlined for the scope of the future work;

- Optimization of enzymatic electrodes (anode and cathode) to be used in enzymatic fuel cells will be carried out. Especially more work needs to be carried out for P2O and GOx such as testing same unit of enzymes for better comparison of the enzymes between each other and the reported values in literature.
- Testing optimized electrodes in an enzymatic fuel cells design (stack) with/without oxygen present for comparative study by using carbon paper electrodes (alternative electrodes could also be used) and using different modes (batch, continuous, closed and air-breathing mode).
- Stability experiments for the enzymatic fuel cell in a continuous flow mode. This can be further expanded to a microfluidic system using different electrodes such as gold.
- Testing the enzymatic fuel cell for real samples such as blood, fruit juice and *etc.*

5.2.2. Enzymes

Pyranose-2-Oxidase mutant T169G (P2O-T169G) was shown to have good electrochemical performance for biofuel cells applications, however, genetic modifications are needed to obtain this enzyme which might be a limitation for mass production. Pyranose dehydrogenase (PDH) on the other hand, is a fungal flavin-dependent sugar oxidoreductase with a molecular mass of 66.5 kD, related to the P2O both structurally and catalytically (Tan *et al.*, 2013). It was also reported to show similar biological functions (Tan *et al.*, 2013). The main difference between PDH and P2O is that, PDH does not utilise oxygen as an electron acceptor which can be

important for membrane-less biofuel cell design where oxygen is also needed for the cathodic reaction (Yakovleva *et al.*, 2012). The structure of PDH is shown in Figure 5.1.

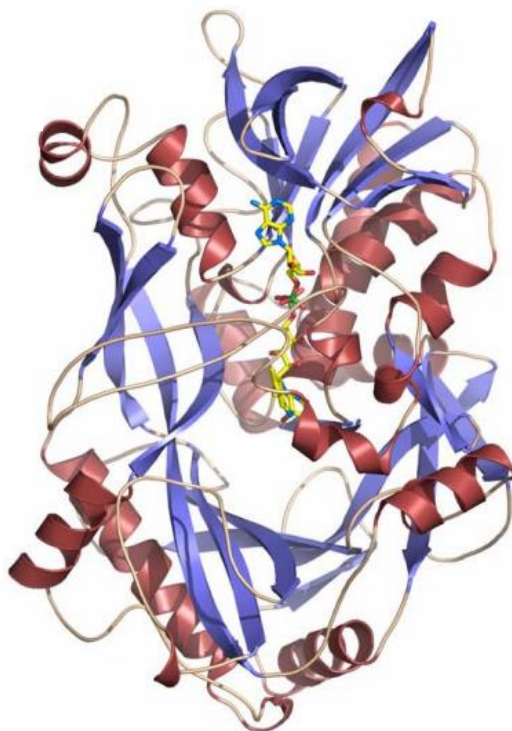


Figure 5. 1. Structure of PDH from *Agaricus meleagris* (Tan *et al.*, 2013)

The enzymatic biofuel cells utilising PDH enzyme show promising results when used with osmium polymers (Shao *et al.*, 2013; Ó Conghaile *et al.*, 2016). Osmium polymer, as explained in Chapter 2, is still a concern especially for long term stable biofuel cell applications due to their toxic and non-biocompatible natures (Hao Yu and Scott, 2010). However, a novel immobilization method developed in this study incorporating ferrocene, nafion and multi-walled carbon nanotubes would be a good alternative to utilise PHD for bio-sensing and biofuel cell applications.

5.2.3. Materials for Electrode Fabrication

Graphene has become very popular in enzymatic biofuel cell electrode fabrication due to its promising properties such as very high surface areas ($2630 \text{ m}^2 \text{ g}^{-1}$), high mechanical conductivity and easy of functionalization. (Babadi *et al.*, 2016). Electron transfer abilities of graphene was already presented in literature for anodic or cathodic electrode fabrication (Shan *et al.*, 2009; Lalaoui *et al.*, 2015). Figure 5.2 shows a representation of the use of graphene with multi-walled carbon nanotubes (MWCNTs) in oxygen reduction by laccase.

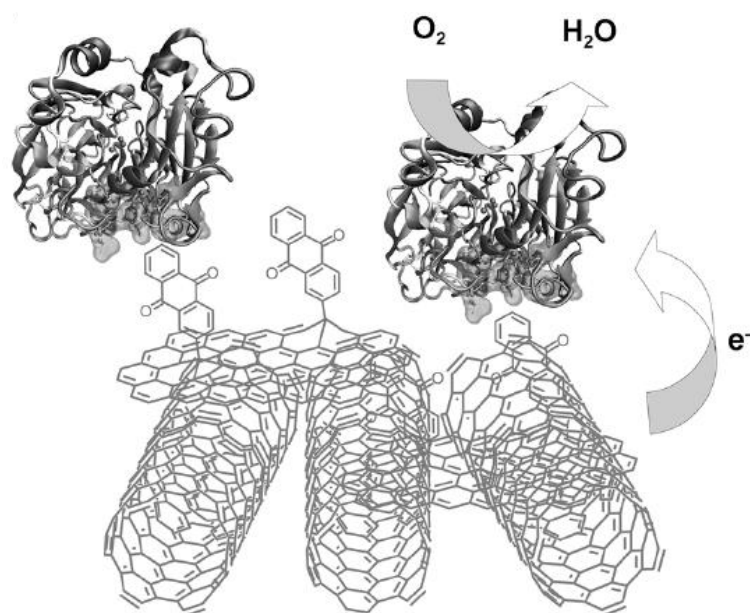


Figure 5. 2. Schematic for oxygen reduction by laccase using graphene-multi-walled carbon nanotubes assembly (Lalaoui *et al.*, 2015)

The feasibility of using reduced graphene oxide (rGO) was tested using different dispersions in ethanol (1 mg mL^{-1}) and mixture with MWCNTs (rGO-MWCNTs) were tested when for oxygen reduction by bilirubin oxidase (BOD). BOD was immobilised on modified electrodes as explained in Chapter 4 and tested in PBS at pH 7.

Figure 5.3 shows the CVs of BOD immobilised on rGO and rGO+MWCNTs modified electrodes. The electrochemical activity of BOD using graphene as electrode material has been successfully achieved. A mixture of MWCNTs and rGO was also prepared and it can be seen from Figure 5.3 (B) that the catalytic current response of MWCNTs was enhanced when mixed with rGO. Scanning-electrode microscopy (SEM) images of rGO and rGO+MWCNTs show the incorporation of rGO in MWCNTs structure (Figure 5 insets). rGO was observed to form thin flat flakes on the electrode surface, on the other hand when mixed with MWCNTs, it wraps around the nanotubes and creates intermolecular connections. This might be the reason of the enhanced catalytic current response. These results are very encouraging towards the use of graphene in fabricating enzyme electrodes as it could also be used to improve the electron transfer for glucose oxidation.

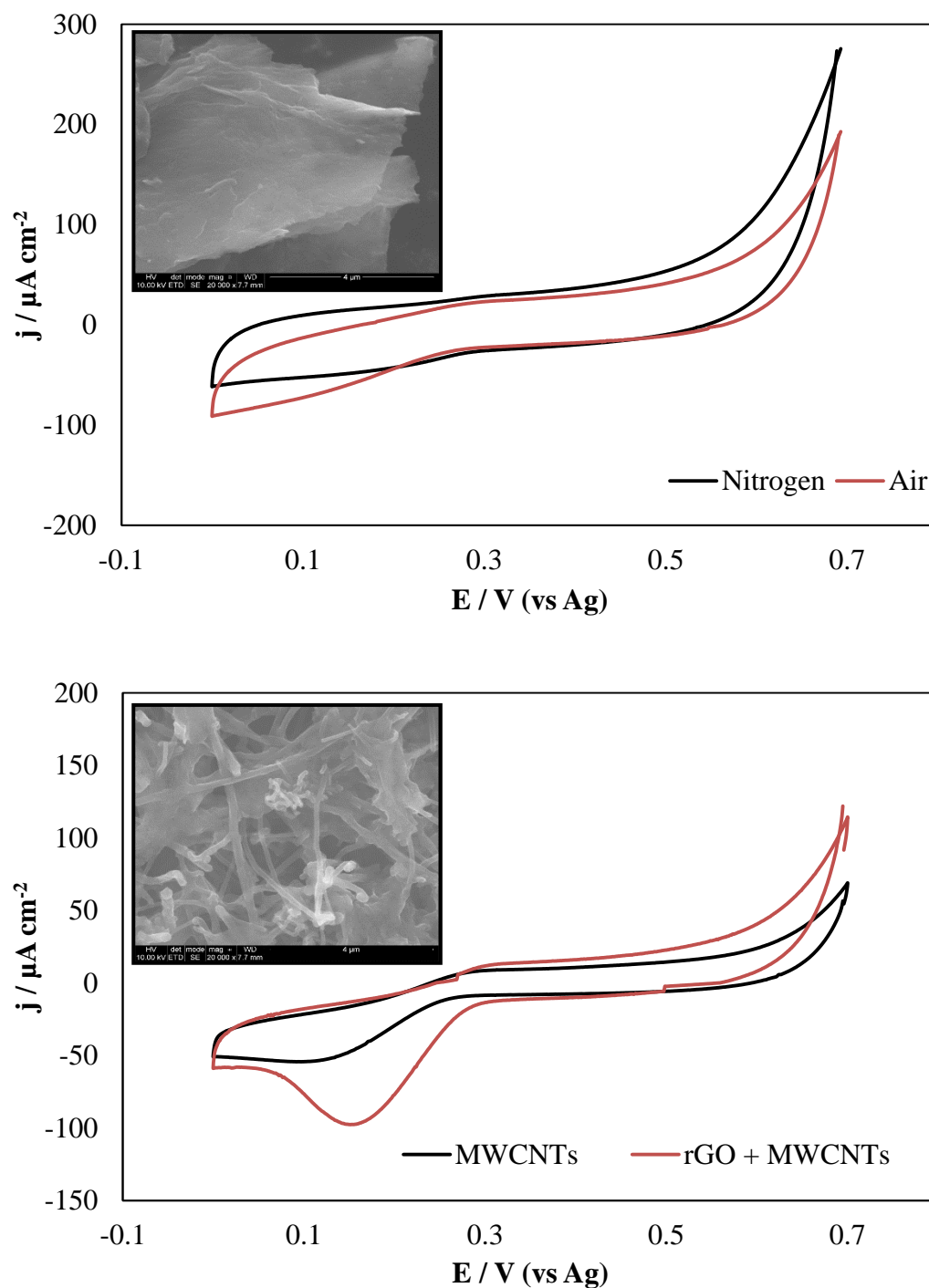


Figure 5. 3. CVs of BOD immobilised on (A) rGO (inset: SEM image, 4 μm magnification) and (B) rGO+MWCNTs (inset: SEM image, 4 μm magnification) modified electrodes, tested in air and/or nitrogen saturated PBS at pH 7, 5 mV s^{-1} scan rate

5.2.4. Biofuel Cell Design

Different strategies can be used to design enzymatic biofuel cells where micro chemical systems have several advantages towards the miniaturization of energy conversion for implantable

applications (Zebda *et al.*, 2011). Therefore, microfluidic systems have been popular in the field of enzymatic biofuel cell design (Togo *et al.*, 2007; Zebda *et al.*, 2009; González-Guerrero *et al.*, 2013). Figure 5.4 shows a glucose/O₂ microfluidic biofuel cell which can produce a power density of 110 $\mu\text{W cm}^{-2}$ at 0.3 V with 10 mM glucose at 23 C.

This type of fuel cells based on non-mixing two streams due to laminar fluid flows, therefore specific streams can be fed for anode and cathode to eliminate negative effects such as oxygen at the anode (Zebda *et al.*, 2011). However, when used with enzymes such as P2O-T169G, the complication of the design in microfluidic systems can be eliminated as it does not utilise oxygen for glucose oxidation. Furthermore, air-breathing add-on could also be added to this type of fuel cells. As a result, a novel microfluidic enzymatic fuel cell based on P2O-T169G at the anode combined with air-breathing cathode based on BOD would be promising for future studies.

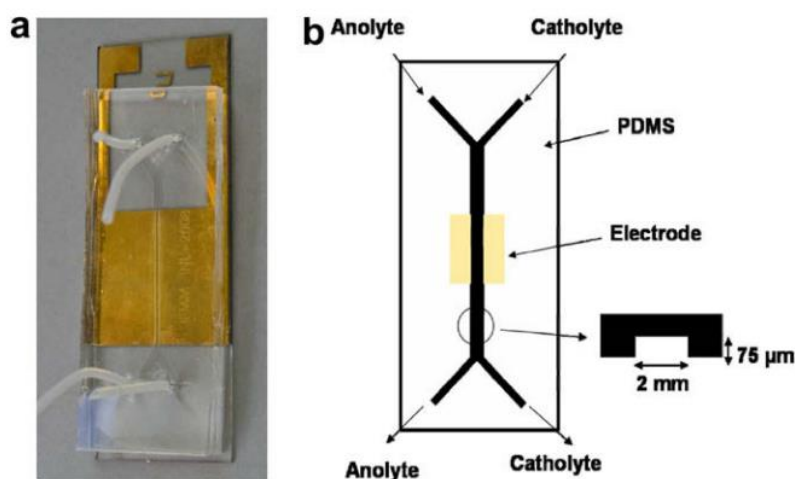


Fig. 1. Glucose/O₂ microfluidic biofuel cell, (a) PDMS-glass device, (b) Scheme of the device consisted in a Y-shaped microfluidic channel with 2 inlets and 2 outlets.

Figure 5. 4. (A) Scheme of Y-shaped glucose/O₂ microfluidic biofuel cell (B) PDMS-glass device.

Appendix

Appendix A

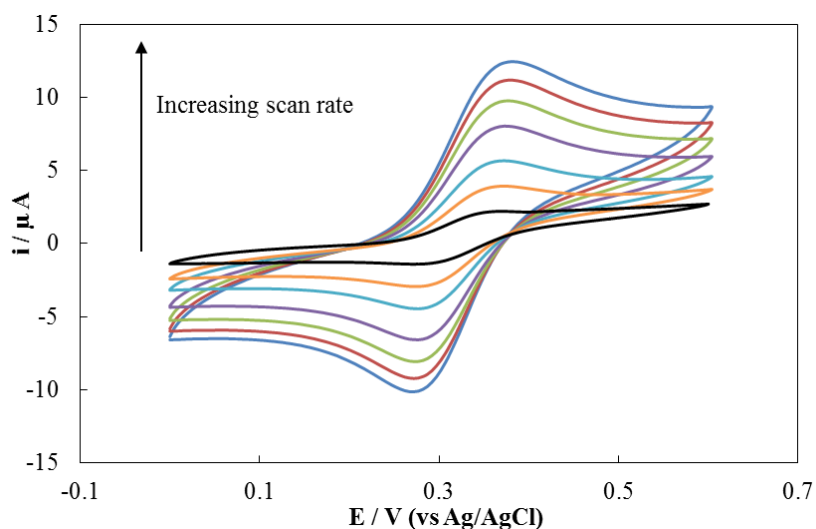


Figure A. 1. CV (scan rate: 10 mV s^{-1}) scans of nitrogen saturated solution experiments with P2O-WT. Tests were performed at various scan rates of 0.5 V s^{-1} (outer scan), 0.4 V s^{-1} , 0.3 V s^{-1} , 0.2 V s^{-1} , 0.1 V s^{-1} , 0.05 V s^{-1} and 0.01 V s^{-1} (inner scan) with 0 mM glucose concentration of 0.5 mM FcCOOH in PBS at pH 7. (GCE surface area: 0.071 cm^2).

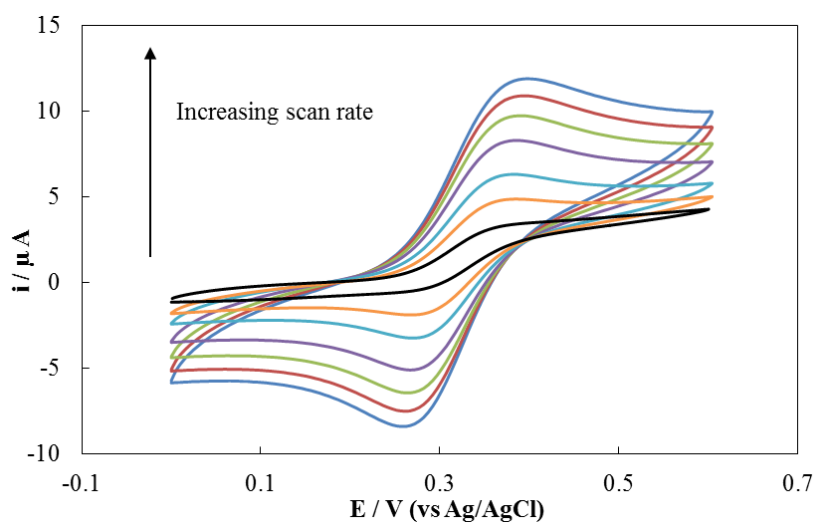


Figure A. 2. CV (scan rate: 10 mV s^{-1}) scans of nitrogen saturated solution experiments with P2O-WT. Tests were performed at various scan rates of 0.5 V s^{-1} (outer scan), 0.4 V s^{-1} , 0.3 V s^{-1} , 0.2 V s^{-1} , 0.1 V s^{-1} , 0.05 V s^{-1} and 0.01 V s^{-1} (inner scan) with 2 mM glucose concentration of 0.5 mM FcCOOH in PBS at pH 7. (GCE surface area: 0.071 cm^2).

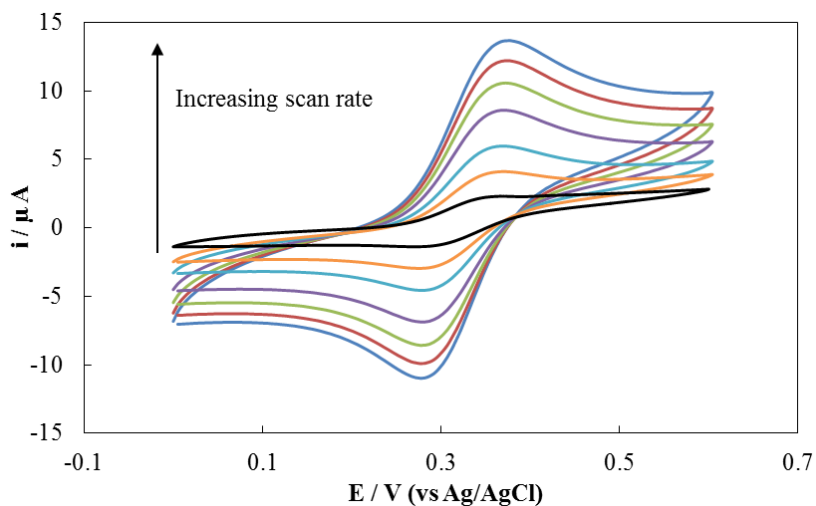


Figure A. 3. CV (scan rate: 10 mV s^{-1}) scans of nitrogen saturated solution experiments with P2O-T169S. Tests were performed at various scan rates of 0.5 V s^{-1} (outer scan), 0.4 V s^{-1} , 0.3 V s^{-1} , 0.2 V s^{-1} , 0.1 V s^{-1} , 0.05 V s^{-1} and 0.01 V s^{-1} (inner scan) with 0 mM glucose concentration of 0.5 mM FcCOOH in PBS at pH 7. (GCE surface area: 0.071 cm^2).

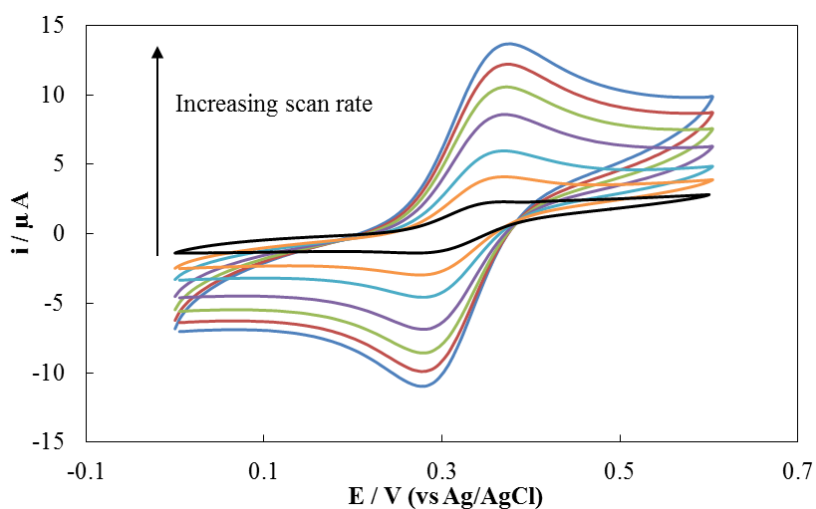


Figure A. 4. CV (scan rate: 10 mV s^{-1}) scans of nitrogen saturated solution experiments with P2O-T169S. Tests were performed at various scan rates of 0.5 V s^{-1} (outer scan), 0.4 V s^{-1} , 0.3 V s^{-1} , 0.2 V s^{-1} , 0.1 V s^{-1} , 0.05 V s^{-1} and 0.01 V s^{-1} (inner scan) with 2 mM glucose concentration of 0.5 mM FcCOOH in PBS at pH 7. (GCE surface area: 0.071 cm^2).

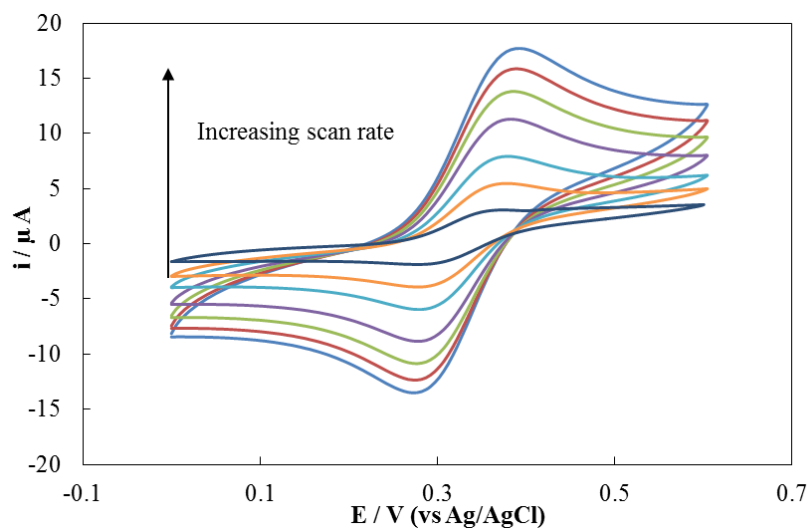


Figure A. 5. CV (scan rate: 10 mV s^{-1}) scans of nitrogen saturated solution experiments with P2O-T169G. Tests were performed at various scan rates of 0.5 V s^{-1} (outer scan), 0.4 V s^{-1} , 0.3 V s^{-1} , 0.2 V s^{-1} , 0.1 V s^{-1} , 0.05 V s^{-1} and 0.01 V s^{-1} (inner scan) with 0 mM glucose concentration of 0.5 mM FcCOOH in PBS at pH 7. (GCE surface area: 0.071 cm^2).

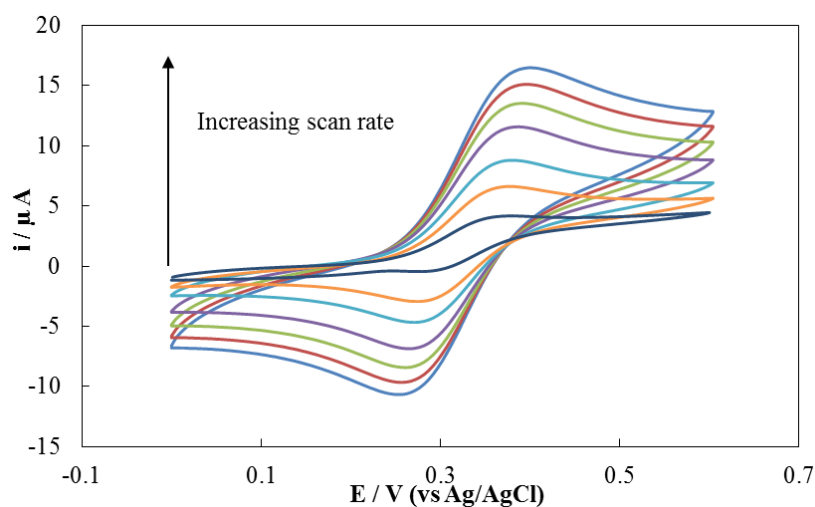


Figure A. 6. CV (scan rate: 10 mV s^{-1}) scans of nitrogen saturated solution experiments with P2O-T169G. Tests were performed at various scan rates of 0.5 V s^{-1} (outer scan), 0.4 V s^{-1} , 0.3 V s^{-1} , 0.2 V s^{-1} , 0.1 V s^{-1} , 0.05 V s^{-1} and 0.01 V s^{-1} (inner scan) with 2 mM glucose concentration of 0.5 mM FcCOOH in PBS at pH 7. (GCE surface area: 0.071 cm^2).

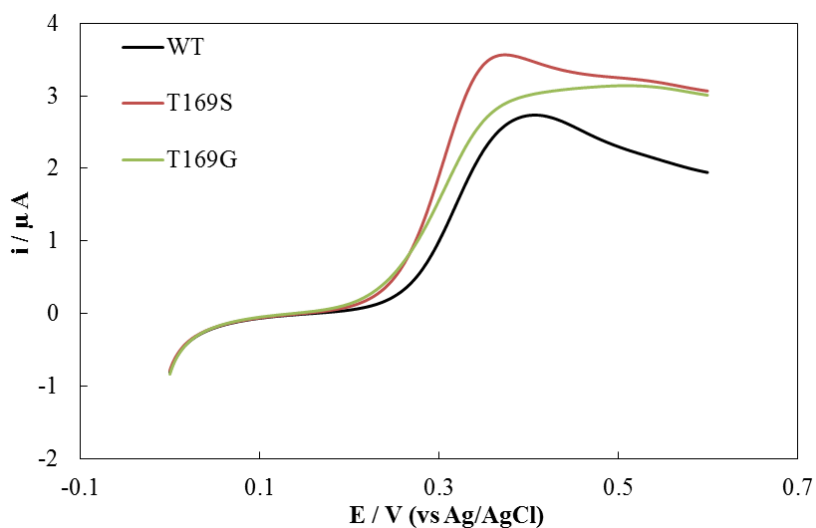


Figure A. 7. Raw data for the LSV (scan rate: 1 mV s^{-1}) scans of nitrogen saturated solutions with 2 mM concentrations of glucose added to the solution containing 0.5 mM FcCOOH and 1 mg mL^{-1} concentrations of P2O-WT, P2O-T169S and P2O-T169G at pH 7. (GCE surface area: 0.071 cm^2)

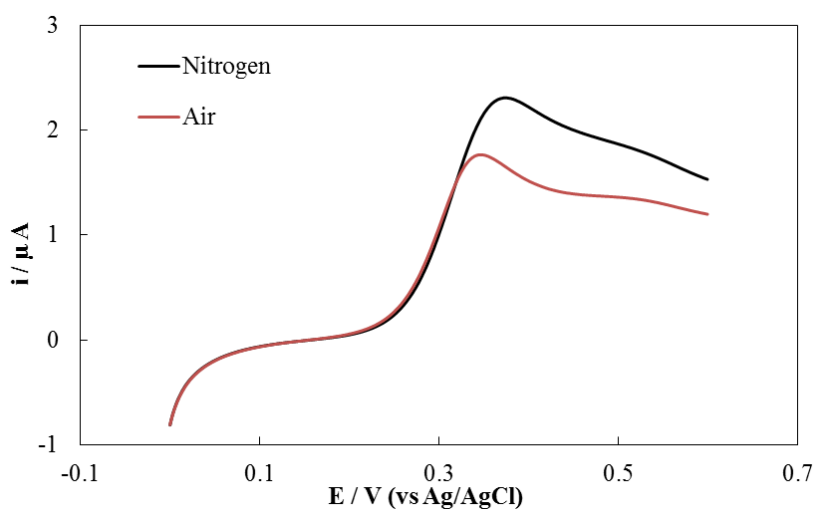


Figure A. 8. LSV (scan rate: 1 mV s^{-1}) scans of P2O-WT (1 mg mL^{-1} in PBS) in nitrogen and air saturated solutions with 1 mM concentrations of glucose added to the solution containing 0.5 mM FcCOOH in PBS at pH 7. (GCE surface area: 0.071 cm^2).

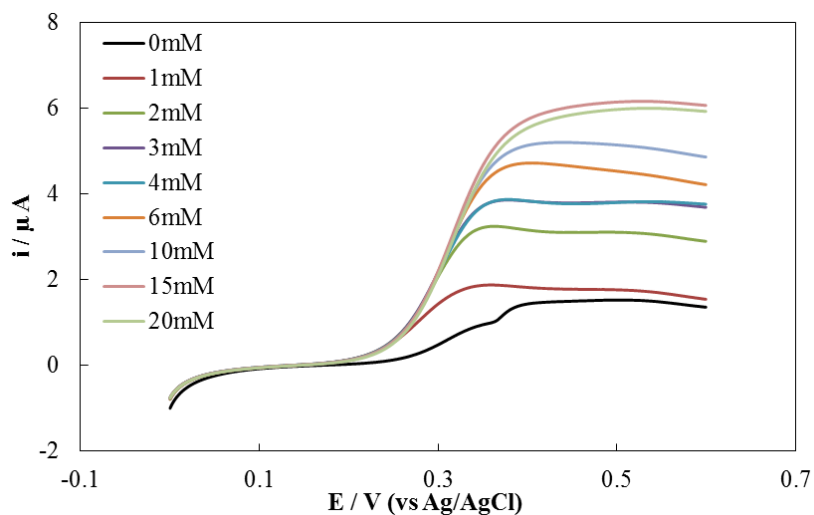


Figure A. 9. LSV (scan rate: 1 mV s^{-1}) scans of nitrogen saturated solutions with various glucose concentrations added to the solution containing 0.5 mM FcCOOH and $1 \text{ mg mL}^{-1} \text{ GOx}$ in PBS at pH 7. (GCE surface area: 0.071 cm^2).

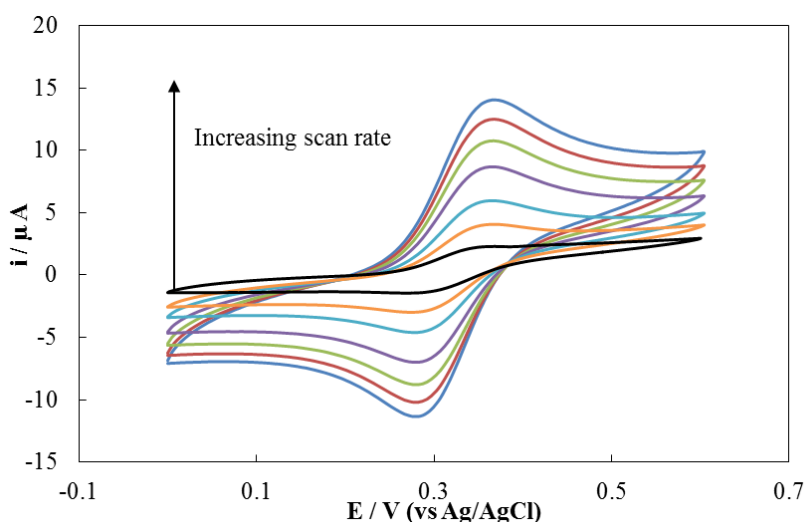


Figure A. 10. CV (scan rate: 10 mV s^{-1}) scans of nitrogen saturated solution experiments with GOx. Tests were performed at various scan rates of 0.5 V s^{-1} (outer scan), 0.4 V s^{-1} , 0.3 V s^{-1} , 0.2 V s^{-1} , 0.1 V s^{-1} , 0.05 V s^{-1} and 0.01 V s^{-1} (inner scan) with 0 mM glucose concentration of 0.5 mM FcCOOH in PBS at pH 7. (GCE surface area: 0.071 cm^2).

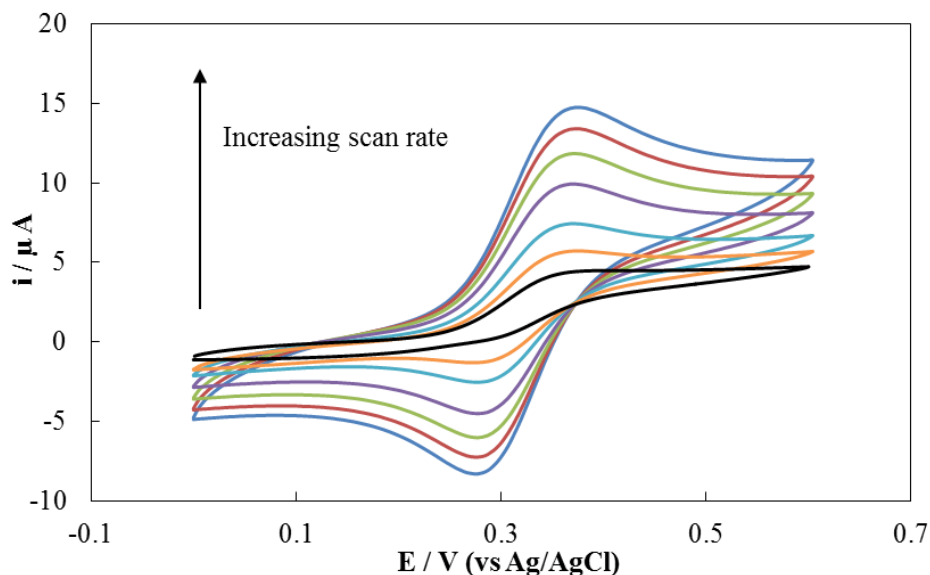


Figure A. 11. CV (scan rate: 10 mV s^{-1}) scans of nitrogen saturated solution experiments with GOx. Tests were performed at various scan rates of 0.5 V s^{-1} (outer scan), 0.4 V s^{-1} , 0.3 V s^{-1} , 0.2 V s^{-1} , 0.1 V s^{-1} , 0.05 V s^{-1} and 0.01 V s^{-1} (inner scan) with 2 mM glucose concentration of 0.5 mM FcCOOH in PBS at pH 7. (GCE surface area: 0.071 cm^2).

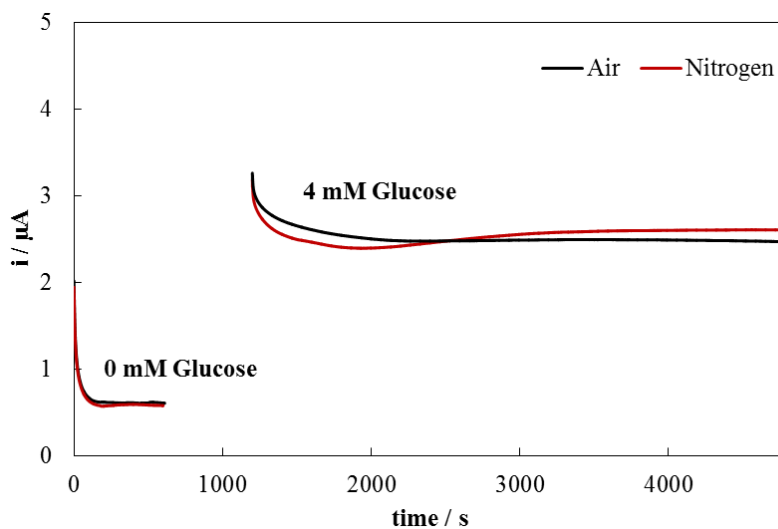


Figure A. 12. CAs (1 h length) of air saturated solutions for P2O-T169G (1 mg mL^{-1}) at 0.350 V for 0 mM and 4 mM concentrations of glucose added to the solution containing 0.5 mM FcCOOH, at pH 7. (GCE, surface area: 0.071 cm^2).

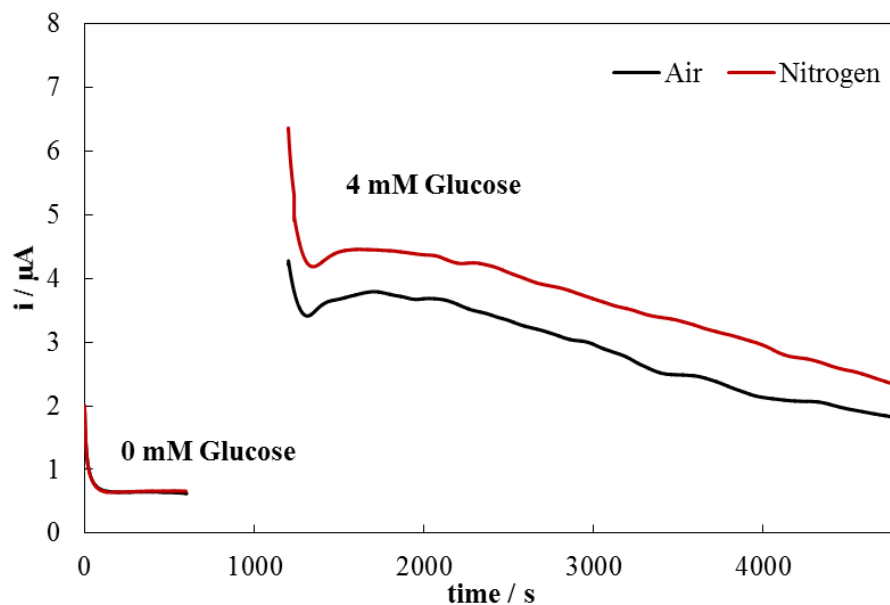


Figure A. 13. CAs (1 h length) of air saturated solutions for GOx (1 mg mL^{-1}) at 0.350 V for 0 mM and 4 mM concentrations of glucose added to the solution containing 0.5 mM FcCOOH, at pH 7. (GCE, surface area: 0.071 cm^2).

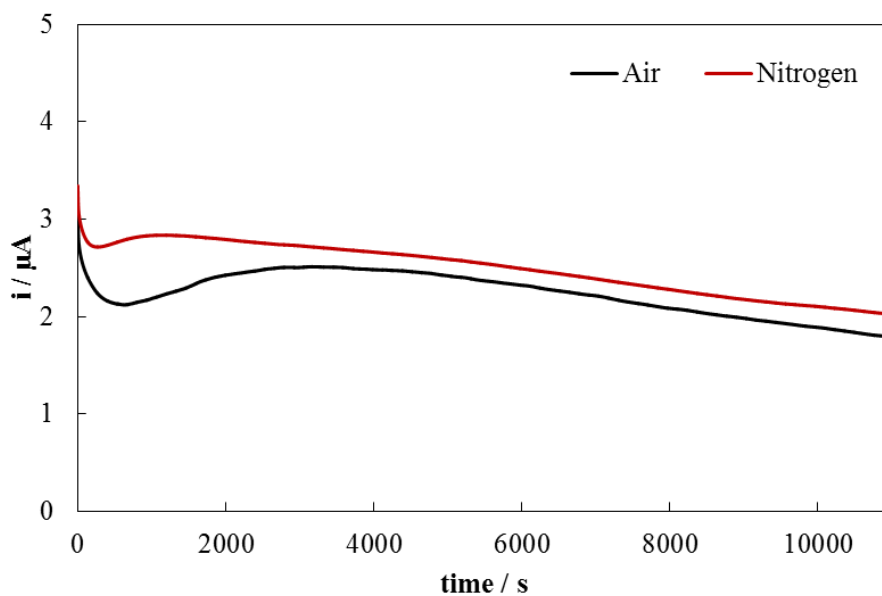


Figure A. 14. CAs (3 h length) of air saturated solutions for P2O-T169G (1 mg mL^{-1}) at 0.350 V for 4 mM concentration of glucose added to the solution containing 0.5 mM FcCOOH, at pH 7. (GCE, surface area: 0.071 cm^2).

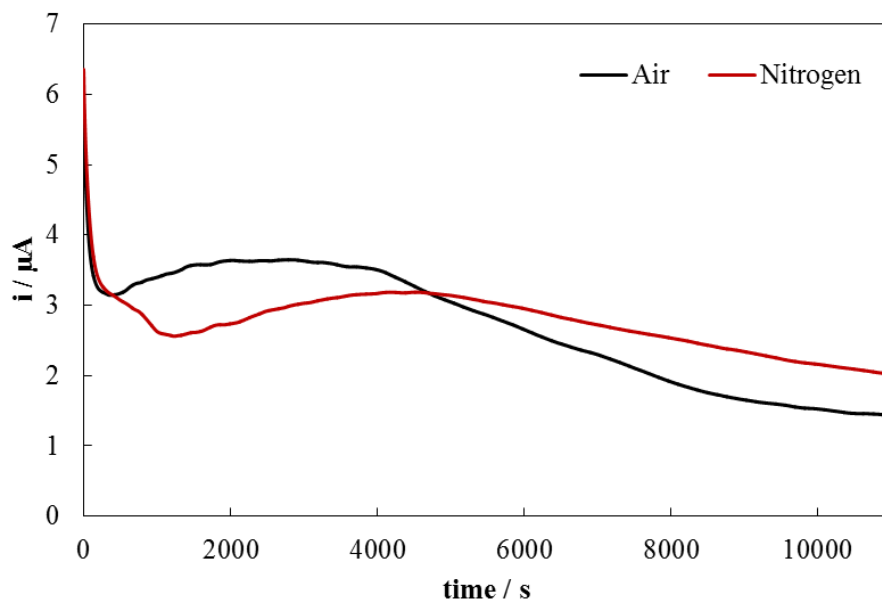


Figure A. 15. CAs (3 h length) of air saturated solutions for GOx (1 mg mL^{-1}) at 0.350 V for 4 mM concentration of glucose added to the solution containing 0.5 mM FcCOOH, at pH 7. (GCE, surface area: 0.071 cm^2).

Appendix B

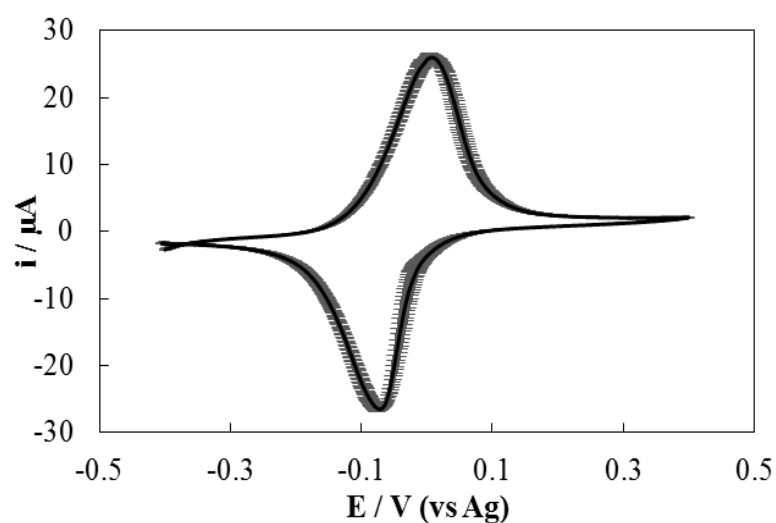


Figure B. 1. CV (scan rate: 5 mV s^{-1}) scans of carbon SPE to show reproducibility of the electrode. Tested in 0.1 M PBS at pH 7. Ag is the silver/silver ion reference electrode used on the SPE (SPE surface area: 0.126 cm^2). Error bars are sample standard deviations of measurements on $n = 4$ samples.

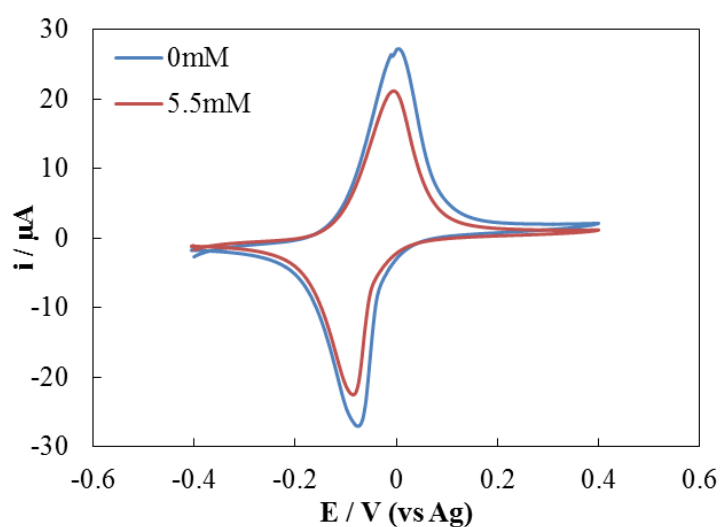


Figure B. 2. CV (scan rate: 5 mV s^{-1}) scans of carbon SPEs to show its activity towards glucose. Tested in 0.1 M PBS at pH 7 containing 0 mM and 5.5 mM glucose. Ag is the silver/silver ion reference electrode used on the SPE (SPE surface area: 0.126 cm^2). Graphs shown are mean values based on $n = 2$ samples.

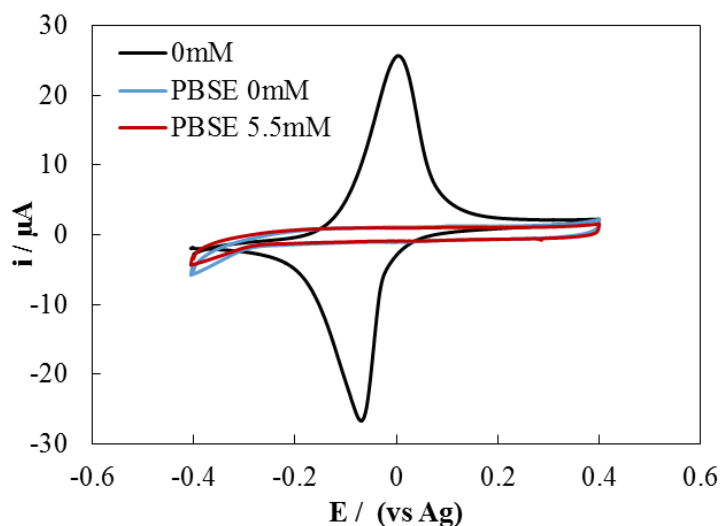


Figure B. 3. CV (scan rate: 5 mV s^{-1}) scans of carbon SPEs modified with Fc-Nafion-MWCNTs and then treated with PBSE to show its activity towards glucose. Tested in 0.1 M PBS at pH 7 containing 0 mM and 5.5 mM glucose. Ag is the silver/silver ion reference electrode used on the SPE (SPE surface area: 0.126 cm^2). Graphs shown are mean values based on $n = 2$ samples.

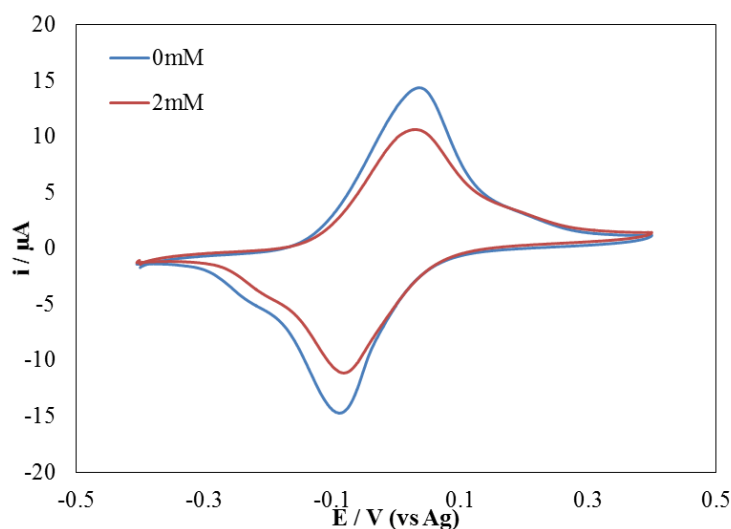


Figure B. 4. CV (scan rate: 5 mV s^{-1}) scans of GOx adsorbed on carbon SPEs to show its activity towards glucose. Tested in 0.1 M PBS at pH 7 containing 0 mM and 2 mM glucose. Ag is the silver/silver ion reference electrode used on the SPE (SPE surface area: 0.126 cm^2).

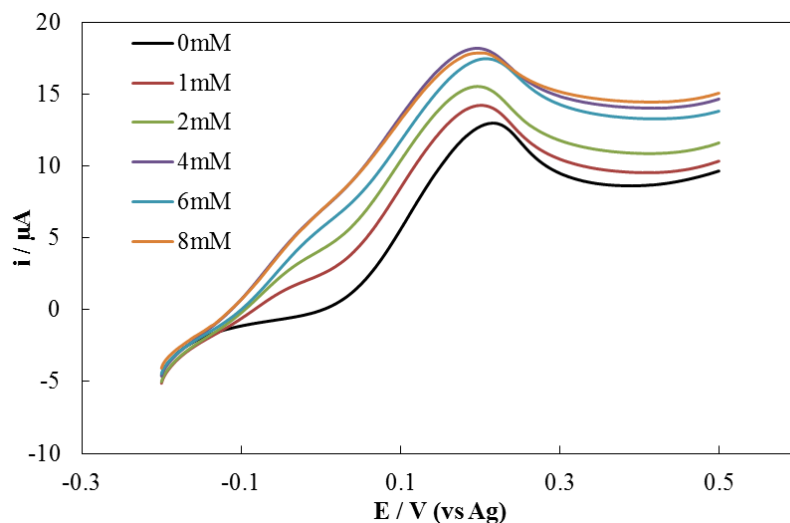


Figure B. 5. LSV (scan rate: 1 mV s^{-1}) scans of P2O-T169G immobilised on carbon SPE. Tested in nitrogen saturated solutions with various glucose concentrations added to the solution containing 0.5 mM FcCOOH in 0.1 M PBS at $\text{pH } 7$. Ag is the silver/silver ion reference electrode used on the SPE (SPE surface area: 0.126 cm^2).

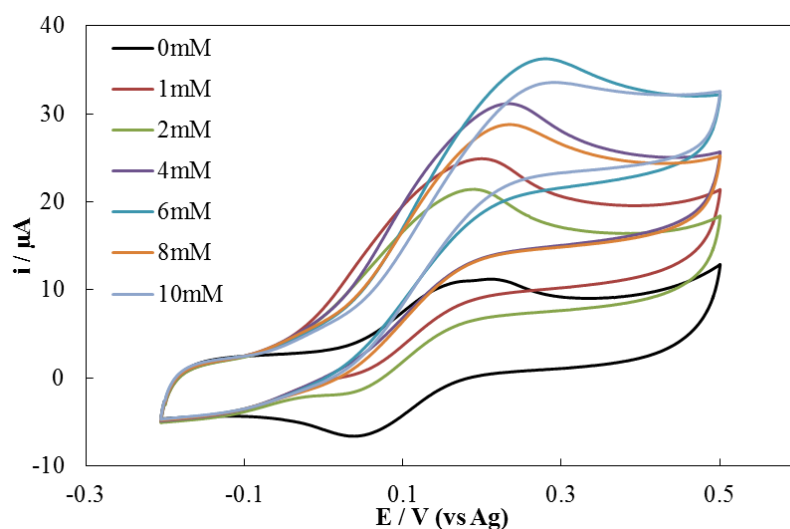


Figure B. 6. CV (scan rate: 5 mV s^{-1}) scans of GOx immobilised on carbon SPE. Tested in nitrogen saturated solutions with various glucose concentrations added to the solution containing 0.5 mM FcCOOH in 0.1 M PBS at $\text{pH } 7$. Ag is the silver/silver ion reference electrode used on the SPE (SPE surface area: 0.126 cm^2).

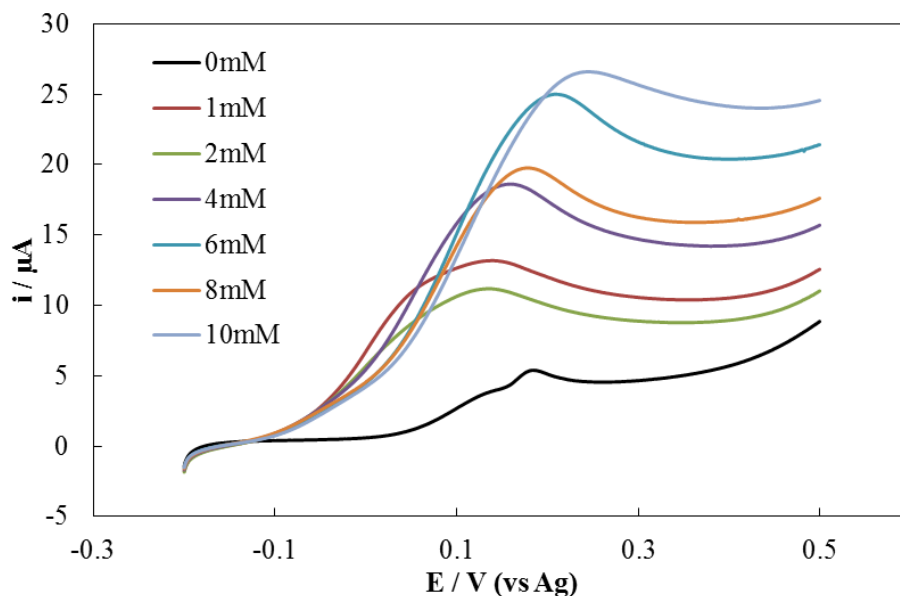


Figure B. 7. LSV (scan rate: 1 mV s^{-1}) scans of GOx immobilised on carbon SPE. Tested in nitrogen saturated solutions with various glucose concentrations added to the solution containing 0.5 mM FcCOOH in 0.1 M PBS at pH 7. Ag is the silver/silver ion reference electrode used on the SPE (SPE surface area: 0.126 cm^2).

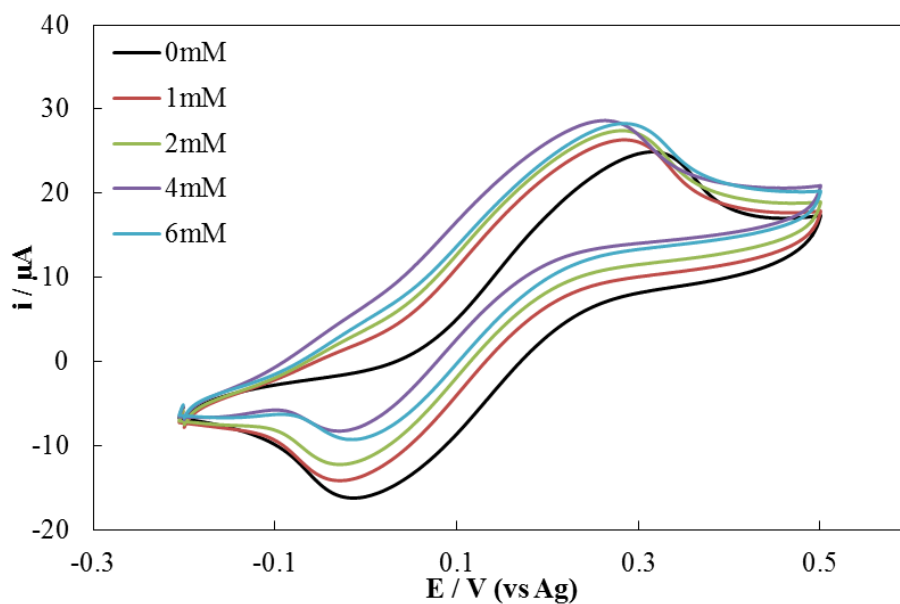


Figure B. 8. CV (scan rate: 5 mV s^{-1}) scans of P2O-T169G immobilised on carbon SPE. Tested in nitrogen saturated solutions with various glucose concentrations added to the solution containing 0.5 mM FcCOOH in 0.1 M PBS at pH 7. Ag is the silver/silver ion reference electrode used on the SPE (SPE surface area: 0.126 cm^2).

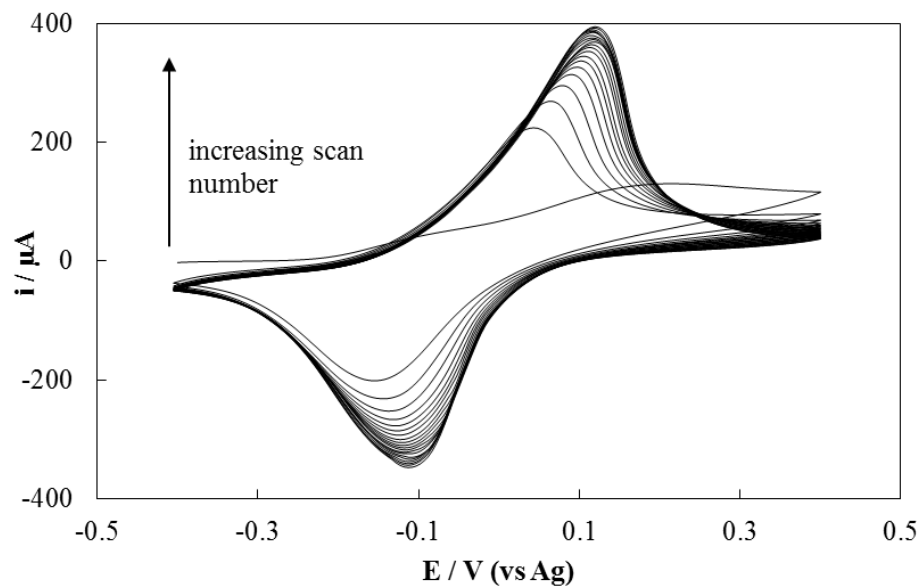


Figure B. 9. CV (scan rate: 50 mV s^{-1}) scans for the pre-conditioning of the carbon SPEs modified with Fc-Nafion. Tested in 0.1 M PBS at pH 7. Fc-Nafion loading is 0.06 mg cm^{-2} . Ag is the silver/silver ion reference electrode used on the SPE (SPE surface area: 0.126 cm^2).

Appendix C

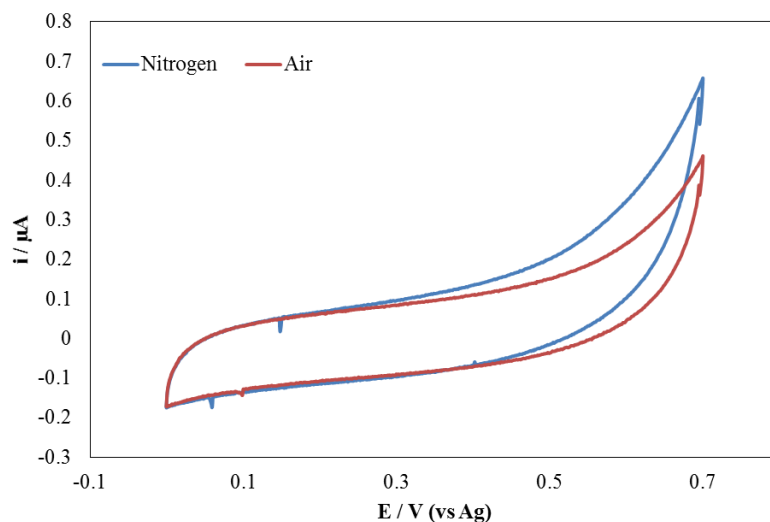


Figure C. 1. CV (scan rate: 5 mV s^{-1}) scans of MWCNTs modified carbon SPE (MWCNTs loading of 0.08 mg cm^{-1}) to show its inactivity towards oxygen present. Tested in nitrogen and air saturated solutions containing 0.1 M PBS at pH 7. Ag is the silver/silver ion reference electrode used on the SPE (SPE surface area: 0.126 cm^2).

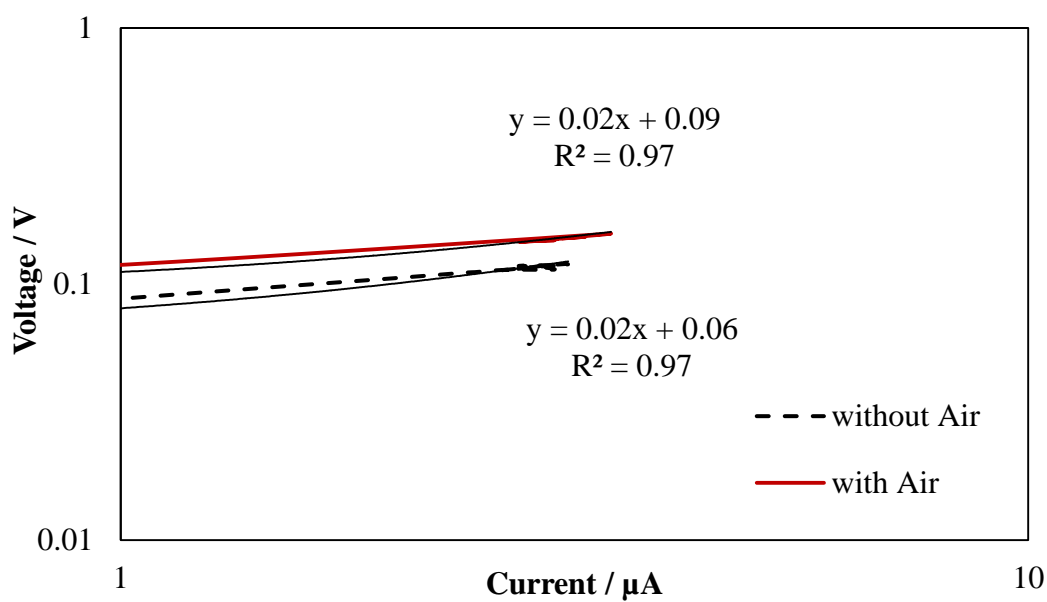


Figure C. 2. Log-log plot of non-aerated and aerated anode-cathode potentials *versus* current curves obtained from enzymatic biofuel cell tests

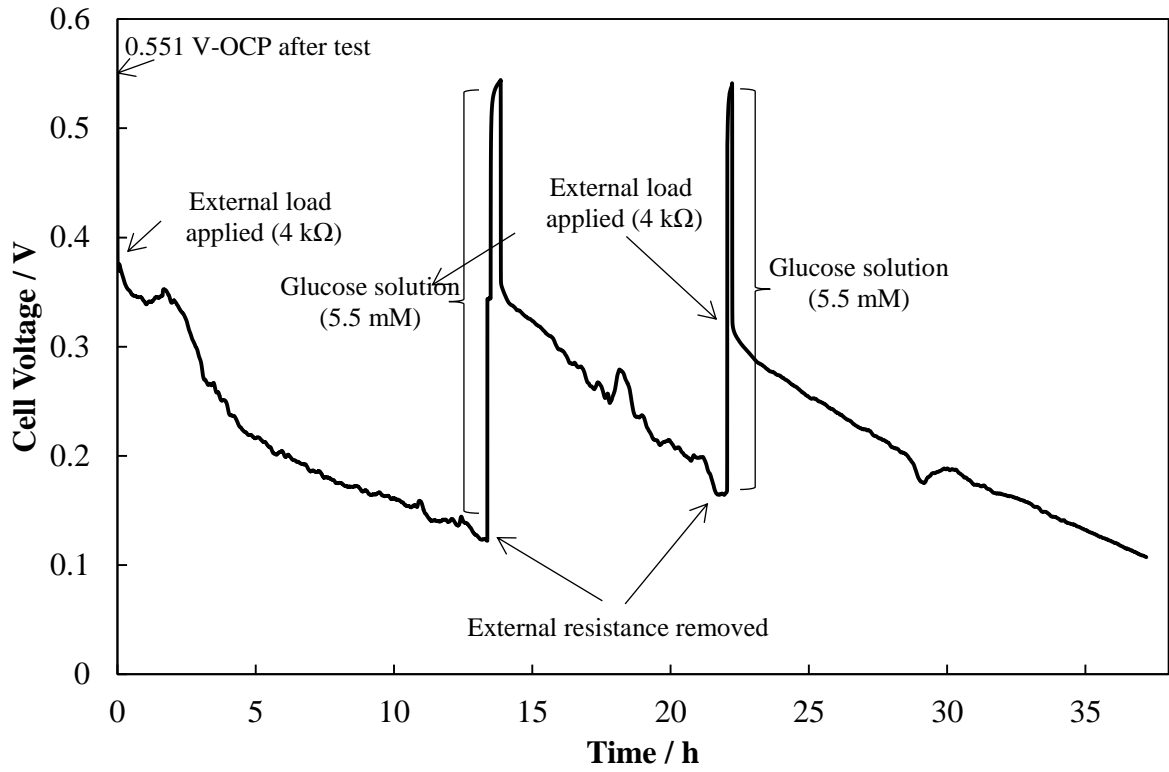


Figure C. 3. Stability of the air-breathing biofuel cell under batch operation

Appendix D

Publications from this work:

Sahin, S., Wongnate, T., Chaiyen, P., and Yu, E.H., Glucose Oxidation Using Oxygen Resistant Pyranose-2-Oxidase for Biofuel Cell Applications. *Chemical Engineering Transactions*, 41, 2014, 367-372.

Oral presentations at conferences:

10th European Symposium on Electrochemical Engineering, Sardinia, Italy, September 28th to October 2nd. Presentation titled 'Glucose Oxidation Using Oxygen Resistant Pyranose-2-Oxidase for Biofuel Cell Applications'.

References

- Ahmadi, M., Vahabzadeh, F., Bonakdarpour, B. and Mehranian, M. (2006) 'Empirical modeling of olive oil mill wastewater treatment using loofa-immobilized *Phanerochaete chrysosporium*', *Process Biochemistry*, 41(5), pp. 1148-1154.
- Alexeyeva, N. and Tammeveski, K. (2008) 'Electroreduction of oxygen on gold nanoparticle/PDDA-MWCNT nanocomposites in acid solution', *Anal Chim Acta*, 618(2), pp. 140-6.
- Alkire, R.C., Kolb, D.M., Lipkowski, J. and Ross, P.N. (2013) *Bioelectrochemistry: fundamentals, applications and recent developments*. John Wiley & Sons.
- Allen, J.B. and Larry, R.F. (2001) 'Electrochemical methods: fundamentals and applications', *Department of Chemistry and Biochemistry University of Texas at Austin, John Wiley & Sons, Inc*, pp. 156-176.
- Andoralov, V., Falk, M., Suyatin, D.B., Granmo, M., Sotres, J., Ludwig, R., Popov, V.O., Schouenborg, J., Blum, Z. and Shleev, S. (2013) 'Biofuel Cell Based on Microscale Nanostructured Electrodes with Inductive Coupling to Rat Brain Neurons', *Scientific Reports*, 3, p. 3270.
- Arribas, A.S., Bermejo, E., Chicharro, M., Zapardiel, A., Luque, G.L., Ferreyra, N.F. and Rivas, G.A. (2007) 'Analytical applications of glassy carbon electrodes modified with multi-wall carbon nanotubes dispersed in polyethylenimine as detectors in flow systems', *Analytica chimica acta*, 596(2), pp. 183-194.
- Babadi, A.A., Bagheri, S. and Hamid, S.B.A. (2016) 'Progress on implantable biofuel cell: Nano-carbon functionalization for enzyme immobilization enhancement', *Biosensors and Bioelectronics*, 79, pp. 850-860.
- Baminger, U., Subramaniam, S.S., Renganathan, V. and Haltrich, D. (2001) 'Purification and Characterization of Cellobiose Dehydrogenase from the Plant Pathogen *Sclerotium (Athelia) rolfsii*', *Applied and Environmental Microbiology*, 67(4), pp. 1766-1774.
- Bard, A.J., Faulkner, L.R., Leddy, J. and Zoski, C.G. (1980) *Electrochemical methods: fundamentals and applications*. Wiley New York.

References

- Barrière, F., Kavanagh, P. and Leech, D. (2006) 'A laccase–glucose oxidase biofuel cell prototype operating in a physiological buffer', *Electrochimica Acta*, 51(24), pp. 5187-5192.
- Bartlett, P.N. and Pratt, K.F.E. (1995) 'A study of the kinetics of the reaction between ferrocene monocarboxylic acid and glucose oxidase using the rotating-disc electrode', *Journal of Electroanalytical Chemistry*, 397(1–2), pp. 53-60.
- Barton, S.C., Kim, H.-H., Binyamin, G., Zhang, Y. and Heller, A. (2001) 'Electroreduction of O₂ to water on the “wired” laccase cathode', *The Journal of Physical Chemistry B*, 105(47), pp. 11917-11921.
- Baughman, R.H., Zakhidov, A.A. and de Heer, W.A. (2002) 'Carbon nanotubes--the route toward applications', *science*, 297(5582), pp. 787-792.
- Bedekar, A.S., Feng, J.J., Krishnamoorthy, S., Lim, K.G., Palmore, G.T.R. and Sundaram, S. (2007) 'Oxygen limitation in microfluidic biofuel cells', *Chemical Engineering Communications*, 195(3), pp. 256-266.
- Berg, J.M., Tymoczko, J.L. and Stryer, L. (2002) 'Biochemistry: International Version'.
- Blake, N.P., Petersen, M.K., Voth, G.A. and Metiu, H. (2005) 'Structure of hydrated Na-Nafion polymer membranes', *The Journal of Physical Chemistry B*, 109(51), pp. 24244-24253.
- Bourourou, M., Elouarzaki, K., Lalaoui, N., Agnès, C., Le Goff, A., Holzinger, M., Maaref, A. and Cosnier, S. (2013) 'Supramolecular immobilization of laccase on carbon nanotube electrodes functionalized with (methylpyrenylaminomethyl) anthraquinone for direct electron reduction of oxygen', *Chemistry–A European Journal*, 19(28), pp. 9371-9375.
- Brett, C., Brett, M.A.O., Brett, A.M.C.M.A. and Brett, A.M.O. (1993) *Electrochemistry: principles, methods, and applications*.
- Britto, P.J., Santhanam, K.S.V., Rubio, A., Alonso, J.A. and Ajayan, P.M. (1999) 'Improved charge transfer at carbon nanotube electrodes', *Advanced Materials*, 11(2), pp. 154-157.
- Brooks, S.L., Ashby, R.E., Turner, A.P.F., Calder, M.R. and Clarke, D.J. (1988) 'Development of an on-line glucose sensor for fermentation monitoring', *Biosensors*, 3(1), pp. 45-56.

References

- Brown, R.S. and Luong, J.H.T. (1995) 'A regenerable pseudo-reagentless glucose biosensor based on Nafion polymer and 1, 1'-dimethylferricinium mediator', *Analytica chimica acta*, 310(3), pp. 419-427.
- Brunel, L., Denele, J., Servat, K., Kokoh, K.B., Jolival, C., Innocent, C., Cretin, M., Rolland, M. and Tingry, S. (2007) 'Oxygen transport through laccase biocathodes for a membrane-less glucose/O₂ biofuel cell', *Electrochemistry Communications*, 9(2), pp. 331-336.
- Bu, H.-Z., Mikkelsen, S.R. and English, A.M. (1998) 'NAD (P) H sensors based on enzyme entrapment in ferrocene-containing polyacrylamide-based redox gels', *Analytical Chemistry*, 70(20), pp. 4320-4325.
- Bullen, R.A., Arnot, T.C., Lakeman, J.B. and Walsh, F.C. (2006) 'Biofuel cells and their development', *Biosensors and Bioelectronics*, 21(11), pp. 2015-2045.
- Bunte, C., Hussein, L. and Urban, G.A. (2014) 'Performance of non-compartmentalized enzymatic biofuel cell based on buckypaper cathode and ferrocene-containing redox polymer anode', *Journal of Power Sources*, 247, pp. 579-586.
- Calabrese Barton, S., Gallaway, J. and Atanassov, P. (2004) 'Enzymatic Biofuel Cells for Implantable and Microscale Devices', *Chemical Reviews*, 104(10), pp. 4867-4886.
- Cass, A.E.G., Davis, G., Francis, G.D., Hill, H.A.O., Aston, W.J., Higgins, I.J., Plotkin, E.V., Scott, L.D.L. and Turner, A.P.F. (1984) 'Ferrocene-mediated enzyme electrode for amperometric determination of glucose', *Analytical chemistry*, 56(4), pp. 667-671.
- Castorena-Gonzalez, J.A., Foote, C., MacVittie, K., Halánek, J., Halámková, L., Martinez-Lemus, L.A. and Katz, E. (2013) 'Biofuel Cell Operating in Vivo in Rat', *Electroanalysis*, 25(7), pp. 1579-1584.
- Chen, J.W., Bélanger, D. and Fortier, G. (1992) *ACS Symposium Series*. American Chemical Soc 1155 16th St, NW, Washington, DC 20036 USA.
- Chen, R.J., Zhang, Y., Wang, D. and Dai, H. (2001a) 'Noncovalent sidewall functionalization of single-walled carbon nanotubes for protein immobilization', *Journal of the American Chemical Society*, 123(16), pp. 3838-3839.

References

- Chen, T., Barton, S.C., Binyamin, G., Gao, Z., Zhang, Y., Kim, H.-H. and Heller, A. (2001b) 'A miniature biofuel cell', *Journal of the American Chemical Society*, 123(35), pp. 8630-8631.
- Cheng, H., Yu, P., Lu, X., Lin, Y., Ohsaka, T. and Mao, L. (2013) 'Biofuel cell-based self-powered biogenerators for online continuous monitoring of neurochemicals in rat brain', *Analyst*, 138(1), pp. 179-185.
- Christenson, A., Shleev, S., Mano, N., Heller, A. and Gorton, L. (2006) 'Redox potentials of the blue copper sites of bilirubin oxidases', *Biochimica et Biophysica Acta (BBA) - Bioenergetics*, 1757(12), pp. 1634-1641.
- Cinquin, P., Gondran, C., Giroud, F., Mazabrard, S., Pellissier, A., Boucher, F., Alcaraz, J.-P., Gorgy, K., Lenouvel, F., Mathé, S., Porcu, P. and Cosnier, S. (2010) 'A Glucose BioFuel Cell Implanted in Rats', *PLoS ONE*, 5(5), p. e10476.
- Cohen, B. (1931) 'The bacterial culture as an electrical half-cell', *J. Bacteriol*, 21(1), pp. 18-19.
- Cooney, M.J., Svoboda, V., Lau, C., Martin, G. and Minteer, S.D. (2008) 'Enzyme catalysed biofuel cells', *Energy & Environmental Science*, 1(3), pp. 320-337.
- Cosnier, S. (2000) 'Biosensors based on immobilization of biomolecules by electrogenerated polymer films', *Applied biochemistry and biotechnology*, 89(2-3), pp. 127-138.
- Cosnier, S., Holzinger, M. and Le Goff, A. (2014) 'Recent advances in carbon nanotube-based enzymatic fuel cells', *Frontiers in bioengineering and biotechnology*, 2.
- Costa, F., Carvalho, I.F., Montelaro, R.C., Gomes, P. and Martins, M.C.L. (2011) 'Covalent immobilization of antimicrobial peptides (AMPs) onto biomaterial surfaces', *Acta Biomaterialia*, 7(4), pp. 1431-1440.
- Courjean, O., Gao, F. and Mano, N. (2009) 'Deglycosylation of glucose oxidase for direct and efficient glucose electrooxidation on a glassy carbon electrode', *Angewandte Chemie International Edition*, 48(32), pp. 5897-5899.
- Cracknell, J.A., McNamara, T.P., Lowe, E.D. and Blanford, C.F. (2011) 'Bilirubin oxidase from *Myrothecium verrucaria*: X-ray determination of the complete crystal structure and a rational surface modification for enhanced electrocatalytic O₂reduction', *Dalton Transactions*, 40(25), pp. 6668-6675.

References

- Cracknell, J.A., Vincent, K.A. and Armstrong, F.A. (2008) 'Enzymes as working or inspirational electrocatalysts for fuel cells and electrolysis', *Chemical Reviews*, 108(7), pp. 2439-2461.
- Danilov, R.A. and Ekelund, N.G.A. (2001) 'Comparison of usefulness of three types of artificial substrata (glass, wood and plastic) when studying settlement patterns of periphyton in lakes of different trophic status', *Journal of Microbiological Methods*, 45(3), pp. 167-170.
- Davis, J.B. and Yarbrough, H.F. (1962) 'Preliminary experiments on a microbial fuel cell', *Science*, 137(3530), pp. 615-616.
- Degani, Y. and Heller, A. (1988) 'Direct electrical communication between chemically modified enzymes and metal electrodes. 2. Methods for bonding electron-transfer relays to glucose oxidase and D-amino-acid oxidase', *Journal of the American Chemical Society*, 110(8), pp. 2615-2620.
- Deng, L., Shang, L., Wang, Y., Wang, T., Chen, H. and Dong, S. (2008) 'Multilayer structured carbon nanotubes/poly-l-lysine/laccase composite cathode for glucose/O₂ biofuel cell', *Electrochemistry Communications*, 10(7), pp. 1012-1015.
- Digital, D. (2016) *Blood Sugar Level Ranges*. Available at: http://www.diabetes.co.uk/diabetes_care/blood-sugar-level-ranges.html (Accessed: 14 May 2016).
- Dong, S., Wang, B. and Liu, B. (1992) 'Amperometric glucose sensor with ferrocene as an electron transfer mediator', *Biosensors and Bioelectronics*, 7(3), pp. 215-222.
- Dörnenburg, H. and Knorr, D. (1995) 'Strategies for the improvement of secondary metabolite production in plant cell cultures', *Enzyme and Microbial Technology*, 17(8), pp. 674-684.
- DropSens (2016) *Screen-printed electrodes*. Available at: http://www.dropsens.com/en/screen_printed_electrodes_pag.html (Accessed: 6 April 2016).
- Du Toit, H. and Di Lorenzo, M. (2014) 'Glucose oxidase directly immobilized onto highly porous gold electrodes for sensing and fuel cell applications', *Electrochimica Acta*, 138, pp. 86-92.

References

du Toit, H., Rashidi, R., Ferdani, D.W., Delgado-Charro, M.B., Sangan, C.M. and Di Lorenzo, M. (2016) 'Generating power from transdermal extracts using a multi-electrode miniature enzymatic fuel cell', *Biosensors & Bioelectronics*, 78, pp. 411-417.

Espenscheid, M.W., Ghatak-Roy, A.R., Moore, R.B., Penner, R.M., Szentirmay, M.N. and Martin, C.R. (1986) 'Sensors from polymer modified electrodes', *Journal of the Chemical Society, Faraday Transactions 1: Physical Chemistry in Condensed Phases*, 82(4), pp. 1051-1070.

Facchini, P.J. and DiCosmo, F. (1990) 'Immobilization of cultured *Catharanthus roseus* cells using a fibreglass substratum', *Applied microbiology and biotechnology*, 33(1), pp. 36-42.

Falk, M., Andoralov, V., Silow, M., Toscano, M.D. and Shleev, S. (2013a) 'Miniature Biofuel Cell as a Potential Power Source for Glucose-Sensing Contact Lenses', *Analytical Chemistry*, 85(13), pp. 6342-6348.

Falk, M., Narváez Villarrubia, C.W., Babanova, S., Atanassov, P. and Shleev, S. (2013b) 'Biofuel Cells for Biomedical Applications: Colonizing the Animal Kingdom', *ChemPhysChem*, 14(10), pp. 2045-2058.

Fatoni, A., Numnuam, A., Kanatharana, P., Limbut, W., Thammakhet, C. and Thavarungkul, P. (2013) 'A highly stable oxygen-independent glucose biosensor based on a chitosan-albumin cryogel incorporated with carbon nanotubes and ferrocene', *Sensors and Actuators B: Chemical*, 185, pp. 725-734.

Fernández, L. and Carrero, H. (2005) 'Electrochemical evaluation of ferrocene carboxylic acids confined on surfactant-clay modified glassy carbon electrodes: oxidation of ascorbic acid and uric acid', *Electrochimica Acta*, 50(5), pp. 1233-1240.

Filik, H., A Avan, A. and Aydar, S. (2015) 'Nafion/Multi-wall Carbon Nanotubes Composite Modified Glassy Carbon Electrode for Sensitive Determination of Bilirubin', *Current Nanoscience*, 11(6), pp. 784-791.

Fiorito, P.A. and Torresi, S.I. (2001) 'Glucose amperometric biosensor based on the co-immobilization of glucose oxidase (GOx) and ferrocene in poly (pyrrole) generated from ethanol/water mixtures', *Journal of the Brazilian Chemical Society*, 12(6), pp. 729-733.

References

Gregg, B.A. and Heller, A. (1991) 'Redox polymer films containing enzymes. 1. A redox-conducting epoxy cement: synthesis, characterization, and electrocatalytic oxidation of hydroquinone', *The Journal of Physical Chemistry*, 95(15), pp. 5970-5975.

Grove, W.R. (1839) 'XXIV. On voltaic series and the combination of gases by platinum', *The London and Edinburgh philosophical magazine and journal of science*, 14(86), pp. 127-130.

Güven, G., Şahin, S., Güven, A. and Yu, E.H. (2016) 'Power Harvesting from Human Serum in Buckypaper-Based Enzymatic Biofuel Cell', *Frontiers in Energy Research*, 4, p. 4.

Habrioux, A., Merle, G., Servat, K., Kokoh, K.B., Innocent, C., Cretin, M. and Tingry, S. (2008) 'Concentric glucose/O₂ biofuel cell', *Journal of Electroanalytical Chemistry*, 622(1), pp. 97-102.

Habrioux, A., Servat, K., Tingry, S. and Kokoh, K.B. (2009) 'Enhancement of the performances of a single concentric glucose/O₂ biofuel cell by combination of bilirubin oxidase/Nafion cathode and Au–Pt anode', *Electrochemistry Communications*, 11(1), pp. 111-113.

Haccoun, J., Piro, B., Noël, V. and Pham, M.C. (2006) 'The development of a reagentless lactate biosensor based on a novel conducting polymer', *Bioelectrochemistry*, 68(2), pp. 218-226.

Halámková, L., Halánek, J., Bocharova, V., Szczupak, A., Alfonta, L. and Katz, E. (2012) 'Implanted Biofuel Cell Operating in a Living Snail', *Journal of the American Chemical Society*, 134(11), pp. 5040-5043.

Hanashi, T., Yamazaki, T., Tsugawa, W., Ikebukuro, K. and Sode, K. (2011) 'BioRadioTransmitter: A Self-Powered Wireless Glucose-Sensing System', *Journal of Diabetes Science and Technology*, 5(5), pp. 1030-1035.

Hao Yu, E. and Scott, K. (2010) 'Enzymatic Biofuel Cells—Fabrication of Enzyme Electrodes', *Energies*, 3(1), p. 23.

Harkness, J.K., Murphy, O.J. and Hitchens, G.D. (1993) 'Enzyme electrodes based on ionomer films coated on electrodes', *Journal of Electroanalytical Chemistry*, 357(1), pp. 261-272.

Harper, A. and Anderson, M.R. (2010) 'Electrochemical glucose sensors—developments using electrostatic assembly and carbon nanotubes for biosensor construction', *Sensors*, 10(9), pp. 8248-8274.

References

- Harrison, D.J., Turner, R.F.B. and Baltes, H.P. (1988) 'Characterization of perfluorosulfonic acid polymer coated enzyme electrodes and a miniaturized integrated potentiostat for glucose analysis in whole blood', *Analytical Chemistry*, 60(19), pp. 2002-2007.
- Hecht, H.J., Kalisz, H.M., Hendle, J., Schmid, R.D. and Schomburg, D. (1993a) 'Crystal structure of glucose oxidase from aspergillus niger refined at 2.3 Å resolution', *Journal of molecular biology*, 229(1), pp. 153-172.
- Hecht, H.J., Schomburg, D., Kalisz, H. and Schmid, R.D. (1993b) 'The 3D structure of glucose oxidase from *Aspergillus niger*. Implications for the use of GOD as a biosensor enzyme', *Biosensors and Bioelectronics*, 8(3), pp. 197-203.
- Heller, A. (2004) 'Miniature biofuel cells', *Physical Chemistry Chemical Physics*, 6(2), pp. 209-216.
- Heller, A. (2006) 'Electron-conducting redox hydrogels: design, characteristics and synthesis', *Current opinion in chemical biology*, 10(6), pp. 664-672.
- Ieropoulos, I., Winfield, J. and Greenman, J. (2010) 'Effects of flow-rate, inoculum and time on the internal resistance of microbial fuel cells', *Bioresourcetechnology*, 101(10), pp. 3520-3525.
- Iqbal, J., Iqbal, S. and Müller, C.E. (2013) 'Advances in immobilized enzyme microreactors in capillary electrophoresis', *Analyst*, 138(11), pp. 3104-3116.
- Ivanov, I., Vidaković-Koch, T. and Sundmacher, K. (2010) 'Recent Advances in Enzymatic Fuel Cells: Experiments and Modeling', *Energies*, 3(4), p. 803.
- Jadhav, D.A., Ghadge, A.N., Mondal, D. and Ghangrekar, M.M. (2014) 'Comparison of oxygen and hypochlorite as cathodic electron acceptor in microbial fuel cells', *Bioresourcetechnology*, 154, pp. 330-335.
- Jönsson-Niedziolka, M., Kaminska, A. and Opallo, M. (2010) 'Pyrene-functionalised single-walled carbon nanotubes for mediatorless dioxygen bioelectrocatalysis', *Electrochimica Acta*, 55(28), pp. 8744-8750.

References

Jung, D., Streb, C. and Hartmann, M. (2010) 'Covalent anchoring of chloroperoxidase and glucose oxidase on the mesoporous molecular sieve SBA-15', *International journal of molecular sciences*, 11(2), pp. 762-778.

Kamitaka, Y., Tsujimura, S., Setoyama, N., Kajino, T. and Kano, K. (2007) 'Fructose/dioxygen biofuel cell based on direct electron transfer-type bioelectrocatalysis', *Physical Chemistry Chemical Physics*, 9(15), pp. 1793-1801.

Kang, C., Shin, H. and Heller, A. (2006) 'On the stability of the "wired" bilirubin oxidase oxygen cathode in serum', *Bioelectrochemistry*, 68(1), pp. 22-26.

Kang, J., Hussain, A.T., Catt, M., Trenell, M., Haggett, B. and Yu, E.H. (2014) 'Electrochemical detection of non-esterified fatty acid by layer-by-layer assembled enzyme electrodes', *Sensors and Actuators B: Chemical*, 190, pp. 535-541.

Kannan, A.M., Renugopalakrishnan, V., Filipek, S., Li, P., Audette, G.F. and Munukutla, L. (2009) 'Bio-batteries and bio-fuel cells: leveraging on electronic charge transfer proteins', *Journal of nanoscience and nanotechnology*, 9(3), pp. 1665-1678.

Karyakin, A.A., Karyakina, E.E., Gorton, L., Bobrova, O.A., Lukachova, L.V., Gladilin, A.K. and Levashov, A.V. (1996) 'Improvement of electrochemical biosensors using enzyme immobilization from water-organic mixtures with a high content of organic solvent', *Analytical Chemistry*, 68(24), pp. 4335-4341.

Kase, Y. and Muguruma, H. (2004) 'Amperometric glucose biosensor based on mediated electron transfer between immobilized glucose oxidase and plasmopolymerized thin film of dimethylaminomethylferrocene on sputtered gold electrode', *Analytical sciences*, 20(8), pp. 1143-1146.

Katz, E. (1994) 'Application of bifunctional reagents for immobilization of proteins on a carbon electrode surface: oriented immobilization of photosynthetic reaction centers', *Journal of Electroanalytical Chemistry*, 365(1-2), pp. 157-164.

Katz, E., Riklin, A., Heleg-Shabtai, V., Willner, I. and Bückmann, A.F. (1999a) 'Glucose oxidase electrodes via reconstitution of the apo-enzyme: tailoring of novel glucose biosensors', *Analytica chimica acta*, 385(1), pp. 45-58.

References

- Katz, E., Willner, I. and Kotlyar, A.B. (1999b) 'A non-compartmentalized glucose | O₂ biofuel cell by bioengineered electrode surfaces', *Journal of Electroanalytical Chemistry*, 479(1), pp. 64-68.
- Kim, H.-H., Mano, N., Zhang, Y. and Heller, A. (2003) 'A miniature membrane-less biofuel cell operating under physiological conditions at 0.5 V', *Journal of The Electrochemical Society*, 150(2), pp. A209-A213.
- Kim, J., Parkey, J., Rhodes, C. and Gonzalez-Martin, A. (2009) 'Development of a biofuel cell using glucose-oxidase-and bilirubin-oxidase-based electrodes', *Journal of Solid State Electrochemistry*, 13(7), pp. 1043-1050.
- Koide, S. and Yokoyama, K. (1999) 'Electrochemical characterization of an enzyme electrode based on a ferrocene-containing redox polymer', *Journal of Electroanalytical Chemistry*, 468(2), pp. 193-201.
- Komaba, S., Mitsuhashi, T. and Shiraishi, S. (2008) 'Optimization of enzyme anode and cathode with polyion complex for the application to biofuel cells', *Electrochemistry*, 76(8), pp. 619-624.
- Krishnan, S. and Armstrong, F.A. (2012) 'Order-of-magnitude enhancement of an enzymatic hydrogen-air fuel cell based on pyrenyl carbon nanostructures', *Chemical Science*, 3(4), pp. 1015-1023.
- Kujawa, M., Ebner, H., Leitner, C., Hallberg, B.M., Prongjit, M., Sucharitakul, J., Ludwig, R., Rudsander, U., Peterbauer, C., Chaiyen, P., Haltrich, D. and Divne, C. (2006) 'Structural Basis for Substrate Binding and Regioselective Oxidation of Monosaccharides at C3 by Pyranose 2-Oxidase', *Journal of Biological Chemistry*, 281(46), pp. 35104-35115.
- Kuwahara, T., Oshima, K., Shimomura, M. and Miyauchi, S. (2007) 'Properties of the enzyme electrode fabricated with a film of polythiophene derivative and its application to a glucose fuel cell', *Journal of applied polymer science*, 104(5), pp. 2947-2953.
- Kwon, K.Y., Kim, J.H., Youn, J., Jeon, C., Lee, J., Hyeon, T., Park, H.G., Chang, H.N., Kwon, Y. and Ha, S. (2014) 'Electrochemical Activity Studies of Glucose Oxidase (GOx)-Based and Pyranose Oxidase (POx)-Based Electrodes in Mesoporous Carbon: Toward Biosensor and Biofuel Cell Applications', *Electroanalysis*, 26(10), pp. 2075-2079.

References

- Lalaoui, N., Le Goff, A., Holzinger, M., Mermoux, M. and Cosnier, S. (2015) 'Wiring Laccase on Covalently Modified Graphene: Carbon Nanotube Assemblies for the Direct Bioelectrocatalytic Reduction of Oxygen', *Chemistry—A European Journal*, 21(8), pp. 3198-3201.
- Lange, M.A. and Chambers, J.Q. (1985) 'Amperometric determination of glucose with a ferrocene-mediated glucose oxidase/polyacrylamide gel electrode', *Analytica Chimica Acta*, 175, pp. 89-97.
- Larminie, J., Dicks, A. and McDonald, M.S. (2003) *Fuel cell systems explained*. Wiley New York.
- Laschi, S., Bulukin, E., Palchetti, I., Cristea, C. and Mascini, M. (2008) 'Disposable electrodes modified with multi-wall carbon nanotubes for biosensor applications', *Irbm*, 29(2), pp. 202-207.
- Leech, D., Kavanagh, P. and Schuhmann, W. (2012) 'Enzymatic fuel cells: Recent progress', *Electrochimica Acta*, 84, pp. 223-234.
- Leitner, C., Volc, J. and Haltrich, D. (2001) 'Purification and Characterization of Pyranose Oxidase from the White Rot Fungus *Trametes multicolor*', *Applied and Environmental Microbiology*, 67(8), pp. 3636-3644.
- Li, J., Chia, L.S., Goh, N.K., Tan, S.N. and Ge, H. (1997) 'Mediated amperometric glucose sensor modified by the sol-gel method', *Sensors and Actuators B: Chemical*, 40(2), pp. 135-141.
- Li, X., Zhou, H., Yu, P., Su, L., Ohsaka, T. and Mao, L. (2008) 'A Miniature glucose/O₂ biofuel cell with single-walled carbon nanotubes-modified carbon fiber microelectrodes as the substrate', *Electrochemistry Communications*, 10(6), pp. 851-854.
- Lidén, H., Volc, J., Marko-Varga, G. and Gorton, L. (1998) 'Pyranose Oxidase Modified Carbon Paste Electrodes for Monosaccharide Determination', *Electroanalysis*, 10(4), pp. 223-230.
- Lim, J., Malati, P., Bonet, F. and Dunn, B. (2007) 'Nanostructured sol-gel electrodes for biofuel cells', *Journal of the Electrochemical Society*, 154(2), pp. A140-A145.

References

- Lim, K.G. and Palmore, G.T.R. (2007) 'Microfluidic biofuel cells: the influence of electrode diffusion layer on performance', *Biosensors and Bioelectronics*, 22(6), pp. 941-947.
- Linford, R. and Schlindwein, W. (2006) 'Medical applications of solid state ionics', *Solid state ionics*, 177(19), pp. 1559-1565.
- Liu, C., Alwarappan, S., Chen, Z., Kong, X. and Li, C.-Z. (2010) 'Membraneless enzymatic biofuel cells based on graphene nanosheets', *Biosensors and Bioelectronics*, 25(7), pp. 1829-1833.
- Liu, Y. and Dong, S. (2007a) 'A biofuel cell harvesting energy from glucose–air and fruit juice–air', *Biosensors and Bioelectronics*, 23(4), pp. 593-597.
- Liu, Y. and Dong, S. (2007b) 'A biofuel cell with enhanced power output by grape juice', *Electrochemistry Communications*, 9(7), pp. 1423-1427.
- Liu, Y., Wang, M., Zhao, F., Liu, B. and Dong, S. (2005) 'A Low-Cost Biofuel Cell with pH-Dependent Power Output Based on Porous Carbon as Matrix', *Chemistry–A European Journal*, 11(17), pp. 4970-4974.
- Luo, X.-L., Xu, J.-J., Wang, J.-L. and Chen, H.-Y. (2005) 'Electrochemically deposited nanocomposite of chitosan and carbon nanotubes for biosensor application', *Chemical communications*, (16), pp. 2169-2171.
- MacVittie, K., Conlon, T. and Katz, E. (2015) 'A wireless transmission system powered by an enzyme biofuel cell implanted in an orange', *Bioelectrochemistry*, 106, Part A, pp. 28-33.
- MacVittie, K., Halamek, J., Halamkova, L., Southcott, M., Jemison, W.D., Lobel, R. and Katz, E. (2013) 'From "cyborg" lobsters to a pacemaker powered by implantable biofuel cells', *Energy & Environmental Science*, 6(1), pp. 81-86.
- Malinauskas, A., Kuzmarskyt, J., Meškys, R. and Ramanavičius, A. (2004) 'Bioelectrochemical sensor based on PQQ-dependent glucose dehydrogenase', *Sensors and Actuators B: Chemical*, 100(3), pp. 387-394.
- Mani, V., Devadas, B. and Chen, S.-M. (2013) 'Direct electrochemistry of glucose oxidase at electrochemically reduced graphene oxide-multiwalled carbon nanotubes hybrid material modified electrode for glucose biosensor', *Biosensors and Bioelectronics*, 41, pp. 309-315.

References

- Mano, N. and Heller, A. (2003) 'A miniature membraneless biofuel cell operating at 0.36 V under physiological conditions', *Journal of The Electrochemical Society*, 150(8), pp. A1136-A1138.
- Mano, N., Kim, H.-H. and Heller, A. (2002a) 'On the Relationship between the Characteristics of Bilirubin Oxidases and O₂ Cathodes Based on Their "Wiring"', *The Journal of Physical Chemistry B*, 106(34), pp. 8842-8848.
- Mano, N., Mao, F. and Heller, A. (2002b) 'A miniature biofuel cell operating in a physiological buffer', *Journal of the American Chemical Society*, 124(44), pp. 12962-12963.
- Mano, N., Mao, F. and Heller, A. (2003a) 'Characteristics of a miniature compartment-less glucose-O₂ biofuel cell and its operation in a living plant', *Journal of the American Chemical Society*, 125(21), pp. 6588-6594.
- Mano, N., Mao, F., Shin, W., Chen, T. and Heller, A. (2003b) 'A miniature biofuel cell operating at 0.78 V', *Chemical Communications*, (4), pp. 518-519.
- Martin, C.R. and Freiser, H. (1981) 'Ion-selective electrodes based on an ionic polymer', *Analytical Chemistry*, 53(6), pp. 902-904.
- Martin Hallberg, B., Leitner, C., Haltrich, D. and Divne, C. (2004) 'Crystal Structure of the 270 kDa Homotetrameric Lignin-degrading Enzyme Pyranose 2-Oxidase', *Journal of Molecular Biology*, 341(3), pp. 781-796.
- Menicucci, J., Beyenal, H., Marsili, E., Veluchamy, Demir, G. and Lewandowski, Z. (2006) 'Procedure for Determining Maximum Sustainable Power Generated by Microbial Fuel Cells', *Environmental Science & Technology*, 40(3), pp. 1062-1068.
- Merchant, S.A., Glatzhofer, D.T. and Schmidtke, D.W. (2007) 'Effects of electrolyte and pH on the behavior of cross-linked films of ferrocene-modified poly (ethylenimine)', *Langmuir*, 23(22), pp. 11295-11302.
- Meredith, M.T., Kao, D.-Y., Hickey, D., Schmidtke, D.W. and Glatzhofer, D.T. (2011) 'High current density ferrocene-modified linear poly (ethylenimine) bioanodes and their use in biofuel cells', *Journal of the Electrochemical Society*, 158(2), pp. B166-B174.

References

- Merle, G., Habrioux, A., Servat, K., Rolland, M., Innocent, C., Kokoh, K.B. and Tingry, S. (2009) 'Long-term activity of covalent grafted biocatalysts during intermittent use of a glucose/O₂ biofuel cell', *Electrochimica Acta*, 54(11), pp. 2998-3003.
- Merotra, J. (2013) 'Fabrication & characterisation of enzyme electrodes for biosensor and biofuel cell applications'.
- Mertens, R. and Liese, A. (2004) 'Biotechnological applications of hydrogenases', *Current opinion in biotechnology*, 15(4), pp. 343-348.
- Miao, Y., Chia, L.S., Goh, N.K. and Tan, S.N. (2001) 'Amperometric glucose biosensor based on immobilization of glucose oxidase in chitosan matrix cross-linked with glutaraldehyde', *Electroanalysis*, 13(4), pp. 347-349.
- Milton, R.D., Lim, K., Hickey, D.P. and Minteer, S.D. (2015) 'Employing FAD-dependent glucose dehydrogenase within a glucose/oxygen enzymatic fuel cell operating in human serum', *Bioelectrochemistry*, 106, pp. 56-63.
- Miyake, T., Haneda, K., Nagai, N., Yatagawa, Y., Onami, H., Yoshino, S., Abe, T. and Nishizawa, M. (2011) 'Enzymatic biofuel cells designed for direct power generation from biofluids in living organisms', *Energy & Environmental Science*, 4(12), pp. 5008-5012.
- Moore, C.M., Akers, N.L., Hill, A.D., Johnson, Z.C. and Minteer, S.D. (2004) 'Improving the environment for immobilized dehydrogenase enzymes by modifying Nafion with tetraalkylammonium bromides', *Biomacromolecules*, 5(4), pp. 1241-1247.
- Nakabayashi, Y., Wakuda, M. and Imai, H. (1998) 'Amperometric Glucose Sensors Fabricated by Electrochemical Polymerization of Phenols on Carbon Paste Electrodes Containing Ferrocene as an Electron Transfer Mediator', *Analytical sciences*, 14(6), pp. 1069-1076.
- Nazaruk, E., Sadowska, K., Biernat, J.F., Rogalski, J., Ginalska, G. and Bilewicz, R. (2010) 'Enzymatic electrodes nanostructured with functionalized carbon nanotubes for biofuel cell applications', *Analytical and bioanalytical chemistry*, 398(4), pp. 1651-1660.
- Nazaruk, E., Smoliński, S., Swatko-Ossor, M., Ginalska, G., Fiedurek, J., Rogalski, J. and Bilewicz, R. (2008) 'Enzymatic biofuel cell based on electrodes modified with lipid liquid-crystalline cubic phases', *Journal of Power Sources*, 183(2), pp. 533-538.

References

Ndlovu, T., Arotiba, O.A., Sampath, S., Krause, R.W. and Mamba, B.B. (2012) 'Reactivities of Modified and Unmodified Exfoliated Graphite Electrodes in Selected Redox Systems', *International Journal of Electrochemical Science*, 7(10), pp. 9441-9453.

Nguyen, Q.T., Glinel, K., Pontié, M. and Ping, Z. (2004) 'Immobilization of bio-macromolecules onto membranes via an adsorbed nanolayer: An insight into the mechanism', *Journal of membrane science*, 232(1), pp. 123-132.

Nicholson, R.S. (1965) 'Theory and Application of Cyclic Voltammetry for Measurement of Electrode Reaction Kinetics', *Analytical Chemistry*, 37(11), pp. 1351-1355.

Nien, P.-C., Lee, C.-Y., Ho, K.-C., Adav, S.S., Liu, L., Wang, A., Ren, N. and Lee, D.-J. (2011) 'Power overshoot in two-chambered microbial fuel cell (MFC)', *Bioresource technology*, 102(7), pp. 4742-4746.

O'Gorman, J. (1998) *Novel electroanalytical methods*. Dublin City University.

Ó Conghaile, P., Falk, M., MacAodha, D., Yakovleva, M.E., Gonaus, C., Peterbauer, C.K., Gorton, L., Shleev, S. and Leech, D. (2016) 'Fully Enzymatic Membraneless Glucose|Oxygen Fuel Cell That Provides 0.275 mA cm⁻² in 5 mM Glucose, Operates in Human Physiological Solutions, and Powers Transmission of Sensing Data', *Analytical Chemistry*, 88(4), pp. 2156-2163.

Odaci, D., Telefoncu, A. and Timur, S. (2008) 'Pyranose oxidase biosensor based on carbon nanotube (CNT)-modified carbon paste electrodes', *Sensors and Actuators B: Chemical*, 132(1), pp. 159-165.

Ozdemir, C., Yeni, F., Odaci, D. and Timur, S. (2010) 'Electrochemical glucose biosensing by pyranose oxidase immobilized in gold nanoparticle-polyaniline/AgCl/gelatin nanocomposite matrix', *Food Chemistry*, 119(1), pp. 380-385.

Palmore, G.T.R. and Kim, H.-H. (1999) 'Electro-enzymatic reduction of dioxygen to water in the cathode compartment of a biofuel cell', *Journal of Electroanalytical Chemistry*, 464(1), pp. 110-117.

References

- Park, H.J., Won, K., Lee, S.Y., Kim, J.H., Kim, W.-J., Lee, D.S. and Yoon, H.H. (2011) 'Fabrication of CNT/ferrocene/glucose oxidase/chitosan-layered bioanode for glucose/oxygen biofuel cells', *Molecular Crystals and Liquid Crystals*, 539(1), pp. 238/[578]-246/[586].
- Piontek, K., Antorini, M. and Choinowski, T. (2002) 'Crystal structure of a laccase from the fungus *Trametes versicolor* at 1.90-Å resolution containing a full complement of coppers', *J Biol Chem*, 277(40), pp. 37663-9.
- Pitsawong, W., Sucharitakul, J., Prongjit, M., Tan, T.-C., Spadiut, O., Haltrich, D., Divne, C. and Chaiyen, P. (2010) 'A Conserved Active-site Threonine Is Important for Both Sugar and Flavin Oxidations of Pyranose 2-Oxidase', *The Journal of Biological Chemistry*, 285(13), pp. 9697-9705.
- Pizzariello, A., Stred'ansky, M. and Miertuš, S. (2002) 'A glucose/hydrogen peroxide biofuel cell that uses oxidase and peroxidase as catalysts by composite bulk-modified bioelectrodes based on a solid binding matrix', *Bioelectrochemistry*, 56(1), pp. 99-105.
- Princeton (2016) *A Review of Techniques for Electrochemical Analysis* Available at: [file://tower7/home42/b2019833/Downloads/Application_Note_E-4%20\(1\).pdf](file://tower7/home42/b2019833/Downloads/Application_Note_E-4%20(1).pdf) (Accessed: 08 May 2016).
- Qiu, J.-D., Zhou, W.-M., Guo, J., Wang, R. and Liang, R.-P. (2009) 'Amperometric sensor based on ferrocene-modified multiwalled carbon nanotube nanocomposites as electron mediator for the determination of glucose', *Analytical biochemistry*, 385(2), pp. 264-269.
- Ramanavicius, A. and Ramanaviciene, A. (2009) 'Hemoproteins in design of biofuel cells', *Fuel cells*, 9(1), pp. 25-36.
- Ramírez, P., Mano, N., Andreu, R., Ruzgas, T., Heller, A., Gorton, L. and Shleev, S. (2008) 'Direct electron transfer from graphite and functionalized gold electrodes to T1 and T2/T3 copper centers of bilirubin oxidase', *Biochimica et Biophysica Acta (BBA)-Bioenergetics*, 1777(10), pp. 1364-1369.
- Rasmussen, M., Abdellaoui, S. and Minteer, S.D. (2016) 'Enzymatic biofuel cells: 30 years of critical advancements', *Biosensors and Bioelectronics*, 76, pp. 91-102.

References

- Rasmussen, M., Ritzmann, R.E., Lee, I., Pollack, A.J. and Scherson, D. (2012) 'An Implantable Biofuel Cell for a Live Insect', *Journal of the American Chemical Society*, 134(3), pp. 1458-1460.
- Rayment, C. and Sherwin, S. (2003) 'Introduction to fuel cell technology', *Department of Aerospace and Mechanical Engineering, University of Notre Dame, Notre Dame, IN, 46556*, pp. 11-12.
- Razumien, J., Marcinkevičien, L., Bachmatova, I., Meškys, R. and Laurinavičius, V. (2003) 'Improvement of screen-printed carbon electrodes by modification with ferrocene derivative', *Sensors and Actuators B: Chemical*, 95(1), pp. 378-383.
- Robertson, M.A.F. and Yeager, H.L. (1996) 'A fluorescent probe investigation of the origin of superselectivity in perfluorinated ionomer membranes', *Macromolecules*, 29(15), pp. 5166-5171.
- Rogers, M.J. and Brandt, K.G. (1971) 'Interaction of D-glucal with *Aspergillus niger* glucose oxidase', *Biochemistry*, 10(25), pp. 4624-4630.
- Rubianes, M.D. and Rivas, G.A. (2007) 'Dispersion of multi-wall carbon nanotubes in polyethylenimine: a new alternative for preparing electrochemical sensors', *Electrochemistry communications*, 9(3), pp. 480-484.
- Rubinstein, I. (1984) 'Voltammetric pH measurements with surface-modified electrodes and a voltammetric internal reference', *Analytical Chemistry*, 56(7), pp. 1135-1137.
- Rubinstein, I. and Bard, A.J. (1980) 'Polymer films on electrodes. 4. Nafion-coated electrodes and electrogenerated chemiluminescence of surface-attached tris (2, 2'-bipyridine) ruthenium (2+)', *Journal of the American Chemical Society*, 102(21), pp. 6641-6642.
- Sakai, H., Nakagawa, T., Tokita, Y., Hatazawa, T., Ikeda, T., Tsujimura, S. and Kano, K. (2009) 'A high-power glucose/oxygen biofuel cell operating under quiescent conditions', *Energy & Environmental Science*, 2(1), pp. 133-138.
- Sales, F.C.P.F., Iost, R.M., Martins, M.V.A., Almeida, M.C. and Crespilho, F.N. (2013) 'An intravenous implantable glucose/dioxygen biofuel cell with modified flexible carbon fiber electrodes', *Lab on a Chip*, 13(3), pp. 468-474.

References

- Sarma, A.K., Vatsyayan, P., Goswami, P. and Minter, S.D. (2009) 'Recent advances in material science for developing enzyme electrodes', *Biosensors and Bioelectronics*, 24(8), pp. 2313-2322.
- Sato, F., Togo, M., Islam, M.K., Matsue, T., Kosuge, J., Fukasaku, N., Kurosawa, S. and Nishizawa, M. (2005) 'Enzyme-based glucose fuel cell using Vitamin K 3-immobilized polymer as an electron mediator', *Electrochemistry Communications*, 7(7), pp. 643-647.
- Scholz, F. (2010) 'Thermodynamics of electrochemical reactions', in *Electroanalytical Methods*. Springer, pp. 11-31.
- Schröder, U. (2012) 'From In Vitro to In Vivo—Biofuel Cells Are Maturing', *Angewandte Chemie International Edition*, 51(30), pp. 7370-7372.
- Scientific, T.F. (2016) *Chemistry of Crosslinking*. Available at: <http://www.piercenet.com/method/chemistry-crosslinking>.
- Sekretaryova, A. (2014) *Novel reagentless electrodes for biosensing*. Linköping University Electronic Press.
- Shan, C., Yang, H., Song, J., Han, D., Ivaska, A. and Niu, L. (2009) 'Direct electrochemistry of glucose oxidase and biosensing for glucose based on graphene', *Analytical Chemistry*, 81(6), pp. 2378-2382.
- Shao, M., Zafar, M.N., Falk, M., Ludwig, R., Sygmund, C., Peterbauer, C.K., Guschin, D.A., MacAodha, D., Ó Conghaile, P., Leech, D., Toscano, M.D., Shleev, S., Schuhmann, W. and Gorton, L. (2013) 'Optimization of a Membraneless Glucose/Oxygen Enzymatic Fuel Cell Based on a Bioanode with High Coulombic Efficiency and Current Density', *ChemPhysChem*, 14(10), pp. 2260-2269.
- Shim, J., Kim, G.-Y. and Moon, S.-H. (2011) 'Covalent co-immobilization of glucose oxidase and ferrocenedicarboxylic acid for an enzymatic biofuel cell', *Journal of electroanalytical chemistry*, 653(1), pp. 14-20.
- Shleev, S., Jarosz-Wilkolazka, A., Khalunina, A., Morozova, O., Yaropolov, A., Ruzgas, T. and Gorton, L. (2005) 'Direct electron transfer reactions of laccases from different origins on carbon electrodes', *Bioelectrochemistry*, 67(1), pp. 115-124.

References

- Shuler, M.L., Hallsby, G.A., Pyne, J.W. and Cho, T. (1986) 'Bioreactors for Immobilized Plant Cell Cultures', *Annals of the New York Academy of Sciences*, 469(1), pp. 270-278.
- Smolander, M., Boer, H., Valkiainen, M., Roozeman, R., Bergelin, M., Eriksson, J.-E., Zhang, X.-C., Koivula, A. and Viikari, L. (2008) 'Development of a printable laccase-based biocathode for fuel cell applications', *Enzyme and Microbial Technology*, 43(2), pp. 93-102.
- Soukharev, V., Mano, N. and Heller, A. (2004) 'A four-electron O₂-electroreduction biocatalyst superior to platinum and a biofuel cell operating at 0.88 V', *Journal of the American Chemical Society*, 126(27), pp. 8368-8369.
- Spadiut, O., Brugger, D., Coman, V., Haltrich, D. and Gorton, L. (2010) 'Engineered Pyranose 2-Oxidase: Efficiently Turning Sugars into Electrical Energy', *Electroanalysis*, 22(7-8), pp. 813-820.
- Stepnicka, P. (2008) *Ferrocenes: ligands, materials and biomolecules*. John Wiley & Sons.
- Stolten, D. (2010) *Hydrogen and fuel cells: fundamentals, technologies and applications*. John Wiley & Sons.
- Svoboda, V., Cooney, M., Liaw, B.Y., Minter, S., Piles, E., Lehnert, D., Calabrese Barton, S., Rincon, R. and Atanassov, P. (2008) 'Standardized characterization of electrocatalytic electrodes', *Electroanalysis*, 20(10), pp. 1099-1109.
- Szczupak, A., Halamek, J., Halamkova, L., Bocharova, V., Alfonta, L. and Katz, E. (2012) 'Living battery - biofuel cells operating in vivo in clams', *Energy & Environmental Science*, 5(10), pp. 8891-8895.
- Tamaki, T. and Yamaguchi, T. (2006) 'High-surface-area three-dimensional biofuel cell electrode using redox-polymer-grafted carbon', *Industrial & engineering chemistry research*, 45(9), pp. 3050-3058.
- Tan, T.C., Spadiut, O., Wongnate, T., Sucharitakul, J., Krondorfer, I., Szymund, C., Haltrich, D., Chaiyen, P., Peterbauer, C.K. and Divne, C. (2013) 'The 1.6 Å crystal structure of pyranose dehydrogenase from *Agaricus meleagris* rationalizes substrate specificity and reveals a flavin intermediate', *PLoS One*, 8(1), p. e53567.

References

- Tan, Y., Deng, W., Ge, B., Xie, Q., Huang, J. and Yao, S. (2009) 'Biofuel cell and phenolic biosensor based on acid-resistant laccase–glutaraldehyde functionalized chitosan–multiwalled carbon nanotubes nanocomposite film', *Biosensors and Bioelectronics*, 24(7), pp. 2225-2231.
- Tan, Y., Deng, W., Li, Y., Huang, Z., Meng, Y., Xie, Q., Ma, M. and Yao, S. (2010) 'Polymeric bionanocomposite cast thin films with in situ laccase-catalyzed polymerization of dopamine for biosensing and biofuel cell applications', *The Journal of Physical Chemistry B*, 114(15), pp. 5016-5024.
- Tasca, F., Gorton, L., Harreither, W., Haltrich, D., Ludwig, R. and Nöll, G. (2008) 'Highly efficient and versatile anodes for biofuel cells based on cellobiose dehydrogenase from *Myriococcum thermophilum*', *The Journal of Physical Chemistry C*, 112(35), pp. 13668-13673.
- Tasca, F., Timur, S., Ludwig, R., Haltrich, D., Volc, J., Antiochia, R. and Gorton, L. (2007) 'Amperometric Biosensors for Detection of Sugars Based on the Electrical Wiring of Different Pyranose Oxidases and Pyranose Dehydrogenases with Osmium Redox Polymer on Graphite Electrodes', *Electroanalysis*, 19(2-3), pp. 294-302.
- Thevenot, D.R., Toth, K., Durst, R.A. and Wilson, G.S. (1999) 'Electrochemical biosensors: recommended definitions and classification', *Pure and Applied Chemistry*, 71(12), pp. 2333-2348.
- Timur, S., Yigzaw, Y. and Gorton, L. (2006) 'Electrical wiring of pyranose oxidase with osmium redox polymers', *Sensors and Actuators B: Chemical*, 113(2), pp. 684-691.
- Tkáč, J., Voštiar, I., Gemeiner, P. and Šturdík, E. (2002) 'Stabilization of ferrocene leakage by physical retention in a cellulose acetate membrane. The fructose biosensor', *Bioelectrochemistry*, 55(1), pp. 149-151.
- Togo, M., Takamura, A., Asai, T., Kaji, H. and Nishizawa, M. (2007) 'An enzyme-based microfluidic biofuel cell using vitamin K 3-mediated glucose oxidation', *Electrochimica Acta*, 52(14), pp. 4669-4674.
- Tran, T.O., Lammert, E.G., Chen, J., Merchant, S.A., Brunski, D.B., Keay, J.C., Johnson, M.B., Glatzhofer, D.T. and Schmidtke, D.W. (2011) 'Incorporation of single-walled carbon nanotubes into ferrocene-modified linear polyethylenimine redox polymer films', *Langmuir*, 27(10), pp. 6201-6210.

References

- Tsujimura, S., Kano, K. and Ikeda, T. (2002) 'Glucose/O₂ biofuel cell operating at physiological conditions', *Electrochemistry*, 70(12), pp. 940-942.
- Turner, R.F.B., Harrison, D.J., Rajotte, R.V. and Baltes, H.P. (1990) 'A biocompatible enzyme electrode for continuous in vivo glucose monitoring in whole blood', *Sensors and Actuators B: Chemical*, 1(1), pp. 561-564.
- Uang, Y.-M. and Chou, T.-C. (2003) 'Fabrication of glucose oxidase/polypyrrole biosensor by galvanostatic method in various pH aqueous solutions', *Biosensors and Bioelectronics*, 19(3), pp. 141-147.
- Vaillancourt, M., Wei Chen, J., Fortier, G. and Bélanger, D. (1999) 'Electrochemical and Enzymatic Studies of Electron Transfer Mediation by Ferrocene Derivatives with Nafion-Glucose Oxidase Electrodes', *Electroanalysis*, 11(1), pp. 23-31.
- Vidal, J.-C., Garcia, E. and Castillo, J.-R. (2002) 'Development of a platinized and ferrocene-mediated cholesterol amperometric biosensor based on electropolymerization of polypyrrole in a flow system', *Analytical sciences*, 18(5), pp. 537-542.
- Vishnyakov, A. and Neimark, A.V. (2001) 'Molecular dynamics simulation of microstructure and molecular mobilities in swollen Nafion membranes', *The Journal of Physical Chemistry B*, 105(39), pp. 9586-9594.
- Wang, S.C., Yang, F., Silva, M., Zarow, A., Wang, Y. and Iqbal, Z. (2009a) 'Membrane-less and mediator-free enzymatic biofuel cell using carbon nanotube/porous silicon electrodes', *Electrochemistry Communications*, 11(1), pp. 34-37.
- Wang, Z.-G., Wan, L.-S., Liu, Z.-M., Huang, X.-J. and Xu, Z.-K. (2009b) 'Enzyme immobilization on electrospun polymer nanofibers: an overview', *Journal of Molecular Catalysis B: Enzymatic*, 56(4), pp. 189-195.
- Wei, X., Cruz, J. and Gorski, W. (2002) 'Integration of enzymes and electrodes: spectroscopic and electrochemical studies of chitosan-enzyme films', *Analytical chemistry*, 74(19), pp. 5039-5046.

References

- Weigel, M.C., Tritscher, E. and Lisdat, F. (2007) 'Direct electrochemical conversion of bilirubin oxidase at carbon nanotube-modified glassy carbon electrodes', *Electrochemistry Communications*, 9(4), pp. 689-693.
- White, H.S., Leddy, J. and Bard, A.J. (1982) 'Polymer films on electrodes. 8. Investigation of charge-transport mechanisms in Nafion polymer modified electrodes', *Journal of the American Chemical Society*, 104(18), pp. 4811-4817.
- Wieckowski, A. (2009) *Fuel cell catalysis: a surface science approach*. John Wiley & Sons.
- Willner, I., Arad, G. and Katz, E. (1998a) 'A biofuel cell based on pyrroloquinoline quinone and microperoxidase-11 monolayer-functionalized electrodes', *Bioelectrochemistry and Bioenergetics*, 44(2), pp. 209-214.
- Willner, I., Katz, E., Patolsky, F. and F. Buckmann, A. (1998b) 'Biofuel cell based on glucose oxidase and microperoxidase-11 monolayer-functionalized electrodes', *Journal of the Chemical Society, Perkin Transactions 2*, (8), pp. 1817-1822.
- Willner, I., Yan, Y.M., Willner, B. and Tel-Vered, R. (2009) 'Integrated Enzyme-Based Biofuel Cells—A Review', *Fuel Cells*, 9(1), pp. 7-24.
- Wilson, R. and Turner, A.P.F. (1992) 'Glucose oxidase: an ideal enzyme', *Biosensors and Bioelectronics*, 7(3), pp. 165-185.
- Winfield, J., Ieropoulos, I., Greenman, J. and Dennis, J. (2011) 'The overshoot phenomenon as a function of internal resistance in microbial fuel cells', *Bioelectrochemistry*, 81(1), pp. 22-27.
- Wongnate, T., Sucharitakul, J. and Chaiyen, P. (2011) 'Identification of a Catalytic Base for Sugar Oxidation in the Pyranose 2-Oxidase Reaction', *ChemBioChem*, 12(17), pp. 2577-2586.
- Woodward, J., Mattingly, S.M., Danson, M., Hough, D., Ward, N. and Adams, M. (1996) 'In vitro hydrogen production by glucose dehydrogenase and hydrogenase', *Nature Biotechnology*, 14(7), pp. 872-874.
- Wu, J.C.Y., Hutchings, C.H., Lindsay, M.J., Werner, C.J. and Bundy, B.C. (2015) 'Enhanced Enzyme Stability Through Site-Directed Covalent Immobilization', *Journal of Biotechnology*, 193, pp. 83-90.

References

- Wu, X., Zhao, F., Varcoe, J.R., Thumser, A.E., Avignone-Rossa, C. and Slade, R.C.T. (2009) 'A one-compartment fructose/air biological fuel cell based on direct electron transfer', *Biosensors and Bioelectronics*, 25(2), pp. 326-331.
- Yahiro, A.T., Lee, S.M. and Kimble, D.O. (1964) 'Bioelectrochemistry: I. Enzyme utilizing bio-fuel cell studies', *Biochimica et Biophysica Acta (BBA)-Specialized Section on Biophysical Subjects*, 88(2), pp. 375-383.
- Yakovleva, M.E., Killyéni, A., Ortiz, R., Schulz, C., MacAodha, D., Conghaile, P.Ó., Leech, D., Popescu, I.C., Gonaus, C. and Peterbauer, C.K. (2012) 'Recombinant pyranose dehydrogenase—A versatile enzyme possessing both mediated and direct electron transfer', *Electrochemistry Communications*, 24, pp. 120-122.
- Yan, Y.-M., Baravik, I., Yehezkeli, O. and Willner, I. (2008) 'Integrated electrically contacted glucose oxidase/carbon nanotube electrodes for the bioelectrocatalyzed detection of glucose', *The Journal of Physical Chemistry C*, 112(46), pp. 17883-17888.
- Yan, Y., Su, L. and Mao, L. (2007a) 'Multi-walled carbon nanotube-based glucose/O₂ biofuel cell with glucose oxidase and laccase as biocatalysts', *Journal of nanoscience and nanotechnology*, 7(4-5), pp. 1625-1630.
- Yan, Y., Zheng, W., Su, L. and Mao, L. (2006) 'Carbon-Nanotube-Based Glucose/O₂ Biofuel Cells', *Advanced Materials*, 18(19), pp. 2639-2643.
- Yan, Y.M., Yehezkeli, O. and Willner, I. (2007b) 'Integrated, Electrically Contacted NAD (P)⁺-Dependent Enzyme–Carbon Nanotube Electrodes for Biosensors and Biofuel Cell Applications', *Chemistry—A European Journal*, 13(36), pp. 10168-10175.
- Yang, X.-Y., Tian, G., Jiang, N. and Su, B.-L. (2012) 'Immobilization technology: a sustainable solution for biofuel cell design', *Energy & Environmental Science*, 5(2), pp. 5540-5563.
- Yang, X., Hua, L., Gong, H. and Tan, S.N. (2003) 'Covalent immobilization of an enzyme (glucose oxidase) onto a carbon sol–gel silicate composite surface as a biosensing platform', *Analytica chimica acta*, 478(1), pp. 67-75.

References

- Yin, D.-M., Wu, J.-C. and Yuan, Y.-J. (2006) 'Spatio-temporal distributions of metal ions and Taxol of *Taxus cuspidata* cells immobilized on polyurethane foam', *Biotechnology letters*, 28(1), pp. 29-32.
- Zafar, M.N., Tasca, F., Boland, S., Kujawa, M., Patel, I., Peterbauer, C.K., Leech, D. and Gorton, L. (2010) 'Wiring of pyranose dehydrogenase with osmium polymers of different redox potentials', *Bioelectrochemistry*, 80(1), pp. 38-42.
- Zebda, A., Cosnier, S., Alcaraz, J.P., Holzinger, M., Le Goff, A., Gondran, C., Boucher, F., Giroud, F., Gorgy, K., Lamraoui, H. and Cinquin, P. (2013) 'Single Glucose Biofuel Cells Implanted in Rats Power Electronic Devices', *Scientific Reports*, 3, p. 1516.
- Zebda, A., Innocent, C., Renaud, L., Cretin, M., Pichot, F., Ferrigno, R. and Tingry, S. (2011) 'Enzyme-based microfluidic biofuel cell to generate micropower', *Enzyme*, 2, p. O2.
- Zebda, A., Renaud, L., Cretin, M., Pichot, F., Innocent, C., Ferrigno, R. and Tingry, S. (2009) 'A microfluidic glucose biofuel cell to generate micropower from enzymes at ambient temperature', *Electrochemistry Communications*, 11(3), pp. 592-595.
- Zhang, L.P., Gong, W.J., Pan, Y. and Zhang, Y.Z. (2008) 'Fabrication of multilayer-film-modified gold electrode composed of myoglobin, chitosan, and polyelectrolyte-wrapped multi-wall carbon nanotubes by layer-by-layer assembled technique and electrochemical catalysis for hydrogen peroxide and trichloroacetic acid', *Russian Journal of Electrochemistry*, 44(11), pp. 1271-1279.
- Zhang, M., Smith, A. and Gorski, W. (2004a) 'Carbon nanotube-chitosan system for electrochemical sensing based on dehydrogenase enzymes', *Analytical Chemistry*, 76(17), pp. 5045-5050.
- Zhang, S., Yang, W., Niu, Y. and Sun, C. (2004b) 'Multilayered construction of glucose oxidase on gold electrodes based on layer-by-layer covalent attachment', *Analytica chimica acta*, 523(2), pp. 209-217.
- Zhang, X.-C., Ranta, A. and Halme, A. (2006) 'Direct methanol biocatalytic fuel cell—Considerations of restraints on electron transfer', *Biosensors and Bioelectronics*, 21(11), pp. 2052-2057.

References

Zhao, H.Y., Zhou, H.M., Zhang, J.X., Zheng, W. and Zheng, Y.F. (2009) 'Carbon nanotube–hydroxyapatite nanocomposite: A novel platform for glucose/O₂ biofuel cell', *Biosensors and Bioelectronics*, 25(2), pp. 463-468.

Zheng, L., Yao, X. and Li, J. (2006) 'Layer-by-layer assembly films and their applications in electroanalytical chemistry', *Current Analytical Chemistry*, 2(3), pp. 279-296.

Zhou, K., Zhu, Y., Yang, X. and Li, C. (2010) 'Electrocatalytic Oxidation of Glucose by the Glucose Oxidase Immobilized in Graphene-Au-Nafion Biocomposite', *Electroanalysis*, 22(3), pp. 259-264.

Zhou, M., Deng, L., Wen, D., Shang, L., Jin, L. and Dong, S. (2009) 'Highly ordered mesoporous carbons-based glucose/O₂ biofuel cell', *Biosensors and Bioelectronics*, 24(9), pp. 2904-2908.

Zhou, Q., Xie, Q., Fu, Y., Su, Z., Jia, X.e. and Yao, S. (2007) 'Electrodeposition of carbon nanotubes-chitosan-glucose oxidase biosensing composite films triggered by reduction of p-benzoquinone or H₂O₂', *The Journal of Physical Chemistry B*, 111(38), pp. 11276-11284.

Zhu, X., Tokash, J.C., Hong, Y. and Logan, B.E. (2013) 'Controlling the occurrence of power overshoot by adapting microbial fuel cells to high anode potentials', *Bioelectrochemistry*, 90, pp. 30-35.

Zhu, Z., Momeu, C., Zakhartsev, M. and Schwaneberg, U. (2006) 'Making glucose oxidase fit for biofuel cell applications by directed protein evolution', *Biosensors and Bioelectronics*, 21(11), pp. 2046-2051.